

**DEVELOPMENT OF BIO-WASTE BASED  
CARBOXYMETHYL CELLULOSE, SPINEL FERRITES  
AND POLYMER COMPOSITES AS ADSORBENTS FOR  
WASTEWATER TREATMENT**

Thesis Submitted for the Award of the Degree of

**DOCTOR OF PHILOSOPHY**

**in**

**Chemistry**

**By Rajinder Singh**

**Registration Number: 41500068**

**Supervised By**

**Dr. Harminder Singh (11839)**

**Department of Chemistry (Professor)**

**Lovely Professional University, Phagwara, Punjab**



**LOVELY PROFESSIONAL UNIVERSITY, PUNJAB**

**2025**

## **DECLARATION**

I, hereby declared that the presented work in the thesis entitled “DEVELOPMENT OF BIO-WASTE BASED CARBOXYMETHYL CELLULOSE, SPINEL FERRITES AND POLYMER COMPOSITES AS ADSORBENTS FOR WASTE WATER TREATMENT” in fulfillment of degree of **Doctor of Philosophy (Ph.D.)** is outcome of research work carried out by me under the supervision of Dr. Harminder Singh, working as Professor, in the School of Chemical Engineering and Physical Sciences of Lovely Professional University, Punjab, India. In keeping with general practice of reporting scientific observations, due acknowledgements have been made whenever work described here has been based on findings of other investigator. This work has not been submitted in part or full to any other University or Institute for the award of any degree.

**(Signature of Scholar)** Rajinder Singh

Registration No. 41500068

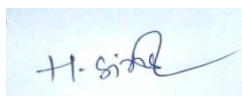
School of Chemical Engineering and Physical Sciences

Lovely Professional University,

Phagwara, Punjab, India

## **CERTIFICATE**

This is to certify that the work reported in the Ph.D. thesis entitled **“DEVELOPMENT OF BIO-WASTE BASED CARBOXYMETHYL CELLULOSE, SPINEL FERRITES AND POLYMER COMPOSITES AS ADSORBENTS FOR WASTEWATER TREATMENT”** submitted in fulfillment of the requirement for the award of degree of **Doctor of Philosophy (Ph.D.) CHEMISTRY** in the School of Chemical Engineering and Physical Sciences, is a research work carried out by Rajinder Singh, Registration No. 41500068, is bonafide record of his original work carried out under my supervision and that no part of thesis has been submitted for any other degree, diploma or equivalent course.



**(Signature of Supervisor)**

Dr. Harminder Singh

Professor in Chemistry

School of Chemical Engineering and Physical Sciences

Lovely Professional University, Phagwara, Punjab-144001

## **Acknowledgement**

I am deeply grateful to almighty God and my organization School Education Department, Punjab to provide me an opportunity to enhance my scientific research aptitude.

I wish to express my sincere appreciation and gratitude to my research advisor, Dr. Harminder Singh, Professor, Lovely Professional University, Phagwara, Punjab, for his continuous guidance, support and encouragement all through this work.

I also thankfully acknowledge the assistance of my fellow colleagues for their constant encouragement and aid in various ways. I would like to express deep appreciation to my research fellows and Laboratory Technicians at Lovely Professional University for their cooperation and helpfulness during this work.

My parents, Sh. Bachitter Singh and Smt. Daljit Kaur deserve special appreciation and gratitude for their inseparable support and prayers. Thanks for supporting me during my studies. Last, but not the least, a special gratitude to my wife Mrs. Tejinder Kaur, without whose incessant moral support this work could not have been a success.

Date: 21-07-2025

Rajinder Singh



## ABSTRACT

Water pollution is one of the major environmental problems globally caused by rapid industrialization, urbanization and intensified agricultural practices that need much attention of the researchers worldwide. The primary reason behind water contamination is direct disposal of effluents without treatment into water bodies by textile, dyes and tanning industries, painting, mining, petrochemical and fertilizer/ pesticides industries. The dyes and heavy metals are especially harmful both for human beings and aquatic life. They tend to accumulate in human bodies and pose severe health issues. Therefore, their removal from the wastewater is necessary. Different traditional approaches and methodologies such as coagulation, filtration, precipitation, ion-exchange, solvent extraction, reverse osmosis, electrochemical treatment and evaporation etc. have been explored for the removal of dyes and heavy metals. These technologies are generally complicated, expensive, time consuming and require sophisticated instrumentation. Thus, keeping these drawbacks into mind, there is need of low cost and less maintenance requiring technique and one such beneficial technique is 'adsorption'. The adsorption is a promising technique due to its environmental friendly, simple, fast and economical nature for removing certain dyes and heavy metals. Various types of natural adsorbents have been explored for the adsorption purpose owing of their low cost and large availability but they show less potentiality for removing the pollutants from waste water. So, there is the need of synthetic adsorbents. The synthetic adsorbents are synthesized either from natural adsorbents or industrial wastes. The potentiality of these adsorbents is remarkable in removing the pollutants from wastewater. Over the years, to enhance the adsorption process, nano materials in the form of nano ferrites, nano fibres, mesoporous compounds, oxides of metals were explored. The nano ferrites give good results in removing the pollutants from water but their stability in aqueous medium is less. To enhance their stability, the surface of these ferrites is modified by the application of various surfactants, doping and polymer coating. Various biopolymers like chitosan, alginates, cellulose, silica, gum Arabic etc. are obtained as agricultural waste and abundantly available. The biopolymer modified spinel ferrites are termed as magnetic bio-composites.

Recently, in wastewater treatment, magnetic bio-composites are frequently investigated as an adsorbent due to their great capacity for adsorption, selectivity, reactivity, large surface area and affordability. Cellulose and its derivatives have practical applications

and are inexpensive, non-toxic, renewable, biocompatible, and environmentally friendly. One such derivatives of cellulose is carboxymethyl cellulose (CMC), which is anionic, water soluble polysaccharide has wide application in food, detergents, pharmaceuticals, textile, paper and paint industries and adhesive industries. The present study aims to synthesize transition metal ferrites of nickel, zinc, cobalt and modified their surface with carboxymethyl cellulose and alginate and used as adsorbents for the removal of dyes (crystal violet and methylene blue) and metal ions in both single as well as binary dye system.

To study the adsorption behaviour of these adsorbents, the preliminary studies were conducted with various types of dyes and metal ions. Batch mode of adsorption process was followed for remediation purpose. It was observed that NiFCMC, NiFCMC-Alg and ZnFCMC and ZnFCMC-Alg composites showed good adsorption potential to remove MB and CV dyes and nickel metal ions. Several techniques were utilized to characterize these synthesized CMC and adsorbents including FTIR (Fourier Transform Infrared Spectroscopy), XRD (X-Ray Diffraction), FESEM (Field emission scanning electron microscopy), EDS (Energy-dispersive spectra), TGA (Thermogravimetric analysis), BET (Brunauer-Emmett-Teller), VSM (Vibration sample magnetometry) and  $\text{pH}_{\text{pzc}}$  (pH of point zero charge). These adsorbents were explored to check their potentiality to remove Ni (II) ions in aqueous medium in single ion system and MB and CV dyes in single and binary dye systems on various parameters such as contact time, initial dye/metal ion concentration, pH, adsorbent dose and temperature. The adsorption behaviour was studied with several adsorption isotherms including Langmuir, Freundlich, Temkin and Dubinin-Radushkevich (D-R) and kinetic models Lagergren pseudo-first order model, Lagergren pseudo-second order, Weber-Morris intra-particle diffusion model and Elovich model. The optimum pH for removing dyes and nickel ions was 8 for all adsorbents. The adsorption behaviour of selected cationic dyes and Ni (II) ions was examined at varying concentration (50-250 mg/L) for single dye /metal ion system and 20-100 mg/L for binary dye systems) using magnetic biopolymer composites. The adsorption capabilities of the adsorbents increased as the initial concentration of the dye/metal ion solution increased as revealed by the results. As the dye/ metal ion concentration rises, more interactions occur between the adsorbent and adsorbate. On the other hand, in metal ion system and both dye systems, the removal percentage decreased as the solution's concentration increased. This may be the result of the adsorbent's surface having less

accessible active sites as the concentration increases. The adsorption behaviour of the dyes/metal ion for the adsorbents increases with increase in temperature. It is because the interaction between the adsorbent and adsorbate occurs more quickly as temperature rises. As the temperature rises, number of pores increased whereby increasing the surface area and speeding up the adsorption process. Results of kinetic studies revealed that for the metal ion/dyes adsorption, the Lagergren pseudo second order mode best fit the data indicating the chemisorption nature. Likewise, the Langmuir isotherm model also showed good agreement with adsorption equilibrium data for all adsorbents. The thermodynamic parameters like  $\Delta H^\circ$ ,  $\Delta G^\circ$  and  $\Delta S^\circ$  were calculated and it was found that value of  $\Delta H^\circ$ ,  $\Delta S^\circ$  was positive suggesting the endothermic nature and increase in randomness at the interface of adsorbate and adsorbent. Similarly, the value of  $\Delta G^\circ$  was found to be negative suggesting the spontaneous nature of adsorption process. The regeneration efficiency of both adsorbents was studied for five cycles and showed significant results. It was found that NiFCMC and NiFCMC-Alg retained the regeneration efficiency of 81.3% and 77.2% for Ni (II) ions, 78.6%, 81.3% for MB and 72.2%, 76.1% for CV in single dye system. Whereas for ZnFCMC and ZnFCMC-Alg, the regeneration efficiency remained 78.8%, 81.3% for MB and 70.8%, 76.4% for CV in single dye system. The findings showed that the synthesized NiFCMC, ZnFCMC, NiFCMC-Alg and ZnFCMC-Alg composites are in-expensive, eco-friendly, selective and efficient alternatives for the removal of both metal ions and cationic dyes from water.

## **Table of Content**

Declaration	
Certificate	ii
Acknowledgements	iii
Abstract	iv
List of Tables	xiii
List of Figures	xvi
List of Abbreviations	xx
Symbols used	xxi

<b>Sr. no.</b>	<b>Content</b>	<b>Page no.</b>
----------------	----------------	-----------------

### **CHAPTER 1: INTRODUCTION**

<b>1.0</b>	General Introduction	1
<b>1.1</b>	Various methods for wastewater treatment	1
<b>1.2</b>	Physical Methods for Wastewater Treatment	1
<b>1.2.1</b>	Adsorption	1
<b>1.2.2</b>	By using Ion–Exchanger	2
<b>1.2.3</b>	Membrane Filtration	2
<b>1.3</b>	Chemical methods for Treatment of Wastewater	2
<b>1.3.1</b>	Coagulation	2
<b>1.3.2</b>	Oxidation	2
<b>1.3.3</b>	Chemical Precipitation	2

<b>1.4</b>	Biological Methods for Treatment of Wastewater	3
<b>1.5</b>	Types of Adsorbent	3
<b>1.5.1</b>	Natural	3
<b>1.5.2</b>	Synthetic	4

## **CHAPTER 2: REVIEW OF LITERATURE**

<b>2.0</b>	Synthesis of Carboxymethyl cellulose (CMC) from Cellulose	6
<b>2.1</b>	Use of Nano Material as Adsorbents	8
<b>2.1.1</b>	Metal Ferrites as Adsorbent	9
<b>2.1.2</b>	Modification of Metal Ferrites' Surface	12
<b>2.1.3</b>	Metal oxide coating	12
<b>2.1.4</b>	Surfactant coating	13
<b>2.1.5</b>	Polymer coating	13
<b>2.1.6</b>	Use of Carboxymethyl cellulose (CMC) in Adsorption field	18
<b>2.2</b>	Regeneration of Adsorbent	25
<b>2.3</b>	Research Gap	27
<b>2.4</b>	Objectives of the Research	27

## **CHAPTER 3: MATERIALS AND METHODS**

<b>3.0</b>	Materials	29
<b>3.1</b>	Experimental Method	29
<b>3.1.1</b>	Synthesis of Nano Metal Ferrites	29
<b>3.1.2</b>	Extraction of Cellulose from Corncob	29
<b>3.1.3</b>	Bleaching	30
<b>3.1.4</b>	Synthesis of Carboxymethyl cellulose from Cellulose	30

<b>3.1.5</b>	Isolation of Lignin	30
<b>3.1.6</b>	Surface Modification with Carboxymethyl cellulose	32
<b>3.1.7</b>	Preparation of Metal Ferrite-Carboxymethyl cellulose-Alginate Composite	32
<b>3.2</b>	Preliminary Adsorption Studies	32
<b>3.2.1</b>	Preliminary adsorption studies with different dyes	35
<b>3.2.2</b>	Preliminary adsorption studies with metal and fluoride ion	36
<b>3.3</b>	Estimation of synthesized Carboxymethyl cellulose	39
<b>3.3.1</b>	CMC yield calculation	39
<b>3.3.2</b>	Degree of Substitution (DS)	39
<b>3.3.2.1</b>	Method of Titration	39
<b>3.3.3</b>	Molecular weight calculation	40
<b>3.3.4</b>	Water retaining/ holding capacity (WHC) and Oil retaining/ holding capacity (OHC)	40
<b>3.3.5</b>	Content of CMC (%)	40
<b>3.3.6</b>	Content of Sodium chloride in CMC	41
<b>3.3.7</b>	Fourier Transform Infra Red (FTIR) Analysis	41
<b>3.3.8</b>	Scanning Electron Microscope (SEM) analysis	41
<b>3.3.9</b>	Energy Dispersive Spectra Analysis (EDS)	42
<b>3.3.10</b>	Brunauer-Emmett-Teller Analysis (BET)	42
<b>3.3.11</b>	Thermo Gravimetric Analysis (TGA)	42
<b>3.3.12</b>	X-Ray Diffraction Analysis (XRD)	42
<b>3.3.13</b>	pH of Point Zero Charge (pHpzc) Analysis	43
<b>3.3.14</b>	Vibration Sample Magnetometer (VSM) Analysis	43

<b>3.4</b>	Adsorption Studies by Batch method	43
<b>3.4.1</b>	Single and Binary Dye system	44
<b>3.4.2</b>	Single Dye system	44
<b>3.4.3</b>	Binary Dye System	44
<b>3.5</b>	Regeneration Studies	45
<b>3.6</b>	Adsorption Kinetics	45
<b>3.6.1</b>	Lagergren Pseudo first Order Model	45
<b>3.6.2</b>	Lagergren Pseudo second Order Model	46
<b>3.6.3</b>	Elovich Model	46
<b>3.6.4</b>	Weber Morris Model	46
<b>3.7</b>	Adsorption Isotherms	46
<b>3.7.1</b>	Langmuir Model	47
<b>3.7.2</b>	Freundlich Isotherm	47
<b>3.7.3</b>	Temkin Isotherm	48
<b>3.7.4</b>	Dubinin-Radushkevich (D-R) Isotherm	48
<b>3.8</b>	Adsorption Thermodynamics	49

## **CHAPTER 4: RESULTS AND DISCUSSION**

### **Part -I**

<b>4.0</b>	<b>Characterization of Extracted Cellulose and synthesized Carboxymethyl cellulose (CMC)</b>	50
<b>4.1</b>	Purification and Isolation of Cellulose	50
<b>4.1.2</b>	FTIR Analysis	54
<b>4.1.3</b>	Analysis using X-Ray diffraction	56

4.1.4	SEM Analysis	57
<b>Part-II</b>		
4.2	<b>Characterization and Adsorption studies of Nickel metal ions with metal ferrite-CMC and their biopolymer composite</b>	58
4.2.1	Nickel Ferrite-CMC (NiFCMC) and Nickel ferrite CMC-Alginate (NiFCMC-Alg) Composite	58
4.2.2	Characterization and Morphological Studies	59
4.2.3	FTIR Spectroscopy	59
4.2.4	X-ray Diffraction (XRD)	60
4.2.5	Field Emission Scanning Electron Microscopy (FESEM)	61
4.2.6	Energy Dispersive Spectra (EDS)	63
4.2.7	Thermogravimetric Analysis (TGA)	64
4.2.8	Vibration Scanning Magnetometry (VSM)	64
4.2.9	Point zero charge pH (pH <sub>PZC</sub> )	65
4.2.10	Brunauer-Emmett-Teller (BET) Analysis	66
4.3	Batch Adsorption Studies with Ni (II) ions	67
4.3.1	Effect of contact time	67
4.3.2	Effect of adsorbent dose	68
4.3.3	Effect of pH	68
4.3.4	Adsorption Kinetics	69
4.3.5	Effect of Concentration and temperature	72
4.3.6	Adsorption Isotherms	73



4.3.7	Adsorption Thermodynamics	77
4.3.8	Regeneration of Adsorbent	79

### **Part-III**

4.4	<b>Result of Batch Adsorption Studies of single and binary dye systems for NiFCMC and NiFCMC-Alg composite</b>	80
4.4.1	Effect of Contact Time	80
4.4.2	Effect of adsorbent dose	81
4.4.3	Effect of pH	81
4.4.4	Adsorption Kinetics	82
4.4.5	Effect of Concentration	84
4.4.6	Adsorption Isotherms	88
4.4.7	Adsorption Thermodynamics	93
4.4.8	Regeneration of Adsorbent	96

### **Part-IV**

4.5	<b>ZnFCMC and ZnFCMC-Alg composite</b>	98
4.5.1	Characterization and Morphological Studies	98
4.5.2	FTIR Spectroscopy	98
4.5.3	X-ray Diffraction (XRD)	99
4.5.4	Field Emission Scanning Electron Microscopy (FESEM)	100
4.5.5	Energy Dispersive Spectra (EDS)	102
4.5.6	Thermogravimetric Analysis (TGA)	103
4.5.7	Vibration Scanning Magnetometry (VSM)	104
4.5.8	pH of point zero charge (pH <sub>PZC</sub> )	105

<b>4.5.9</b>	Brunauer-Emmett-Teller (BET) Analysis	106
<b>4.5.10</b>	<b>Result of Batch Adsorption Studies of single and binary dye systems for ZnFCMC and ZnFCMC-Alg composite</b>	106
<b>4.5.11</b>	Effect of contact time	106
<b>4.5.12</b>	Effect of adsorbent dose	107
<b>4.5.13</b>	Effect of pH	108
<b>4.5.14</b>	Adsorption Kinetics	109
<b>4.5.15</b>	Effect of Concentration	113
<b>4.5.16</b>	Adsorption Isotherms	115
<b>4.5.17</b>	Adsorption Thermodynamics	121
<b>4.5.18</b>	Regeneration of Adsorbent	124
<b>4.5.19</b>	Mechanism of Adsorption	127

## **CHAPTER 5: SUMMARY AND CONCLUSIONS**

<b>5.0</b>	Summary and Conclusions	128-132
	<b>References</b>	133-151
	<b>List of publications</b>	152
	<b>List of conferences</b>	
	<b>Appendix</b>	

## **LIST OF TABLES**

<b>Table no.</b>	<b>Title of Table</b>	<b>Page no.</b>
<b>2.1</b>	Properties of CMC synthesized from various cellulosic source	7
<b>2.2</b>	Different methods, characteristics, advantages and disadvantages of different methods of synthesis of	10-11

	ferrites	
<b>2.3</b>	Use of various metal ferrites for the adsorption of various pollutants	12
<b>2.4</b>	Removal capacity of various nano particles, magnetic composites and magnetic nano composites towards metal ions and dyes along with other reaction conditions	14-17
<b>2.5</b>	Adsorption capability of CMC composites for metal ions, anion and dye	21-24
<b>2.6</b>	Various desorption agents used in regeneration of adsorbate containing CMC	25-26
<b>3.1</b>	Preliminary study of percentage removal of Methylene Blue (MB) Cationic dye	33
<b>3.2</b>	Preliminary study of percentage removal of Crystal violet (CV) (Cationic) dye	34
<b>3.3</b>	Preliminary study of percentage removal of Congo Red (CR) (Anionic) dye	34
<b>3.4</b>	Preliminary study of percentage removal of Eosin Blue (EB) (Neutral) dye	35
<b>3.5</b>	Preliminary study of percentage removal of Flouride (F <sup>-</sup> ) ions	37
<b>3.6</b>	Preliminary study of percentage removal of Ni (II) ions	38
<b>4.1.1</b>	DS, percentage yield and solubility of synthesized CMC	51
<b>4.1.2</b>	Calculated values of intrinsic viscosity and molecular weight of CMC	51
<b>4.1.3</b>	Percentage purity, NaCl content, WRC and ORC of synthesized CMC	52
<b>4.2.1</b>	Elemental composition of NiF, NiFCMC, NiFCMC-Alg composite	62-63
<b>4.2.2</b>	Results of BET analysis of NiF, NiFCMC and	67

## NiFCMC-Alg composite

<b>4.3.1</b>	Calculated values of constants of various kinetic models used for NiFCMC and NiFCMC-Alg of Ni (II) ions	71-72
<b>4.3.2</b>	Various adsorption isotherm constants of NiFCMC and NiFCMC-Alg composite for Ni (II) ions	75-76
<b>4.3.3</b>	Comparative study showing adsorption capacity of several adsorbents for Ni (II) ions	77
<b>4.3.4</b>	Calculated thermodynamic parameters for Ni (II) ions	78
<b>4.3.5</b>	Regeneration performance of adsorbent NiFCMC and NiFCMC–Alg composite	79
<b>4.4.1</b>	Computed values of various constants of various kinetic models for NiFCMC and NiFCMC-Alg at 298 K in single and binary dye systems	86
<b>4.4.2</b>	Estimated values for various constants of different adsorption isotherm models at 25°C, 30°C and 35°C in single dye system for NiFCMC and NiFCMC-Alg composite	89
<b>4.4.3</b>	Estimated values for various constants of different adsorption isotherm models at 25°C, 30°C and 35°C in binary dye system for NiFCMC and NiFCMC-Alg composite	90
<b>4.4.4</b>	Computed values of $\Delta H^\circ$ , $\Delta S^\circ$ and $\Delta G^\circ$ in both dye systems	94-95
<b>4.4.5</b>	Percentage regeneration efficiency of NiFCMC and NiFCMC-Alg adsorbent	97
<b>4.5.1</b>	Composition of elements in ZnF, ZnFCMC and ZnFCMC-Alg composite	102
<b>4.5.2</b>	Results of BET analysis of ZnF, ZnFCMC and ZnFCMC-Alg composite	106

<b>4.5.3</b>	Calculated values of adsorption constants of different kinetic models for ZnFCMC and ZnFCMC-Alg at 298K in single dye system	111-112
<b>4.5.4</b>	Calculated values of adsorption constants of different kinetic models for ZnFCMC and ZnFCMC-Alg at 298K in binary dye system	112-113
<b>4.5.5</b>	Computed values for various constants of different adsorption isotherm models at 25°C, 30°C and 35°C in single dye system for ZnFCMC and ZnFCMC-Alg composite	116
<b>4.5.6</b>	Computed values for various constants of different adsorption isotherm models at 25°C, 30°C and 35°C in binary dye system for ZnFCMC and ZnFCMC-Alg composites	117
<b>4.5.7</b>	Comparative study of adsorption capabilities of different adsorption materials for MB and CV dyes	120-121
<b>4.5.8</b>	Calculated values of $\Delta H^\circ$ , $\Delta S^\circ$ and $\Delta G^\circ$ in both dye systems (single and binary)	123-124
<b>4.5.9</b>	Percentage regeneration efficiency of ZnFCMC and ZnFCMC Alg adsorbent	126

### **LIST OF FIGURES**

<b>Figure no.</b>	<b>Title of Figures</b>	<b>Page no.</b>
<b>1.1</b>	Structure of cellulose	4
<b>3.1</b>	Synthesis of carboxymethyl cellulose from cellulose	30
<b>3.2</b>	Flow chart showing the synthesis of CMC from corncob	31
<b>4.1.1</b>	Pictorial representation of synthesis of carboxymethyl cellulose (CMC) from corncob	53
<b>4.1.2</b>	FTIR curve for (a) extracted cellulose (b) corncob (c)	55

	extracted lignin	
<b>4.1.3</b>	FTIR curve shows (a) CMC standard (b) CMC synthesized	56
<b>4.1.4</b>	XRD peaks of (a) extracted cellulose (b) synthesized CMC	57
<b>4.1.5</b>	SEM images of (a) Extracted cellulose (b, c) synthesized CMC (d) extracted lignin	58
<b>4.2.1</b>	FTIR image of (a) NiF (b) NiFCMC and (c) NiFCMC - Alg composite	59
<b>4.2.2</b>	XRD of NiF, NiFCMC and NiFCMC-Alg	60
<b>4.2.3</b>	FESEM pictures of (a) NiF (b) NiFCMC (c) NiFCMC-Alg	61-62
<b>4.2.4</b>	EDS graph for (a) NiF (b) NiFCMC and (c) NiFCMC-Alg	63
<b>4.2.5</b>	TGA curves of NiF, NiFCMC and NiFCMC-Alg composite	64
<b>4.2.6</b>	Magnetization curve of (a) NiF (b) NiFCMC (c) NiFCMC-Alg	65
<b>4.2.7</b>	pH <sub>pzc</sub> of NiFCMC and NiFCMC-Alg	66
<b>4.3.1</b>	Effect of contact time for Ni (II) ions	67
<b>4.3.2</b>	Effect of adsorbent dosage for Ni (II) ions	68
<b>4.3.3</b>	Effect of pH on removal % of Ni (II) ions	69
<b>4.3.4</b>	Various kinetic adsorption models (a) Pseudo first order kinetic model (b) Pseudo second order kinetic model (c) Elovich model (d) Weber-Morris diffusion model	70-71
<b>4.3.5</b>	Effect of concentration for NiFCMC and NiFCMC-Alg composite	73

<b>4.3.6</b>	(a-d) Plot of different adsorption isotherms (a) Langmuir (b) Freundlich (c) Temkin (d) D-R isotherm	74-75
<b>4.3.7</b>	Plot of $\ln K_d$ versus $1/T$ for Ni(II) ions	78
<b>4.3.8</b>	Percentage regeneration efficiency of NiFCMC and NiFCMC-Alg composite	79
<b>4.4.1</b>	Effect of contact time in single and binary dye systems	80
<b>4.4.2</b>	Effect of adsorbent dosage in single as well as binary dye systems	81
<b>4.4.3</b>	Effect of pH on removal % of MB and CV dye	82
<b>4.4.4</b>	Various kinetic models (a) Pseudo first order (b) Pseudo second order (c) Elovich (d) Weber-Morris diffusion model	83-84
<b>4.4.5</b>	Impact of concentration on $Q_e$ and removal % in (a) single and (b) binary dye system	87
<b>4.4.6</b>	Graph of various adsorption isotherms (a) Langmuir (b) Freundlich (c) Temkin (d) D-R isotherm	91-92
<b>4.4.7</b>	Graph between $\ln K_d$ vs $1/T$ in (a) single (b) binary dye system	93-94
<b>4.4.8</b>	Percentage regeneration efficiency of NiFCMC and NiFCMC-Alg adsorbent	96
<b>4.5.1</b>	FTIR spectra of ZnF, ZnFCMC and ZnFCMC-Alg composite	99
<b>4.5.2</b>	XRD spectra of ZnF, ZnFCMC and ZnFCMC-Alg composite	100
<b>4.5.3</b>	FESEM pictures of (a) ZnF (b) ZnFCMC (c) ZnFCMC-Alg	101
<b>4.5.4</b>	Energy Dispersive spectra of (a) ZnF (b) ZnFCMC (c) ZnFCMC-Alg	102-103

<b>4.5.5</b>	TGA curves of ZnF, ZnFCMC and ZnFCMC–Alg composite	104
<b>4.5.6</b>	Magnetization curve of ZnF, ZnFCMC and ZnFCMC-Alg composite	105
<b>4.5.7</b>	pH <sub>pzc</sub> of ZnFCMC and ZnFCMC-Alg	106
<b>4.5.8</b>	Effect of contact time in single as well as binary dye system	107
<b>4.5.9</b>	Effect of adsorbent dosage in single as well as binary dye system	108
<b>4.5.10</b>	Effect of pH on removal percentage of MB and CV dye	109
<b>4.5.11</b>	Various kinetic models (a) Pseudo first order (b) Pseudo second order (c) Elovich (d) Weber-Morris diffusion model	110-111
<b>4.5.12</b>	Effect of concentration on Q <sub>e</sub> and percentage removal in single dye system	114
<b>4.5.13</b>	Effect of concentration on Q <sub>e</sub> and percentage removal in binary dye system	114
<b>4.5.14</b>	Various adsorption isotherms plots (a) Langmuir (b) Freundlich (c) Temkin (d) D-R isotherm	118-119
<b>4.5.15</b>	Graph between ln K <sub>d</sub> vs 1/T for MB and CV in single dye system	122
<b>4.5.16</b>	Graph between ln K <sub>d</sub> vs 1/T for MB and CV in binary dye system	122
<b>4.5.17</b>	Percentage regeneration efficiency of ZnFCMC and ZnFCMC-Alg adsorbent	125
<b>4.5.18</b>	Adsorption mechanism of cationic dyes and metal ion on Metal CMC-Alginate composite surface	127



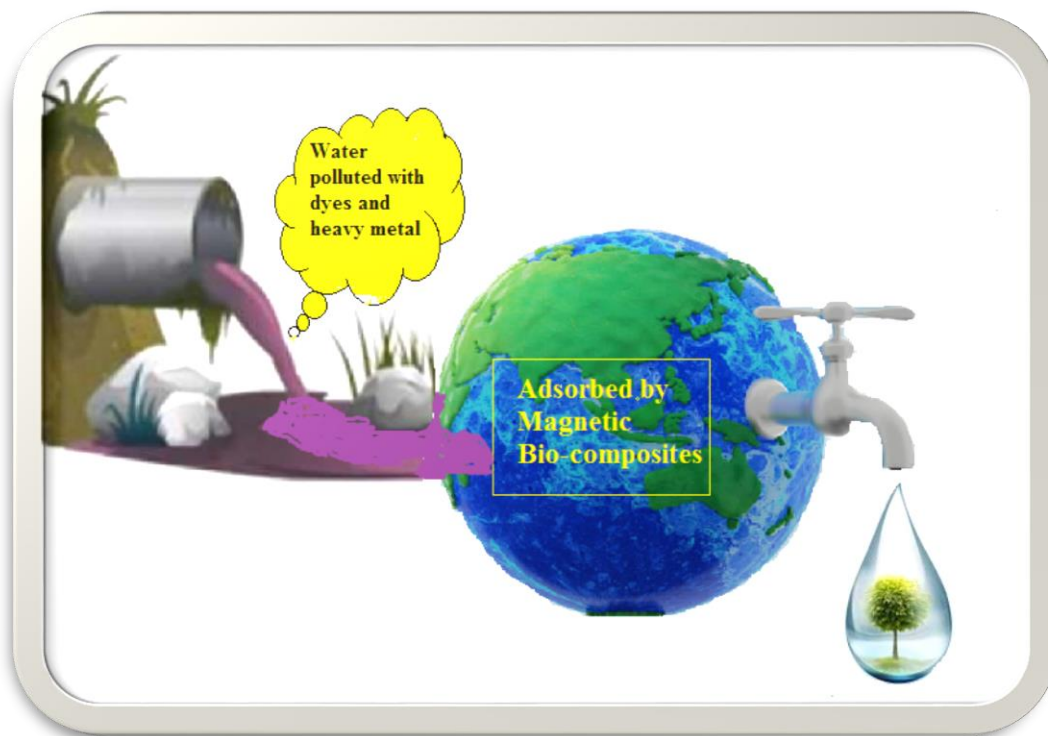
## **Abbreviations**

<b>Abbreviation</b>	<b>Meaning</b>
MB	Methylene blue
CV	Crystal blue
CMC	Carboxymethyl cellulose
NiF	Nickel ferrite
ZnF	Zinc ferrite
CuF	Copper ferrite
CR	Congo red
EB	Eosin blue
NiFCMC	Nickel ferrite carboxymethyl cellulose
ZnFCMC	Zinc ferrite carboxymethyl cellulose
NiFCMC-Alg	Nickel ferrite carboxymethyl cellulose-alginate
ZnFCMC-Alg	Zinc ferrite carboxymethyl cellulose-alginate
OD	Optical density
SWCNT	Single walled carbon nano tube
MWCNT	Multi walled carbon nano tube
ODH	Oxalyl dihydrazide
DS	Degree of substitution
WHC	Water holding capacity
OHC	Oil holding capacity
DW	Distilled water

## **Symbols Used**

<b>Parameter</b>	<b>Symbol</b>	<b>Unit</b>
Percentage	%	-
Temperature	T	°C
Initial concentration	C <sub>o</sub>	mg/L
Concentration at time t	C <sub>t</sub>	mg/L
Adsorption capacity at equilibrium	Q <sub>e</sub>	mg/g
Adsorption capacity at time t	Q <sub>t</sub>	mg/g
Equivalent weight per gram of NaOH	A	G
Volume of NaOH used	B	mL
Normality of NaOH	C	g equ/L
Volume of HCl used	D	mL
Normality of HCl	E	g equ/L
Weight of CMC used	F	G
Intrinsic viscosity	η	dL/g
Solvent constant	K	-
Polymer shape factor	a	-
Crystallite size	D	Nm
Gibbs free energy change	ΔG°	kJ/mol
Enthalpy change	ΔH°	kJ/mol
Entropy change	ΔS°	J/mol/K

Lagergren pseudo first order rate constant	$k_1$	$\text{min}^{-1}$
Lagergren pseudo second order rate constant	$k_2$	$\text{mg/min}$
Chemisorption rate constant	$\alpha$	$\text{g/mg/min}$
Desorption constant	$\beta$	$\text{g/mg}$
Absolute temperature	$T$	$\text{K}$
Maximum binding energy	$A$	$\text{L/g}$
Temkin constant	$bT$	$\text{J/mg}$
Langmuir constant	$b$	$\text{L/mg}$
Langmuir adsorption capacity	$Q$	$\text{mg/g}$
D-R adsorption capacity	$Q_m$	$\text{mg/g}$
Polanyi potential	$\varepsilon$	$\text{kJ/mol}$



## **CHAPTER 1**

### **INTRODUCTION**

## **1.0 General Introduction**

Water pollution is a significant environmental issue globally caused with the rapid industrialization, urbanization and intensified agricultural practices that need much attention of the researchers worldwide. The primary reason behind water contamination is direct disposal of effluents without treatment into water bodies. Various sectors including textile, tanning, mining, petrochemical, painting and fertilizer/pesticide discharge dyes and heavy metals into the water which are the most harmful and hazardous contaminants<sup>1</sup>. Heavy metals and dyes are particularly dangerous because they tend to build up in human bodies causing serious health issues. The dyes and heavy metals being the dangerous, carcinogenic and toxic nature pose serious health issues in human beings and aquatic life<sup>2</sup>. Being toxic, these cause respiratory and digestive disorders, skin problems, cyanosis and carcinogenesis<sup>3, 4</sup>. Therefore, their removal from the wastewater is necessary.

Keeping in mind the above situation, there is a need to explore new methods and technologies to detect and eliminate the toxic pollutants from water in effective and economical manner. Over the years, a number of technologies have been developed to remove heavy metals and other contaminants from effluents from industries. Numerous conventional methods and procedures including filtration, flocculation, oxidation process, photocatalytic, electrochemical treatment, evaporation, bioreactors and others were investigated for the removal of dyes from industrial wastewater<sup>5, 6</sup>.

### **1.1 Various methods for wastewater treatment**

These methods have been categorized in 3 main types viz. physical methods, chemical methods and biological methods

#### **1.2 Physical Methods for Wastewater Treatment**

##### **1.2.1 Adsorption**

Adsorption technique shows high potential for purification of waste water and has emerged as clean, economical, highly selective and efficient technique. Adsorption is a surface phenomenon which involves the adhesion of molecules, atoms or ions on the solid or liquid surface. The main advantage of this method is simple designing, easy, affordable and time-efficient process and less land requirement as compared to other methods. Activated clay, mesoporous materials and industrial and agricultural waste are examples of natural and artificial adsorbents that were utilized to remove various dyes and heavy metals from effluent<sup>7, 8</sup>.

### **1.2.2 By using Ion-Exchanger**

The effective technique for extracting dissolved ions from water is the ion-exchange method. Various types of ion-exchangers viz. cation exchange resins, anion exchange resins, neutral and chelate resins are employed for removing the pollutants from effluent. The primary benefit of the technique is reversible and selective nature making extended utilization of resin. The disadvantages include the periodic regeneration of resins, potential fouling of resins and high maintenance cost <sup>9</sup>.

### **1.2.3 Membrane Filtration**

This technique makes use of a semi-permeable membrane to remove contaminants of organic and inorganic nature. Reverse osmosis, ultra and nano filtration, microfiltration are some types of the membrane filtrations that are used to remove different kinds of pollutants. The advantages of this method includes-high efficiency, compact design and no chemical use. The disadvantages are- high cost, high risk of membrane blockage, consumption of energy and fouling <sup>10, 11</sup>.

## **1.3 Chemical methods for Treatment of Wastewater**

### **1.3.1 Coagulation**

Coagulation is a crucial wastewater treatment procedure that helps to remove colloids, dissolved compounds and particles in suspension from water. It functions by dissolving and binding small particles in water with chemicals known as coagulants. This allows the larger particles to form clusters that are easier to remove by sedimentation or further filtration. It is effective method for removing contaminants and pathogens. The main disadvantages of this method are- choosing the right coagulant and its dosages, production of large amount of sludge and it can be challenging to ensure that chemicals are working properly in wastewater treatment <sup>5, 12</sup>.

### **1.3.2 Oxidation**

In the oxidation process, pollutants are changed into less hazardous readily removable chemicals by using oxidising agents. The various types of oxidising agents like chlorine ( $\text{Cl}_2$ ), ozone ( $\text{O}_3$ ), potassium permanganate ( $\text{KMnO}_4$ ), sodium hypochlorite ( $\text{NaClO}$ ) and hydrogen peroxide ( $\text{H}_2\text{O}_2$ ) are used for pollutant degradation. The advantages of the method include -effective cleaning, degradation of organic matter and remove odour. The disadvantages of this method are its expensive nature and formation of hazardous by-products, difficulties with catalyst activity and recyclability <sup>5</sup>.

### **1.3.3 Chemical Precipitation**

It is a versatile method of treating water that involves adding certain chemicals to remove

dissolved pollutants and converting them into a solid form known as precipitate. By using filtration, sedimentation or other physical techniques, the precipitates are subsequently extracted from the water. The commonly used precipitating agents are lime, ferric chloride, alum, sodium hydroxide etc. The main drawbacks of this method includes production of a large volume of sludge, which necessitates further processing and disposal, raising the overall expense and complexity and change in pH and temperature of wastewater <sup>13</sup>.

#### **1.4 Biological Methods for Treatment of Wastewater**

For sustainable water and wastewater treatment, it is key method for effectively reducing organic and inorganic pollutants and pathogens. This biological method comprises of two types of treatment viz. aerobic and anaerobic. Aerobic treatment refers to the breakdown of inorganic as well as organic matter by microorganisms or bacteria in the presence of oxygen while degradation or break down in the absence of oxygen is called anaerobic mode. Chemical treatment can be performed along with this method. The main limitations of the biological methods are- the necessity for trained operators, sensitivity to environmental changes, potential for prolonged treatment times and vulnerability to harmful compounds <sup>14, 15</sup>.

Adsorption is a physical approach that showed significant potential for the filtration of wastewater that contains various organic and inorganic impurities. Adsorption technique has certain advantages like low cost, effective, less time consuming and less requirement of land. A surface phenomena known as adsorption occurs when molecules, atoms or ions stick to the surface of a solid or liquid. The molecules accumulate on the surface of the adsorbent without entering into the bulk of the material. The material which gets adsorbed on the surface is termed as adsorbate while the surface on which adsorption occurs is called adsorbent. The adsorbent and adsorbate are attracted to one another through an intermolecular force during the adsorption process <sup>16, 17</sup>.

#### **1.5 Types of Adsorbent**

It has been revealed by literature study that in adsorption process, a variety of adsorbents has been used. Adsorbents are of two main types - (a) Natural (b) Synthetic

##### **1.5.1 Natural**

Charcoal, zeolites, chitosan, lignocelluloses and clay minerals come under category of natural adsorbents. These inexpensive natural adsorbents are readily available in bulk and are efficient for removing heavy metals and dyes from effluent. Low cost biosorbents have been explored as material for adsorption during last decades. These adsorbents have been

chemically modified to enhance their adsorption potential in wastewater treatment<sup>16, 18</sup>.

### 1.5.2 Synthetic

Since natural adsorbents have modest adsorption capabilities, their use in removing hazardous pollutants from wastewater has proven less efficient. To remove these pollutants from wastewater, various synthetic adsorbent types have been investigated. The synthetic adsorbents are prepared from natural adsorbents mainly agricultural and industrial waste materials. These include sawdust, rice husk, sugarcane bagasse, coconut shell, fly ash, meso porous material, zeolites etc.<sup>5, 19, 20</sup>.

Nanomaterials have recently shown their efficacy as excellent adsorbents in the treatment of wastewater with high adsorptive capacity such as nano-scale functionalized carbon nanotubes both SWCNT and MWCNT, nano-alumina, hydroxyapatite nanoparticles<sup>21</sup>. To further improve the adsorption capability, the conventional bioadsorbents such as alginate, cellulose, chitosan, gum arabic and polysaccharides have been impregnated with nanomaterials such as zero valent metal (ZVM), magnetic nanoparticles and magnetic synthetic polymers<sup>22, 23</sup>. The adsorbents synthesized in this manner are found to have more porosity, selectivity, reactivity, possess large surface area and enhanced adsorption capability towards removal of heavy metals and dyes. Therefore the use of magnetic nano materials impregnated onto traditional bio-adsorbents has been explored as the thrust area for the wastewater treatment.

Cellulose which is made up of  $\beta$ -1, 4 glycosidic linkages, is a highly abundant natural polymer and a primary component of plant biomass is shown in figure 1.1.

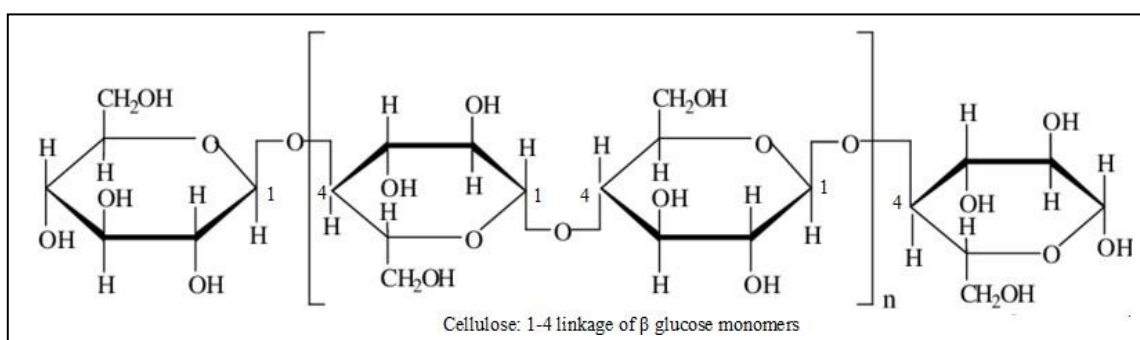


**Figure 1.1–Structure of cellulose**

Cellulose along with its derivatives has practical applications and is inexpensive, non-toxic, renewable, biocompatible, and environmentally friendly. The common derivative of cellulose, CMC (Carboxymethyl cellulose)- is a polymer which is soluble in water and anionic in nature that contains the functional groups- hydroxyl (-OH) and carboxylic (-COOH), where divalent ions get adhered<sup>24</sup>. CMC is extensively used cellulose which has



widespread applications in the field of industries dealing with food, medicines, textile, paint, adhesives and paper<sup>25</sup>.

Therefore, the present study aims to synthesize transition metal ferrites-carboxymethyl cellulose composites modified with biopolymers used as adsorbents and further used them for the removal of CV and MB dyes and metal ions in single and multiple adsorbate systems. To provide an environmentally sustainable, economically viable and selective kind of adsorbent for the treatment of wastewater, metal ferrite-CMC biopolymer composites could be an effective alternative.



## **CHAPTER 2**

### **REVIEW OF LITERATURE**

The current work focuses on surface-modified magnetic metal ferrites by biopolymers and their application as an adsorbent to remove both metal ions and dyes from wastewater. In this chapter, comprehensive literature reviews on different sources of cellulose used for the synthesis of carboxymethyl cellulose, use of nano materials in the form of metal ferrites and their composites for adsorption has been included.

## **2.0 Synthesis of Carboxymethyl cellulose (CMC) from Cellulose**

The primary and most significant natural polymer on earth is cellulose, which can be found in all kind of plants. It is the component of cell wall and plant biomass (30%), wood (over 50%) that can be explored as underdone material for synthesis of various cellulose derivatives. Due to biodegradable nature, low cost and abundant availability of cellulose sources, their use has been increased in material science and innovation. The cellulose fibres are being used in textile, paper, packaging, pharmaceutical industries and many more <sup>26-28</sup>. To meet the increasing demand of cellulose and to reduce dependency on wood sources, non-wood materials are explored as alternative sources of it.

The long and straight polymer- cellulose, is composed of glucose units bonded by  $\beta$ -1, 4 glycosidic linkages formed by condensation process. In plants, it is found along with other substances like lignin and hemicelluloses having composition of 40-55% cellulose, 25-40% hemicelluloses and 15-35% lignin. The common derivative of cellulose, CMC (carboxymethyl cellulose)- is a polymer which is soluble in water and anionic in nature that contains the functional groups- hydroxyl (-OH) and carboxylic (-COOH), where divalent ions get adhered <sup>24, 26</sup>.

Various sources of cellulose have been explored such as wood residue, cotton linters, sago waste, waste paper sludge, cotton stalk, corncob, water hyacinth, cotton gin waste, office waste paper, corn husk, oil palm fronds, corn stalk, sugarcane bagasse and almond shells, almond stem and fig stem for the synthesis of carboxymethyl cellulose <sup>25-32</sup>. Extraction of cellulose from these agricultural wastes involved sophisticated and expensive instruments such as microwave, autoclave reactor, high pressure cooking pot and high temperature and pressure conditions <sup>25, 30</sup>.

The various characteristics of synthesized CMC along with the source of cellulose from which, it has been prepared are listed in table 2.1.

**Table 2.1- Properties of CMC synthesized from various cellulosic source**

<b>Source of cellulose</b>	<b>DS of CMC</b>	<b>Yield (%)</b>	<b>Purity (%)</b>	<b>Reference</b>
Corncob	1.18	-	-	26
Cotton Gin waste	0.874	143.7	-	29
Water Hyacinth	1.76	179.04	93.24	27
Office waste paper	1.07	150.8	-	33
Corn Husk	2.41	240	99.99	28
Oil Palm Fronds	1.1	170.1	97.3	34
Corncob	1.02	-	-	25
Cornstalk	0.85	-	-	30
Sugarcane Bagasse	0.78	180	-	31
Baobab Fruit Shell	0.94	164	86.2	35
Almond Shell, Almond Stem, Fig Stem	0.43-2.83	-	-	32
Asparagus Stalk End	0.98	44.04	-	36
Wheat Straw	1.23	141.4	-	37
Rice Stubble Waste	0.64	90.18	-	38
Oil Palm Fruit Bunch	0.16	248	124	39
Hard Wood Pulp	2.4	162	-	40
Palm Fiber Waste	1.05	79.6	-	41
Coconut Fibres	1.82	9.45g	-	42
Pineapple Leaf Fibres	0.45	-	-	43

## 2.1 Use of Nano Material as Adsorbents

Nano science is becoming one of the most appealing fields for worldwide research and development over the past few decades. Because of their unusual size, shape and physical-chemical characteristics, nano materials such as nano wires, rods, tubes and nano particles have gained a great deal of interest. Applications for these nano materials are numerous in various scientific areas including material science, food science, environmental science, biomedical, bioengineering and technology and space science <sup>44</sup>. The use of nano materials with high adsorptive capabilities in wastewater treatment has produced amazing results. Due to their certain physical and chemical properties, the application of nano materials in water treatment is receiving a lot of attention <sup>45, 46</sup>. These nano materials have certain properties which make them suitable in adsorption field. These are:

1. Ability to remove heavy metals and dyes at minimal concentrations because of its great adsorption capacity and selectivity.
2. Due to their reduced size and greater surface area.
3. The tendency to decrease a pollutant's toxicity by lowering its oxidation state.
4. Due to their high surface reactivity and surface can be modified by changing functional group or active site.
5. It is simple to remove the adsorbed species from the surface of adsorbents i.e. desorption is easy.
6. They show high regeneration efficiency.

A review of the literature reveals that nano ferrites along with their composites exhibit high adsorption potential for various dyes and heavy metals from effluents. Certain metal oxides of Fe, Al and Ti like  $\text{Fe}_2\text{O}_3$ ,  $\text{Fe}_3\text{O}_4$ ,  $\text{Al}_2\text{O}_3$  and  $\text{TiO}_2$  in single or combined form are considered as first line of material as adsorbents <sup>47</sup>. The use of metal oxides as adsorbent in singular or composite form first generation materials and grafting or coating of these nano particles by surfactants or polymers to form magnetic nanocomposites form next generation materials, found application in sequestration of heavy metals and toxic effluents from wastewater. Different types of spinel ferrites are synthesized having general formula  $\text{MFe}_2\text{O}_4$  -where M is metal cation (Mn, Co, Ni, Zn) which is chemically and thermally stable magnetic materials <sup>48, 49</sup>. The size and structure of the lattice determined the characteristics of nano ferrites which in term depend upon method of synthesis.

From the literature review, it has been observed that the synthesis of ferrites can be categorized into two main types: (a) Solid-state methods (b) Wet Chemical methods

(a) **Solid–State methods:** These methods are simple and conventional type of methods which involve the metal oxides reactions at high temperature. Examples- Ceramic method and Mechanical or Ball milling method <sup>50, 51</sup>.

(b) **Wet Chemical methods:** Being the versatile method, certain characteristics like particle size, morphology and stoichiometry can be precisely controlled in these methods. Examples- Sol-gel method, Co-precipitation method, Hydrothermal method, Microwave- assisted synthesis and Spray pyrolysis <sup>52, 53</sup>.

The different methods of synthesis of ferrites and their characteristics along with advantages and disadvantages of these methods have been described in table 2.2.

### **2.1.1 Metal Ferrites as Adsorbent**

Different types of metal ferrites have been used as adsorbents for the removal of heavy metals and different dyes. Considering their high surface area, magnetic characteristics, and capacity to bind with pollutants, metal ferrites are frequently employed in adsorption for the treatment of wastewater, environmental clean-up, and pollutant removal. The application of different metal ferrites for the removal of heavy metals and dyes are shown in table 2.3.

**Table 2.2- Different methods, characteristics, advantages and disadvantages of different methods of synthesis of ferrites**

<b>Synthesis Method</b>	<b>Reaction Temperature</b>	<b>Key Characteristics</b>	<b>Example Ferrite</b>	<b>Reference</b>	<b>Advantages</b>	<b>Disadvantages</b>
Solid-State Reaction	800–1200°C	Mixing of solid oxides, high-temperature sintering	NiFe <sub>2</sub> O <sub>4</sub> Mn <sub>1-x</sub> Zn <sub>x</sub> Fe <sub>2</sub> O <sub>4</sub>	54 55	Simple, cost- effective, large-scale production	High energy use, large grain size, long processing
Co-precipitation	Room temp to 200°C	Precipitation of metal salts in solution	MnFe <sub>2</sub> O <sub>4</sub> FeFe <sub>2</sub> O <sub>4</sub> FeFe <sub>2</sub> O <sub>4</sub> FeFe <sub>2</sub> O <sub>4</sub> NiFe <sub>2</sub> O <sub>4</sub> FeFe <sub>2</sub> O <sub>4</sub> FeFe <sub>2</sub> O <sub>4</sub> FeFe <sub>2</sub> O <sub>4</sub>	56 23 57 58 59 53 60 61	Fine particles, high purity, low temperature	Requires pH control, lengthy filtration
Sol-Gel Method	300–600°C	Formation of gel from metal alkoxides, drying and calcination	CoFe <sub>2</sub> O <sub>4</sub> ZnFe <sub>2</sub> O <sub>4</sub> BiFeO <sub>3</sub>	62 63 64	Controlled size, low temperature, complex compositions	Expensive precursors, sensitive to impurities

Hydrothermal Synthesis	100–300°C	High-pressure reaction in an autoclave	MnFe <sub>2</sub> O <sub>4</sub>	<sup>65</sup>	High crystallinity, less defects, controlled morphology	Specialized equipment, limited scalability
Microwave-Assisted	Room temp to 200°C	Microwave heating to accelerate reactions	Ni <sub>0.5</sub> Zn <sub>0.5</sub> Fe <sub>2</sub> O <sub>4</sub> (Ni-Zn Ferrite)  CoFe <sub>2</sub> O <sub>4</sub>	<sup>66</sup>  <sup>67</sup>	Fast synthesis, homogeneous particles, energy saving	Requires microwave equipment, limited scalability
Combustion Synthesis	300–700°C	Exothermic reaction using metal nitrates and fuel	NiFe <sub>2</sub> O <sub>4</sub>  ZnFe <sub>2</sub> O <sub>4</sub>  CoFe <sub>2</sub> O <sub>4</sub>  Ni <sub>1-x</sub> Zn <sub>x</sub> Fe <sub>2</sub> O <sub>4</sub>	<sup>68</sup>  7  <sup>69</sup>  70	Rapid synthesis, porous structures	Non-uniform particles, risk of impurities
Spray Pyrolysis	200–800 °C	Atomization of solution with rapid heating	BaFe <sub>12</sub> O <sub>19</sub>	<sup>71</sup>	Fine particles, continuous production	Specialized equipment, requires post-processing
Mechanical Milling	Room temp to 100 °C	High energy milling of powders	CoFe <sub>2</sub> O <sub>4</sub>	<sup>72</sup>	Cost-effective, low-temperature	Irregular particles, contamination risk



**Table 2.3- Use of various metal ferrites for the adsorption of various pollutants**

<b>Ferrites</b>	<b>Pollutant</b>	<b>% Removal</b>	<b>Adsorption Capacity (mg/g)</b>	<b>Reference</b>
CoFe <sub>2</sub> O <sub>4</sub>	Titan Yellow	-	212.8	73
	Congo Red		200.0	
Fe/BaFe <sub>12</sub> O <sub>19</sub>	Methylene Blue	-	189.3	74
MgFe <sub>2</sub> O <sub>4</sub>	Co (II)	99.2	67.41	75
CaFe <sub>2</sub> O <sub>4</sub>	Congo Red	95	18.19	69
	Crystal violet		10.67	
BiFeO <sub>3</sub>	Tetracycline	79	-	76
Fe <sub>3</sub> O <sub>4</sub> (Magnetite)	Cu (II)	-	4.02	77
CoFe <sub>2</sub> O <sub>4</sub>	Crystal Violet	98	105	78
Co <sub>0.5</sub> Ni <sub>0.5</sub> Fe <sub>2</sub> O <sub>4</sub>	Methylene Blue (MB)	-	162	79
MgFe <sub>2</sub> O <sub>4</sub>	Pb (II)	-	283.1	80
ZnFe <sub>2</sub> O <sub>4</sub>	Cr (VI)	-	82.7	81

### 2.1.2 Modification of Metal Ferrites' Surface

Despite being an excellent class of adsorbents, nano-ferrites show rapid degradation and limited stability in solution <sup>82</sup>. The application of compounds of organic and inorganic nature on the surface of metal ferrites is the most important of the several ways to stabilize them against oxidation, corrosion and agglomeration. Additionally, surface modification is a crucial step to enhance adsorption capability by increasing the selectivity as well as surface area of the adsorbent <sup>83</sup>. From the review of literature, it has been found that there are few methods for the surface modification of metal ferrites viz. metal oxide coating, surfactant coating and polymer coating.

### 2.1.3 Metal / Metal oxide coating

Applying a layer of certain transition metals like nickel, cobalt and rare earth metals like lanthanum, cerium, neodymium to ferrites is called doping and metal oxides such as

silica, titanium dioxide or aluminium oxide to ferrite nano particles is known as metal oxide coating. Certain properties like stability, compatibility can be enhanced by this method. Coating is performed by sol-gel method and hydrothermal method <sup>84, 85</sup>.

#### **2.1.4 Surfactant coating**

This method typically involves dispersing the nanoparticles in a solution containing the surfactant, which adsorbs onto the surface and prevents agglomeration. Surfactants like cetyl trimethylammonium bromide (CTAB), polyvinyl alcohol (PVA), SDS (Sodium dodecyl sulphate) and oleic acid are used to give stability to the ferrites <sup>78, 86, 87</sup>.

#### **2.1.5 Polymer coating**

The coating of the polymers is employed by the methods like in situ polymerisation, layer-by-layer deposition or covalent bonding. Certain polymers like polyethylene glycol (PEG), polylactic acid (PLA), chitosan, carboxymethyl cellulose and alginates which are biocompatible with ferrites are used for this purpose. Certain properties like stability and solubility are improved by these polymers. The polymers contain long chains of molecules having higher molecular mass which contain different functional groups that form a strong interaction with the ferrites, stabilize the ferrites and thus increase the adsorption capacity <sup>49, 53, 88</sup>.

Various low cost, efficient and environmentally friendly nano materials have been explored and developed each have potential application in purification of water/wastewater. Among these various nano-adsorbents, inorganic- (e.g. silica, clay, carbon nanotubes (CNT) - both single walled (SWCNT) and multi walled (MWCNT), graphene and organic- polymers, nano composites have been used for removal of heavy metals and dyes from water.

It has been observed that at saturation of adsorption, there is difficulty in desorption of small sized adsorbents. This problem has been solved by using magnetic nano adsorbents since it caused no contamination due to flocculants and large sample can be purified in less time. The magnetic composites (MC) have been functionalized to get magnetic nanocomposites (MNC). These magnetic nanocomposites due to its remarkable rapidity and effectiveness have been examined for their application in detection and separation of toxic dyes and heavy metal from water <sup>47</sup>.

**Table 2.4- Removal capacity of CNT's, Modified CNT and other magnetic nano composites towards metal ions and dyes**

Adsorbate	Adsorbent	%Removal /Adsorption Capacity(mg/g)	Best fit Adsorption Isotherm	Best fit Kinetic model	Reference
Cd (II)	MWCNTs	55%	Langmuir	-	89
Pb (II)	CNT	17.4	Freundlich	-	90
Reactive Yellow 15 Reactive Yellow 42	CNT	36.0 48.1	Langmuir and Freundlich	Pseudo 2 <sup>nd</sup> order	91
<b>Use of Modified CNT</b>					
Co (II)	PAA@ MWCNT	$1.49 \times 10^{-4}$ (mol/g)	Langmuir	Pseudo 2 <sup>nd</sup> order	92
Cu (II)	Magnetic-MWCNTs	97%	Langmuir	Pseudo 2 <sup>nd</sup> order	93
Pb (II)	PVA@ MWCNT	80%	Freundlich	Pseudo 2 <sup>nd</sup> order	94
Hg (II)	Sulphur containing MWCNTs	72.8	Freundlich	-	95
Pb (II)	MWCNTs/ MnO <sub>2</sub> nano composite	98.9%	Elovich	Pseudo 2 <sup>nd</sup> order	96

Acid Blue 45 Acid Black 1	Amine functionalized CNT	714.0 666.0	Langmuir	Pseudo 2 <sup>nd</sup> order	<sup>97</sup>
Cd (II)	Humic acid modified MWCNTs	18.4	-	-	<sup>98</sup>
F <sup>-</sup> ions	Hydroxypatite@ MWCNT	97.2	Langmuir and Freundlich	Pseudo 2 <sup>nd</sup> order	<sup>99</sup>
Methyl Orange	Starch-vitamin C@ magnetic MWCNT	11.1	Langmuir	Pseudo 2 <sup>nd</sup> order	<sup>100</sup>
Ni (II)	Deep Eutectic Solvent @MWCNT	115.8	-	Pseudo 2 <sup>nd</sup> order	<sup>101</sup>
Tetracycline	Fe <sub>3</sub> O <sub>4</sub> @MWCNT	84.1, 99.2%	-	Pseudo 2 <sup>nd</sup> order	<sup>102</sup>
Congo Red	Magnetic Fe <sub>3</sub> O <sub>4</sub> @ graphene	33.06	Langmuir	Pseudo 2 <sup>nd</sup> order	<sup>103</sup>
Basic Blue9	Magnetic ferrite nanoparticle alginate composite	106.0	Langmuir	Pseudo 2 <sup>nd</sup> order	<sup>104</sup>

Cd (II) MB Orange G	Magnetic Graphene Oxide	91.29 64.23 20.85	Langmuir	Pseudo 2 <sup>nd</sup> order	105
As (III) As (V)	Fe <sub>3</sub> O <sub>4</sub> @CuO-GO	70.7 62.6	Langmuir and Elovich	Pseudo 2 <sup>nd</sup> order	106
Ni (II)	Cellulose – alginate hydroxyapatite beads	41.95	Langmuir	Pseudo 2 <sup>nd</sup> order	21
Ni (II)	Alginate - magadiite Di- (2-ethylhexyl) phosphoric acid	44.0	Langmuir	Pseudo 2 <sup>nd</sup> order	107
MB MG MV	Alginate coatedperlite beads	104.1 74.6 149.2	Langmuir	Pseudo 2 <sup>nd</sup> order	108
Cr (VI) Pb (II)	Chitosan microspheres/ Alginate beads	16.0 180.0	Langmuir	Pseudo 2 <sup>nd</sup> order	109
MB	Fe <sub>3</sub> O <sub>4</sub> /Activated Charcoal/Cyclo Dextrin Alginate nanocomposite	2.07 10.63 99.53	Langmuir	Pseudo 2 <sup>nd</sup> order	110

MB	Activated carbon-CuF- Alginate beads	400.0	Langmuir	Pseudo 2 <sup>nd</sup> order	<sup>111</sup>
Cd (II) Pb (II)	Alginate-chitosan composite	0.81 0.41	Langmuir and Sip	Pseudo 2 <sup>nd</sup> order	<sup>112</sup>
MB	Sodium Alginate/ Lignin microbeads	254.3	Langmuir	Pseudo 2 <sup>nd</sup> order	<sup>113</sup>
CV	Alginate/ Clinoptilolite/ Fe <sub>3</sub> O <sub>4</sub>	16.52 (single) 15.79 (binary)	Langmuir	Pseudo 2 <sup>nd</sup> order	<sup>61</sup>
Pb (II) Fe (II) Zn (II)	Carboxymethyl- Chitosan	4.78 147.06 238.10	Langmuir	Pseudo 2 <sup>nd</sup> order	<sup>114</sup>
Methyl Violet 2B	CS-PVA/FGA/ MMT	105.7	Langmuir	Pseudo 2 <sup>nd</sup> order	<sup>115</sup>
CV BG MB	ZnF-Mango Starch	142.9 101.2 105.8	Langmuir	Pseudo 2 <sup>nd</sup> order	<sup>116</sup>

As the polymer chains contain a variety of reactive chemical groups, biopolymers have attracted a lot of attention for their usage as adsorbents due to their high reactivity, physical and chemical properties and chemical stability, which specifically targets heavy metal ions and dyes <sup>47</sup>. Since these are biodegradable and environmental friendly and hence are widely used. There are two types of biopolymers- naturally occurring biopolymers like proteins and carbohydrates (like starch, cellulose, chitosan, alginate) and synthetically produced polymers that can be degraded known as biodegradable like polyethylene glycol, polyglycolic acid and polyvinyl alcohol and microbial polyesters like polyhydroxyl butyrate, polyhydroxyl alkanoates <sup>53, 88</sup>.

Cellulose is the most abundant natural polymer and main component of plant biomass which is made up of  $\beta$ -1, 4 glycosidic linkages. Cellulose and its derivatives have practical applications due to biocompatible, biodegradable, renewable, low priced, non-toxic and environment friendly nature. The common derivative of cellulose, Carboxymethyl cellulose (CMC), which is a water soluble, anionic polysaccharide contains carboxyl and hydroxyl groups for interactions with positively charged ionic species <sup>24</sup>. CMC is widely used derivative having applications in food, biomedicine, dyeing, detergent, paper, textile, pharmaceutical and paint industries etc. <sup>25, 53, 65</sup>.

#### **2.1.6 Use of Carboxymethyl cellulose (CMC) in Adsorption field**

Literature studies reveal that carboxymethyl cellulose is widely used in food industry, pharmacy, biomedicine, textiles, printing, ceramics, dyeing etc. <sup>33, 117</sup>. Recently CMC has been utilized as adsorbent material increasingly in pollution control <sup>118</sup>.

The removal of Cr (VI) has been done using CMC stabilised zero-valent iron particles from water <sup>22</sup>. FTIR, SEM and TEM techniques were used for the characterization of CMC-ZVI adsorbent. The stabilization of Nzvi particles with CMC seem to prevent aggregation and show high reactivity. The pseudo first order kinetic model best fit the adsorption data having calculated value of constant  $K_1$  for Cr (VI) as  $0.019 \text{ min}^{-1}$ .

Magnetic carboxymethyl cellulose beads coated with polyaniline have been developed for the purpose of selectively removing uranium ions U (VI) from water <sup>57</sup>. The adsorbent was characterized by FTIR, SEM, DTA techniques. It was revealed from the results that magnetic CMC beads' surface was successfully grafted by aniline. At a pH of 4.5, the maximum adsorption capacity ( $Q_e$ ) of the mCMC and mCMC-g-PANI beads for U (VI) ions was found to be 129.4 and 386.5 mg/g, respectively. The kinetic and isotherm model that fitted well with the adsorption data was found to be pseudo second order and

Langmuir model respectively.

In another study, core-shell structured, CMC-modified  $\text{Fe}_3\text{O}_4$  ( $\text{Fe}_3\text{O}_4\text{@CMC}$ ) was synthesized and was tested for removal of Eu (III) from aqueous system. The results of characterization by FTIR, zeta-potential and TGA showed that CMC gets successfully coated on  $\text{Fe}_3\text{O}_4$  surface. The adsorption capacity has been found to be  $2.78 \times 10^{-4}$  mol/g at 293 K and adsorption data was found to be better fitted by Lagergren pseudo second order kinetic model and Langmuir model of isotherm<sup>23</sup>.

A peculiar hydrogel of magnetic polysaccharides was created by combining sodium alginate with CMC (carboxymethyl cellulose) filled with magnetic nanoparticle. The composite was used for the removal of Mn (II), Pb (II) and Cu (II). From the Langmuir model, the maximal adsorption capacity was determined to be 71.83, 89.49, and 105.93 mg/g for Mn (II), Pb (II) and Cu (II) respectively. The pseudo second order kinetics best fitted the data<sup>53</sup>.

Similar work was also done by synthesizing calcium alginate-carboxymethyl cellulose@ $\text{MnFe}_2\text{O}_4$  composite (CA-CMC@  $\text{MnFe}_2\text{O}_4$ ) and explored for its capacity to remove copper ions. The pseudo second order kinetic model and Langmuir isotherm was found to be best fitted with the adsorption data. The maximum  $Q_e$  (adsorption capacity) of 77.22 mg/g was observed at pH of 5 and 298 K. The research revealed that mechanism through which the removal of copper ions occurred was ion-exchange and complex formation<sup>65</sup>.

In another study, the nanosorbent (CMC-PA-PAA) was fabricated by coating  $\text{Fe}_3\text{O}_4$  with carboxymethyl cellulose with poly (acrylic acid-co-acrylamide) and tested for the adsorption of MB dye from aqueous solution. The adsorption performance was investigated as the effects of solution pH, adsorbent dose, initial dye concentration and contact time. The experimental data of MB adsorption were fit to Langmuir isotherm model and pseudo-second-order kinetic model with maximum adsorption of 34.3 mg/g.<sup>60</sup>

A copolymer was prepared from carboxymethyl cellulose (CMC) modified with acrylamide (AM) and N-vinylpyrrolidone (NVP). The potentiality of the synthesized adsorbent was explored for removing MB (methylene blue) dye. For MB dye, the adsorption kinetic model as well as isotherm model that fitted well for CMC-AM-NVP composite was pseudo-second order and Langmuir isotherm model. The maximum removal percentage was found to be 99.4%<sup>119</sup>.

In another study, a novel eco-friendly hydrogel beads based on carboxymethyl cellulose



(CMC), alginate (Alg) and graphene oxide (GO) were synthesized and evaluated for removal of MB dye. The prepared hydrogel beads were characterized by Fourier transform infrared spectroscopy (FTIR), scanning electron microscopy (SEM), thermogravimetric analysis (TGA), differential thermal analysis (DTA) and point of zero charge (pHpzc). The maximum removal percentage of 96.2% was observed at pH of 9.5. The adsorption experimental data was well described by the Freundlich model.<sup>120</sup>

A novel adsorbent (CMC-PBQ-IDA) was synthesized by surface functionalization of p-benzoquinonecarboxymethyl cellulose (CMC-PBQ) activated microbeads with iminodiacetic acid (IDA) in another study. The prepared microbeads were characterized by FTIR, TGA, SEM, XPS and zeta potential analysis techniques. These beads were tested for the removal of CV dye from aqueous solution under various adsorption conditions. The removal percentage was found to be 91.6% with 0.15 M IDA concentration. The experimental data were well-fitted with both Langmuir and Freundlich isotherms with a maximum adsorption capacity of 107.52 mg/g<sup>121</sup>.

Similar work was done by fabricating PVA/CMC/Turmeric film from turmeric, polyvinyl alcohol and carboxymethyl cellulose for MB dye removal. The adsorbent was characterized by FTIR, TGA, XRD and SEM analysis. Maximum dye adsorption (83%) was achieved at initial dye concentration of 10 mg/L with contact time 170 min at room temperature. The adsorption isotherm studies showed that both Langmuir and Freundlich isotherm was suitable for the MB adsorption. The maximum adsorption capacity was found to be 6.27 and the kinetic followed pseudo-second order model<sup>122</sup>.

Table 2.5 shows the adsorption capability of carboxymethyl cellulose and its various composites for different metal ions, anions and dyes that have been studied.

**Table 2.5- Adsorption capability of CMC composites for the removal of metal ions and dyes**

Adsorbent used	Adsorbate used	% Removal/ Q <sub>e</sub> (mg/g)	Kinetic model followed	Isotherm Model followed	Reference
<b>CMC composites for metal ions</b>					
SA/CMC	Cr (II)	16.67	-	Langmuir	<sup>123</sup>
Semi IPN CMC/Poly (Acrylamide) MNHs	Cu (II)	0.74	-	Langmuir	<sup>124</sup>
	Ni (II)	0.88			
Starch(S)/ CMC (C) stabilized Nzvi particles	As (III)	12.2	Pseudo 2 <sup>nd</sup> order	Langmuir	<sup>125</sup>
	As (V)	14.0			
CMC-stabilized Nzvi particles	Cr (VI)	87.65	Pseudo 2 <sup>nd</sup> order	Langmuir	<sup>22</sup>
	Cu (II)	94.65			
mCMC-g-PANI(Polyaniline)	U (VI)	386.5	Pseudo 2 <sup>nd</sup> order	Langmuir	<sup>57</sup>
Fe <sub>2</sub> O <sub>3</sub> @CMC	Eu (III)	2.78×10 <sup>-4</sup> (mol/g)	Pseudo 2 <sup>nd</sup> order	Langmuir	<sup>23</sup>
CMC-g-CMPVA	Cu (II)	35.34	Pseudo 2 <sup>nd</sup> order	Langmuir	<sup>58</sup>
Thiosemicarbazide-CMC (T-CMC)	Cu (II)	144.92	Pseudo 2 <sup>nd</sup> order	Langmuir	<sup>126</sup>

CMC-g-PAA	Cu (II)	154.0	Pseudo 2 <sup>nd</sup> order	Langmuir	127
CMC-EDTA- Chitosan	Cu (II)	142.95	Pseudo 2 <sup>nd</sup> order	Langmuir	128
MnF-CMC MnF-SCM	Pb (II)	34.0 46.0	Pseudo 2 <sup>nd</sup> order	Langmuir	56
SA/CMC/ Fe <sub>3</sub> O <sub>4</sub> nano particles	Mn (II) Pb (II) Cu (II)	71.83 89.49 105.93	Pseudo 2 <sup>nd</sup> order	Langmuir	53
CA/CMC-MnFe <sub>2</sub> O <sub>4</sub>	Cu (II)	77.22	Pseudo 2 <sup>nd</sup> order	Langmuir	65
Sodium Alginate/CMC/ Zinc ferrite Nanoparticles	Cu (II) Cr (VI)	63.29 10.15	Pseudo 2 <sup>nd</sup> order	Langmuir	129
CMC-Montmorillonite (CMC-MMT)	As (III)	85.0	Pseudo 2 <sup>nd</sup> order	Langmuir	130
Polyaniline/TiO <sub>2</sub> /CMC powder	Ni (II)	97.88	-	-	131

CMC composites for dyes					
CMC-Acrylic Acid	Methyl Orange	84.2	Pseudo 2 <sup>nd</sup> order	Temkin	132
	Disperse Blue (2BLN)	79.6			
	Malachite Green	99.9			
MCA-E <sub>0.7</sub> /CMC-g-PDMAAC	MB OR (Orange) II	210.0 149.0	Pseudo 2 <sup>nd</sup> order	Langmuir	133
CMC/k-carrageenan/ Montmorillonite composite beads	MB	12.25	Pseudo 2 <sup>nd</sup> order	Langmuir	134
CMC-Alginate-Graphene Oxide	MB	96.22	Pseudo 2 <sup>nd</sup> order	Freundlich	120
CMC-PBQ-IDA	CV	91.56 107.52	Pseudo 2 <sup>nd</sup> order	Langmuir	121
CMC –PA-PAA nanocomposite	MB	34.3	Pseudo 2 <sup>nd</sup> order	Langmuir	60

CMC/ PVA/Turmeric film	MB	6.27	Pseudo 2 <sup>nd</sup> order	Langmuir Freundlich	<sup>122</sup>
CMC/Gelatin Hydrogel	MB	943.40	Pseudo 2 <sup>nd</sup> order	Langmuir	<sup>135</sup>
CMC/Acrylamide/NVinylpyrrolidine (CMC-AM-NVP) copolymer	MB	81.96	Pseudo 2 <sup>nd</sup> order	Langmuir	<sup>119</sup>
CMC/GO/ZnO	Fuchsin Dye	172.41	Pseudo 2 <sup>nd</sup> order	Langmuir Temkin	<sup>136</sup>
CMC-SA- $\beta$ -CD/NCO CMC-Succinicacid- $\beta$ - Cyclodextrin/ Nickel cobaltite	Malachite Green (MG)	182	Pseudo 2 <sup>nd</sup> order	Langmuir	<sup>137</sup>

## 2.2 Regeneration of Adsorbent

In wastewater treatment, an adsorbent's potential is determined by both its adsorption capacity and its power of regeneration and reusability. In addition to economic aspect, it also restricts the utilization of fresh adsorbent. The literature studies reveals that various types of desorption agents have been used for regeneration of different composites of CMC which are shown in table 2.6 <sup>47</sup>.

**Table 2.6- Various desorption agents used in regeneration of adsorbate containing CMC**

Adsorbent	Adsorbate	Desorption agent	Conc. (mol L <sup>-1</sup> )	% Regeneration Efficiency	Reference
Semi IPN CMC/ Poly (Acrylamide) MNHs	Cu (II)	HCl	0.1	80	124
	Ni (II)	EDTA	0.1	90	
mCMC-g-PANI	U(VI)	HCl	0.1	97	57
Fe <sub>2</sub> O <sub>3</sub> @CMC	Eu (III)	EDTA-2Na	5.0×10 <sup>-3</sup>	100	23
MCA-E <sub>0.7</sub> /CMC- g-PDMDAAC	MB	HCl	0.1	210	127
	OR (Orange) II	NaOH	0.1	149	
CMC-g-CMPVA	Cu (II)	HCl	0.1	86	58
Thiosemicarbazide -CMC (T-CMC)	Cu (II)	HCl	0.1	>90	126
CMC-Alg/GO	MB	HCl	0.5	76.07	120
MnF-CMC MnF-SCM	Pb (II)	EDTA-2Na	5.0×10 <sup>-3</sup>	90	56

Chitosan-EDTA- CMC	Cu (II)	EDTA	0.1	>90	128
CMC-PBA-IDA	CV	HCl	0.5	65	121
CA/CMC@ MnFe <sub>2</sub> O <sub>4</sub>	Cu (II)	HNO <sub>3</sub>	0.1	99	65
SA/CMC@Fe <sub>3</sub> O <sub>4</sub>	Mn (II)	NaOH	0.1	58.6	53
	Pb (II)			65.3	
	Cu (II)			61.7	
CMC/Gelatin Hydrogel	MB	HCl	1.0	85	135
Carboxymethyl- Chitosan	Pb	HCl	0.1	53.73	114
	Fe			61.82	
	Zn			64.51	
CMC-SA-β- CD/NCO (CMC-Succinic acid-β- Cyclodextrin/ Nickel cobaltite)	Malachite Green (MG)	Acetone	-	> 70	137

Today, there is a growing global need for clean water on a regular basis. Studies have demonstrated that the adsorption process has a great deal of potential for efficiently treating wastewater. Adsorption is a promising technique due to inexpensive, easy to use and less area requirement than others techniques, it is frequently employed for water purification. To clean up contaminated water, a variety of adsorbents have been applied which are of natural and synthetic nature. Using nanomaterials, particularly metal ferrites, to treat wastewater is a rapidly developing and promising field of adsorbent technology. The survey of the literature indicates that for the synthesis of metal ferrites, the combustion method at low temperature is simplest, least time-consuming and most affordable ways among other methods. Apart from this, Stoichiometrically, pure and single-phase ferrites are obtained by this method. Ferrites particles obtained by this method are of small size and have greater surface area.

The biopolymers have been used to modify the surface of these metal ferrites to develop metal ferrite-biopolymer composites which have high adsorption capabilities.

These adsorbents need to be tested for their potential to remove heavy metals and dyes from wastewater.

### **2.3 Research Gap**

Research indicates that there are lesser reports on the adsorption behaviour of nano ferrites modified with CMC and alginate and thus it is largely unexplored topic. The literature review also makes evident that the natural biopolymers carboxymethyl cellulose and sodium alginate have effective adsorption capabilities for the removal of variety of pollutants from effluent. Utilising biopolymers like alginate and carboxymethyl cellulose to alter the surface of spinel metal ferrite in order to develop selective adsorbents has drawn relatively little attention, this research gap need to be filled up. Consequently, additional research in this field is required. In most of the previous work, it has been observed that the carboxymethyl cellulose (CMC) used was purchased from the market as analytical grade sample. However, an attempt was made to synthesize CMC from the cellulose extracted from the corncob which is an agricultural waste in the present work. From the literature review, it has been observed that in most of the studies, only the synthesis and characterization of the carboxymethyl cellulose have been reported but the application of the synthesized carboxymethyl cellulose for the removal of various pollutants has been less reported. Agricultural waste can be managed and turned into resources at a minimal cost by using such strategy. After adsorption, regeneration of the adsorbent is one of the cost-effective measures for which a few studies have been reported.

The current research work aims to synthesize different transition metal ferrites and modify their surface by CMC and alginate biosorbents which have high surface area and selectivity and explore their potentiality for removing dyes and nickel metal from water. The study on the reusability capacity of these adsorbents is also done. The application of biopolymer-coated metal ferrites in adsorption is a trending field of study that is both economical and environmentally benign.

### **2.4 Objectives of the Research**

1. To synthesize carboxymethyl cellulose (CMC) from cellulose obtained from corncob.
2. To develop selected transition metal spinel ferrite-CMC and selected polymer modified spinel ferrite- CMC adsorbents and their characterization.



3. To test the adsorption potential of synthesized adsorbents for the removal of heavy metals or dyes on various parameters such as pH, temperature, initial metal-ion concentration, adsorbent dose and contact time.
4. To study the adsorption behaviour in single and multiple adsorbate systems for metal ions or dyes.
5. To study regeneration of these polymer modified ferrite-CMC adsorbent and to reuse the adsorbent.



## **CHAPTER 3**

### **MATERIALS AND METHODS**

### 3.0 Materials

Every chemical utilized in this investigation was of analytical quality and was used just as supplied, requiring no additional purification. Nickel Chloride, Zinc Nitrate, Ferric Chloride, Hydrazine Hydrate, Diethyl Oxalate, Sodium Alginate, Sodium Hydroxide, Mono Chloroacetic Acid (MCA), Methanol, Glacial Acetic Acid, Sodium Chlorite ( $\text{NaClO}_2$ ), Acetone, Silver Nitrate ( $\text{AgNO}_3$ ), Hydrochloric acid, Nitric acid, Nickel sulphate, Sodium Citrate, Potassium Iodide, Dimethyl Glyoxime, Ammonia,  $\text{CaCl}_2$ , Sodium Fluoride, Crystal Violet and Methylene Blue dye were purchased from Loba Chemie Ltd. India. Corncobs were collected from local fields in Pathankot district of Punjab.

### 3.1 Experimental Method

#### 3.1.1 Synthesis of Nano Metal Ferrites

Low temperature combustion method was used to synthesize different types of spinel nano metal ferrites such as  $\text{NiFe}_2\text{O}_4$ ,  $\text{ZnFe}_2\text{O}_4$  and  $\text{CoFe}_2\text{O}_4$ <sup>49, 138</sup>. The general formula of metal spinel ferrite is  $\text{MFe}_2\text{O}_4$  (Where M = Ni, Zn and Co). As shown in the metal ferrite stoichiometric equation, the ratio of each component in the intended result should be 1:2:4. Using this stoichiometric ratio, the saturated hydrous solutions of required metal salt and iron salt were mixed with double distilled water in two separate beakers. Oxalyldihydrazide (ODH) served as the source of oxygen component in the required product. The ODH was synthesized by mixing 1 mole of diethyl oxalate and 2 moles of hydrazine hydrate in w/w 1:2 with constant stirring at ambient conditions. The resulting white coloured solid powder was dried at room temperature. After concentrating the resultant solution for an hour at 70°C on a water bath, the concentrate was annealed for three hours at 600°C in a muffle furnace. The coloured product formed at last was labelled as desired metal ferrite<sup>49, 139</sup>.

#### 3.1.2 Extraction of Cellulose from Corncob

Corncobs were locally collected, washed with water to remove dirt and sun dried to make them free from moisture. The dried cobs were cut into small pieces (1 cm) and milled with a grinder to obtain powder. The powdered corncob was sieved (0.5 mm sieve) and stored in air tight container. A suitable amount of corncob powder was treated with 2% (w/w) of sodium hydroxide at 100°C for 4 h under mechanical stirring in 500 mL flat bottomed flask. The product was filtered, washed with distilled water for several time till product was alkali free. The resulting fibres were

subsequently dried for 24 hours at 40°C in an air-circulating oven<sup>28, 33, 35</sup>.

### 3.1.3 Bleaching

The fibres were bleached with a solution made up of equivolumes of acetate buffer, pH = 4.71 (by dissolving 27 g NaOH in 75 mL glacial acetic acid and diluted to 1 L) and 1.7 wt % of aqueous sodium chlorite (NaClO<sub>2</sub>) for 6 h at 80°C. The product obtained was then washed with distilled water for several times until neutral (pH=7) and dried at 40°C in air circulating oven for 24 h<sup>28, 33, 35</sup>.

### 3.1.4 Synthesis of Carboxymethyl cellulose from Cellulose

The cellulose extracted from corncob was used for the preparation of carboxymethyl-cellulose. It involved two steps viz. alkalization and etherification:

In alkalization process, a suitable amount (5 g) cellulose fibers were treated with 30% (w/v) NaOH solution in 150 mL ethanol as solvent (cellulose to liquor ratio = 1:2.7) and stirred at 30°C for one hour. In etherification, monochloroacetic acid (120% w/v) was added drop wise with constant stirring into the reaction mixture for 30 minutes (cellulose to liquor ratio = 1:1.2) and this step was continued at 55°C for three and half hours (figure 3.1). The product was filtered, washed with methanol (200 mL) and glacial acetic acid was used to neutralize it. After that, the sample was cleaned four times with 70% ethanol and then once more with 100% alcohol to eliminate any leftover residue like sodium glycolate and sodium chloride. In an oven, the residue was dried at 60°C<sup>30, 33, 41</sup>.

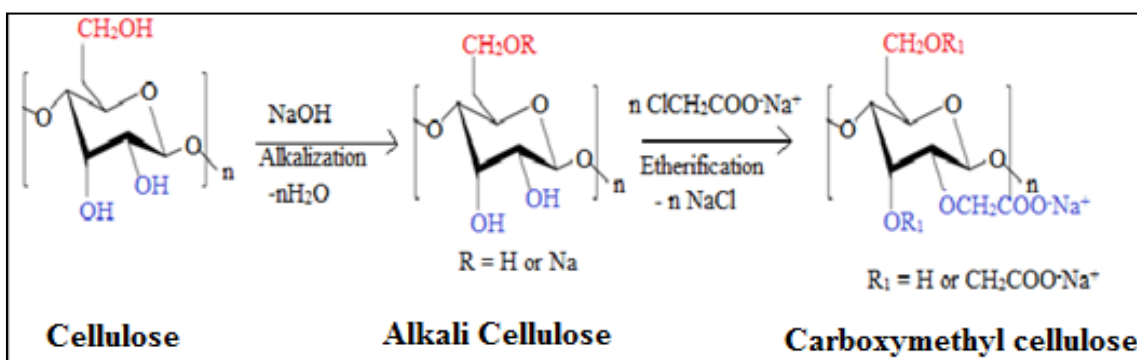
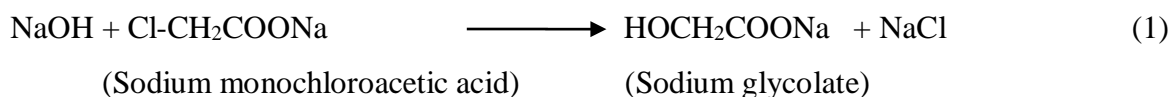


**Figure 3.1- Synthesis of carboxymethyl cellulose from cellulose**



### 3.1.5 Isolation of Lignin

From the alkali extraction, the black coloured liquor was acidified with concentrated sulphuric acid (H<sub>2</sub>SO<sub>4</sub>) to pH 1.5 by drop wise addition of it. Then the mixture was

heated in water bath at 100°C with constant stirring for one hour. The mixture was allowed to cool to room temperature before the lignin was filtered through a Buchner funnel and rinsed with hot water until it reached a neutral pH. Under normal conditions, the product was allowed to air dry. By maintaining a pH of 1.5, the separated lignin was again dissolved in NaOH (17.5% w/v) and precipitated by using concentrated sulphuric acid (H<sub>2</sub>SO<sub>4</sub>) following above mentioned method. After filtering the precipitated lignin in a Buckner funnel, the filtrate was cleaned with hot water. The product was dried in air under ambient laboratory conditions <sup>140</sup>. The flow chart for the synthesis of CMC from corncob has been shown in figure 3.2.

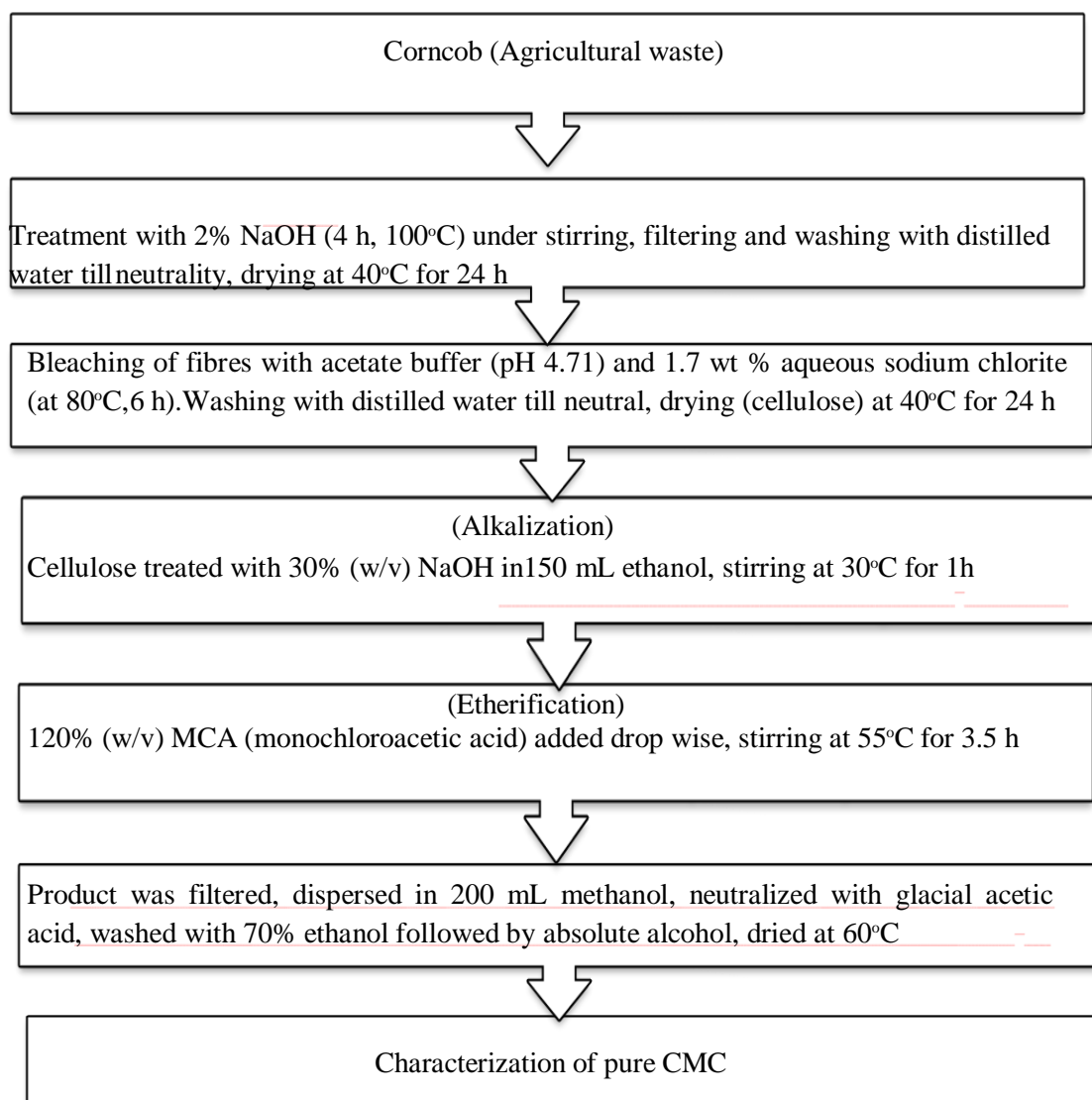


**Figure 3.2- Flow chart showing the synthesis of CMC from corncob**

The surface modification is discussed in the following sections:

### **3.1.6 Surface Modification with Carboxymethyl cellulose**

To prepare metal ferrite-CMC composite, the cross-linking technique was used. By dissolving 2 g of CMC in 50 mL of double distilled water, a homogenous solution of CMC was prepared. 2 g of metal ferrite was immersed in 10 mL distilled water to form the ferro fluid solution. This ferro fluid solution was then mixed into the above 2% CMC solution and for two hours, the solution was stirred. Using a syringe needle having 1 mm needle size, the resulting hydrogel was then mixed with 0.5 M  $\text{CaCl}_2$  (5.5 g in 100 mL distilled water).  $\text{CaCl}_2$  served as an agent for cross-linking. The composite was kept undisturbed for 24 hours in  $\text{CaCl}_2$  solution. After that, the composite was repeatedly cleaned with double-distilled water and dried at 50°C in a hot air oven<sup>53, 65</sup>. Using the same process, the composites of nickel ferrite-carboxymethyl cellulose (NiFCMC) and zinc ferrite-carboxymethyl cellulose (ZnFCMC) were prepared.

### **3.1.7 Preparation of Metal Ferrite-Carboxymethyl cellulose-Alginate Composite**

The surface modification of metal ferrite-CMC composite was done by using the sodium alginate polymer (Na-Alg). This method involved mixing of CMC (2% solution in double distilled water) and spinel metal ferrite ferro fluid solution (2 g of metal ferrite in 10 mL double distilled water) in the stoichiometric ratio of 1:1 by continuously stirring for 15 minutes. A 4% solution of sodium alginate was made in double-distilled water by heating it at 50°C for an hour while stirring constantly with a magnetic stirrer. This solution of sodium alginate was then mixed with above mixture and after stirring for 2 hours introduced into 0.5 M  $\text{CaCl}_2$  (5.5 g in 100 mL distilled water) solution with a syringe needle having 1 mm needle size. For 24 hours, the solution was kept undisturbed and the resulting mixture was filtered, cleaned several times with double distilled water and dried at 50°C in hot air oven<sup>53, 65</sup>. Using the same process, the composites of nickel ferrite-carboxymethyl cellulose-alginate (NiFCMC-Alg) and zinc ferrite-carboxymethyl cellulose-alginate (ZnFCMC-Alg) were prepared.

## **3.2 Preliminary Adsorption Studies**

The adsorption potential of the different prepared spinel metal ferrites, CMC-spinel ferrites composites and polymer modified CMC-spinel ferrites composites for the different types of dyes such as cationic dyes (Methylene blue, Crystal violet), anionic dyes (Congo red) and neutral dye (Eosin B) has been done as pilot study. Batch mode of adsorption process was followed for remediation purpose. In 250 mL conical flasks, 0.1

g of the adsorbents was added with known concentration (50mg/L MB, CV, CR and 20 mg/L Eosin Blue dye solution) and kept for 3 hours in thermostatic shaker at 150 rpm. After stipulated time, the samples were taken out, magnetically separated and by using UV-visible spectrophotometer (Shimadzu 8400S), the reduced dye concentration of solution was calculated by analyzing the absorbance for MB, CV, CR and EB dye at 664, 590, 497 and 522 nm respectively <sup>49</sup>. Table 3.1, 3.2, 3.3 and 3.4 shows the findings of preliminary studies with various metal ferrites and their composites respectively.

**Table 3.1- Preliminary study of percentage removal of Methylene Blue (MB)**

**Cationic dye**

S. No.	Adsorbent	Blank OD at 664 nm (50 mg/L)	OD with adsorbent	Concentration (Ce)	% Removal
1	CoFe <sub>2</sub> O <sub>4</sub>	1.588	1.074	33.82	32.37
2	CoFe <sub>2</sub> O <sub>4</sub> -CMC	1.588	0.843	26.54	46.91
3	CoFe <sub>2</sub> O <sub>4</sub> CMC-Alg	1.588	0.642	20.21	59.57
4	CuFe <sub>2</sub> O <sub>4</sub>	1.588	1.070	33.69	32.62
5	CuFe <sub>2</sub> O <sub>4</sub> -CMC	1.588	0.925	29.13	41.75
6	CuFe <sub>2</sub> O <sub>4</sub> CMC-Alg	1.588	0.707	22.26	55.48
7	NiFe <sub>2</sub> O <sub>4</sub>	1.588	0.990	31.71	37.66
8	NiFe <sub>2</sub> O <sub>4</sub> -CMC	1.588	0.669	21.06	57.87
9	NiFe <sub>2</sub> O <sub>4</sub> CMC-Alg	1.588	0.380	11.96	76.07
10	Zn Fe <sub>2</sub> O <sub>4</sub>	1.588	1.067	33.59	32.81
11	Zn Fe <sub>2</sub> O <sub>4</sub> -CMC	1.588	0.563	17.73	64.55
12	Zn Fe <sub>2</sub> O <sub>4</sub> CMC-Alg	1.588	0.302	11.39	77.20

**Table 3.2- Preliminary study of percentage removal of Crystal violet (CV)  
(Cationic) dye**

S. No.	Adsorbent	Blank OD at 590 nm (50 mg/L)	OD with adsorbent	Concentration (Ce)	% Removal
1	NiFe <sub>2</sub> O <sub>4</sub>	0.199	0.153	38.44	23.11
2	NiFe <sub>2</sub> O <sub>4</sub> -CMC	0.199	0.104	26.13	47.74
3	NiFe <sub>2</sub> O <sub>4</sub> CMC- Alg	0.199	0.062	15.58	68.8
4	Zn Fe <sub>2</sub> O <sub>4</sub>	0.199	0.166	41.71	16.58
5	ZnFe <sub>2</sub> O <sub>4</sub> -CMC	0.199	0.112	28.14	43.72
6	ZnFe <sub>2</sub> O <sub>4</sub> CMC-Alg	0.199	0.088	22.11	55.78

**Table 3.3- Preliminary study of percentage removal of Congo Red (CR)  
(Anionic) dye**

S.No.	Adsorbent	Blank OD at 497 nm (50 mg/L)	OD with adsorbent	Concentration (Ce)	% Removal
1.	NiFe <sub>2</sub> O <sub>4</sub>	0.917	0.502	54.72	45.28
2.	NiFe <sub>2</sub> O <sub>4</sub> -CMC	0.917	0.683	74.45	25.55
3.	NiFe <sub>2</sub> O <sub>4</sub> CMC- Alg	0.917	0.745	81.21	18.80
4.	Zn Fe <sub>2</sub> O <sub>4</sub>	0.917	-	-	-
5.	ZnFe <sub>2</sub> O <sub>4</sub> -CMC	0.917	0.592	64.53	35.47
6.	ZnFe <sub>2</sub> O <sub>4</sub> CMC-Alg	0.917	0.875	95.38	4.63



**Table 3.4- Preliminary study of percentage removal of Eosin Blue (EB)  
(Neutral) Dye**

S.No.	Sample	OD Blank	Absorbance at 522 nm (20 mg/L)	Concentration (Ce)	% Removal
1.	NiFe <sub>2</sub> O <sub>4</sub>	0.997	0.759	15.23	23.87
2.	NiFe <sub>2</sub> O <sub>4</sub> -CMC	0.997	0.786	15.77	21.16
3.	NiFe <sub>2</sub> O <sub>4</sub> CMC-Alg	0.997	0.828	16.61	16.95
4.	ZnFe <sub>2</sub> O <sub>4</sub>	0.997	0.738	16.81	15.95
5.	ZnFe <sub>2</sub> O <sub>4</sub> -CMC	0.997	1.517	30.33	-
6.	ZnFe <sub>2</sub> O <sub>4</sub> CMC-Alg	0.997	2.591	51.97	-

### 3.2.1 Preliminary adsorption studies with different dyes

The adsorption behaviour of different metal ferrite, metal ferrite-CMC and their composites with alginate were studied with different cationic, anionic and neutral dyes in aqueous solution. In order to study the adsorption capacity of the synthesized adsorbents, various types of dyes such as Methylene Blue (MB), Crystal Violet (CV), Congo Red (CR) and Eosin Blue were utilized. The adsorption behaviour of different dyes was investigated using the batch adsorption method <sup>49, 78</sup>. Using a Shimadzu, 1800 scanning Double beam UV-VIS spectrophotometer, the absorbance was measured to examine the decreased dye concentration. The maximum wavelength ( $\lambda_{max}$ ) for MB, CV, CR and EB used were 664 nm, 590 nm, 497 nm and 522 nm respectively.

It was observed that NiFCMC, NiFCMC-Alg and ZnFCMC and ZnFCMC-Alg composites showed the maximum percentage removal to remove MB and CV dyes when compared with their metal ferrites. The percentage removal of CR anionic dye with NiFCMC, NiFCMC-Alg and ZnFCMC and ZnFCMC-Alg composites decreased as compared NiF and ZnF. Because of the surface modification of metal ferrites with CMC

and alginate, the percentage removal decreased. As there are negatively charged functional groups  $\text{-COO}^-$  and  $\text{-OH}$  present in the structure of CMC and alginate so surface become negatively charge. These functional groups that are negatively charged operate as active locations where the various dyes can attach. On the surface of adsorbents, the positive charged dyes are attracted towards the functional groups which have negative charge and then adsorbed on it and their removal percentage increased. However, in the case of CR anionic dye, their removal percentage decreased because the adsorbent and anionic dye surfaces have identical charges. In case of neutral dye (Eosin Blue), the removal percentage decreased in NiFCMC and NiFCMC-Alg and no results were observed with ZnFCMC and ZnFCMC-Alg. It can be inferred that the synthesized adsorbents have high selectivity towards cationic dyes only. So, for studying the adsorption behaviour of cationic dyes MB and CV, the composites NiFCMC, NiFCMC-Alg, ZnFCMC and ZnFCMC-Alg were used in aqueous medium.

### 3.2.2 Preliminary adsorption studies with metal and fluoride ions

The synthesized composites were also utilized to examine the adsorption of cationic metal ions and anionic fluoride ( $\text{F}^-$ ) ions. Adsorption behaviour of cationic and anionic ion such as Ni (II) ions and fluoride ( $\text{F}^-$ ) ions with pure metal ferrites, metal ferrite-carboxymethyl cellulose composite and metal ferrite-carboxymethyl cellulose - alginate composite were examined. The reduced concentration of nickel ion samples was measured by producing more intense colour by using dimethylglyoxime and fluoride ions samples were measured with SPADNS (1,8-Dihydroxy-2-) 4- sulphophenylazo) naphthalene-3, 6-disulphonic acid trisodium salt) method by using Shimadzu 1800 scanning double beam UV-Visible spectrophotometer<sup>141, 142</sup>.

Various reagent solutions were produced for the spectrophotometric measurement of fluoride ions. 0.958 g of SPADNS reagent, which was dissolved in 500 mL of distilled water, was labelled as reagent A. 0.133 g of zirconyl chloride octahydrate was dissolved in 25 mL of distilled water to which 350 mL of concentrated hydrochloric acid was added. Subsequently, 500 mL of distilled water was further added and reagent B be labelled to the resultant solution. A standard solution known as reagent S was made by mixing an equal volume of reagents A and B. Mix 5 mL of reagent S in 50 mL distilled water to make the reference solution<sup>69</sup>.

In order to make a solution of sodium flouride ( $\text{NaF}$ ) (100 mg/L), 0.221 g of it was dissolved in one litre distilled water. After testing the adsorption performance with

different adsorbents, the adsorbent was separated from the aqueous solution. 5 mL of reagent S was added to 1 mL of used NaF solution and the solution was kept for 30 minutes. With the use of a spectrophotometer set at 570 nm, the decreased concentration of fluoride ions was determined. The preliminary study of percentage removal of fluoride ions with various synthesized adsorbents are shown in table 3.5.

It is clear from table 3.5 that metal ferrites and their composites with CMC and alginate biopolymer did not give reproducible results with fluoride ions. The reason behind this could be that adsorbent surfaces which have functional groups like -OH and -COO- and fluoride ions have similar negative charge that repel each other resulting in less removal percentage.

**Table 3.5- Preliminary study of percentage removal of Fluoride (F<sup>-</sup>) ions**

S.No.	Sample	OD Blank	Absorbance at 570 nm (5 mg/L)	Concentration (Ce)	% Removal
1.	NiF	0.788	0.482	3.06	38.83
2.	NiFCMC	0.788	0.470	2.98	40.36
3.	NiFCMC-Alg	0.788	0.488	3.10	38.07
4.	ZnF	0.788	0.491	3.12	37.69
5.	ZnFCMC	0.788	0.468	2.97	40.61
6.	ZnFCMC-Alg	0.788	0.482	3.06	38.83
7.	CoF	0.788	0.530	3.36	32.74
8.	CoFCMC	0.788	0.481	3.05	38.96
9.	CoFCMC-Alg	0.788	0.477	3.03	39.47

**Table 3.6- Preliminary study of percentage removal of Ni (II) ions**

S. No.	Sample	OD Blank	Absorbance at 470 nm (100 mg/L)	Concentration (Ce)	% Removal
1.	NiFe <sub>2</sub> O <sub>4</sub>	0.924	0.540	58.44	41.56
2.	NiFe <sub>2</sub> O <sub>4</sub> -CMC	0.924	0.450	48.70	51.30
3.	NiFe <sub>2</sub> O <sub>4</sub> CMC-Alg	0.924	0.429	46.43	53.57
4.	ZnFe <sub>2</sub> O <sub>4</sub>	0.924	0.596	64.51	35.50
5.	ZnFe <sub>2</sub> O <sub>4</sub> -CMC	0.924	0.480	51.95	48.05
6.	ZnFe <sub>2</sub> O <sub>4</sub> CMC-Alg	0.924	0.456	49.35	50.65

The stock solution of NiSO<sub>4</sub>.6H<sub>2</sub>O was prepared by dissolving 4.479 g in 1000 mL of distilled water. The reagents used for the procedure were prepared as follows:

1. HCl solution (0.5 N): 50 mL of concentrated HCl was diluted to 1000 mL with distilled water.
2. Sodium Citrate solution: The solution of sodium citrate was made by dissolving 125 g of sodium citrate (Na<sub>3</sub>C<sub>6</sub>H<sub>5</sub>O<sub>2</sub>.2H<sub>2</sub>O) in 500 mL distilled water.
3. Iodine Solution (0.005 N): 20 g of potassium iodide (KI) was dissolved in 5 mL distilled water. To this solution, 6.4 g of iodine crystals were dissolved and solution was diluted to 1000 mL with distilled water.
4. Dimethylglyoxime (DMG): Dissolve 1 g of dimethylglyoxime in 100 mL of concentrated ammonia followed by addition of 100 mL of distilled water to it.

Procedure: In 50 mL volumetric flask, 1 mL of aliquot of Ni (II) ion sample not containing more than 2 µg/ mL of solution was taken. 20 mL of 0.5 N HCl was then added, followed by addition of 10 mL solution of sodium citrate. Further iodine solution (2 mL) and dimethylglyoxime solution (4 mL) was added to it. The solution in titration flask was made 50 mL with distilled water and the solution was kept undisturbed for

20 minutes to develop the colour. The absorbance of this solution was measured at  $\lambda_{\text{max}}$  of 470 nm by UV-spectrophotometer.

The findings of the preliminary investigation of removal percentage of nickel ions by using NiF and ZnF with their composites with CMC and alginate were displayed in table 3.6. From the above table, it was clear that removal percentage of nickel ions was found to more than by using NiFCMC and NiFCMC-Alg as compared to pure NiF as well as ZnFCMC and ZnFCMC-Alg composite. So, for further detailed study of removal of nickel ions from aqueous medium, NiFCMC and NiFCMC-Alg composites were selected.

### **3.3 Estimation of Synthesized Carboxymethyl cellulose**

#### **3.3.1 CMC yield calculation**

To calculate the yield of CMC, gravimetric method has been used. The yield was calculated by dividing the net weight of dried CMC (in grams) by the dried weight of cellulose (in grams) <sup>28, 33, 35</sup>.

$$\% \text{ Yield of CMC} = \frac{\text{Weight of dried CMC (in g)}}{\text{Dried weight of cellulose (in g)}} \times 100 \quad (2)$$

#### **3.3.2 Degree of Substitution (DS)**

It is by definition, the average number of sodium carboxymethyl groups that replaced hydroxyl groups at C2, 3, and 6 in the cellulose chain. Back Titration method was employed for calculating DS <sup>28, 33</sup>.

This method was adopted because the results obtained were very reproducible and no sophisticated instruments and chemicals were required. In this method, Na-CMC was first converted into H-CMC by the following method:

2 g of dry powdered Na-CMC was dissolved in acetone by stirring. To this dispersion, 6 mL of hydrochloric acid (6 N) was added with continuous stirring for 30 minutes. The dispersion was filtered and precipitates were washed with a solution made up of methanol: water (80:20 v/v). The precipitates were spread further in acetone, filtered and dried in oven at 50°C. The dried product (H-CMC) was grinded and utilized for titration.

##### **3.3.2.1 Method of Titration**

0.5 g of H-CMC was dissolved in 20 mL of 0.2 N sodium hydroxide (NaOH) and to it 50 mL of double distilled water was added. The solution was transferred into 100 mL volumetric flask and filled upto the mark by double distilled water. In a 100 mL

Erlenmeyer flask, 25 mL of the above solution was taken and filled up to mark by adding double distilled water. Phenolphthalein was used as an indicator to back titrate the excess sodium hydroxide using a standard solution of 0.05 N hydrochloric acid. The above titration was done in triplicate to find mean volume of HCl used for calculation. The degree of substitution was calculated by following equations:

$$A = \frac{BC - DE}{F} \quad (3)$$

$$\text{Degree of substitution (DS)} = \frac{0.162 \times A}{1 - (0.0058 \times A)} \quad (4)$$

where: A represents equivalent weight per gram of sample of NaOH used, B shows volume of sodium hydroxide (in mL), C represents normality of sodium hydroxide (N), D = volume of hydrochloric acid consumed (mL), E = normality of HCl solution (N), F = sample weight of CMC (in g), 162 represents mol. wt. of glucose unit (anhydrous), 58 denotes net increase in mass of glucose unit per added carboxymethyl group.

### 3.3.3 Molecular weight calculation

The calculation of molecular weight of CMC was done with the help of Mark-Houwink-Sakurada equation<sup>28,33</sup>. The equation is as follows:

$$[\eta] = KM^a \quad (5)$$

Where  $[\eta]$  is the intrinsic viscosity, K = solvent's constant, 'a' represents factor associated with shape of polymer, molecular weight is denoted by M. To calculate the molecular weight, dissolve 2% solution of CMC in a solution of 0.78M sodium hydroxide. The Ostwald's Viscometer was used to measure the intrinsic viscosity of CMC. The viscosity is determined by using the data obtained from the time it takes for a solvent to move between two points using a viscometer and by comparing the result to that of a CMC solution. The molecular weight was determined from  $\eta$  value.

### 3.3.4 Water retaining/holding capacity (WHC) and Oil retaining/ holding capacity (OHC)

To 25 mL of distilled water and mustard oil, dissolve 1 g dried CMC separately. The mixture was agitated and then incubated for one hour at 40°C in an oven. The residue (remaining material) was weighed following the centrifugation of the sample. Water and oil retaining capacity was examined by dividing water and oil in gram per dry weight of sample respectively<sup>28</sup>.

### 3.3.5 Content of CMC (%)

1.5 gram of CMC sample was dissolved in 100 mL of 80% methanol aqueous solution and the mixture was swirled. The mixture was filtered after 10 minutes. The sample was

again cleaned using 100 mL of 80% methanol aqueous solution, washed and then filtered and put to dry in order to obtain pure CMC sample <sup>28, 35</sup>.

The CMC content was calculated by using following formula:

$$\text{Content of CMC (\%)} = W / W_o \times 100 \quad (6)$$

where, W and W<sub>o</sub> denotes weight of CMC sample after and before washing.

### **3.3.6 Content of Sodium chloride in CMC**

Dissolve 2 g of CMC in 250mL of methanol solution (60%) and the mixture was left undisturbed for 5 hours. 100 mL of this mixture solution was titrated with 0.1N AgNO<sub>3</sub> solution after being neutralized with 0.1 N nitric acid (HNO<sub>3</sub>) <sup>28, 35</sup>. The content of sodium chloride in the sample was estimated as follows:

$$\text{Content of sodium chloride(\%)} = \frac{1.461}{M} \times V \quad (7)$$

where, V denotes amount of AgNO<sub>3</sub> solution (in mL), M is weight of the dried sample of CMC in (g).

### **3.3.7 Fourier Transform Infra Red (FTIR) Analysis**

FTIR spectrophotometer (Shimadzu 8400S double beam spectrophotometer) was used to characterize and detection of functional groups in prepared cellulose, lignin and carboxymethyl cellulose (CMC), different metal ferrite, metal ferrite-CMC and metal ferrite-CMC-Alginate composites using KBr method. The dried sample of about 0.2 g was mixed with 2 mg of KBr, grounded and compressed to transparent disk. Wave numbers are used to measure the frequency range, which is usually between 4000 cm<sup>-1</sup> and 400 cm<sup>-1</sup>. The FTIR works on the principle that the majority of organic and inorganic molecules absorb light in the IR region of the electromagnetic radiation spectrum. The absorbance exactly corresponds to the molecule's bonds. Different peaks within particular region indicate the existence of distinct functional groups.

### **3.3.8 Scanning Electron Microscope (SEM) analysis**

By using a scanning electron microscope (SEM), the surface morphology was investigated. It is based on the principle of applying a small beam of electrons of high energy to the surface of the specimen and measuring the different signals from the surface to determine its properties. In SEM technique, the microscopic image was captured with the Zeiss Crossbeam 340. Smaller pieces (5×5×5) were cut out of the specimen and coated with gold and examined with 2-10 kV accelerating voltage. By this technique, the particle shape, size and surface morphology can be accessed. The surface

morphology of cellulose, lignin and CMC, various synthesized metal ferrites, metal ferrite-CMC and metal ferrite-CMC-Alginate was determined by SEM (JOEL JSM-7610).

### **3.3.9 Energy Dispersive Spectra Analysis (EDS)**

The chemical characterization as well as elemental composition of the material was determined by analytical technique known as Energy dispersive spectra (EDS). EDS uses the X-ray spectrum that is produced when a solid sample is subjected to an intense electron beam. Elements having atomic number ranging from 4 (Be) and 92 (U) can be determined by this technique. It is helpful in examining the surface modification. The elemental peaks and composition of different metal ferrites, metal ferrite-CMC and metal ferrite CMC-Alginate was analyzed by EDS (OXFORD EDS LN2).

### **3.3.10 Brunauer-Emmett-Teller Analysis (BET)**

The Brunauer-Emmett-Teller (BET) method can be used to determine the material's specific surface area, pore size and pore volume. The fundamental idea behind this method is that the particular area of the material can be ascertained by the physisorption of gas molecules on the solid surface of the adsorbent. The BET analysis of different metal ferrites, metal ferrite-CMC and metal ferrite CMC-Alginate was done with BET (Anton Par, Nova-600 BET).

### **3.3.11 Thermo Gravimetric Analysis (TGA)**

The amount of biopolymer bonded to the metal ferrite and its thermal stability is assessed by using thermogravimetric analysis (TGA). (Perkin Elmer TGA 4000). The TGA method involves heating the sample at a controlled rate in a certain atmosphere (air, N<sub>2</sub>, CO<sub>2</sub>, He, Ar etc.) The sample's weight change is noted in relation to either temperature or time. TGA analysis of various metal ferrites, metal ferrite-CMC and metal ferrite CMC-Alginate was done with Perkin Elmer TGA 4000.

### **3.3.12 X-Ray Diffraction Analysis (XRD)**

The crystallite structure, geometry and shape were calculated by using X-ray diffraction technique. It is based on the principle of constructive interference of monochromatic x-ray. When a material is exposed to incoming X-rays, XRD measures the intensities and scattering angles of the X-rays that exit the substance. Using CuK $\alpha$  as the radiation source, a 45 kV and generator of 40 mA was used to capture the diffraction patterns between 2 $\theta$ , which ranged from 20° to 80°. XRD analysis of cellulose, CMC, various metal ferrites, metal ferrite-CMC and metal ferrite CMC-alginate was done with XRD



Bruker D8.

The Scherrer formula was used to determine the average size of the crystallite of metal ferrite and its composites as shown below <sup>7</sup>.

$$D = \frac{0.89\lambda}{\beta \cos \theta} \quad (8)$$

Where the crystallite size is denoted by D,  $\lambda$  represents X-ray wavelength, diffraction angle is represented by  $\theta$  while broadening peak is denoted by  $\beta$ .

### **3.3.13 pH of Point Zero Charge (pHpzc Analysis)**

The adsorption process is significantly influenced by the pH of point zero charge (pHpzc). It stands for the pH value at which the adsorbent's surface has no net surface charge. The pHpzc of the sample was calculated by employing solid addition method <sup>49, 143</sup>.

In this method, 50 mL solution of KNO<sub>3</sub> (0.1 M) was placed in 250 mL conical flasks and using 0.1 N HCl and 0.1 N NaOH, the pH of the solution was changed between 2 and 10. Then in each flask 0.1 g of the adsorbent was added and kept the conical flasks on thermo shaker for 24 hours at 298 K. Following filtering, the solution's final pH was recorded. The graph was plotted between  $\Delta$  pH (initial-final) vs pH (initial) to calculate pH of point zero charge.

### **3.3.14 Vibration Sample Magnetometer (VSM) Analysis**

The magnetic property of the magnetic material was determined by VSM analysis by measuring magnetic moment of the material. This technique uses the homogenous magnetic field H to cause the magnetic material to vibrate, creating an electric current in sensing coils that are positioned correctly. The working of this analysis includes an electromagnet which produces a homogeneous magnetic field that surrounds a sample. Along a predetermined axis, the sample vibrates, usually in a sinusoidal manner. The magnetic flux changes as a result of this vibration through pick-up coils, which are stationary coils placed close to the sample. In the pick-up coils, a voltage is induced by the fluctuating magnetic flux. The magnetic moment of the sample is directly correlated with the amplitude of induced voltage amplitude and phase. By analyzing the induced voltage, the magnetic moment of the sample can be determined. VSM analysis of different metal ferrites, metal ferrite-CMC and metal ferrite-CMC-alginate was determined by VSM-7400.

### **3.4 Adsorption Studies by Batch method**

To investigate the metal ferrite-CMC and metal ferrite CMC-alginate's adsorption

capacity for MB, CV cationic dyes and Ni (II) ions, batch adsorption method was done on various adsorption parameters in both single and binary dye systems. This approach involves putting a fixed amount of adsorbent (0.1 g) in a 250 mL flask with a known volume (50 mL) of adsorbate at a fixed concentration. The flask is then placed on a thermoshaker set at 150 rpm for a predetermined time. After the completion of the experiment, the samples were taken from the thermo shaker and adsorbent was magnetically separated. The absorbance of the resultant solution was measured using a UV-visible spectrophotometer (Shimadzu, 1800 scanning double beam UV-VIS spectrophotometer) at 664 nm, 590 nm and 470 nm respectively to ascertain the decreased concentration of the dye and metal ion solution. The effects of several adsorption factors were investigated, including temperature, the amount of adsorbent, starting dye/metal ion concentration, time and pH with metal ferrite-CMC and metal ferrite CMC-alginate composites by following above described procedure by maintaining other parameters fixed.

### 3.4.1 Single and Binary Dye system

#### 3.4.2 Single Dye system

Adsorption capability ( $Q_e$  mg/g) and percentage (%) removal of dyes and Ni (II) ions were determined using equations (9) and (10) respectively <sup>49, 78</sup>.

$$Q_e = (C_o - C_e) / m \times V \quad (9)$$

$$\% \text{ Removal} = (C_o - C_t) / C_o \times 100 \quad (10)$$

where  $C_o$  denotes concentration (mg/L) of dyes or metal ions at initial time,  $C_t$  is concentration at time 't' and  $C_e$  shows concentration at equilibrium,  $m$  = mass of adsorbent (in gram),  $V$  is volume of solution (in Litre).

#### 3.4.3 Binary Dye System

The concentration of different components A and B can be ascertained by using the equations (11) and (12) in binary dyes system <sup>49, 144</sup>.

$$C_A = (K_{B2}d_1 - K_{B1}d_2) / (K_{A1}K_{B2} - K_{A2}K_{B1}) \quad (11)$$

$$C_B = (K_{A1}d_2 - K_{A2}d_1) / (K_{A1}K_{B2} - K_{A2}K_{B1}) \quad (12)$$

Where,  $K_{A1}$ ,  $K_{B1}$ ,  $K_{A2}$  and  $K_{B2}$  represents the constants for calibration at two wavelengths  $\lambda_1$  and  $\lambda_2$  for components A and B in a binary mixture. The optical densities of the dye mixture at  $\lambda_1$  and  $\lambda_2$  are  $d_1$  and  $d_2$  respectively. The coefficients of adsorption are denoted

by  $K_{A1}$  of pure component A for CV whereas  $K_{B1}$  represents for pure components B (MB) at  $\lambda_1$  (590 nm). Likely,  $K_{A2}$  represents coefficients of adsorption of pure component A for CV and  $K_{B2}$  for pure components B (MB) at  $\lambda_2$  (664 nm).

### 3.5 Regeneration Studies

After studying the adsorption behaviour with dyes and metal ions in both single as well as binary systems, the adsorbent dose of predetermined amount was used for regeneration. In 250 mL conical flask, 1 g of spent adsorbent saturated with dye / metal ions was taken and 50 mL of 0.1 N HCl (desorbing agent) was added to it. The mixture was shaken for an hour at 150 rpm in a thermostatic shaker. To make the adsorbent useful again, it was filtered, cleaned and dried. The equation (13) was used to calculate the adsorbents' percentage regeneration capacity<sup>65, 69</sup>.

$$\text{Regeneration Efficiency \%} = \frac{\text{Adsorbed dye amount in (n+1)th cycle}}{\text{Adsorbed dye amount in nth cycle}} \quad (13)$$

### 3.6 Adsorption Kinetics

The adsorption behaviour in relation to time is determined by adsorption kinetics. Several kinetic models including the Lagergren pseudo first and second order model, Weber-Morris intra-particle diffusion model and the Elovich model were used to determine the kinetic behaviour of adsorption of different metal ferrite-CMC and metal ferrite CMC-alginate composites with specific dyes and metal ions in both single as well as binary dye systems. The data that was obtained from adsorption study in relation to time, fitted to general linear equation<sup>49, 94, 104</sup>.

#### 3.6.1 Lagergren Pseudo first Order Model

Bimolecular reactions that have first-order characteristics are known as pseudo-first-order reactions. The first order occurs when the concentration of one of the reacting substance is kept constant in relation to the other or when it is present in large excess. The adsorption process will be physical in nature since the rate determining step involves diffusion rather than the concentrations of both reactants<sup>49, 145</sup>.

The equation for pseudo-first order kinetics in linear form is shown as:

$$\log(Q_e - Q_t) = \log Q_e - \frac{k_1}{2.303} t \quad (14)$$

Where, adsorption capacities (mg/g) of dye/metal ions at equilibrium and time 't' is shown as  $Q_e$  and  $Q_t$ . The rate constants for Lagergren pseudo first order is represented by the values  $k_1$  ( $\text{min}^{-1}$ ). The different values of constant are calculated from the values of intercept and slope of plot between  $\log(Q_e - Q_t)$  and t.

### 3.6.2 Lagergren Pseudo second Order Model

The underlying premise of the pseudo second order kinetic model is that chemical adsorption is the rate-determining step that determines behaviour throughout the entire adsorption process. Under such conditions, adsorption capacity rather than adsorbate concentration determines the adsorption rate<sup>49, 146</sup>.

The pseudo second order kinetics is shown in linear form as follows

$$\frac{t}{Q_t} = \frac{1}{k_2 Q_e^2} + \frac{t}{Q_e} \quad (15)$$

Where adsorption capacities (mg/g) at equilibrium and at time 't' is denoted as  $Q_e$  and  $Q_t$  for dyes and metal ions,  $h = k_2 Q_e^2$  is initial sorption rate and the equilibrium rate constant for pseudo second order kinetics is represents as  $k_2$  (mg/min). The values of the various constants  $Q_e$  and  $k_2$  are ascertained from the slope and intercept of the linear relationship provided by the plot of  $t/Q_t$  vs  $t$ .

### 3.6.3 Elovich Model

The basic assumption of this model is that as the amount of adsorbed solute increased, the adsorption rate of that solute is expected to decrease exponentially. It is often applicable in the systems which have heterogeneous adsorbing surface and depicts the nature of adsorption as chemisorptions. The Elovich model in the linear form is represented as below<sup>49, 146</sup>.

$$Q_t = \frac{1}{\beta} \ln \alpha \beta + \frac{1}{\beta} \ln t \quad (16)$$

Where, the initial chemisorption rate is indicated by  $\alpha$  (g/mg/min) and desorption constant is represented by  $\beta$  (g/mg). From the plot of  $\ln t$  versus  $Q_t$ , the values of constants can be calculated from the slope ( $1/\beta$ ) and intercept  $1/\beta \ln(\alpha\beta)$ .

### 3.6.4 Weber Morris Model

Weber and Morris presented the intra particle diffusion to determine the diffusion mechanism in adsorption process. The linear form of the Weber Morris intra-particle diffusion model is represented as<sup>7, 104</sup>.

$$Q_t = K_{int} t^{0.5} \quad (17)$$

Where,  $K_{int}$  denotes rate constant for the intra-particle diffusion. The rate determining step is shown by the plot of  $Q_t$  vs  $t^{0.5}$ , which shows the adsorbent's diffusion behaviour. The origin must be crossed by the straight line if this is the only step for rate measuring.

## 3.7 Adsorption Isotherms

The relationship between the adsorbate in the surrounding phase and the adsorbate on the

adsorbent's surface at equilibrium and constant temperature is represented by the adsorption isotherm. Various kinds of adsorption isotherms were employed for determination of adsorption equilibrium of preapred magnetic biopolymer composites.

The present study examined the adsorption behaviour of metal ions and dyes using a number of adsorption isotherm models, such as the Langmuir, Freundlich, Temkin and Dubinin-Radushkevich (D-R) models.

### 3.7.1 Langmuir Model

- This model describes the equilibrium between the adsorbent and adsorbate system as a function of concentration. It characterises the region on the surface of solid adsorbents that is covered by adsorbate molecules in relation to concentration or partial pressure at a set temperature <sup>78, 146, 147</sup>. The main assumptions of this model are following:
- Every adsorption site is equal and the adsorbent surface is uniform.
- Adsorption creates an adsorbate's monolayer on the surface with just one adsorbate molecule adsorbed at a time on each available site.
- The molecules on separate sites do not interact with one another.
- The number of sites and the heat of adsorption are unrelated to one another. For every site, it is the same.

The Langmuir isotherm in linear form is displayed as <sup>49, 146</sup>.

$$\frac{1}{Q_e} = \frac{1}{Q} + \frac{1}{bQC_e} \quad (18)$$

Where, Q (mg/g) represents the Langmuir adsorption capacity; b = Langmuir constant (L/mg); Q<sub>e</sub> is the quantity of adsorbate adsorbed per adsorbent weight; C denotes concentration of dye/metal ions at equilibrium. A straight line with a slope of 1/bQ and an intercept of 1/Q is produced by plotting 1/Q<sub>e</sub> against 1/C<sub>e</sub>.

### 3.7.2 Freundlich Isotherm

The heterogeneous surface of adsorptive materials that follow the Freundlich isotherm equation is thought to have sites with varying adsorption potentials and each kind of site is thought to adsorb molecules. According to this model, multilayer is formed in the adsorption process <sup>49, 146</sup>.

Equation (19) showed the linearized form of Freundlich isotherm model

$$\log Q_e = \log K_f + \frac{1}{n} \log C_e \quad (19)$$

Where, Q<sub>e</sub> (mg/g) denotes the Freundlich adsorption capacity; K<sub>f</sub> = Freundlich constant

and  $n$  denotes the Freundlich exponent (dimensionless). The plot of  $\log Q_e$  versus  $\log C_e$ , gives a straight line. The values of constants like  $K_f$  and  $1/n$  will be computed from the graph's slope and intercept.

### 3.7.3 Temkin Isotherm

The indirect interactions between the adsorbent and adsorbate are taken into account by the Temkin isotherm model when studying the adsorption process. The basic assumption is that the heat of adsorption of each molecule in the layer decreases linearly with increasing adsorbent surface coverage. Binding energy defines the nature of adsorption.

Temkin Isotherm in linear form is shown as <sup>49, 146</sup>.

$$Q_e = \frac{RT}{b_T} \ln A + \frac{RT}{b_T} \ln C_e \quad (20)$$

Where, adsorption heat is expressed as  $B = RT/b_T$ ,  $A$  denotes binding equilibrium constant (L/g);  $T$  shows absolute temperature (Kelvin)); Temkin constant (J/mg) =  $b_T$ ;  $R$  is universal gas constant (8.314 J/K mol). An exothermic form of adsorption is indicated by a positive value for  $b_T$ . When the value is negative, it indicates that the adsorption is endothermic.

### 3.7.4 Dubinin-Radushkevich (D-R) Isotherm

The adsorption mechanisms can be better described by this isotherm. It also aids in the distinction between chemisorption and physisorption by determining the apparent free energy change.

D-R isotherm in linear form is represented as <sup>49, 146, 148</sup>.

$$\ln Q_e = \ln Q_m - K\varepsilon^2 \quad (21)$$

$$\varepsilon = RT \ln (1+1/C_e) \quad (22)$$

Where, adsorption capability is shown as  $Q_m$ (mg/g);  $K$  represents DR constant;  $\varepsilon$  is Polanyi potential (kJ/mol),  $R$  (8.314J/K/mol) shows Universal gas constant;  $T$  is absolute temperature (Kelvin).

Adsorption energy ( $E$ ) is one of the metrics used to determine the type of adsorption behaviour. It is computed using the equation shown here <sup>78, 147</sup>.

$$E = 1/\sqrt{2} K \quad (23)$$

Where,  $K$  is D-R constant shows adsorption free energy ( $\text{mol}^2\text{J}^{-2}$ ). It is possible to predict the kind of adsorption process using the computed value of " $E$ ." If the value of  $E < 40$  kJ/mol then physical adsorption will take place otherwise chemisorption is the adsorption process <sup>49</sup>.

### 3.8 Adsorption Thermodynamics

In an adsorption process, the amount of energy released from the start to the final state is specified by adsorption thermodynamics. The change in  $H^\circ$  (Adsorption enthalpy),  $G^\circ$  (Gibbs free energy) and  $S^\circ$  (entropy) are three thermodynamic characteristics that have been used to determine the type of adsorption process<sup>49, 147, 149</sup>.

The adsorption thermodynamics is studied by using various thermodynamic equations.

According to Van't Hoff

$$\Delta G^\circ = RT \ln K_d \quad (24)$$

$$K_d = C_o - C_e / C_e \quad (25)$$

As per Gibb's Helmholtz equation

$$\Delta G^\circ = \Delta H^\circ - T\Delta S^\circ \quad (26)$$

Equations (24) and (26) are combined to produce:

$$\ln K_d = \frac{\Delta S^\circ}{R} - \frac{\Delta H^\circ}{RT} \quad (27)$$

$C_o$  and  $C_e$  are the initial and final concentrations of the adsorbate (in mg per litre),  $K_d$  denotes dimensionless distribution equilibrium constant,  $T$  is the absolute Kelvin temperature,  $R$  represents the universal gas constant (8.314 J/K/mol).

The values of  $H^\circ$  and  $S^\circ$  are obtained by calculating the slope and intercept of the linear plot between  $\ln K_d$  and  $1/T$ .



## **CHAPTER 4**

### **RESULTS AND DISCUSSION**



On the basis of preliminary studies' finding, various metal ferrites CMC and their alginate biopolymer composites were chosen to explore the in-depth studies of adsorption with various cationic dyes (MB and CV) and Ni (II) ions in both adsorbate systems i.e. single as well as binary. Consequently, two sections are presented discussing the results of adsorption experiments: one section deals with dyes and the other with Ni metal ion using various metal ferrite CMC and alginate biopolymer composites. Additionally, each section has been divided into sub-sections for the purpose of characterizing the adsorbents and the results of the adsorption tests are thoroughly examined.

## **Part-I**

### **4.0 Characterization of Extracted Cellulose and synthesized Carboxymethyl cellulose (CMC)**

#### **4.1 Purification and Isolation of Cellulose**

The treatment of dried and powdered corncobs with NaOH was done to remove lignin and hemicelluloses. NaOH is the key chemical reagent which dissolves lignin and hemicellulose but not cellulose. Bleaching with equimolar (1:1) mixture of acetate buffer (NaOH: acetic acid) and sodium chlorite was used to take off lignin and hemicelluloses<sup>28, 33</sup>. The corncob powder after pre-treatment with NaOH (light brown in colour) gave a yield of 71.67% which after bleaching process produced cellulose (white in colour) had a yield of 48.78% by dry mass (figure 4.1.1 (c) and (d)). The extracted lignin was brown in colour with a yield of 9.67% by dry mass was obtained.

The treatment with sodium hydroxide (NaOH) not only affects the crystalline structure of cellulose but also increases the surface roughness due to removal of lignin and hemicelluloses<sup>27, 28</sup>. The change of crystallinity and molecular orientation was due to suspending of cellulose in the mixture of NaOH and ethanol where NaOH was uniformly distributed within the cellulose during alkalization step. NaOH act as a swelling agent as well as a dilutant and it facilitated good penetration of solvent into cellulose structure. Sodium carboxymethyl cellulose was produced by heterogenous reaction in which rate depends upon the diffusion rate of NaOH and monochloroacetic acid inside cellulose<sup>28, 33</sup>. CMC produced was a white coloured powder.

Table 4.1.1 displays the yield, DS and solubility of synthesized CMC. The high yield of CMC was attributed to the fact of addition of monochloroacetic acid on cellulose during etherification.

The percentage yield of CMC was calculated by dividing the amount or mass of dry CMC in gram by amount or mass of cellulose in gram <sup>28, 35</sup>.

**Table 4.1.1- DS, percentage yield and solubility of synthesized CMC**

DS	CMC Yield %	Solubility
2.27	120	Soluble

DS value of CMC has been observed to affect its solubility. It was found that CMC with a DS value less than 0.4 was insoluble in water and its solubility increases as the DS value increases <sup>33</sup>.

It has been found that the value of degree of substitution of CMC (2.27) in the present work is higher than 1.02, 1.18 and 0.85 using the same source of cellulose as corncob and corn stalk <sup>26, 30</sup>. The yield and purity of CMC sample 120% and 91.65% was also high. The findings proved the validity of the techniques used in the present research as these require low acid and alkali concentration and did not require sophisticated instruments like high pressure cooking pot used in similar work using corncob <sup>25</sup>. Table 4.1.2 displays the calculated value of intrinsic viscosity and molecular weight of prepared CMC.

**Table 4.1.2- Calculated values of intrinsic viscosity and molecular weight of CMC**

Sample	Intrinsic Viscosity ( $\eta$ )	Molecular Weight (Da)
Synthesized CMC	1.02	436515.83

Mark-Houwink-Sakurada equation was used to calculate the value of molecular weight of synthesized CMC as  $\eta = KM^a$ ; where the value of K is  $37 \times 10^{-5}$  dl/g and 'a' is factor associated with shape of polymer having value of 0.61 at 35°C.

It has been found that value of DS increases when the more numbers of free -OH groups in cellulose chain are available and substituted by monochloroacetic acid. It is because larger groups (monochloroacetic acid) cause substitution of the smaller groups (-OH) thereby increases molecular weight. The viscosity of a polymer depends upon its size (molecular weight) and concentration. It also increases with increase in DS value because more hydrophilic hydroxyl groups are substituted by carboxymethyl groups and thereby viscosity increases. The prepared CMC has intrinsic viscosity of 1.02. The low intrinsic

viscosity value may be due to the formation of sodium glycolate as by product in side reaction where monochloroacetic acid is used up in the step of etherification <sup>25, 28, 31</sup>. The synthesized CMC has been characterized by percentage purity, NaCl content, water retention capacity (WRC) and oil retention capacity (ORC) that has been shown in table 4.1.3.

**Table 4.1.3- Percentage purity, NaCl content, WRC and ORC of synthesized CMC**

<b>Sample</b>	<b>Percentage Purity</b>	<b>NaCl content</b>	<b>WRC</b>	<b>ORC</b>
Synthesized CMC	91.65	0.37	3.81	1.66

The synthesized CMC was treated with 70% ethanol and then with absolute alcohol to measure purity of CMC. This treatment eliminated the byproducts formed during alkalization and etherification process. The water holding capacity of prepared CMC was due to hydrophilic nature of CMC. It is because that more -OH groups which have hydrophilic nature are substituted by carboxymethyl groups in etherification process <sup>28</sup>. The purity of CMC greatly depends upon concentration of NaOH (30%) and monochloroacetic acid (120%). Above this concentration, side reaction starts in which monochloroacetic acid is inactivated and consumed, results in the formation of sodium glycolate (equation 3.1). Similar findings have been reported in the study of water hyacinth, corn husk and Baobab fruit shell <sup>27, 28, 35</sup>.

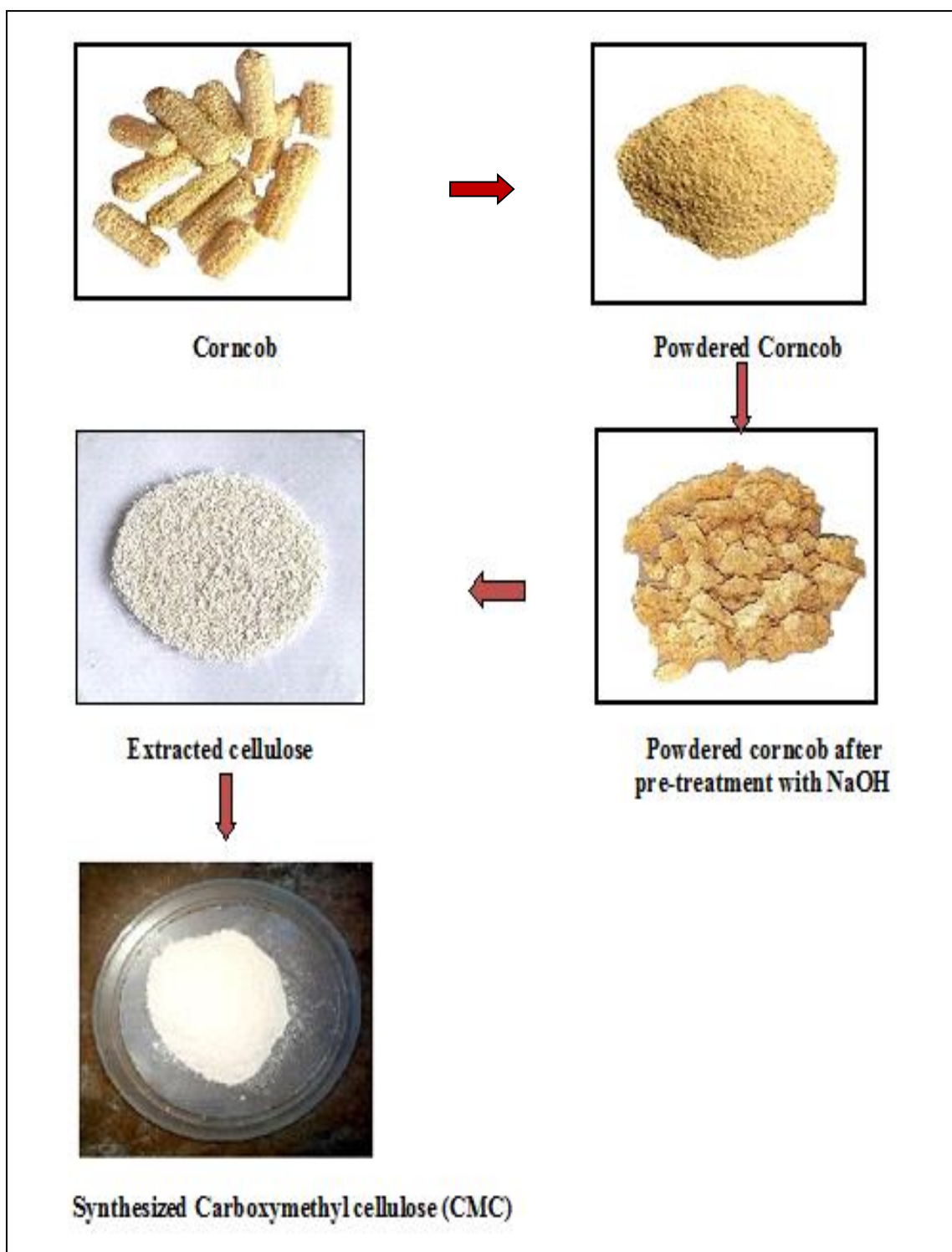


**Figure 4.1.1- Pictorial representation of Synthesis of Carboxymethyl cellulose (CMC) from corncob**

#### 4.1.2 FTIR Analysis

The prepared CMC was characterized by FTIR technique. Figure 4.1.2 (a, b and c) shows the FTIR spectra of extracted cellulose, corncob and extracted lignin. The spectra of extracted cellulose, corncob and extracted lignin lie in the region between 1800  $\text{cm}^{-1}$  and 800  $\text{cm}^{-1}$  shows the main difference. The absorption bands near 1730.21  $\text{cm}^{-1}$ , 1599.04  $\text{cm}^{-1}$  and 1506.46  $\text{cm}^{-1}$  in spectra of corncob were not found in spectra of cellulose. The absorption bands near 1506.46  $\text{cm}^{-1}$  and 1255.70  $\text{cm}^{-1}$  are removed or reduced in the spectra of extracted cellulose. This showed that most of the lignin has been removed<sup>28, 35</sup>. This was also revealed from the spectra of lignin where absorption bands were found at 1506.46  $\text{cm}^{-1}$  and 1222.91  $\text{cm}^{-1}$  in figure 4.1.2 (c). The band at 1730.21  $\text{cm}^{-1}$  was due to labile ester bonds which were completely cleaved while the absorption band at 1458.23  $\text{cm}^{-1}$  was attributed to methoxyl groups.

In figure 4.1.2 (a), the two peaks at 1159.26  $\text{cm}^{-1}$  and 1028.09  $\text{cm}^{-1}$  shows vibration and elongation of -OH (hydroxyl) linkages. The peak at 896.93  $\text{cm}^{-1}$  indicates 1, 4  $\beta$ - (glycosidic linkage), -CH<sub>2</sub> scissoring and -(O-H) bending motion is demonstrated by the peaks at 1427.37  $\text{cm}^{-1}$  and 1315.50  $\text{cm}^{-1}$ . The peak at 2891.75  $\text{cm}^{-1}$  represents -C-H stretching vibration while peak at 3325.39  $\text{cm}^{-1}$  is attributed to stretching vibration frequency of -OH group<sup>33</sup>.

The figure 4.1.3 (a) shows the spectra of CMC purchased from the market which has been assigned as standard CMC whereas figure 4.1.3 (b) showed the FTIR spectra of the synthesized CMC.

It was significant to see that a new, powerful absorption band appeared at 1599.40  $\text{cm}^{-1}$ , confirming the existence of the -COO group. The peak at 1411.94  $\text{cm}^{-1}$  represented -CH<sub>2</sub> (methyl) and 1321.28  $\text{cm}^{-1}$  depicts -O-H bending. While the peak at 2877.89  $\text{cm}^{-1}$  was ascribed to the -C-H stretching vibration and the wide peak at 3375.54  $\text{cm}^{-1}$  demonstrated the stretching frequency of the hydroxyl (-OH) group. The peaks at 1599.40  $\text{cm}^{-1}$  and 1411.94  $\text{cm}^{-1}$  represented specific characteristics of CMC according to literature review<sup>28, 33–35, 40</sup>. The >CH-O-CH<sub>2</sub> stretching peak appeared at 1031.95  $\text{cm}^{-1}$ <sup>35, 40</sup>. It is significant to observe that the spectrum of prepared CMC is almost same as that of spectra of CMC purchased from market. It showed that CMC has been successfully prepared from cellulose which was extracted from corncobs.

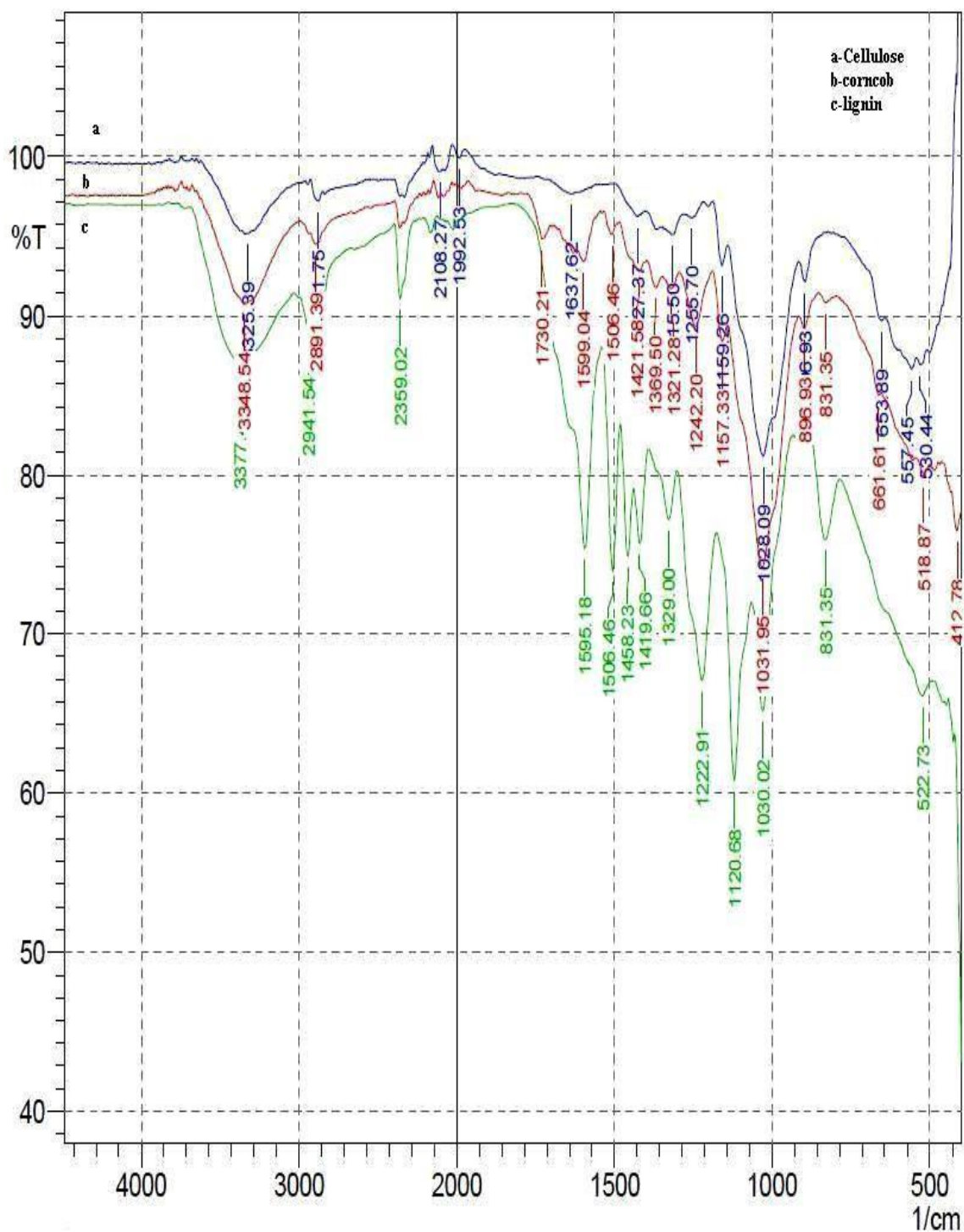
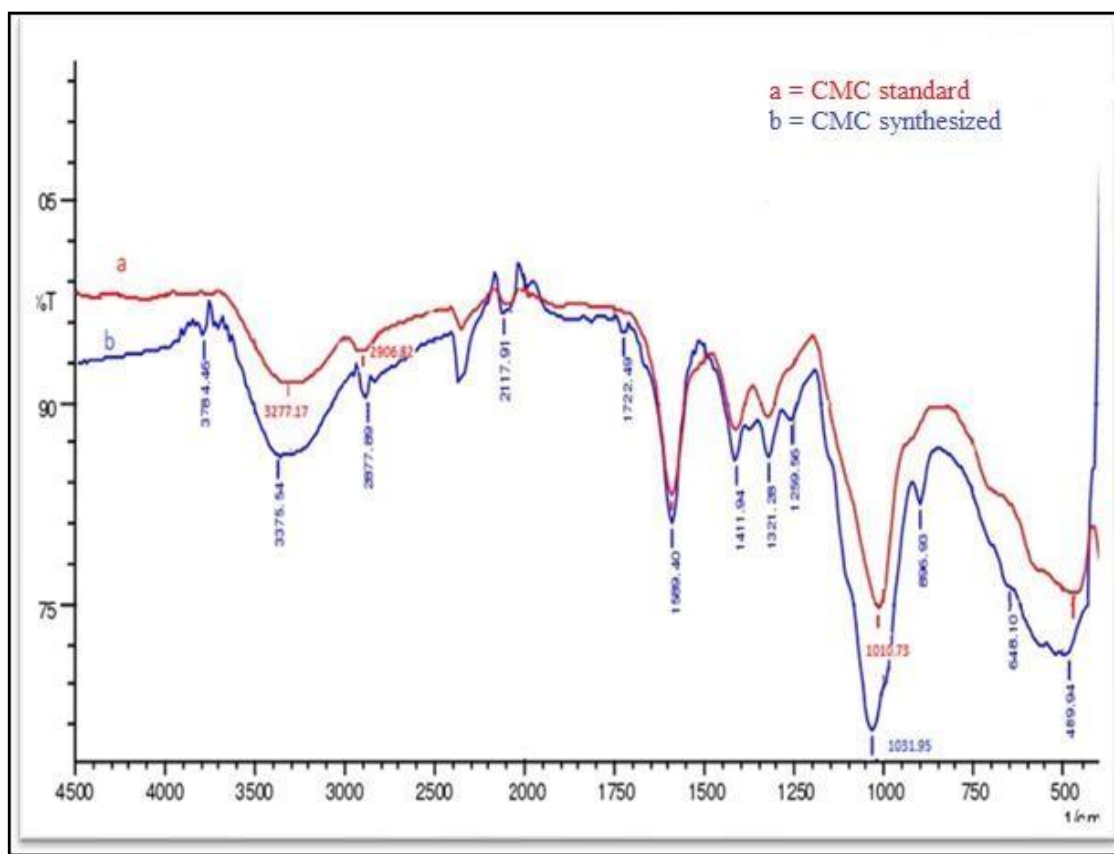


Figure 4.1.2- FTIR curve for (a) extracted cellulose (b) corncob (c) extracted lignin

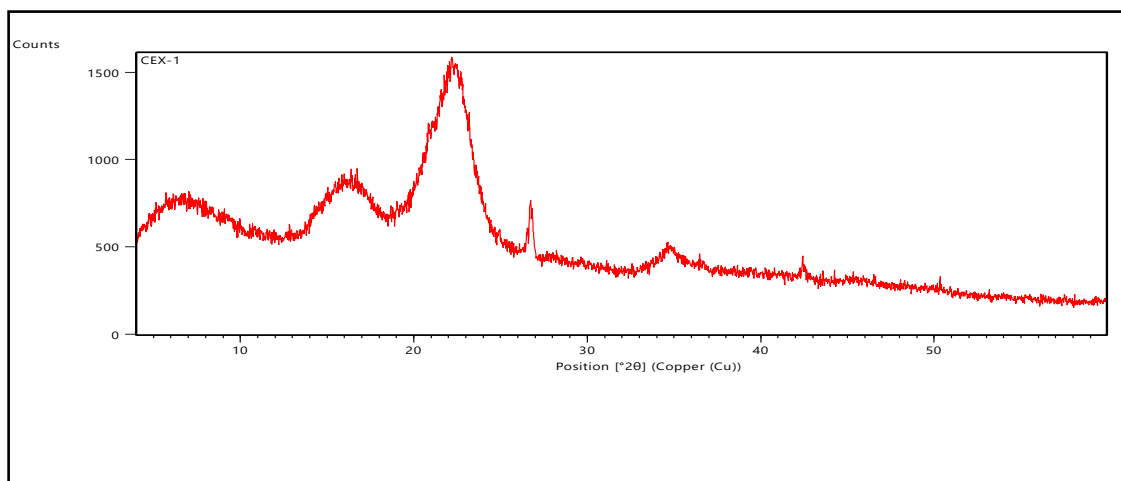


**Figure 4.1.3- FTIR curve shows (a) CMC standard (b) CMC synthesized**

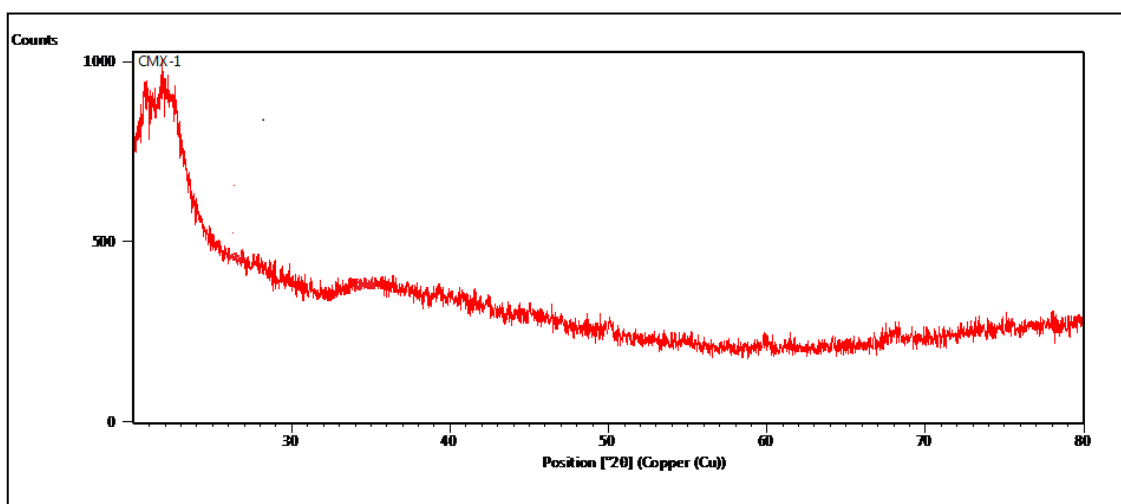
#### 4.1.3 Analysis using X-Ray diffraction

An essential technique for determining a polymer's degree of crystallinity is X-ray diffraction or XRD. The cellulose molecule has semi-crystalline structure. Figure 4.1.4 (a, b) illustrates the diffraction patterns of extracted cellulose and synthesized carboxymethyl cellulose respectively. The crystalline phase in the sample was represented by peaks while the plane region represented the amorphous phase.

The broad peaks were due to the presence of crystallites in the cellulose molecule. In the spectra of CMC, certain peaks that appeared in the sample of cellulose were found to be lowered or disappeared and changed into amorphous phase. It was due to the reason that in carboxymethylation process, 30% NaOH used causes swelling of chains of cellulose molecule thereby creating pressure on neighboring crystallites resulting in unwinding or breaking of helical structure by cleavage of hydrogen bonds and also its crystalline structure<sup>28, 150</sup>.



(a)



(b)

**Figure 4.1.4- XRD peaks of (a) extracted cellulose (b) synthesized CMC**

#### 4.1.4 SEM Analysis

The scanning electron microscope (SEM) technique is helpful in elucidating the surface morphology. The figure 4.1.5 (a, b, c and d) shows the surface morphology of extracted cellulose, synthesized CMC and extracted lignin. The surface of cellulose was found to be rough and particles have average length and breadth of 645.83  $\mu\text{m}$  and 309.99  $\mu\text{m}$  respectively. The CMC molecules have smooth surface with rod or ribbon like shaped with average length and breadth of 154.48  $\mu\text{m}$  and 23.84  $\mu\text{m}$  respectively which was same as observed in other reported images of CMC molecule<sup>28, 34, 35</sup>. Consequently, due to carboxymethylation, the particles of CMC shows decrease in the average size and consequently the morphology of surface of CMC appeared as ribbon shape.



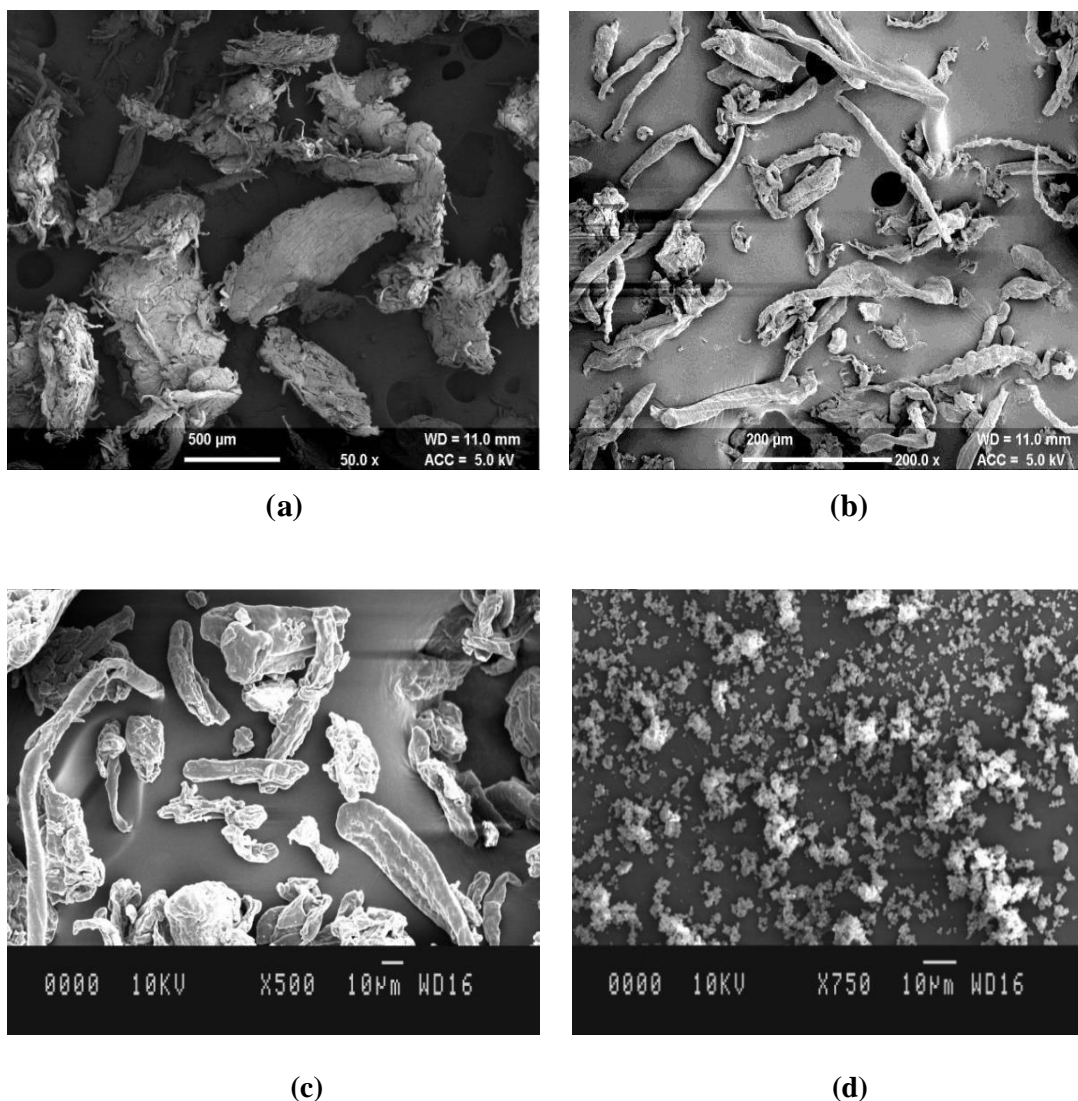


**Figure 4.1.5- SEM images of (a) Extracted cellulose (b, c) synthesized CMC (d) extracted lignin**

## **Part -II**

### **4.2 Characterization and Adsorption studies of Nickel metal ions with metal ferrite-CMC and their biopolymer composite**

Nickel Ferrite-CMC and Nickel Ferrite CMC-Alginate were selected as adsorbents to remove Ni (II) ions in single dye system from aqueous medium. The following section provides a full discussion of the surface characterization, morphology and adsorption study results of Nickel Ferrite-CMC and Nickel Ferrite CMC-Alginate composite

#### **4.2.1 Nickel Ferrite-CMC (NiFCMC) and Nickel ferrite CMC-Alginate (NiFCMC-Alg) Composite**

## 4.2.2 Characterization and Morphological Studies

### 4.2.3 FTIR Spectroscopy

Figure 4.2.1 illustrates FTIR spectra of NiF, NiFCMC and NiFCMC-Alg composites in between 4000-400  $\text{cm}^{-1}$  wavenumber range. There are two distinct strong peaks at 500-600  $\text{cm}^{-1}$  and 400-450  $\text{cm}^{-1}$  which are associated with the metal-oxygen bond in the tetrahedral site and metal-oxygen bond in the octahedral sites respectively which confirmed formation of a spinel metal ferrite. Both NiFCMC and NiFCMC-Alg showed a common strong characteristic peak at 3317.7  $\text{cm}^{-1}$  which corresponds to hydroxyl (-OH) group stretching and 2913  $\text{cm}^{-1}$  for aliphatic -CH stretching of the ether group resulting from carboxymethylation of cellulose. At 1594.9  $\text{cm}^{-1}$  and 1428.4  $\text{cm}^{-1}$  in the spectra of NiFCMC, the peak corresponds to vibrations owing to both symmetric and asymmetric COO- stretching of carboxylate group has been shifted to 1582.9  $\text{cm}^{-1}$  and 1416.3  $\text{cm}^{-1}$  in the spectra NiFCMC-Alg respectively indicating -COO<sup>-</sup> may take part in cross linking process<sup>53, 151</sup>. The distinct spectral bands at 1323  $\text{cm}^{-1}$  corresponds to C-O stretching and the peak at 1036.1  $\text{cm}^{-1}$  is due to >CH-O-CH<sub>2</sub> stretching of saccharide in the spectra of NiFCMC has been shifted to 1024  $\text{cm}^{-1}$  in the spectra of NiFCMC-Alg which confirmed that sodium alginate has been attached on the surface of NiFCMC<sup>53, 152, 153</sup>.

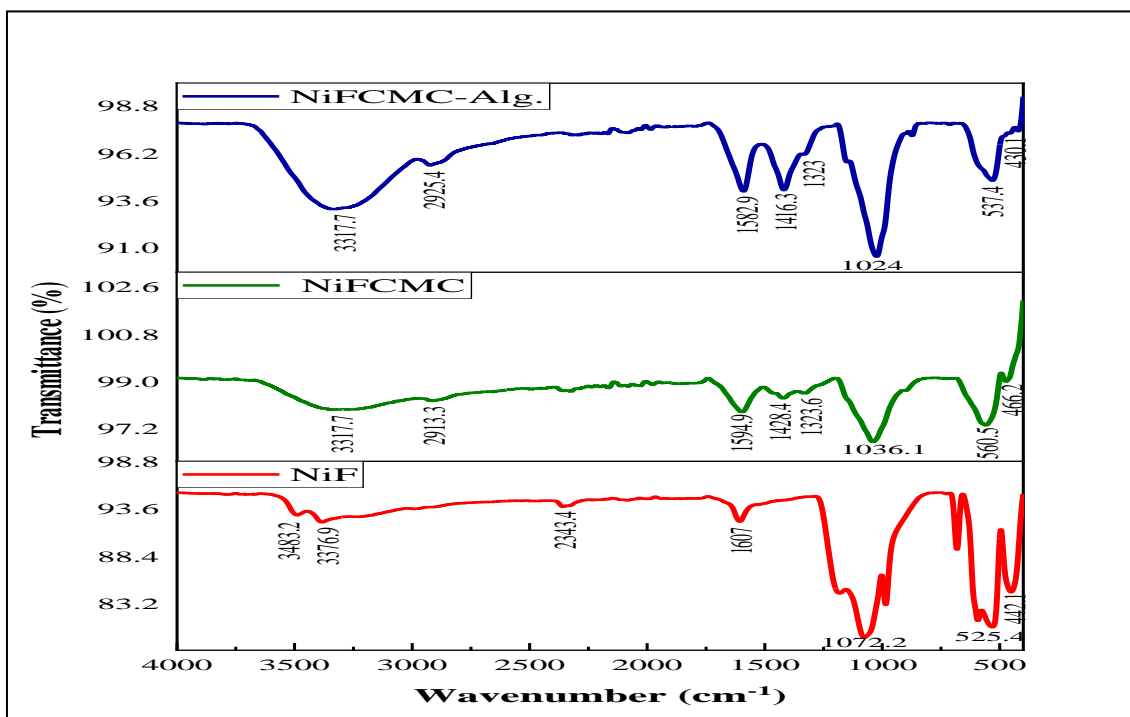


**Figure 4.2.1- FTIR image of (a) NiF (b) NiFCMC and (c) NiFCMC –Alg composite**

#### 4.2.4 X-ray Diffraction (XRD)

XRD pattern of NiF, NiFCMC and NiFCMC-Alg composite was represented in figure 4.2.2. Different diffraction peaks of NiF appeared at  $2\theta \sim 30.2, 33.1, 35.6, 37.2, 43.3, 53.8, 62.9$  and  $74.5^\circ$  showing peaks as (220), (311), (222), (400), (422), (511), (440), (620) known as Bragg's reflection <sup>154</sup>. The peaks showed that NiF in the spinel-like structure has greater crystallinity and phase purity. However, similar diffraction peaks with slight difference seemed in XRD pattern of NiFCMC and NiFCMC-Alg composite. The reason could be that on modification of surface, magnetic composite's size is increased. That cause the shift in the XRD angle <sup>155</sup>. The NiCMC and NiFCMC-Alg retained crystallinity and spinel character afterwards surface modification as indicated by result. The Scherrer formula was used to calculate the mean crystalline size of NiF, NiFCMC and NiFCMC-Alg as 21 nm, 25.63 nm and 38.42 nm.

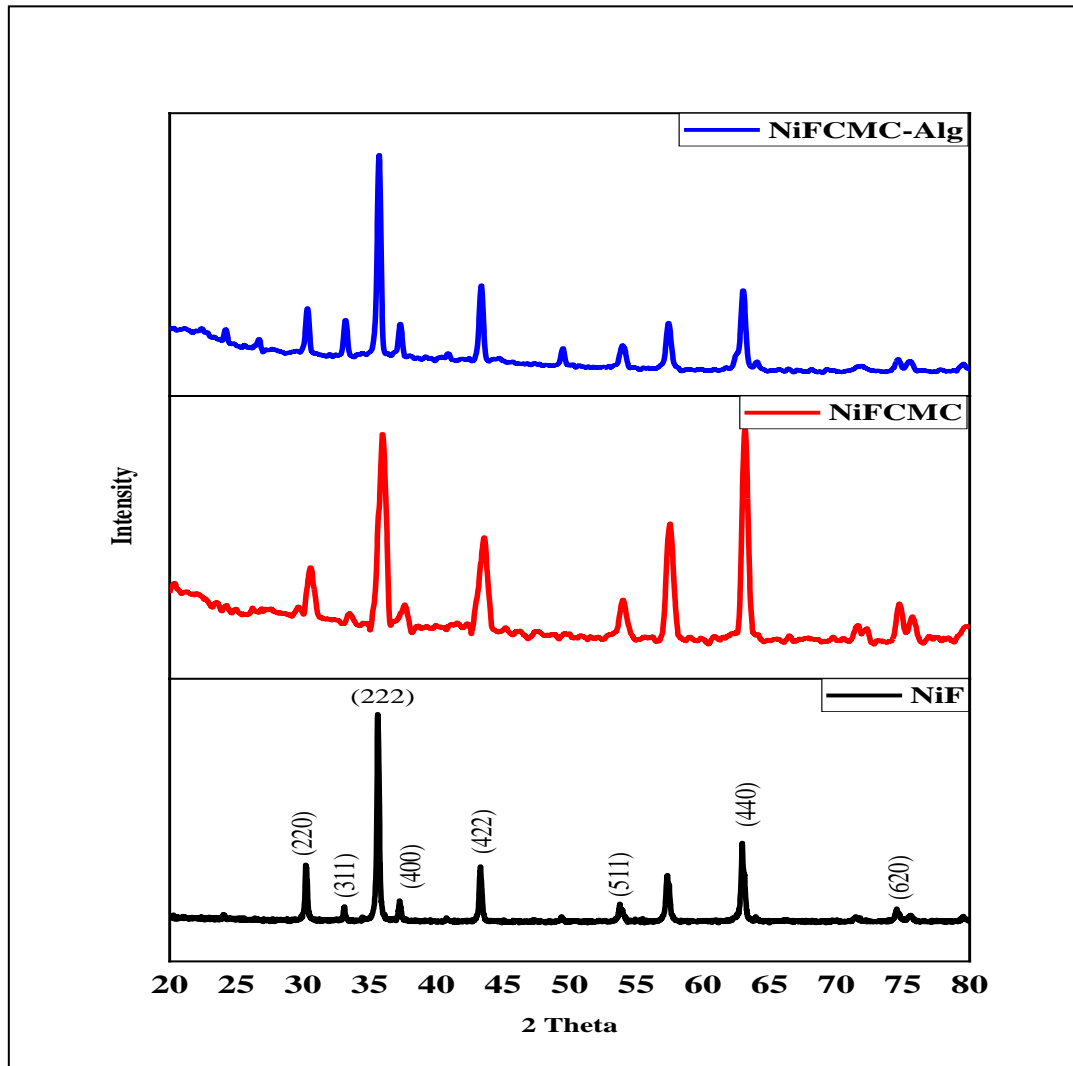
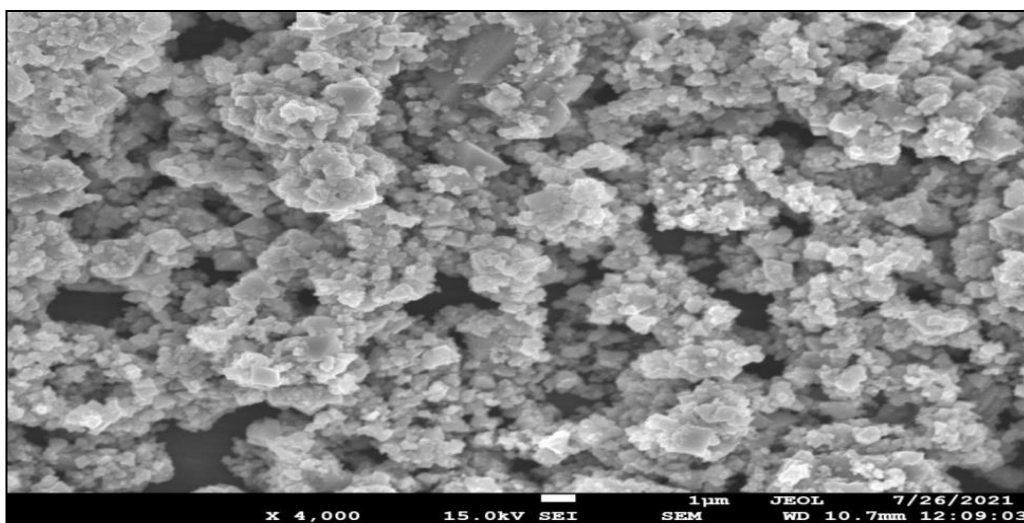


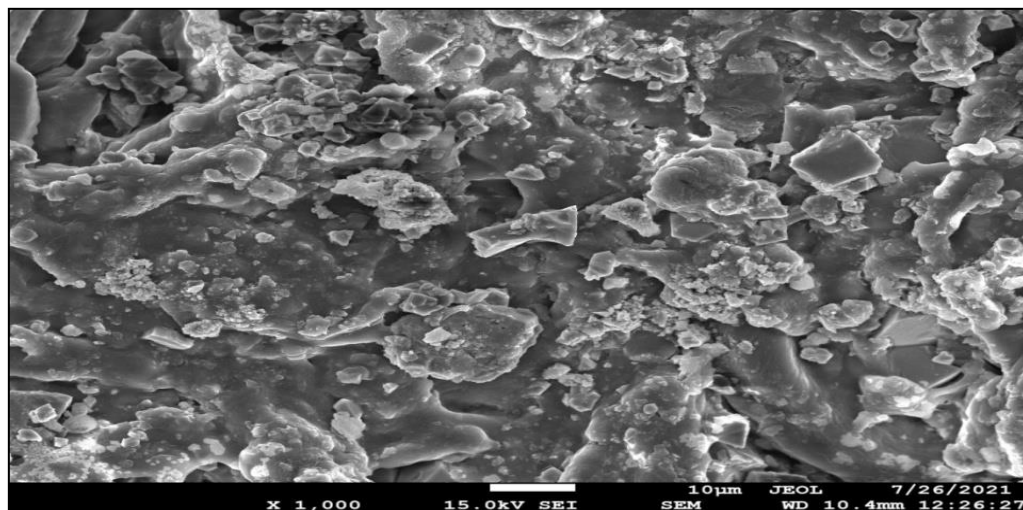
Figure 4.2.2- XRD of NiF, NiFCMC and NiFCMC-Alg

#### 4.2.5 Field Emission Scanning Electron Microscopy (FESEM)

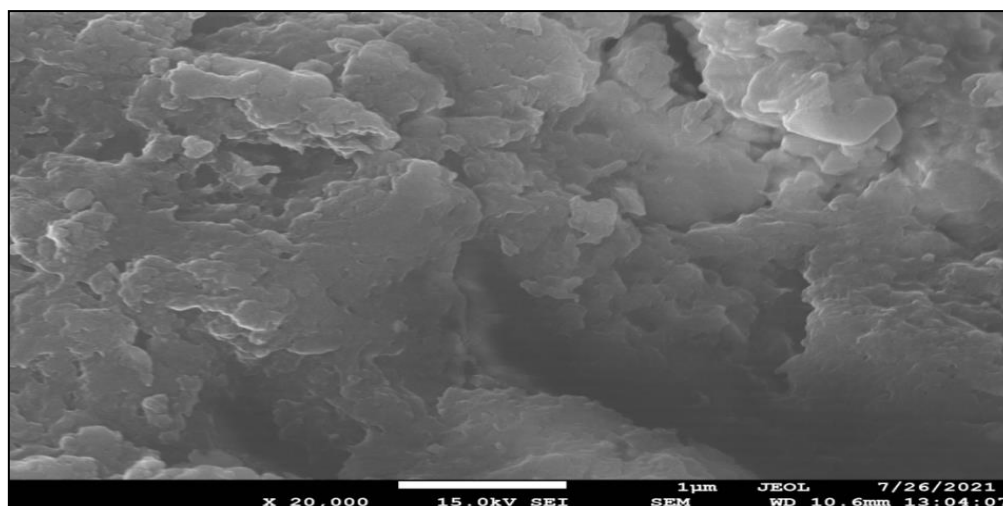
Figure 4.2.3 (a, b and c) shows the SEM images of NiF, NiFCMC and NiFCMC-Alg respectively. The crystalline structure of nickel ferrite, which is also indicated by the XRD spectra confirmed the spherical shaped homogeneous particles which are uniformly distributed. Some of the particles are also agglomerated <sup>156</sup>. The average size range of nickel ferrite was found to be 0.549  $\mu\text{m}$  and in case of NiFCMC, it was 3.54  $\mu\text{m}$  that indicated that the size of NiFCMC was larger than uncoated NiF. The surface was uneven but became more porous in NiFCMC as shown in figure 4.2.3 (b).



(a)



(b)



(c)

**Figure 4.2.3- FESEM pictures of (a) NiF (b) NiFCMC (c) NiFCMC-Alg**

The agglomeration was reduced which may be due to the layer of organic biopolymer content covering the magnetic nano particles <sup>156</sup>. Further in NiFCMC-Alg composite, the cross-section showed interior with more porosity on the surface. On the surface of the composite, the increased porosity may allow Ni (II) ions and dye particles to freely diffuse <sup>129</sup>.

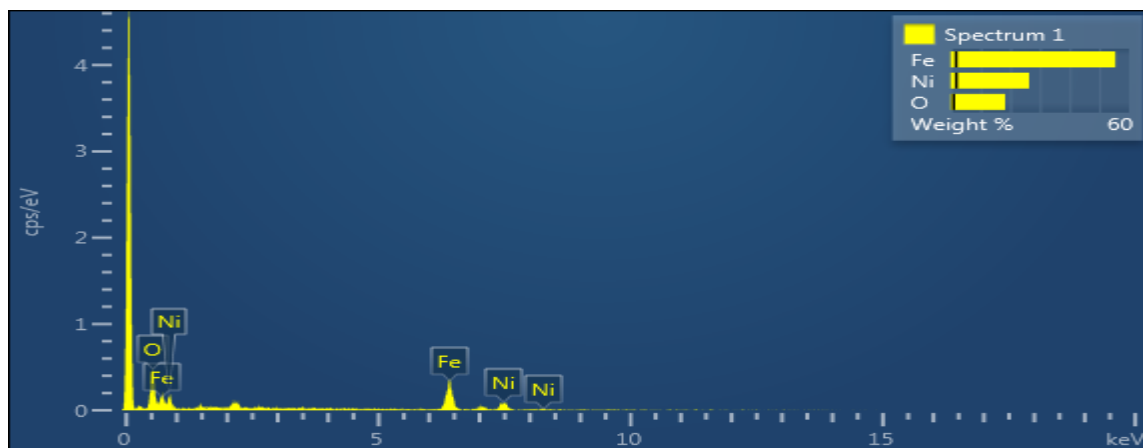
#### 4.2.6 Energy Dispersive Spectra (EDS)

Figure 4.2.4 (a, b and c) shows the EDS spectrum of NiF, NiFCMC, NiFCMC-Alg composites which represents distinct peak for each of constituent elements. The elemental makeup of each sample is shown in table 4.2.1 along with its atomic and weight percentages. The percentage of carbon content increased in NiFCMC-Alg composite as compared to NiFCMC as revealed by the results. It confirmed that sodium alginate and carboxymethyl cellulose were adhered to the nickel ferrite surface <sup>49</sup>.

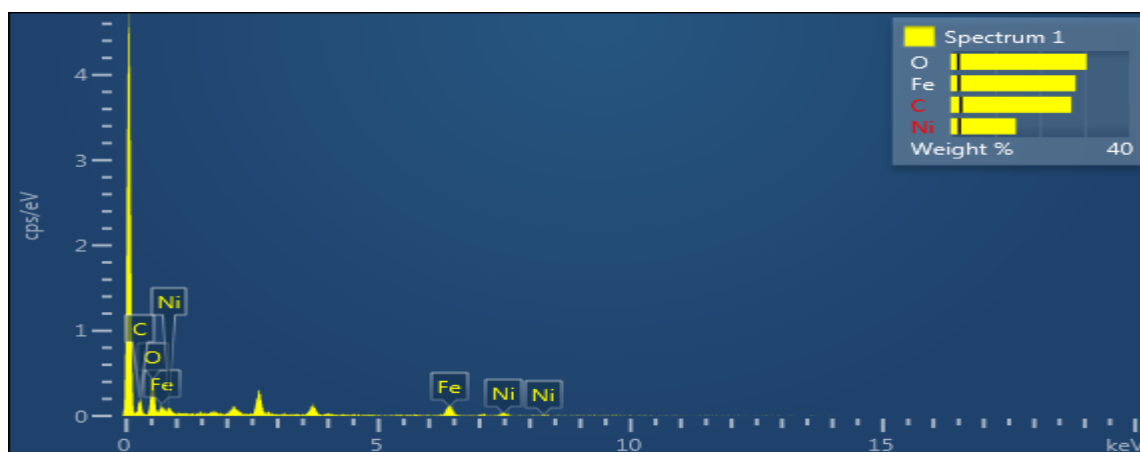
**Table 4.2.1- Elemental composition of NiF, NiFCMC, NiFCMC-Alg composite**

Element	NiF		NiFCMC		NiFCMC-Alg composite	
	Weight %	Atomic %	Weight %	Atomic %	Weight %	Atomic %
C	-	-	27.02	45.90	36.20	51.88
O	18.28	44.24	30.44	38.82	37.28	40.11
Fe	55.39	38.40	27.97	10.22	15.53	4.79

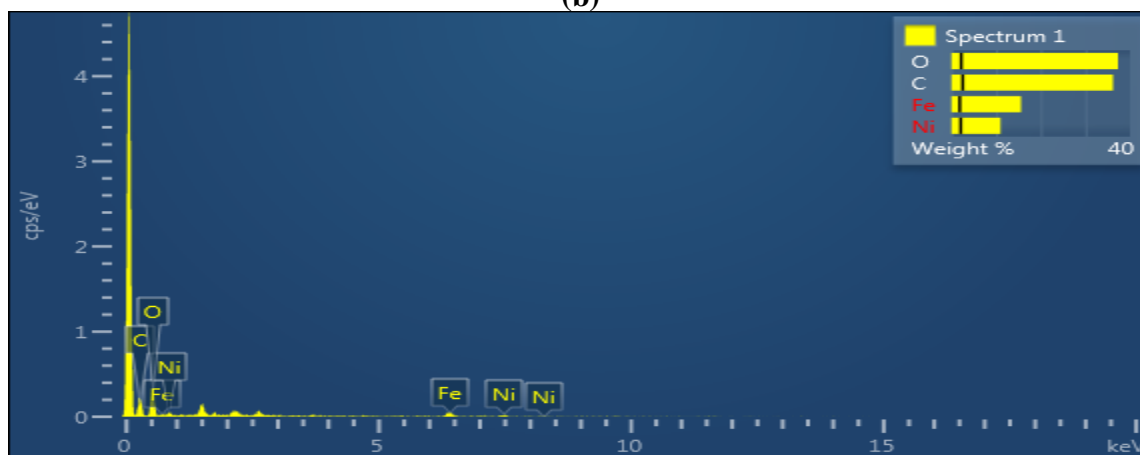
Ni	26.33	17.36	14.57	5.07	10.99	3.22
Total	100.00	-	100.00	-	100.00	-



(a)



(b)



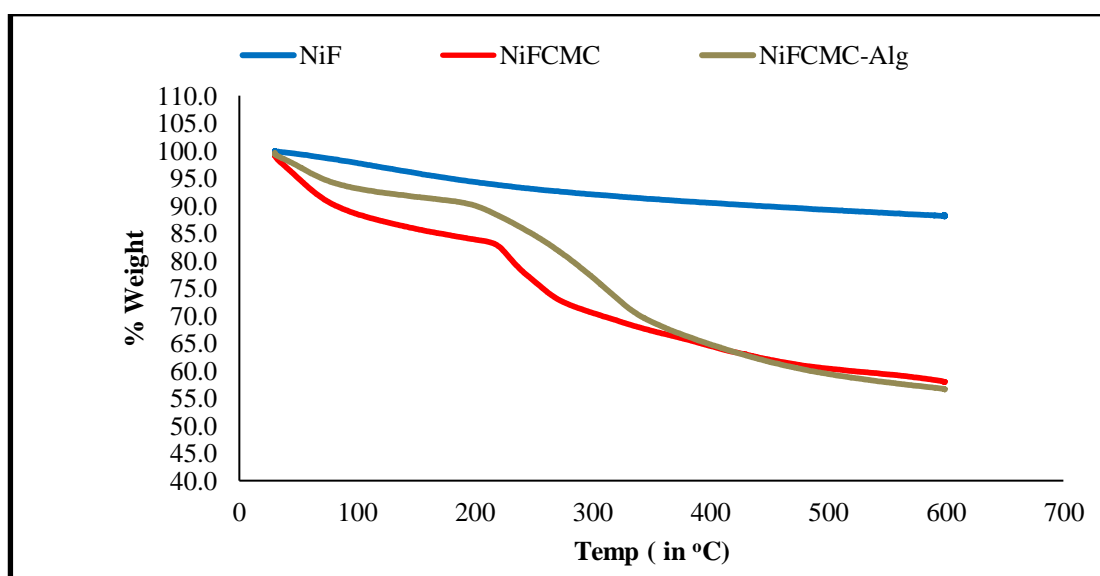
(c)

Figure 4.2.4- EDS graph for (a) NiF (b) NiFCMC (c) NiFCMC-Alg

#### 4.2.7 Thermogravimetric Analysis (TGA)

By the technique of thermo gravimetric analysis, thermal stability of the NiF, NiFCMC and NiFCMC-Alg was investigated. The sample was heated in air atmosphere with temperature ranged from 30 to 800°C having heating rate 10°C/minute. Figure 4.2.5 shows TGA of NiF, NiFCMC, NiFCMC-Alg.

A weight loss of 6–10% was observed at temperatures about 100°C, which may be caused by evaporation of trapped moisture in the samples. Around 250°C, additional weight loss of 4-8% was observed for NiFCMC and NiFCMC-Alg while 10-21 % weight loss at 350°C in NiFCMC and NiFCMC-Alg composite. The degradation and breakdown of organic functional groups of polymeric chain in the composite may be the cause of this weight loss. No further weight loss was noticed up to temperature 600-800°C<sup>155, 157</sup>. These results suggested that in 1 g of composite around 0.193 g of CMC and 0.245 g of CMC-sodium alginate was attached.



**Figure 4.2.5- TGA curves of NiF, NiFCMC and NiFCMC-Alg composite**

#### 4.2.8 Vibration Scanning Magnetometry (VSM)

Magnetic properties were calculated by measuring change in magnetization of sample with respect to changing magnetic field. Figure 4.2.6 (a, b and c) depicts the measurement from which a mild magnetization saturation of 0.59 emu/g, 0.43 emu/g and 0.21 emu/g was established for NiF, NiFCMC and NiFCMC-Alg respectively. This mild magnetization was attributed to presence of Fe<sub>3</sub>O<sub>4</sub> nanoparticles. As a result of polymerization, the slight increase in mass of NiFCMC and NiFCMC-Alg and decrease in percentage content of Fe from 55.39% in NiF to 27.97% in NiFCMC and

15.53% in NiFCMC-Alg as revealed in table 4.2.1 may be the cause of reduced magnetization. The composite still has magnetic properties and can be separated by the using magnet <sup>57</sup>.

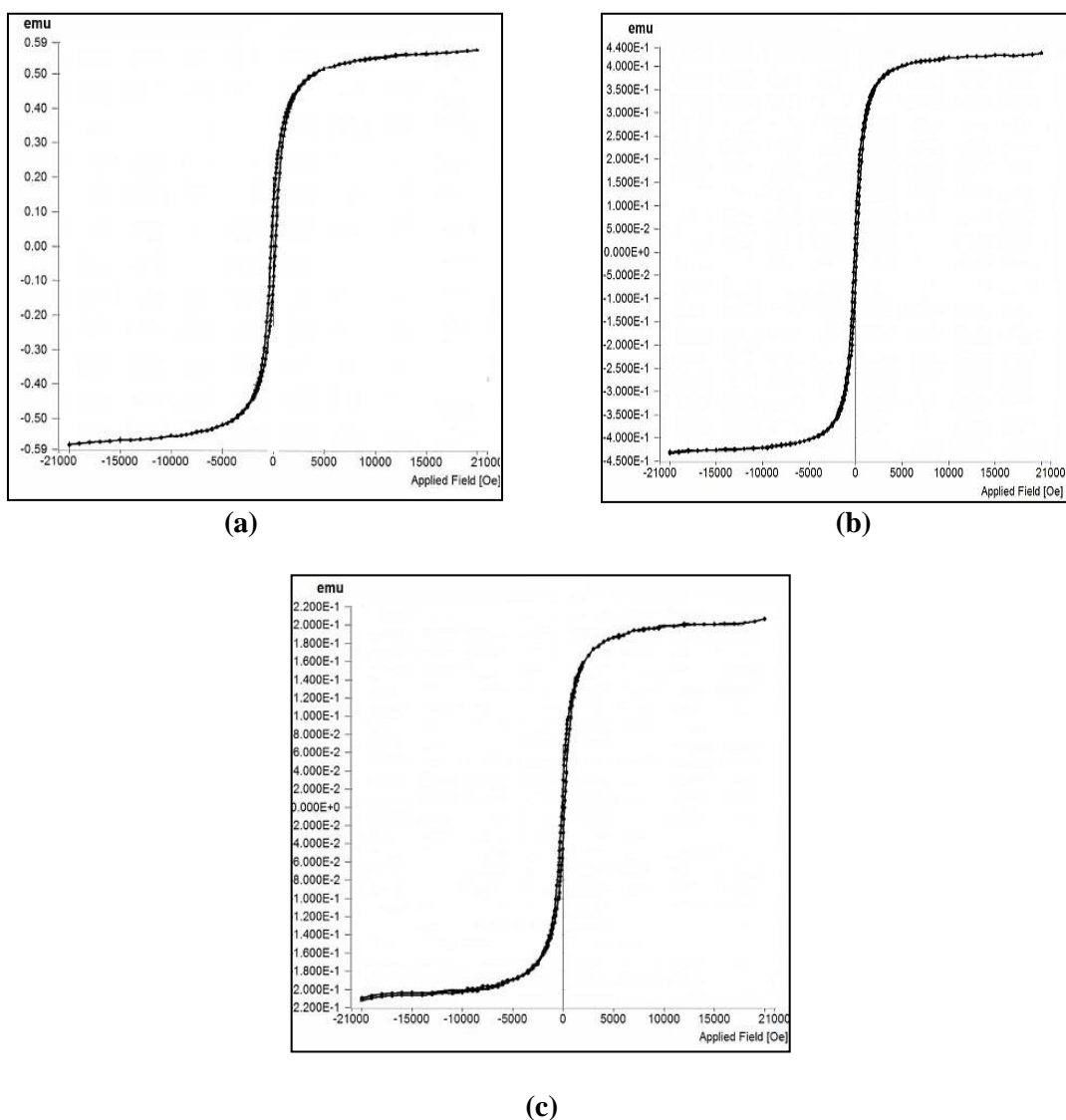


**Figure 4.2.6- Magnetization curve of (a) NiF (b) NiFCMC (c) NiFCMC-Alg**

#### 4.2.9 Point zero charge pH (pHpzc)

The pH of point zero charge (pHpzc) of prepared material represents the value of pH at which net surface charge of adsorbent is nil. Solid addition method was employed for calculating the pHpzc of magnetic composite. Figure 4.2.7 shows the graph between  $\Delta$  pH (initial –final) versus pH (initial) for NiFCMC and NiFCMC-Alg composite. The calculated values of pHpzc for NiFCMC and NiFCMC–Alg composite the computed values of pHpzc were 6.8 and 7.7 respectively.

The pHpzc value is important factor in adsorption process as it would depict the charge



on the adsorbent's surface. If the pH of the solution is less than pH<sub>pzc</sub> value, then the surface charge on the adsorbent would become positive and negatively charged species (anions) would be adsorbed. Conversely, if the pH of the solution is above the pH<sub>pzc</sub> value, then there would be net negative charge on the surface of adsorbent and it would attract positively charged species (cations). It revealed that there would be net positive and negative charge below and above this pH on the surface of magnetic composite <sup>143</sup>,  
158 .

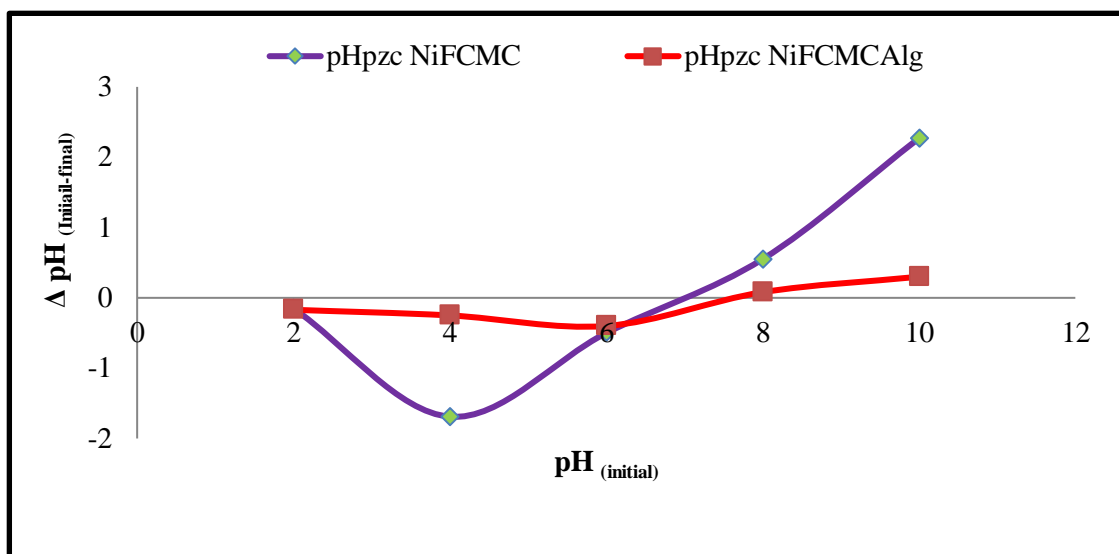


**Figure 4.2.7- pH<sub>pzc</sub> of NiFCMC and NiFCMC-Alg**

#### 4.2.10 Brunauer-Emmett-Teller (BET) Analysis

To characterize NiF, NiFCMC and NiFCMC-Alg composite in terms of specific area, pore volume and pore diameter, BET analysis is used. Table 4.2.2 shows the results of BET analysis. As compared to pure NiF, the surface area is decreased while pore diameter of the NiFCMC and NiFCMC-Alg composite were larger, which supports the successful surface modification of pure NiF due to increase in the size of the particle. These findings confirm the effective attachment of the CMC and alginate component to the pure NiF surface.

**Table 4.2.2- Results of BET analysis of NiF, NiFCMC and NiFCMC-Alg composite**

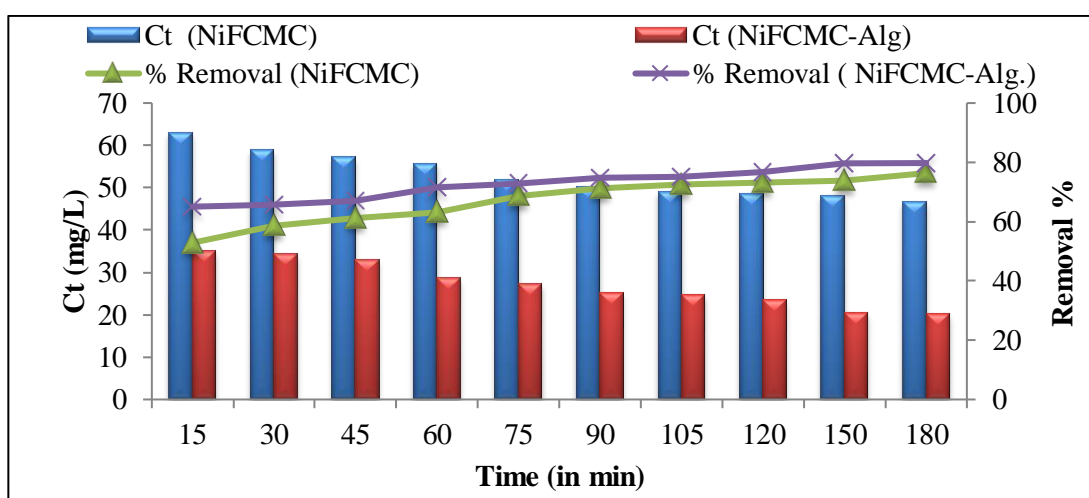
Parameters	NiF	NiFCMC	NiFCMC-Alg
Specific surface Area (in m <sup>2</sup> / g)	8.532	1.889	0.985
Total pore volume (cm <sup>3</sup> /g)	0.0250	0.00588	0.00235
Average Pore diameter (nm)	11.751	12.471	12.550

### 4.3. Batch Adsorption Studies with Ni (II) ions

NiFCMC and NiFCMC-Alg are used as adsorbents to study the adsorption behavior of Ni (II) ions in single metal ion system.

#### 4.3.1 Effect of contact time

Time is the factor on which the adsorption largely depends. For studying this effect, Ni (II) ions solution with known concentration (100 mg/L) and known volume (50 mL) were taken along with fixed amount of adsorbent in Erlenmeyer flasks for fixed temperature in thermostatic shaker. The flasks were removed from shaker at fixed time interval and reduced concentration of metal ion was noted by UV-spectrophotometer (Shimadzu UV-1800). The effect of time on concentration and percentage removal of Ni (II) ions using NiFCMC and NiFCMC-Alg is displayed in figure 4.3.1. It was evident from the figure that percentage removal proceeded quickly at the beginning and attained equilibrium after passage of time. This resulted from more available empty sites on the surface of the adsorbent at the initial stage and after sometime vacant sites got totally occupied and the rate of adsorption decreased until it reached equilibrium<sup>49, 78</sup>.

**Figure 4.3.1- Effect of contact time for Ni (II) ion**

#### 4.3.2 Effect of adsorbent dose

The influence of the dose of adsorbent on percentage removal for NiFCMC and NiFCMC-Alg is shown in Figure 4.3.2. To study this effect, a solution of known Ni (II) ion concentration (100 mg/L) with varying adsorbent dose (0.1 g to 0.5 g) was taken. The graph clearly showed an increase in removal percentage from 41.77 to 57.57% for NiFCMC and 75.22 to 95.78% for NiFCMC-Alg with increased amount of adsorbent. The increase in amount of dose cause the increase in number of active sites that cause the rise in removal percentage<sup>144</sup>. The optimum adsorbent dosage in the study was kept at 0.5 g.

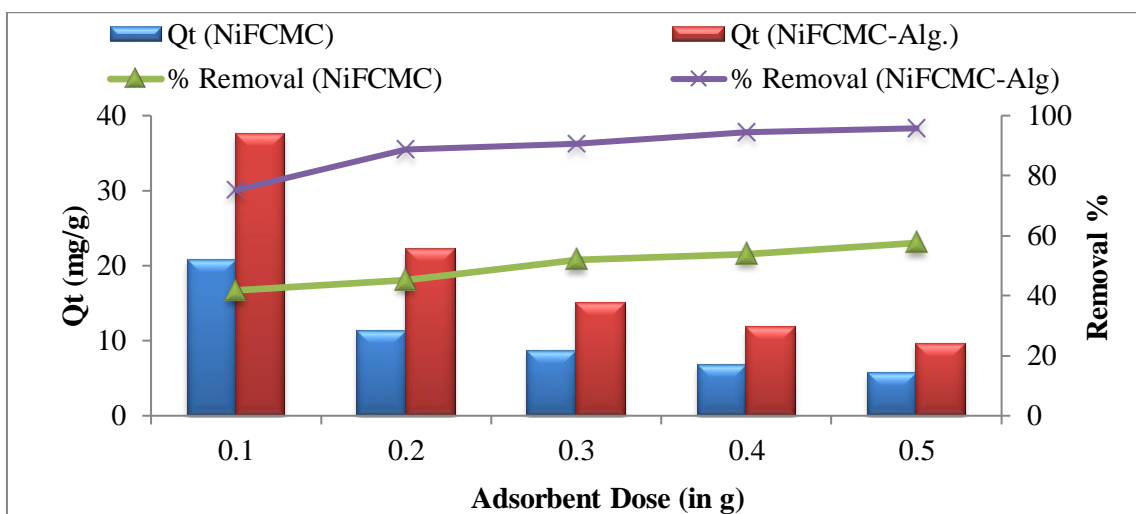


**Figure 4.3.2- Effect of adsorbent dosage for Ni (II) ions**

#### 4.3.3 Effect of pH

The pH of solution has direct effect upon adsorption behavior of adsorbent as adsorbent surface charge is influenced by pH. The experiment was carried at various pH levels from 2-10 which have 0.1 g adsorbent dose and fixed concentration of 100 mg/L of Ni (II) ion solution for equilibrium time of 3 h to explore the impact of pH. Figure 4.3.3 represents the effect of pH on the removal percentage of Ni ion solution for NiFCMC and NiFCMC-Alg. The maximum removal percentage was 43.55% for NiFCMC and 69.23% for NiFCMC-Alg respectively at pH 8 and further decreased. At higher pH  $>8$ , the removal percentage is decreased due to precipitation of Ni (II) ions and formation of Ni (OH)<sub>2</sub> species<sup>53</sup>.

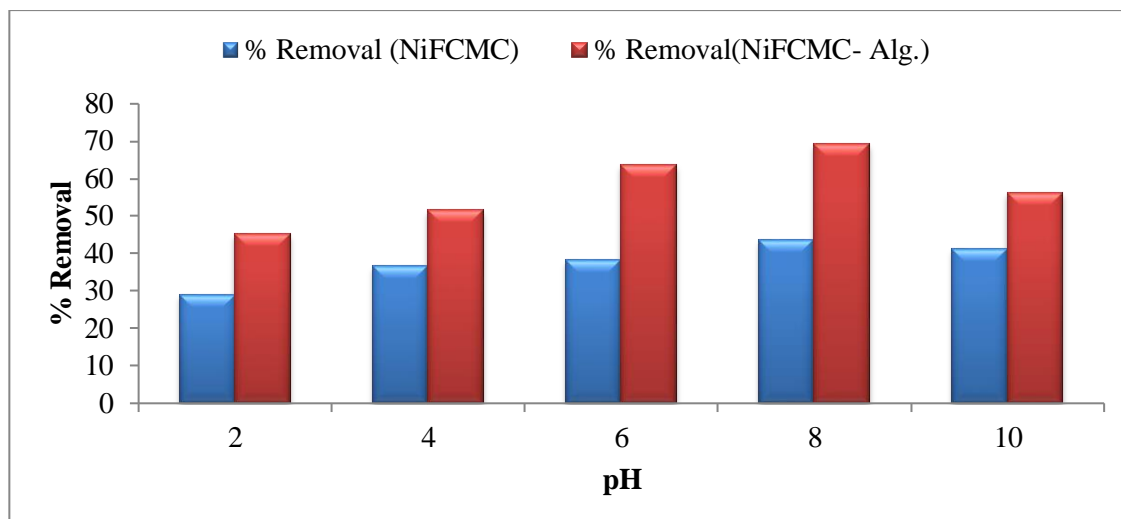


**Figure 4.3.3- Effect of pH on removal % of Ni (II) ions**

The NiFCMC-Alg composite behaved ionic above point zero charge value ( $pH_{pzc} = 7.7$ ) and at low pH, the electrostatic attraction was lesser. Because at lower pH value, there were more  $H^+$  ions in the aqueous solution both  $H^+$  and Ni (II) ions compete with one another to stick to the adsorbent surface. Smaller  $H^+$  ions bind to the empty site more quickly, while Ni (II) ions interact less electrostatically with the adsorbent surface. Since surface charge density decreased due to increase in electrostatic interaction that existed between molecules of adsorbent and metal ion, the degree of adsorption increased as pH increased <sup>53, 78</sup>.

#### 4.3.4 Adsorption Kinetics

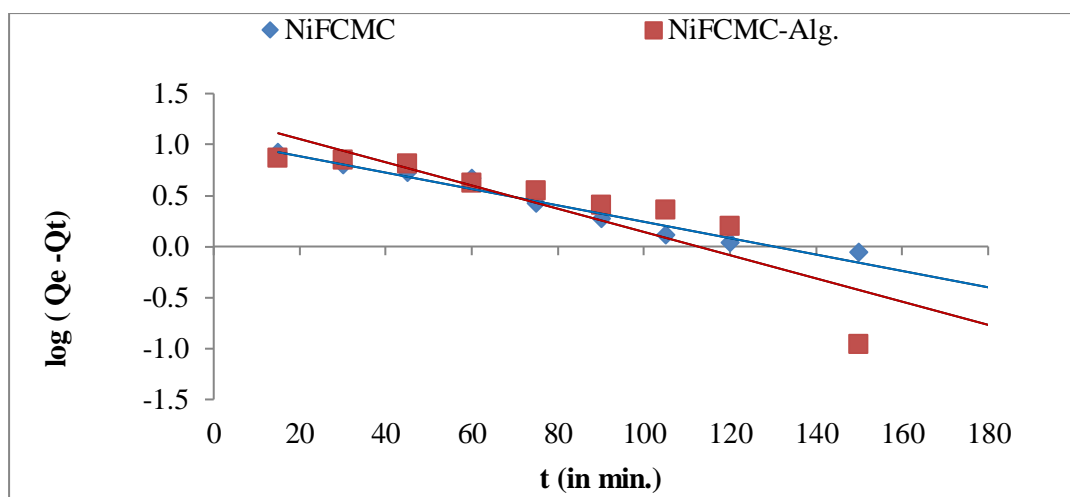
Adsorption kinetics defines the adsorption behaviour with respect to time. To ascertain the adsorption behaviour, different kinetic models like Lagergren pseudo first order, pseudo second order, Elovich and Weber- Morris diffusion model were investigated <sup>93, 104, 116</sup>. These models were fitted with data from adsorption investigations with regard to time and from the values of slope and intercept, the values of various constants were calculated.

The time study data was plotted after being fitted to the kinetic models mentioned above. Figure 4.3.4 (a-d) depicts Lagergren pseudo first, Lagergren pseudo second order, Elovich model and Intra particle diffusion model of kinetics respectively.

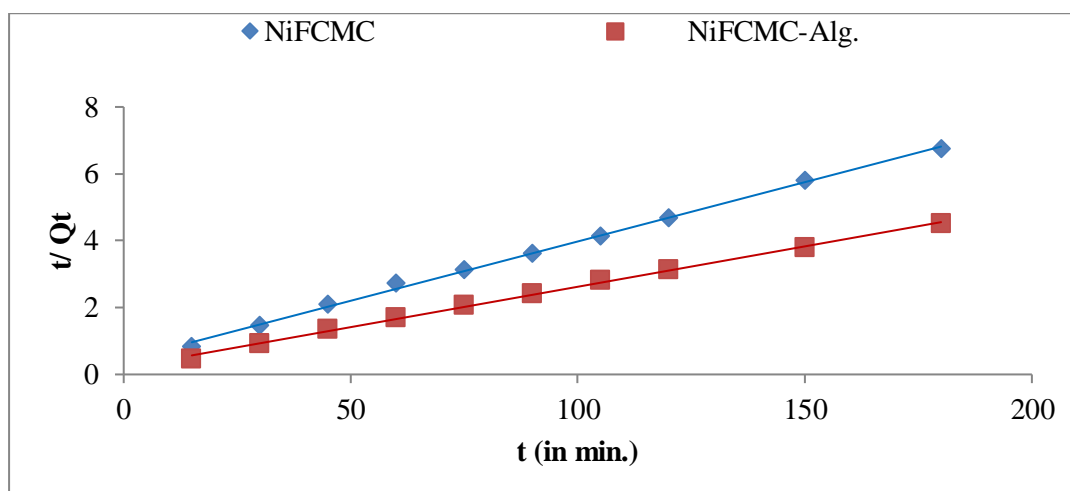
Table 4.3.1 provides a summary of the different calculated kinetic constants related to various models. The value of calculated correlation coefficients ( $R^2$ ) of different models was compared and best fitted value among various kinetic models was determined. Adsorption will be a physical process if the data meet pseudo first order kinetics while chemisorption will be the adsorption behaviour if the data is fitted effectively by pseudo second order

kinetic model <sup>78</sup>. From the table 4.3.1, it was revealed the data was most well fit by the Lagergren pseudo second order model, which had the greatest  $R^2$  value 0.998 and 0.998 whereas for Lagergren pseudo firstorder model,  $R^2$  value is 0.966 and 0.786 and for Elovich model the value of  $R^2$  was found to be 0.971 and 0.923 for NiFCMC and NiFCMC-Alg composite. It implied that for the adsorption of Ni (II) ions, the adsorption behaviour is chemisorption in nature.

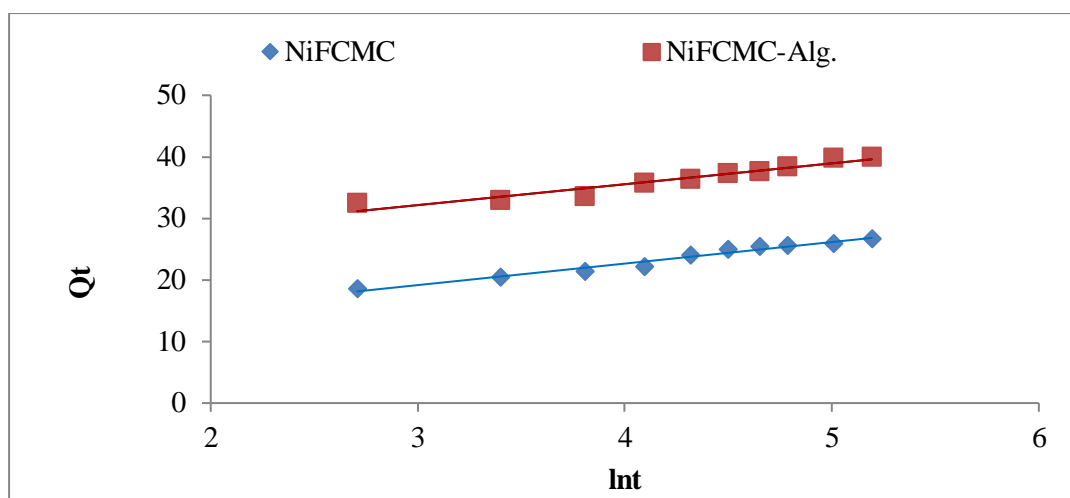
To study the intra-particle diffusion behaviour, Weber Morris diffusion model was used by plotting a graph between  $Q_t$  versus  $t^{0.5}$ . A straight line must pass through the origin if that step is the sole one that determines rate. The plot is not linear and line is not passing through the origin in case of both adsorbents as shown in figure 4.3.4 (d). It showed that there are other elements besides intra particle diffusion that have an impact on the adsorption rate <sup>69</sup>.



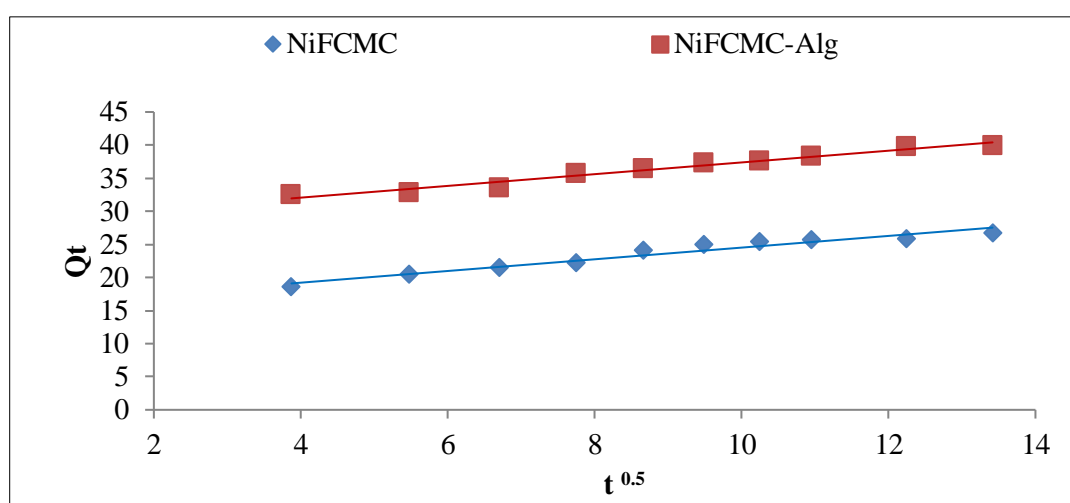
(a)



(b)



(c)



(d)

**Figure 4.3.4- Various kinetic adsorption models (a) Pseudo first order kinetic model (b) Pseudo second order kinetic model (c) Elovich model (d) Weber-Morris diffusion model**

**Table 4.3.1- Calculated values of constants of various kinetic models used for NiFCMC and NiFCMC-Alg of Ni (II) ions**

System→ Kinetic model ↓	Parameter	For NiFCMC	For NiFCMC-Alg
Lagergren Pseudo first order	$Q_e$	11.117	19.138
	$k_1$	0.0184	0.0262
	$R^2$	0.966	0.786

<b>Lagergren Psuedo second order</b>	$Q_e$	28.169	41.493
	$h$	2.327	4.831
	$K_2$	0.0029	0.0028
	$R^2$	0.998	0.998
<b>Elovich model</b>	$\alpha$	2222.11	41.872
	$\beta$	0.294	0.286
	$R^2$	0.971	0.923

#### 4.3.5 Effect of Concentration and temperature

Ni (II) ions solution at varying concentrations (100 to 300 mg/L) was used for studying adsorption. It was evident from figure 4.3.5 that with the increase in initial concentration of metal ion solution, the adsorption capability ( $Q_e$ ) of both adsorbents increases and found maximum at 300 mg/L. On increasing the metal ion concentration, there are more interactions occur between adsorbate and adsorbent<sup>49, 149</sup>. However, with increased concentration of the solution, there showed a decrease in removal percentage of Ni (II) ions. This might be because as the concentration of metal ions increase, fewer active sites become available on surface of the adsorbent.

At various temperatures (25°C, 30°C and 35°C), the impact of concentration was investigated. The adsorption behaviour of Ni (II) ions increased with rise in temperature in both adsorbents. It was due to the reason that with increase in temperature, the adsorbate and adsorbent interact more readily<sup>7</sup>. The temperature rise cause an increase in number of pores which increases the surface area of the adsorbent and speeds up the adsorption process<sup>78, 159</sup>.

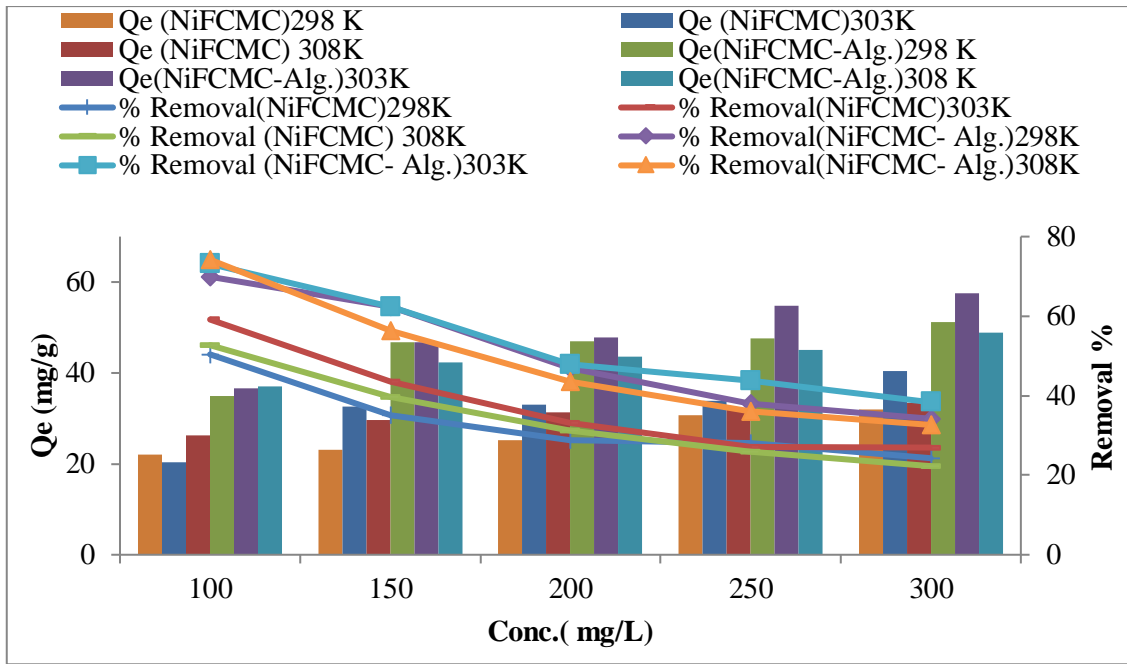


**Figure 4.3.5- Effect of concentration for NiFCMC and NiFCMC-Alg composite**

#### 4.3.6 Adsorption Isotherms

Under equilibrium conditions, numerous isotherms models like Langmuir, Freundlich, Temkin and Dubinin-Radushkevich (D-R) were employed to study the adsorption behaviour.

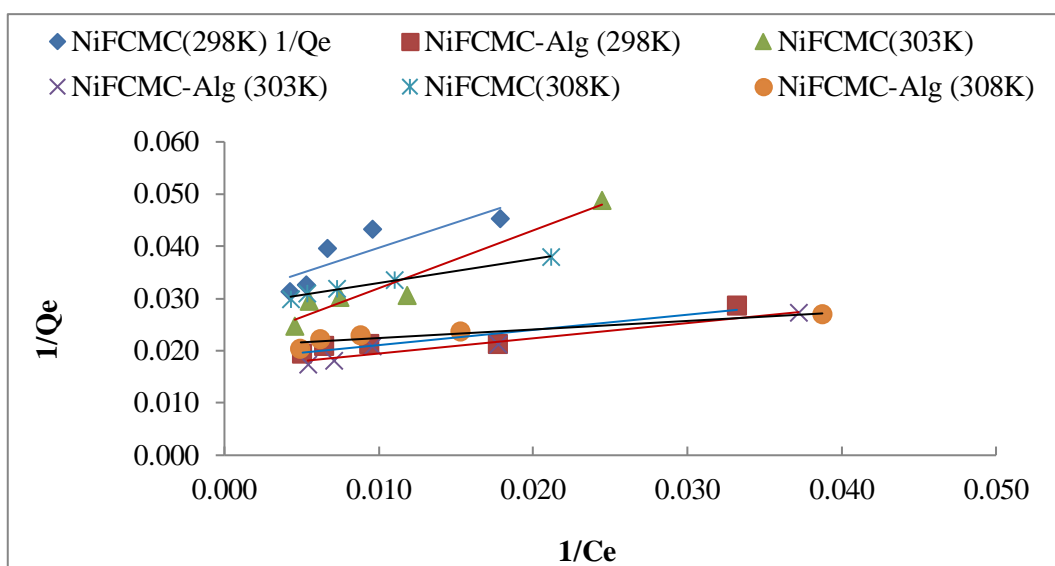
The slope and intercept of the graphs shown in figure 4.3.6 were used to compute values of different constants. Different adsorption isotherm models correlation coefficients ( $R^2$ ) were compared and it was observed that the  $R^2$  value of the Langmuir isotherm model was higher (0.916, 0.938, 0.992 for NiFCMC and 0.892, 0.947 and 0.904 for NiFCMC - Alg) than those of the Freundlich (0.836, 0.867, 0.986 for NiFCMC and 0.773, 0.941 and 0.947 for NiFCMC-Alg, Temkin (0.814, 0.873, 0.993 for NiFCMC and 0.791, 0.941 and 0.934 for NiFCMC-Alg and D-R models (0.551, 0.927, 0.928 for NiFCMC and 0.944, 0.861 and 0.792 for NiFCMC-Alg at 298 K, 303 K and 308 K respectively) as computed in the table 4.3.2 and the Langmuir model provided the greatest fit for the adsorption data. NiFCMC and NiFCMC-Alg were found to have Langmuir adsorption capabilities of 47.84 and 60.24 mg/g.

One of the crucial variables associated with the Langmuir adsorption isotherm is the separation factor ( $R_L$ ). According to the computed value of  $R_L$ , there are four types of adsorption behaviour: unfavourable ( $R_L > 1$ ), linear ( $R_L = 1$ ), favourable ( $0 < R_L < 1$ ) and

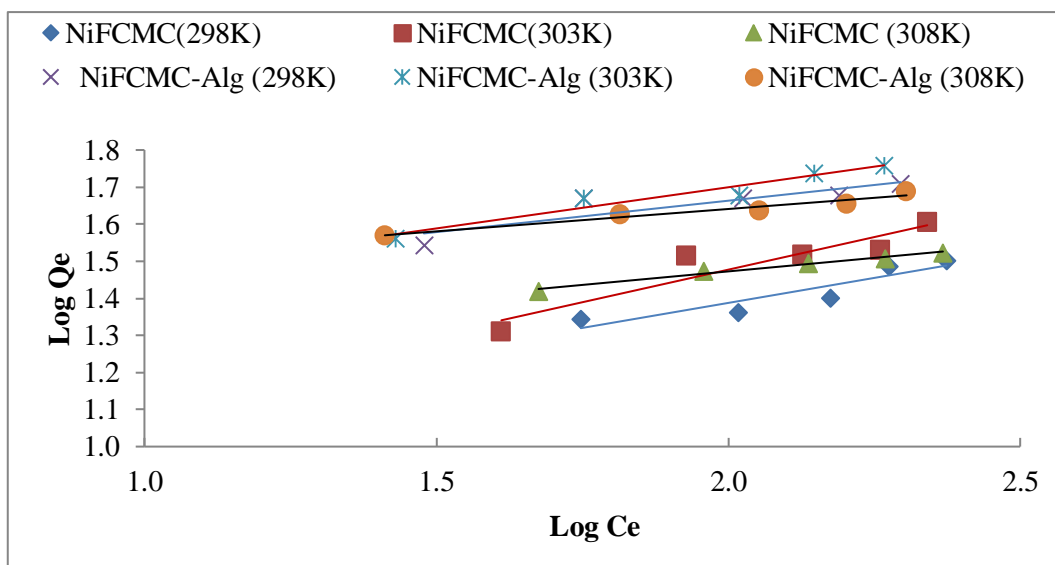


irreversible ( $R_L=0$ ). Langmuir adsorption process was advantageous in the current study as evidenced by  $R_L$  value which ranges between 0 and 1.

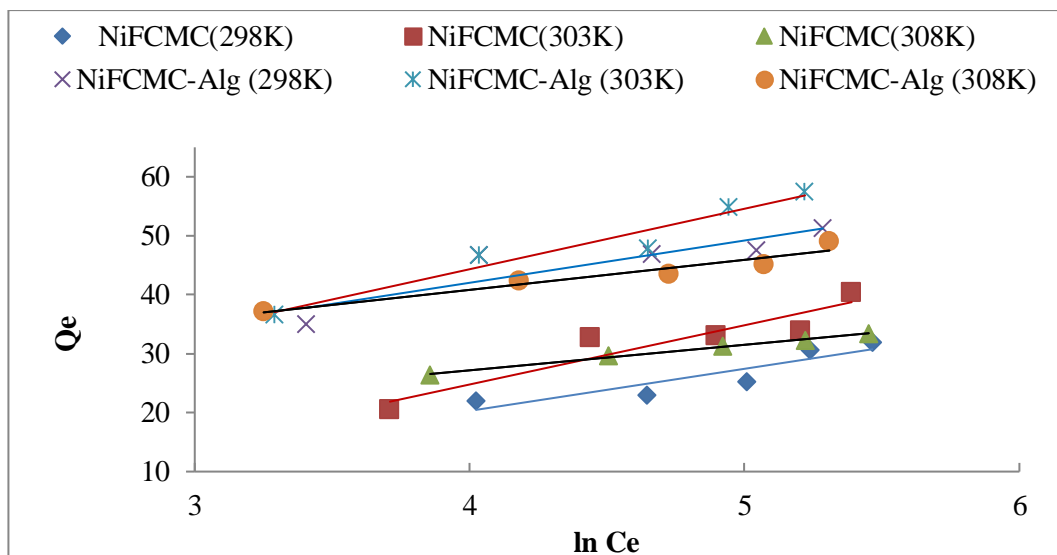
One of the parameters which is used in the D-R model called adsorption energy is helpful in determining the kind of adsorption. If predicted energy of adsorption is above 40 kJ/mol, in that scenario chemisorption will occur; otherwise physical adsorption will occur. Table 4.3.2 showed the calculated value of adsorption energy more than 50 kJ/mol for NiFCMC and more than 100 kJ/mol for NiFCMC-Alg adsorbent revealed that chemisorption occurred in the current work.



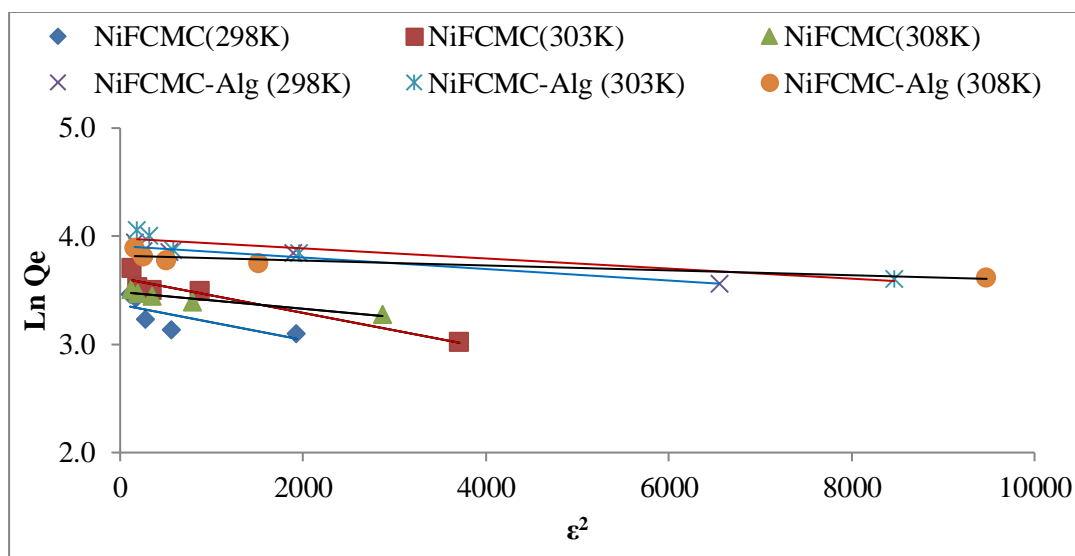
(a)



(b)



(c)



(d)

**Figure 4.3.6- (a-d) Plot of different adsorption isotherms (a) Langmuir (b) Freundlich (c) Temkin (d) D-R isotherm**

**Table 4.3.2- Various adsorption isotherm constants of NiFCMC and NiFCMC-Alg composite for Ni (II) ions**

System→ Isotherm model ↓	Constant	For NiFCMC			For NiFCMC-Alg		
Temperature		25°C	30°C	35°C	25°C	30°C	35°C

<b>Langmuir</b>	<b>Q</b>	33.33	47.84	35.21	54.94	60.24	48.07
	<b>B</b>	0.031	0.018	0.061	0.062	0.057	0.127
	<b>R<sup>2</sup></b>	0.916	0.938	0.992	0.892	0.947	0.904
	<b>R<sub>L</sub></b>	0.244	0.347	0.139	0.138	0.149	0.073
<b>Freundlich</b>	<b>K<sub>f</sub></b>	7.0	5.9	15.1	21.1	18.0	25.1
	<b>1/n</b>	0.269	0.351	0.146	0.169	0.222	0.120
	<b>R<sup>2</sup></b>	0.836	0.867	0.986	0.773	0.941	0.947
<b>Temkin</b>	<b>b<sub>T</sub></b>	353.4	250.8	581.7	351.4	245.5	494.3
	<b>A</b>	0.316	0.215	9.733	6.442	1.378	55.14
	<b>R<sup>2</sup></b>	0.814	0.873	0.993	0.791	0.941	0.934
<b>D-R model</b>	<b>Q<sub>m</sub></b>	29.0	37.1	32.6	49.9	53.5	45.6
	<b>K</b>	2×10 <sup>-4</sup>	2×10 <sup>-4</sup>	8×10 <sup>-5</sup>	5×10 <sup>-5</sup>	5×10 <sup>-5</sup>	2×10 <sup>-5</sup>
	<b>R<sup>2</sup></b>	0.551	0.927	0.928	0.944	0.861	0.792
	<b>E</b>	50.0	50.0	79.1	100.0	100.0	158.1

As per the literature review, the adsorption studies for Ni (II) ions with different adsorbents were reviewed. Table 4.3.3 represents the Langmuir adsorption capacity (Q<sub>e</sub>) of different adsorbents for adsorption of Ni (II) ions as reported in previous studies. On comparing, it was observed that NiFCMC and NiFCMC-Alg composites might be suitable eco-friendly adsorbent to remove Ni (II) ions from aqueous solution. Among these two composites, NiFCMC-Alg composite showed high adsorption capacity to remove Ni (II) ions from aqueous solution.

**Table 4.3.3- Comparative study showing adsorption capacity of several adsorbents for Ni (II) ions**

Adsorbent used	Q <sub>e</sub> (mg/g)	Reference
Cellulose alginate hydroxyapatite beads	41.95	<sup>21</sup>
Calcium alginate/ coffee beads	20.96	<sup>160</sup>
Alginate and magadiite Di-(2-ethylhexyl) phosphoric acid	44	<sup>107</sup>
Ca-alginate impregnated hemp fibers	12	<sup>161</sup>
Nickel ferrite CMC Nickel ferrite CMC-Alginate composite	47.84 60.24	Present study

#### 4.3.7 Adsorption Thermodynamics

Adsorption thermodynamic describes the energy evolution in adsorption reaction proceeding from initial state to final state. To define the kind of adsorption process, different thermodynamic characteristics have been used including  $H^\circ$ ,  $G^\circ$  and  $S^\circ$ . From the values of slope and intercept of linear plot of  $\ln K_d$  vs  $1/T$  are used to compute the values of  $H^\circ$  and  $S^\circ$  as shown in figure 4.3.7.

Table 4.3.4 contains the various adsorption thermodynamic parameters that were determined. For both adsorbents, calculated values for  $\Delta H^\circ$  and  $\Delta S^\circ$  were found to be positive indicating the endothermic nature of the adsorption process and also signifies strong interactions between adsorbate and adsorbent molecule. The calculated value  $\Delta G^\circ$  was negative at 25°C, 30°C and 35°C for concentrations 100, 150 and 200 mg/L for NiFCMC-Alg while for NiFCMC composite,  $\Delta G^\circ$  was negative at concentration 150 to 250 mg/L at 25°C, 30°C and 35°C g/L respectively suggest spontaneous. The calculated  $\Delta G^\circ$  values were found to be less than 5 kJ/mol that indicated that adsorbents were easily regenerable <sup>70, 78, 147</sup>.

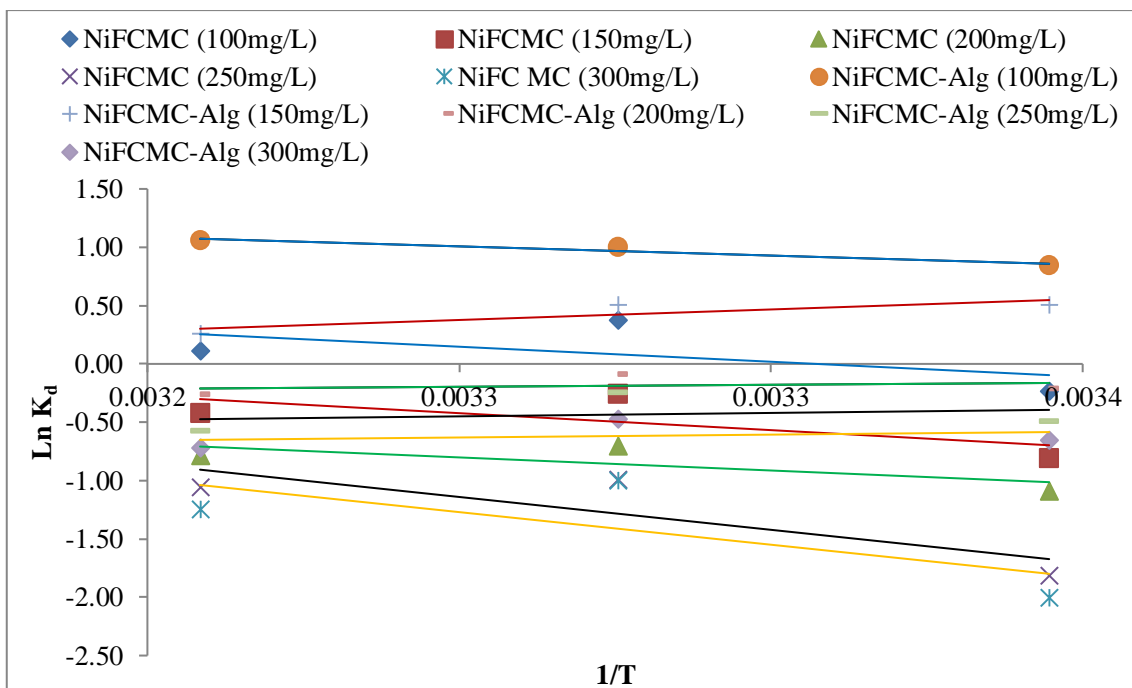


Figure 4.3.7- Plot of  $\ln K_d$  versus  $1/T$  for Ni (II) ions

Table 4.3.4- Calculated thermodynamic parameters for Ni (II) ions

System	Conc. (mg/L)	$\Delta H^\circ$ (KJ/mol)	$\Delta S^\circ$ (KJ/mol/ K)	$\Delta G^\circ$ (25°C) (KJ/mol)	$\Delta G^\circ$ (30°C) (KJ/mol)	$\Delta G^\circ$ (35°C) (KJ/mol)
<b>NiFCMC</b>	100	26.8	0.089	0.589	0.370	-0.275
	150	30.2	0.096	-2.018	-0.259	-1.080
	200	23.3	0.070	-2.698	-0.706	-2.012
	250	58.5	0.182	-4.504	-0.990	-2.704
	300	58.1	0.180	4.964	-0.998	3.199
<b>NiFCMC-Alg</b>	100	16.37	0.062	-2.086	-2.521	-2.704
	150	2.74	0.013	-1.241	-1.274	-1.374
	200	1.70	0.005	0.304	-0.219	-0.261
	250	-0.86	0.006	1.206	0.621	1.283
	300	-5.08	0.022	1.622	1.197	1.855

#### 4.3.8 Regeneration of Adsorbent

Regeneration efficiency is an important component to define the performance and cost effectiveness of adsorbent after recycling. In the present study, NiFCMC and NiFCMC-Alg composite were regenerated with 0.1N HCl as desorbing solvent. The regeneration efficiency was studied up to five cycles. Regeneration efficiency and percentage weight loss for both adsorbents are shown in table 4.3.5 and figure 4.3.8. It was evident from the table 4.3.5 that regeneration efficiency % for NiFCMC and NiFCMC-Alg after five cycles was still 81.3% and 77.2%. The weight loss after five cycles of adsorption-desorption was also studied after five cycles and a loss of 18.7% and 22.8% weight for NiFCMC and NiFCMC-Alg adsorbent was reported respectively. The results revealed that NiFCMC and NiFCMC-Alg composite was suitable cost effective alternative for the removal of Ni (II) ions from aqueous medium <sup>49, 53</sup>.

**Table 4.3.5- Regeneration performance of adsorbent NiFCMC and NiFCMC-Alg composite**

Regeneration Cycle	Regeneration Efficiency		Wt. loss % of adsorbent after five cycles	
	NiFCMC	NiFCMC-Alg	NiFCMC	NiFCMC-Alg
1	98.3	97.7	18.7	22.8
2	93.8	92.5		
3	89.8	87.2		
4	85.6	82.6		
5	81.3	77.2		

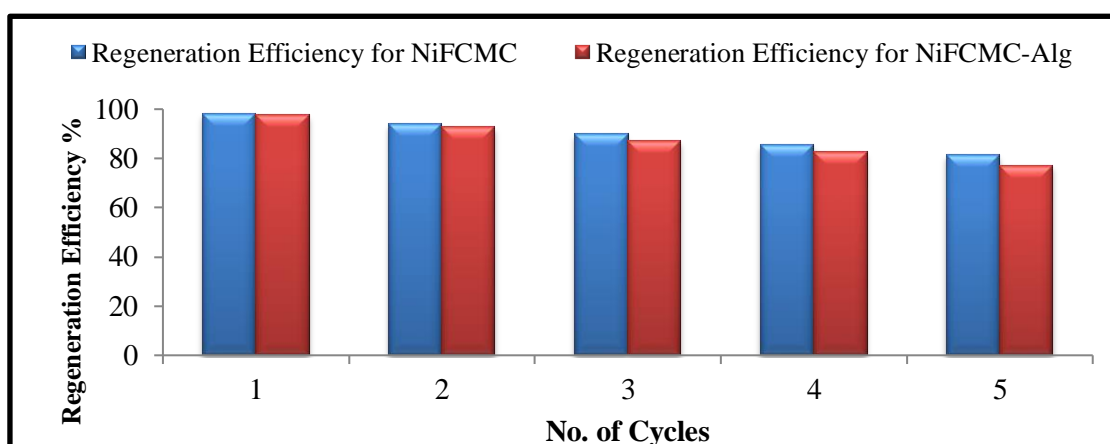


**Figure 4.3.8- Percentage regeneration efficiency of NiFCMC and NiFCMC-Alg composite**

### Part –III

#### 4.4 Result of Batch Adsorption Studies of single and binary dye systems for NiFCMC and NiFCMC-Alg composite

##### 4.4.1. Effect of Contact Time

Adsorption changes as the time changes. To study this effect, a known quantity (0.1 g) of adsorbent (NiFCMC and NiFCMC-Alg) was added to dye solutions with known concentrations (50 mg/L for single and 20 mg/L for binary systems) and 50 mL volumes in 250 mL Erlenmeyer flasks for fixed temperature at 150 rpm in a thermostatic shaker. The flasks were taken out of the shaker after the fixed time interval and lowered concentrations of dyes were measured with the help of the UV spectrophotometer (Shimadzu UV-1800).

Figure 4.4.1 illustrates the influence of contact time on concentration (Ct) and removal percentage for CV and MB in both single as well as binary dye systems. The removal percentage tends to increase rapidly before reaching equilibrium over time. This was caused by the adsorbent's surface having more available empty spaces. Consequently, empty spaces eventually filled up entirely and the adsorption rate slowed down till equilibrium was reached over time <sup>49, 143</sup>.

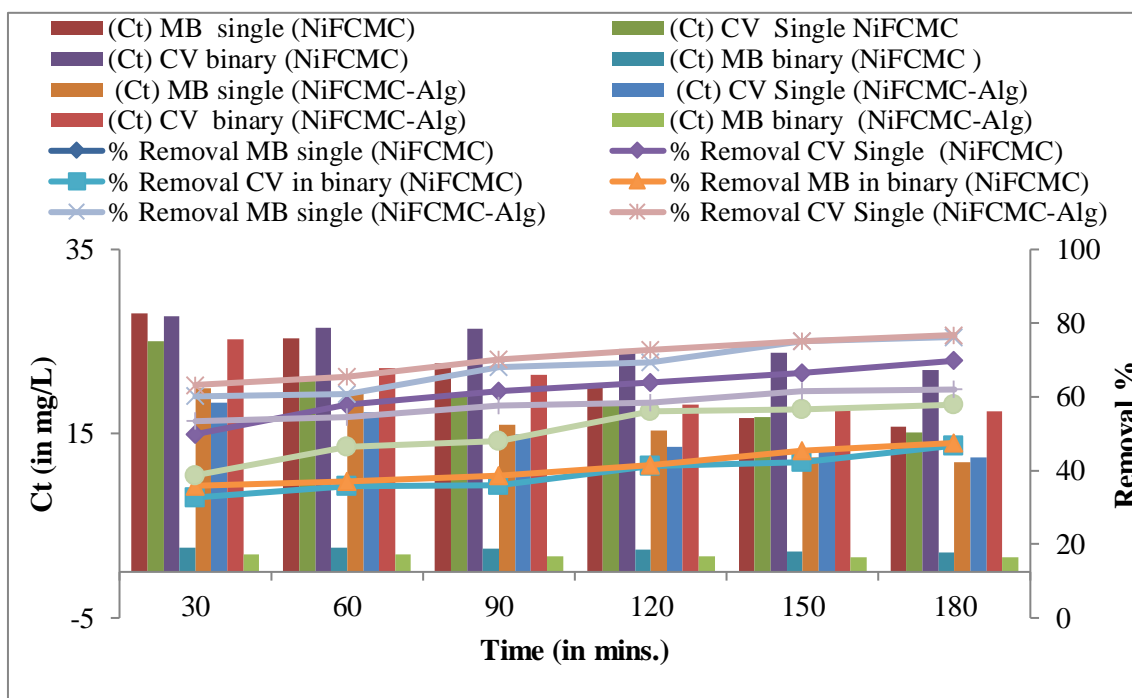


Figure 4.4.1- Effect of contact time in single and binary dye systems

#### 4.4.2 Effect of adsorbent dose

Figure 4.4.2 shows the effect of adsorbent dose on percentage removal for NiFCMC and NiFCMC-Alg in both single as well as binary systems. A solution with known dye concentrations (50 mg/L for single dye system and 20 mg/L for binary dye system) and adsorbent doses (0.1 g to 0.5 g) was used to study this effect. It was found that adding more adsorbent enhanced the removal percentage from 50.21% to 71.40% of MB and 50.51% to 63.19% of CV by NiFCMC while 64.80% to 75.02% for MB and 60.74% to 74.03% of CV by NiFCMC-Alg in single dye system. Percentage removal of dyes is found to be less in binary system as compared to single dye system. An increase in the removal percentage could be the result of more active sites available as the adsorbent dosage increases in single and binary systems<sup>53, 69</sup>. In the present work, 0.5 g of adsorbent was the optimal adsorbent dosage.

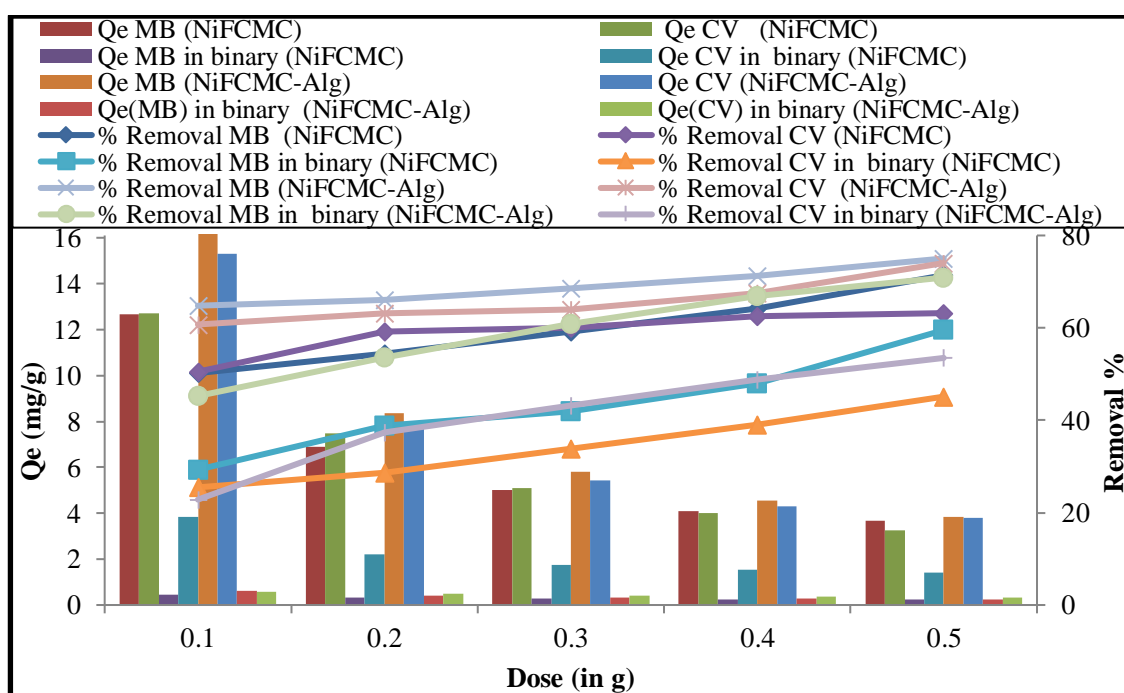


Figure 4.4.2- Effect of adsorbent dosage in single as well as binary dye systems

#### 4.4.3 Effect of pH

The material's adsorption behaviour is directly impacted by pH since it changes the charge on the adsorbent's surface. The investigation was carried out with a single dye system at different pH values between 2 and 10, with 50 mg/L initial dye concentration and 0.1 g adsorbent dose allowing for 3 hours time to attain equilibrium. The effect of pH on removal percentage of MB and CV dye solution for adsorbents is displayed in



figure 4.4.3. At pH 8, the maximum removal percentage was 62.19% and 62.87% in NiFCMC for MB dye while 64.34% and 65.84% in NiFCMC-Alg for CV dye respectively and then further decreased.

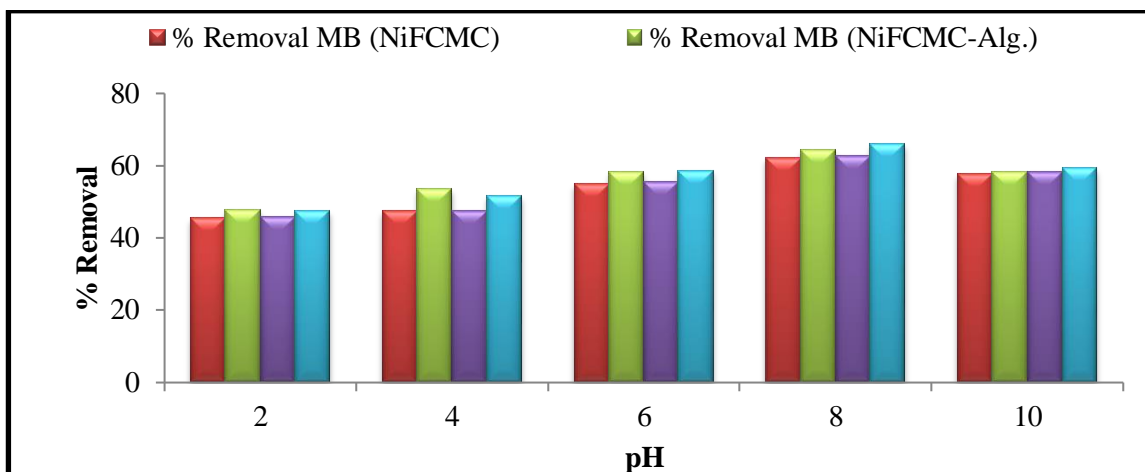


**Figure 4.4.3- Effect of pH on removal % of MB and CV dye**

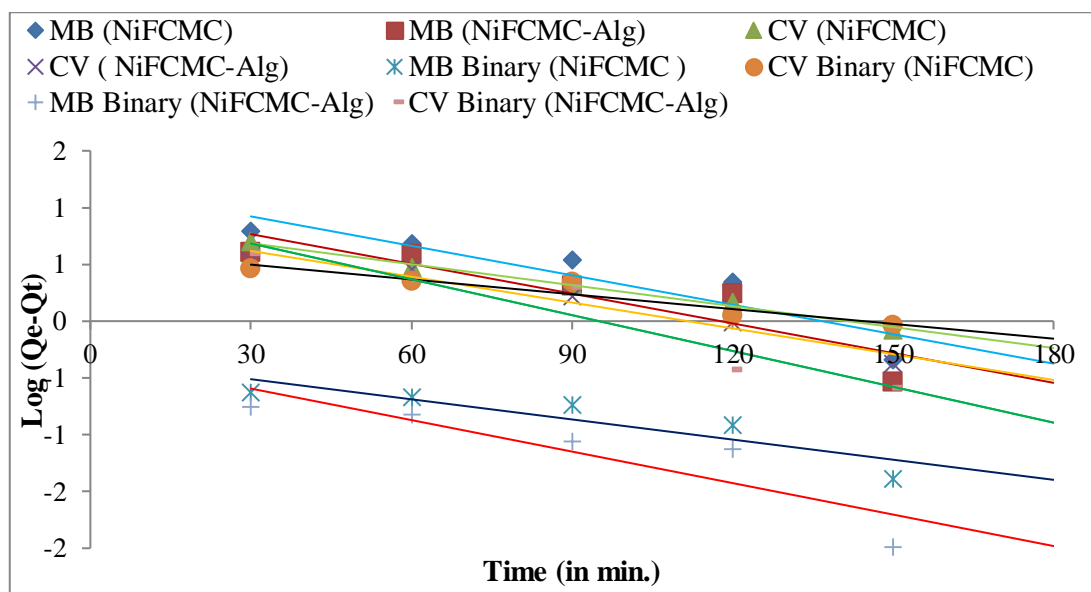
The NiFCMC-Alg composite behaved anionic below  $pH_{pzc} = 7.7$  and at low pH values, the electrostatic attractive forces were reduced. MB dye molecules and  $H^+$  ions competed to stick to the adsorbent surface because at lower pH values, there were more  $H^+$  ions in the aqueous solution. While comparing with  $H^+$  ions, these  $H^+$  ions are smaller and bind to the empty site more quickly, cationic dye molecules interact less electrostatically with the adsorbent surface. As pH increased, the adsorbent and dye molecules' electrostatic interaction intensified leading to increase in the degree of adsorption due to drop in surface charge density<sup>49, 116, 143</sup>.

#### 4.4.4 Adsorption Kinetics

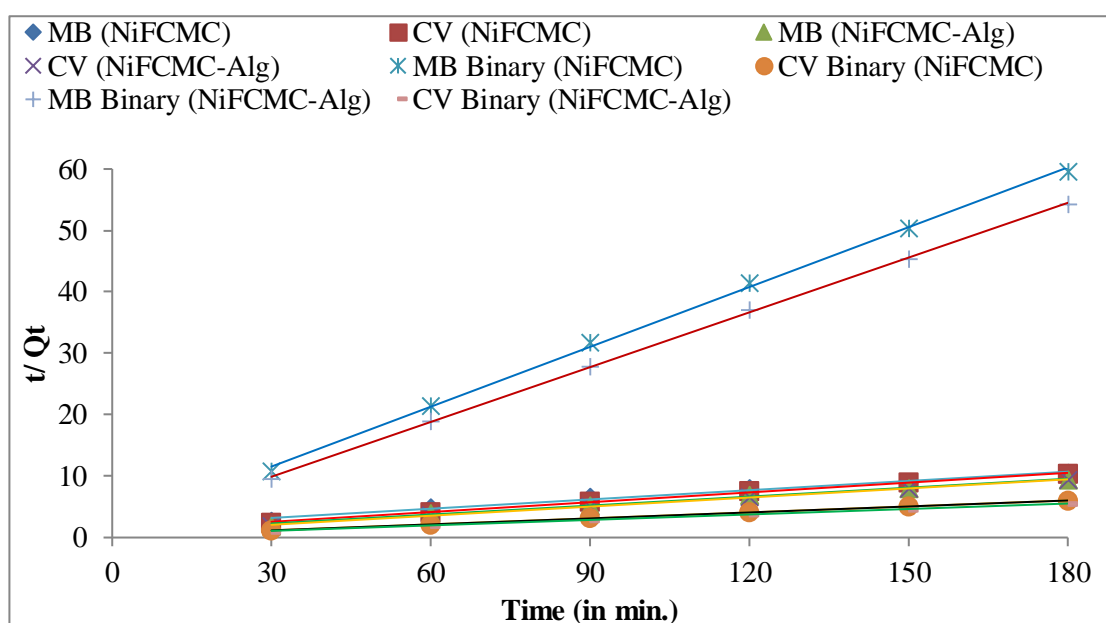
The adsorption behaviour in relation to time is determined by adsorption kinetics. Several models like the Lagergren pseudo-first order model, Lagergren pseudo-second order, Weber-Morris diffusion model and Elovich model of kinetics were used<sup>78, 158</sup>.

A summary of the different adsorption constants computed for different models is shown in Table 4.4.1. The computed correlation coefficients ( $R^2$ ) values were compared to assess the fitness of several kinetic models. The adsorption behaviour will be chemisorption in nature if the data fits the kinetic model of pseudo second order; if not, it will be physical adsorption provided the data fulfill pseudo first order kinetics<sup>78</sup>. The results showed that out of all the kinetic models, the Lagergren pseudo-second order model best fit the data since it had the highest  $R^2$  value. It showed that adsorption

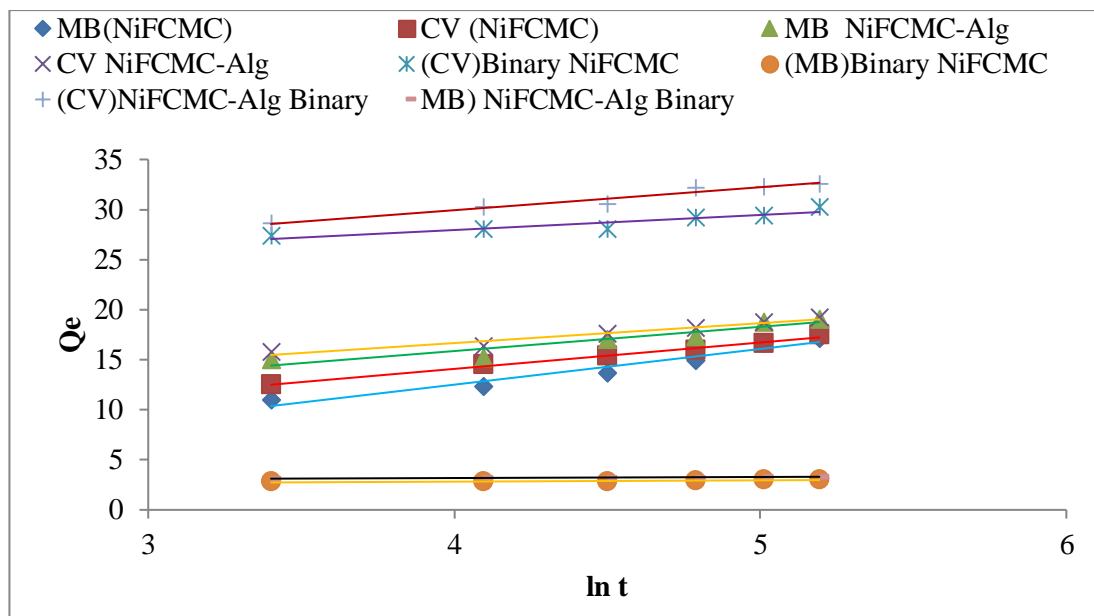
process between adsorbent and adsorbate follows chemisorption mode. To study the intra-particle diffusion behaviour, Weber-Morris diffusion model was used by plotting a graph between  $Q_t$  versus  $t^{0.5}$ . If that is the only rate determining step, then the origin must be crossed by a straight line. Figure 4.4.4 (d) showed that in the case of both adsorbents in both single as well as binary systems, there is non-linear plot and the line does not pass through the origin. It showed that factors other than intra particle diffusion may influence the rate of adsorption<sup>7, 78</sup>.



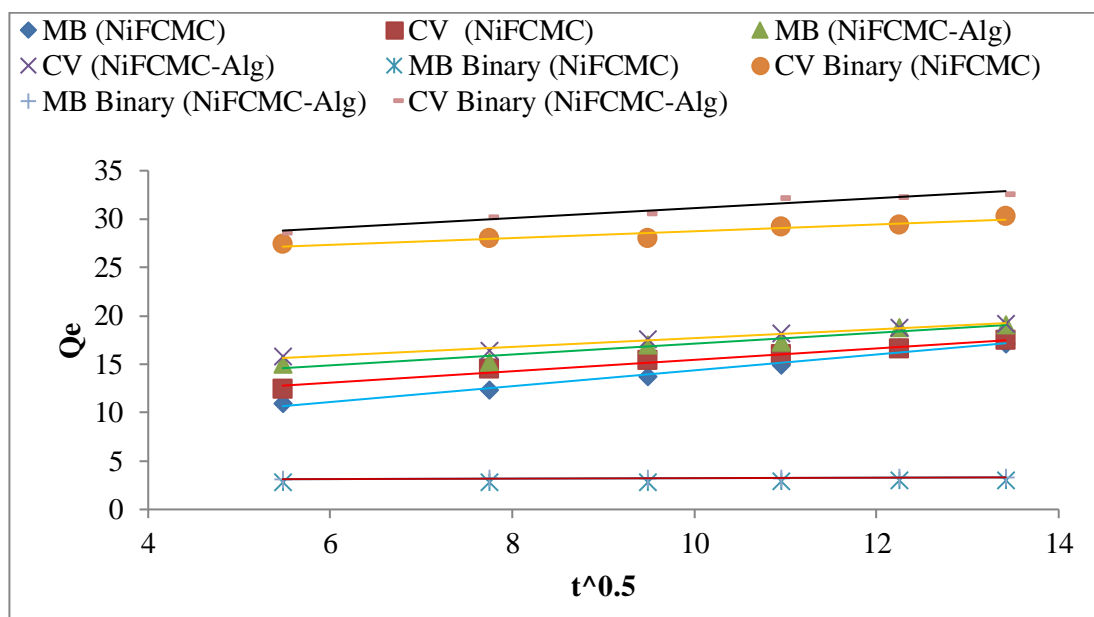
(a)



(b)



(c)



(d)

**Figure 4.4.4- Various kinetic models– (a) Pseudo first order (b) Pseudo second order (c) Elovich (d) Weber-Morris diffusion model**

#### 4.4.5 Effect of Concentration

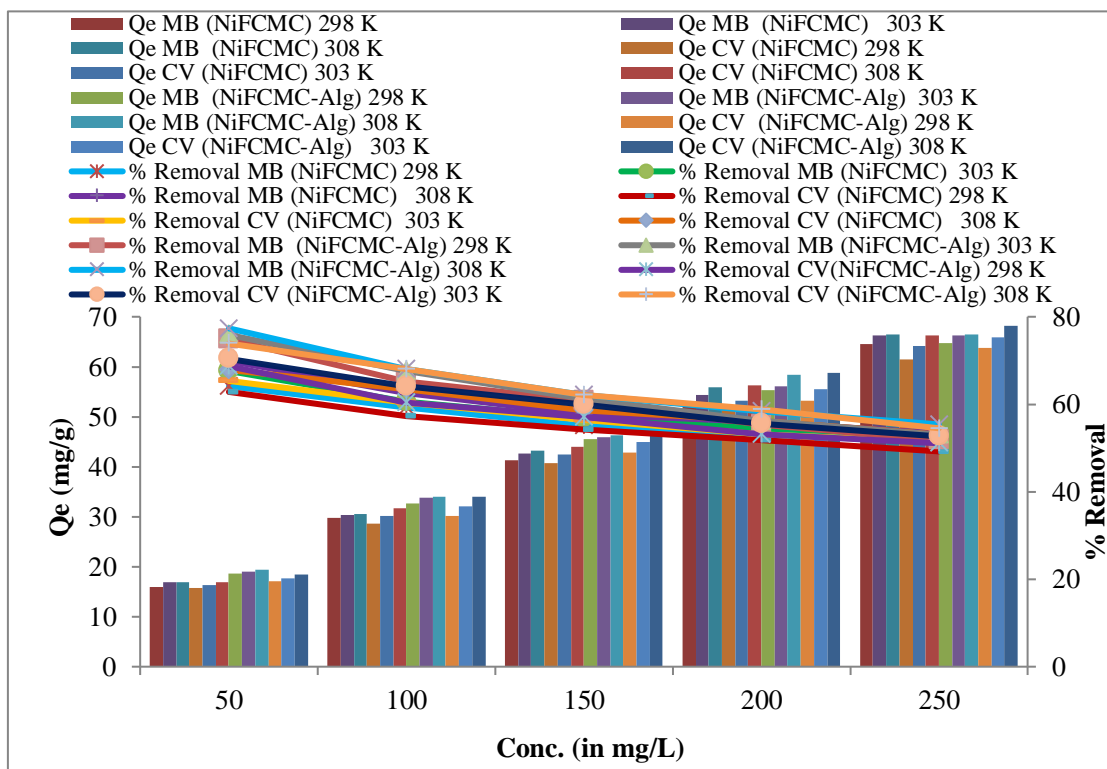
The effect of MB and CV dye concentrations was investigated for single as well as binary systems by using NiFCMC and NiFCMC-Alg adsorbents. The initial dye concentration was taken between 50-250 mg/L (for single dye system) and 20-100 mg/L (for binary dye system) respectively. The adsorption capabilities for both adsorbents

increased as the initial concentration of the dye solution increased as shown in figure 4.4.5 reaching a maximum at 250 mg/L in single dye system and 100 mg/L in binary dye system. As the dye concentration rises, more interactions occur between the adsorbent and adsorbate. Conversely, the removal percentage in both dye systems decreased as the solution's concentration increased. This may be the result of the adsorbent's surface having less accessible active sites as the dye concentration increases<sup>7</sup>.

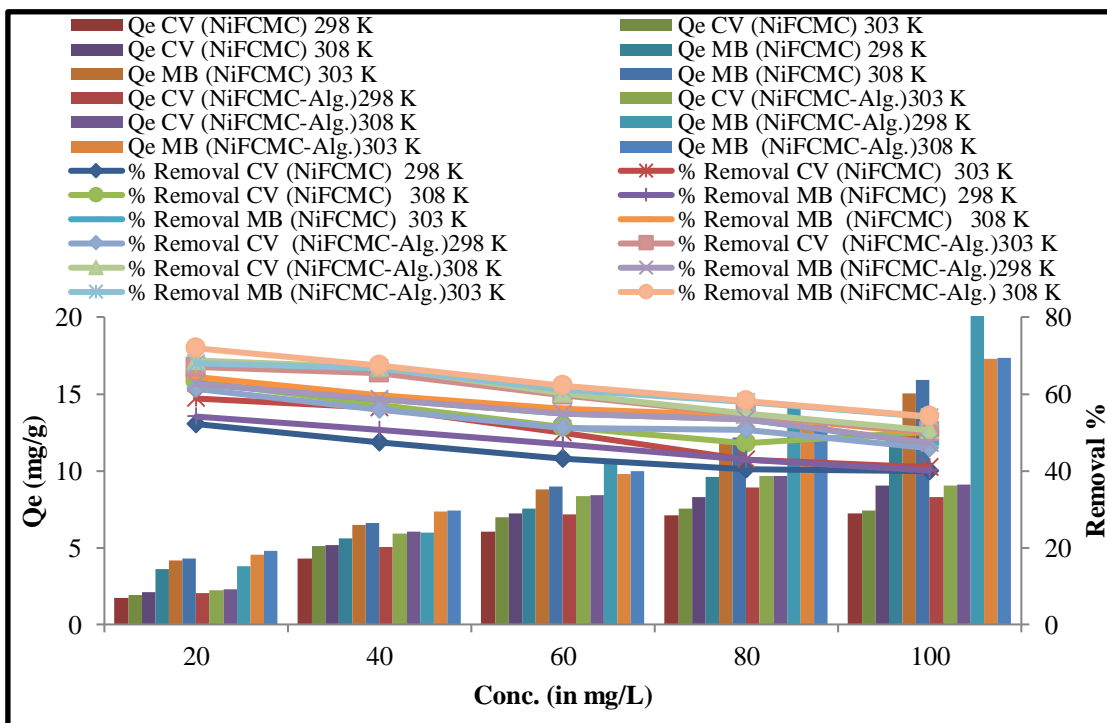
At various temperatures (25°C, 30°C and 35°C), the impact of concentration was investigated. For both adsorbents, the adsorption capacity increased as the temperature increased. It was because both the adsorbent as well as adsorbate interact more quickly as the temperature rises. Because of an increase in pores brought on by a rise in temperature, the adsorbent's surface area has increased, speeding up the adsorption process<sup>49, 78, 143</sup>.

**Table 4.4.1- Computed values of various constants of various kinetic models for NiFCMC and NiFCMC-Alg at 298 K in single and binary dye system**

System→	Parameter	Single MB (NiFCMC)	Single CV (NiFCMC)	Single MB (NiFCMC -Alg)	Single CV (NiFCMC -Alg)	MB in binary (NiFCMC)	CV in binary (NiFCMC)	MB in binary (NiFCMC -Alg)	CV in binary (NiFCMC -Alg)
Kinetic model ↓									
<b>Lagergren Pseudo first order</b>	<b>Q<sub>e</sub></b>	15.18	7.41	10.66	7.01	2.16	4.25	2.07	9.98
	<b>k<sub>1</sub></b>	0.019	0.019	0.020	0.018	0.014	0.01	0.021	0.024
	<b>R<sup>2</sup></b>	0.842	0.991	0.803	0.953	0.809	0.908	0.786	0.912
<b>Lagergren Psuedo second order</b>	<b>Q<sub>e</sub></b>	19.92	18.79	20.58	20.28	3.08	30.86	3.36	33.67
	<b>H</b>	0.593	1.046	1.120	1.684	0.551	5.058	1.023	5.048
	<b>K<sub>2</sub></b>	0.002	0.003	0.003	0.004	0.058	0.005	0.090	0.005
	<b>R<sup>2</sup></b>	0.986	0.997	0.994	0.998	0.998	0.998	0.999	0.999
<b>Elovich model</b>	<b>A</b>	2.178	10.074	31.08	160.31	426.45	324.62	429.00	192.65
	<b>B</b>	0.280	0.379	0.413	0.504	7.553	0.665	9.671	0.435
	<b>R<sup>2</sup></b>	0.947	0.991	0.884	0.954	0.827	0.855	0.915	0.959
<b>Weber – Morris Model</b>	<b>K<sub>id</sub></b>	0.818	0.589	0.561	0.454	0.031	0.351	0.024	0.513
	<b>I</b>	6.19	9.56	11.53	13.16	2.58	25.23	2.99	26.0
	<b>R<sup>2</sup></b>	0.984	0.979	0.936	0.983	0.911	0.919	0.958	0.948



(a)



(b)

#### 4.4.5- Impact of concentration on $Q_e$ and removal % in (a) single and (b) binary dye system

#### 4.4.6 Adsorption Isotherms

Under equilibrium conditions, numerous isotherms models like Langmuir, Freundlich, Temkin and Dubinin-Radushkevich (D-R) were employed to study the adsorption behaviour.

Figure 4.3.6 shows the values of several constants that were calculated using the slope and intercept of graphs. In table 4.4.2, various adsorption isotherm models were compared for their correlation values ( $R^2$ ) and it was revealed from the findings that the model that was most fit was Langmuir model for the adsorption data with highest  $R^2$  value among different isotherm models. It showed that the active sites are consistently arranged on the surface of magnetic bio-composite. It was found that the Langmuir adsorption capabilities in single dye system were 113.6 and 99.01 mg/g for MB, 112.3 and 97.08 mg/g for CV while 16.10, 21.23 mg/g for CV and 25.57 and 29.85 mg/g for MB in binary dye system for NiFCMC and NiFCMC-Alg respectively. Due to the antagonistic effects of both cationic dyes, each dye's removal efficiency was lower in the binary dye system than in the single dye system. Different dye molecules exhibit a variety of attractive forces that combine to form strong bonds in binary dye system<sup>93</sup>. The decrease in dye adsorption behaviour in binary systems is a result of this strong bonding.

One of the crucial variables associated with the Langmuir adsorption isotherm is the separation factor ( $R_L$ ), which depicts the spontaneity of the adsorption process. According to the computed value of  $R_L$ , there are four types of adsorption behaviour: unfavourable ( $R_L > 1$ ), linear ( $R_L = 1$ ), favourable ( $0 < R_L < 1$ ) and irreversible ( $R_L = 0$ ). In the present study, the value of  $R_L$  lies in range 0-1 that shows that the Langmuir adsorption isotherm was advantageous in this study. The adsorption energy ( $E$ ) that represents the type of adsorption in D-R model is an important parameter. Physical adsorption will occur if the predicted adsorption energy is less than 50 kJ/mol; if not, chemisorption will occur. Table 4.4.2 showed the determined value of adsorption energy for NiFCMC and NiFCMC-Alg adsorbents in both single as well as binary systems was larger than 100 kJ/mol indicating that chemisorption took place throughout the present work.

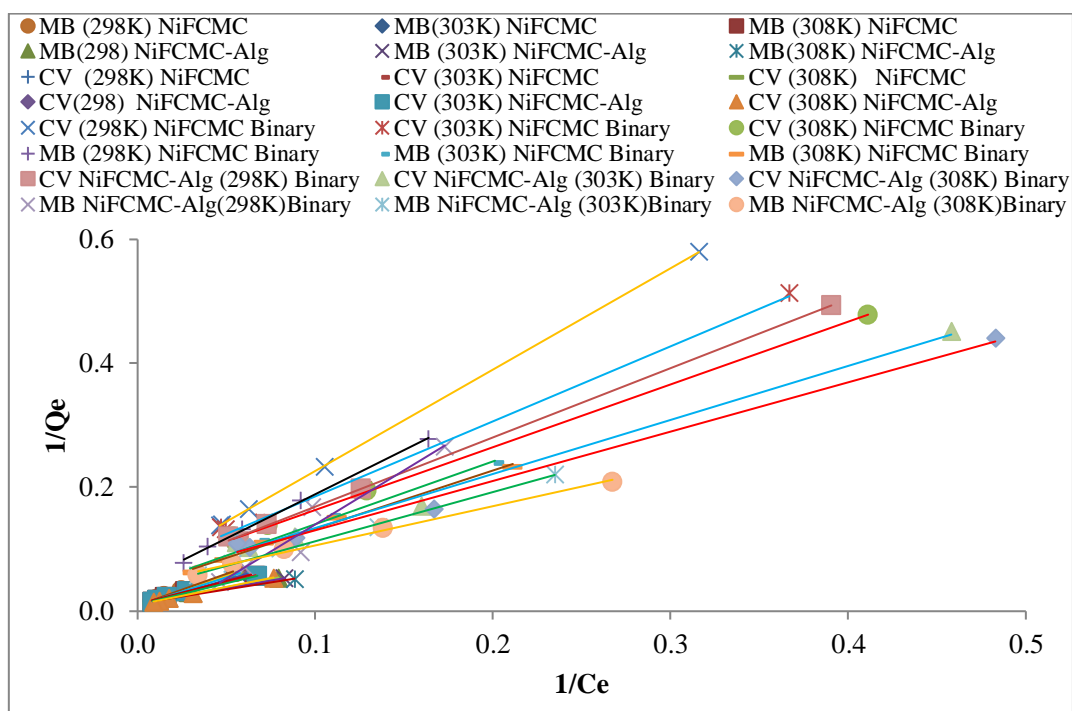
**Table 4.4.2- Estimated values for various constants of different adsorption isotherm models at 25°C, 30°C and 35°C in single dye system for NiFCMC and NiFCMC-Alg composite**

System→	Constant	Single MB (NiFCMC)			Single CV (NiFCMC)			Single MB (NiFCMC-Alg)			Single CV (NiFCMC-Alg)		
Isotherm model ↓													
Temperature		25°C	30°C	35°C	25°C	30°C	35°C	25°C	30°C	35°C	25°C	30°C	35°C
<b>Langmuir</b>	<b>Q</b>	113.60	78.12	93.46	108.69	108.69	112.35	99.01	80.01	80.64	87.72	97.08	95.24
	<b>B</b>	0.009	0.024	0.015	0.009	0.010	0.011	0.012	0.025	0.027	0.015	0.015	0.018
	<b>R<sup>2</sup></b>	0.997	0.997	0.989	0.996	0.998	0.998	0.991	0.992	0.985	0.988	0.997	0.998
	<b>R<sub>L</sub></b>	0.307	0.141	0.210	0.692	0.664	0.647	0.244	0.136	0.128	0.568	0.576	0.523
<b>Freundlich</b>	<b>K<sub>f</sub></b>	1.999	2.473	2.931	1.940	2.254	2.574	4.573	4.920	4.974	3.132	3.235	4.005
	<b>1/n</b>	0.723	0.686	0.655	0.717	0.699	0.687	0.556	0.547	0.557	0.641	0.636	0.606
	<b>R<sup>2</sup></b>	0.984	0.986	0.990	0.985	0.990	0.994	0.990	0.990	0.991	0.987	0.990	0.992
<b>Temkin</b>	<b>b<sub>T</sub></b>	102.3	104.5	107.1	106.5	105.0	102.5	123.8	123.6	118.1	113.2	109.9	110.2
	<b>A</b>	0.094	0.118	0.119	0.092	0.101	0.111	0.165	0.186	0.187	0.119	0.130	0.155
	<b>R<sup>2</sup></b>	0.956	0.950	0.953	0.968	0.969	0.976	0.973	0.975	0.960	0.960	0.979	0.982
<b>D-R model</b>	<b>Q<sub>m</sub></b>	50.6	51.3	51.9	49.2	51.1	53.4	51.5	52.6	53.7	49.9	53.7	54.9
	<b>K</b>	7×10 <sup>-5</sup>	5×10 <sup>-5</sup>	4×10 <sup>-5</sup>	7×10 <sup>-5</sup>	6×10 <sup>-5</sup>	5×10 <sup>-5</sup>	3×10 <sup>-5</sup>	3×10 <sup>-5</sup>	2×10 <sup>-5</sup>	5×10 <sup>-5</sup>	4×10 <sup>-5</sup>	3×10 <sup>-5</sup>
	<b>R<sup>2</sup></b>	0.847	0.822	0.820	0.844	0.854	0.862	0.822	0.836	0.811	0.820	0.856	0.857
	<b>E</b>	84.5	100.0	111.8	84.5	100.0	100.0	129.1	129.1	158.1	100.0	111.8	129.1

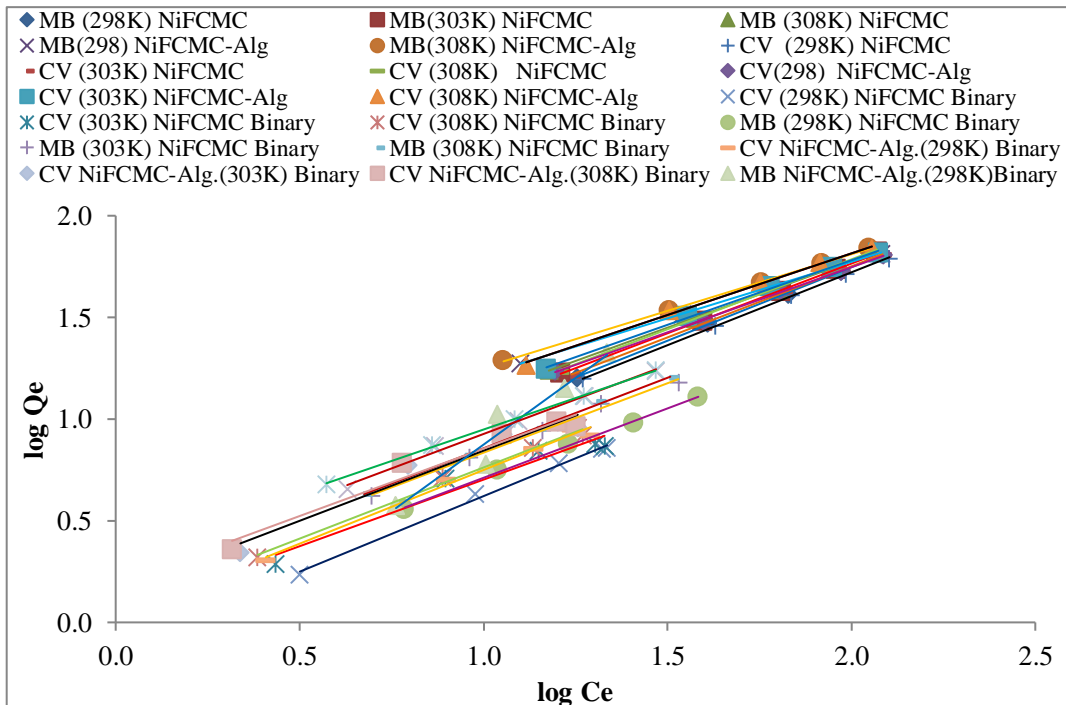


**Table 4.4.3- Estimated values for various constants of different adsorption isotherm models at 25°C, 30°C and 35°C in binary dye system for NiFCMC and NiFCMC-Alg composite**

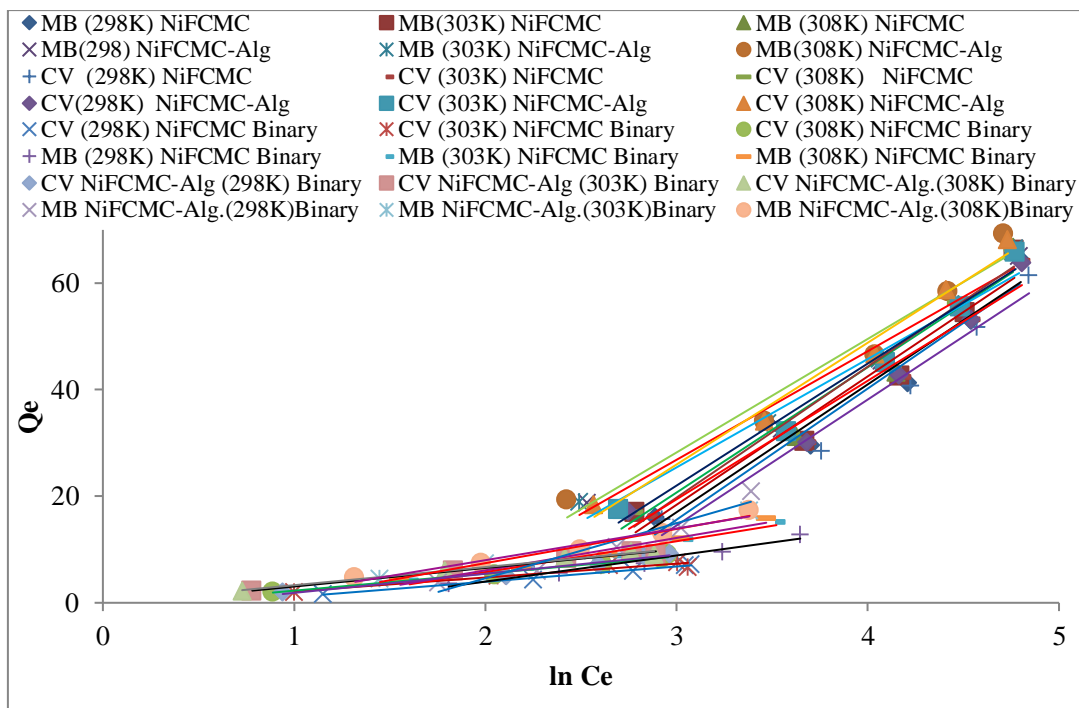
System→	Constant	CV in Binary (NiFCMC)			MB in Binary (NiFCMC)			CV in Binary (NiFCMC-Alg)			MB in Binary ( NiFCMC-Alg)		
Isotherm model ↓													
Temperature		25°C	30°C	35°C	25°C	30°C	35°C	25°C	30°C	35°C	25°C	30°C	35°C
<b>Langmuir</b>	<b>Q</b>	16.03	15.55	16.10	21.65	22.47	25.57	17.58	21.23	19.61	28.90	29.85	23.31
	<b>B</b>	0.038	0.053	0.061	0.032	0.079	0.042	0.051	0.054	0.064	0.019	0.042	0.068
	<b>R<sup>2</sup></b>	1.000	0.992	0.999	0.998	0.978	0.993	0.998	0.993	0.993	0.990	0.996	0.993
	<b>R<sub>L</sub></b>	0.567	0.485	0.449	0.607	0.387	0.546	0.495	0.481	0.438	0.716	0.542	0.425
<b>Freundlich</b>	<b>K<sub>f</sub></b>	1.325	1.144	1.154	1.068	1.418	1.454	5.305	4.897	1.553	2.735	1.773	2.173
	<b>1/n</b>	0.743	0.655	0.699	0.692	0.682	0.694	0.725	0.69	0.664	1.311	0.678	0.619
	<b>R<sup>2</sup></b>	0.995	0.951	0.992	0.991	0.985	0.992	0.988	0.956	0.954	0.937	0.993	0.991
<b>Temkin</b>	<b>b<sub>T</sub></b>	882.8	968.9	778.4	514.3	435.1	414.3	762.2	722.1	740	195.9	392.3	423.3
	<b>A</b>	0.542	0.839	0.742	0.305	0.366	0.368	0.675	0.883	0.969	0.200	0.431	0.519
	<b>R<sup>2</sup></b>	0.988	0.954	0.978	0.971	0.976	0.964	0.969	0.981	0.984	0.889	0.974	0.964
<b>D-R model</b>	<b>Q<sub>m</sub></b>	6.6	7.1	7.9	6.6	12.0	12.3	8.1	8.9	8.9	17.3	13.7	13.3
	<b>K</b>	3×10 <sup>-6</sup>	2×10 <sup>-6</sup>	2×10 <sup>-6</sup>	8×10 <sup>-6</sup>	5×10 <sup>-6</sup>	5×10 <sup>-6</sup>	2×10 <sup>-6</sup>	2×10 <sup>-6</sup>	1×10 <sup>-6</sup>	1×10 <sup>-6</sup>	4×10 <sup>-6</sup>	3×10 <sup>-6</sup>
	<b>R<sup>2</sup></b>	0.936	0.976	0.938	0.847	0.837	0.814	0.913	0.965	0.967	0.806	0.866	0.818
	<b>E</b>	408.2	500	500	250	316.2	316.2	500	500	707.1	707.1	353.5	408.2



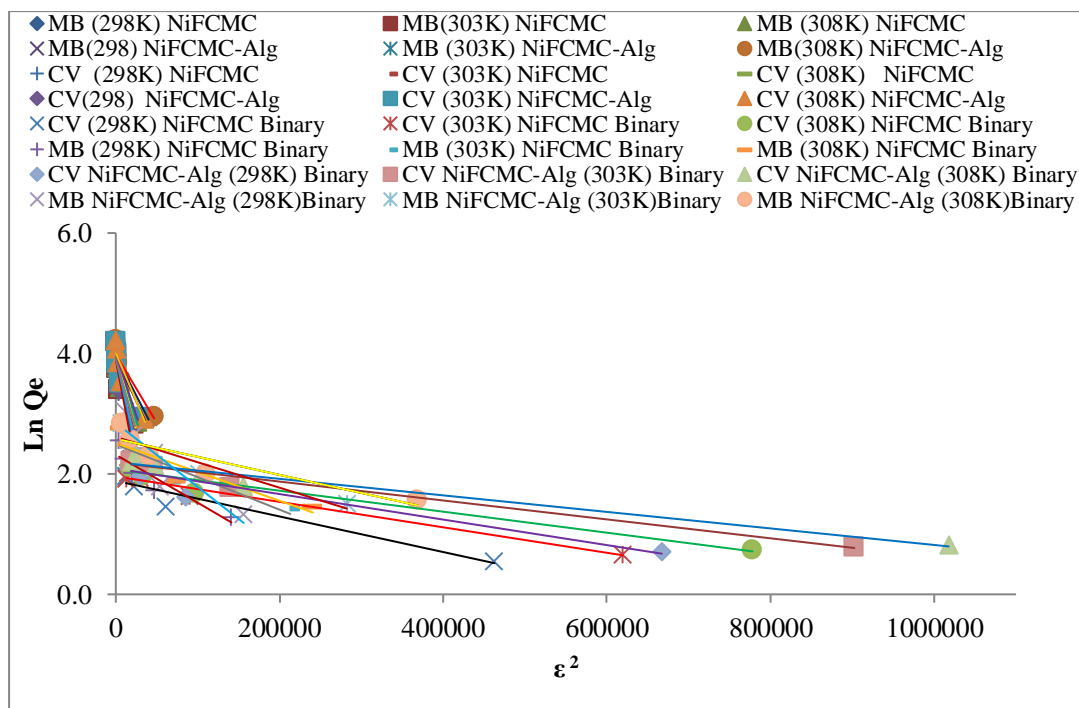
(a)



(b)



(c)



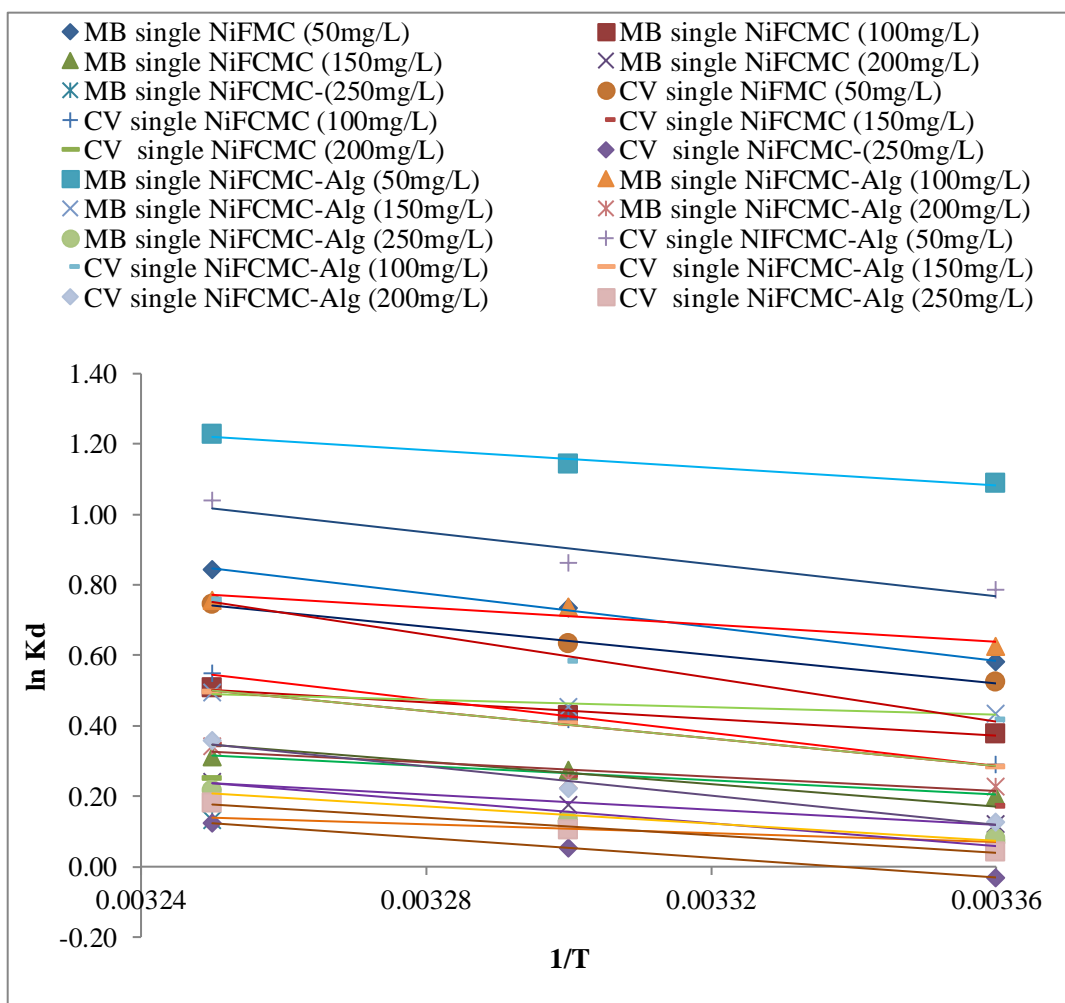
(d)

**Figure 4.4.6- Graph of various adsorption isotherms (a) Langmuir (b) Freundlich (c) Temkin (d) D-R isotherm**

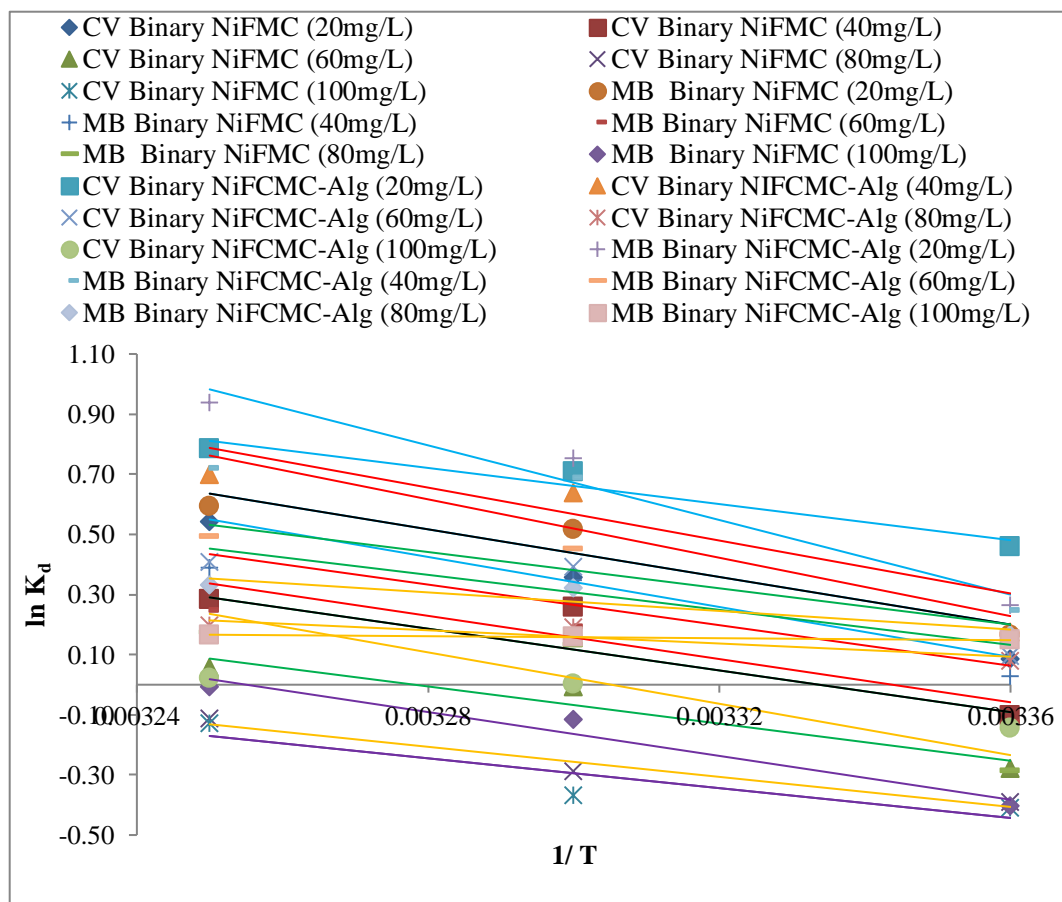
#### 4.4.7 Adsorption Thermodynamics

In an adsorption process, the quantity of energy released from the start to the final state is determined by adsorption thermodynamics.  $H^\circ$ ,  $G^\circ$  and  $S^\circ$  are three thermodynamic characteristics employed to study the adsorption behaviour.

From the values of slope and intercept of linear plot of  $\ln K_d$  vs  $1/T$  the values of  $H^\circ$  and  $S^\circ$  are calculated as shown in figure 4.4.7. Various adsorption thermodynamic parameters were determined and listed in table 4.4.4. The adsorbate and adsorbent exhibited a strong interaction as evidenced by the computed values of two parameters viz.  $\Delta H^\circ$  and  $\Delta S^\circ$  for both adsorbents which were found to be positive suggesting that the adsorption process was endothermic. In both dye systems, the calculated  $\Delta G^\circ$  value was negative predicting the spontaneous nature of adsorption process<sup>49, 78</sup>.



(a)



(b)

Figure 4.4.7- Graph between  $\ln K_d$  vs  $1/T$  (a) single (b) binary dye system

Table 4.4.4- Computed values of  $\Delta H^\circ$ ,  $\Delta S^\circ$  and  $\Delta G^\circ$  in both dye systems

System	Conc. (mg/L)	$\Delta H^\circ$ (kJ/mol)	$\Delta S^\circ$ (kJ/mol/K)	$\Delta G^\circ$ (25°C) (kJ/mol)	$\Delta G^\circ$ (30°C) (kJ/mol)	$\Delta G^\circ$ (35°C) (kJ/mol)
Single MB (NiFCMC)	50	19.9	0.072	-1.439	-1.852	-2.159
	100	9.8	0.036	-0.938	-1.082	-1.303
	150	8.4	0.030	-0.499	-0.691	-0.796
	200	8.9	0.031	-0.303	-0.444	-0.616
	250	5.2	0.018	-0.162	-0.299	-0.341
Single MB (NiFCMC- Alg)	50	10.4	0.044	-2.697	-2.882	-3.144
	100	10.1	0.039	-1.553	-1.856	-1.942
	150	4.4	0.018	-1.079	-1.143	-1.269
	200	8.4	0.030	-0.566	-0.622	-0.876

	250	10.2	0.035	-0.200	-0.326	-0.556
<b>Single CV (NiFCMC)</b>	50	16.7	0.061	-1.299	-1.596	-1.911
	100	19.6	0.068	-0.718	-1.054	-1.410
	150	13.3	0.046	-0.430	-0.657	-0.895
	200	13.5	0.046	-0.176	-0.322	-0.645
	250	11.6	0.039	0.078	-0.137	-0.316
<b>Single CV (NiFCMC- Alg)</b>	50	18.8	0.070	-1.947	-2.177	-2.661
	100	25.7	0.090	-1.037	-1.472	-1.941
	150	16.2	0.057	-0.704	-1.024	-1.274
	200	17.2	0.059	-0.317	-0.562	-0.918
	250	10.4	0.035	-0.106	-0.267	-0.463
<b>CV in binary (NiFCMC)</b>	20	34.6	0.117	-0.213	-0.895	-1.389
	40	29.9	0.100	0.257	-0.648	-0.722
	60	25.7	0.084	0.693	0.022	-0.140
	80	20.8	0.066	0.970	0.730	0.291
	100	20.6	0.066	1.015	0.927	0.334
<b>MB in binary (NiFCMC)</b>	20	25.0	0.088	-0.407	-1.300	-1.518
	40	40.4	0.138	-0.064	-0.876	-0.997
	60	24.2	0.082	0.312	-0.487	-0.637
	80	9.1	0.031	0.706	-0.337	-0.447
	100	20.6	0.066	1.001	0.295	0.019
<b>CV in binary (NiFCMC- Alg)</b>	20	32.9	0.112	-1.138	-1.783	-2.011
	40	28.1	0.095	-0.433	-1.603	-1.788
	60	28.8	0.096	-0.233	-0.987	-1.041
	80	35.5	0.117	-0.196	-0.477	-0.505
	100	30.3	0.099	0.363	-0.004	-0.053
<b>MB in binary (NiFCMC- Alg)</b>	20	51.6	0.176	-0.651	-1.896	-2.403
	40	36.6	0.125	-0.616	-1.734	-1.848
	60	25.1	0.086	-0.417	-1.136	-1.264
	80	12.8	0.045	-0.405	-0.807	-0.843
	100	1.4	0.006	-0.365	-0.401	-0.424

#### 4.4.8 Regeneration of Adsorbent

After recycling, regeneration efficiency significantly influenced the adsorbent performance and cost-effectiveness of the adsorbent. To regenerate the NiFCMC and NiFCMC-Alg composite in the current work, 0.1N HCl was used as the desorbing solvent. The regeneration capacity was examined over a maximum of five cycles. Table 4.4.5 and figure 4.4.8 represented the regeneration capacity and percentage loss of weight for each adsorbent. Based on the table, it was clear that after five cycles, the regeneration efficiency percentages for NiFCMC and NiFCMC-Alg in single dye system remained 78.6%, 81.3% for MB and 72.2%, 76.1% for CV. Additionally, the weight loss following five cycles of adsorption-desorption was examined. In a single MB and CV study, the weight loss was 14.9%, 19.5% and 17.4%, 23.6% for NiFCMC and NiFCMC-Alg adsorbent respectively. The results determined the effectiveness of NiFCMC and NiFCMC-Alg composite in both dye systems and proved fairly inexpensive alternatives for dye removal.

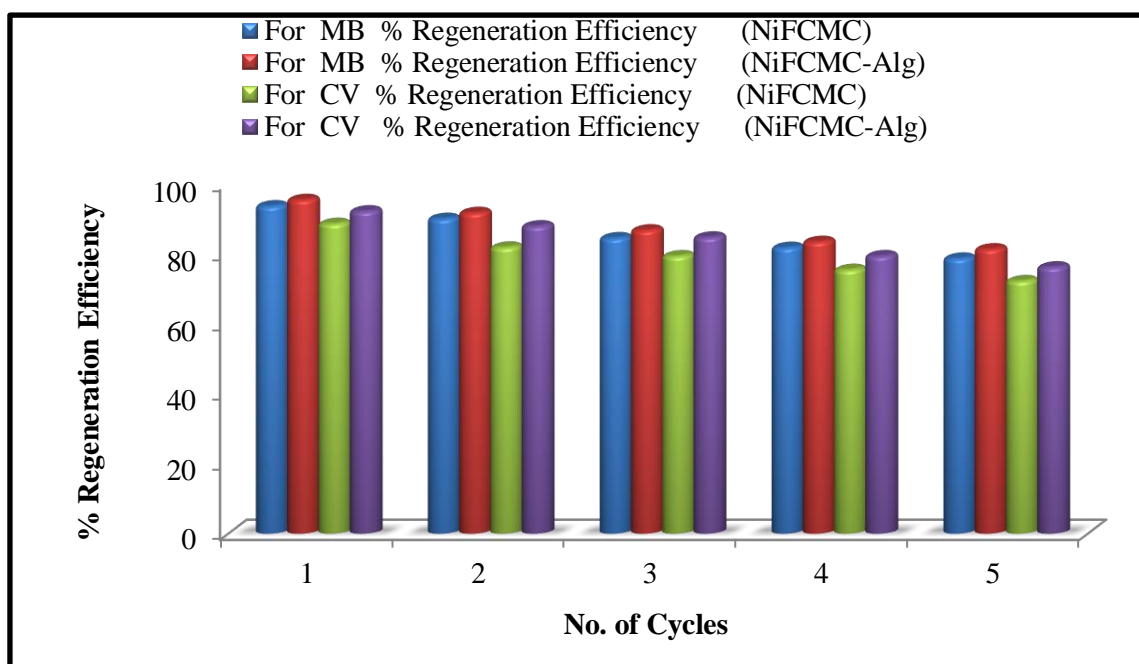


**Figure 4.4.8- Percentage regeneration efficiency of NiFCMC and NiFCMC-Alg adsorbent**

**Table 4.4.5- Percentage regeneration efficiency of NiFCMC and NiFCMC-Alg adsorbent**

<b>No. of Cycles</b>	<b>For MB % Regeneration Efficiency (NiFCMC)</b>	<b>For MB % Regeneration Efficiency (NiFCMC-Alg)</b>	<b>For CV % Regeneration Efficiency (NiFCMC)</b>	<b>For CV % Regeneration Efficiency (NiFCMC-Alg)</b>	<b>Adsorbent weight loss % following five cycles (for MB)</b>		<b>Adsorbent weight loss % following five cycles (for CV)</b>	
					<b>NiFCMC</b>	<b>NiFCMC-Alg</b>	<b>NiFCMC</b>	<b>NiFCMC-Alg</b>
1	93.62	95.44	88.61	92.17				
2	90.02	91.72	81.85	87.90	14.9	19.5	17.64	24.3
3	84.50	86.73	79.36	84.70				
4	81.74	83.44	75.44	79.36				
5	78.66	81.32	72.24	76.16				



## Part –IV

### 4.5 ZnFCMC and ZnFCMC-Alg composite

The general procedure for the surface modification of ZnF with ZnFCMC and ZnFCMC-Alg was described in the section 3.1.6 and 3.1.7. The results of surface characterization and morphological studies are discussed in the following sections.

#### 4.5.1 Characterization and Morphological Studies

##### 4.5.2 FTIR Spectroscopy

Figure 4.5.1 illustrates FTIR spectra of ZnF, ZnFCMC and ZnFCMC-Alg composites in between 4000-400  $\text{cm}^{-1}$  wavenumber range. There are two distinct strong peaks at 500-600  $\text{cm}^{-1}$  and 400–450  $\text{cm}^{-1}$  which are associated with the metal-oxygen bond in the tetrahedral site and metal-oxygen bond in the octahedral sites respectively which confirmed formation of a spinel metal ferrite in the spectra of ZnFCMC and ZnFCMC-Alg in the range between 4000-400  $\text{cm}^{-1}$  <sup>49</sup>. Both ZnFCMC and ZnFCMC-Alg showed a strong characteristic peak at 3305.7  $\text{cm}^{-1}$  and 3311.4  $\text{cm}^{-1}$  that is attributed to stretching vibration of hydroxyl group while peak at 2897.7  $\text{cm}^{-1}$  due to aliphatic -CH stretching of the ether group formed as a result of process of carboxymethylation of cellulose. The common peak at 1591.5  $\text{cm}^{-1}$  and 1417.9  $\text{cm}^{-1}$  in the spectra of ZnFCMC and ZnFCMC-Alg respectively that corresponds to the peak corresponds to vibrations owing to both symmetric and asymmetric -COO- stretching of carboxylate group and C-C bonds in aromatic ring pointing towards that -COO<sup>-</sup> may take part in cross-linking process <sup>53, 151</sup>. The distinct spectral bands at 1322.5  $\text{cm}^{-1}$  in the spectra of ZnFCMC corresponds to C-O stretching which gets shifted to 1310.9  $\text{cm}^{-1}$  in the spectra of ZnFCMC-Alg whereas the spectra at 1034  $\text{cm}^{-1}$  and 1028.3  $\text{cm}^{-1}$  corresponds to >CH-O-CH<sub>2</sub> stretching of saccharide in the spectra of both ZnFCMC and ZnFCMC-Alg which verified sodium alginate's adherence to the ZnFCMC surface <sup>65, 152, 153</sup>.

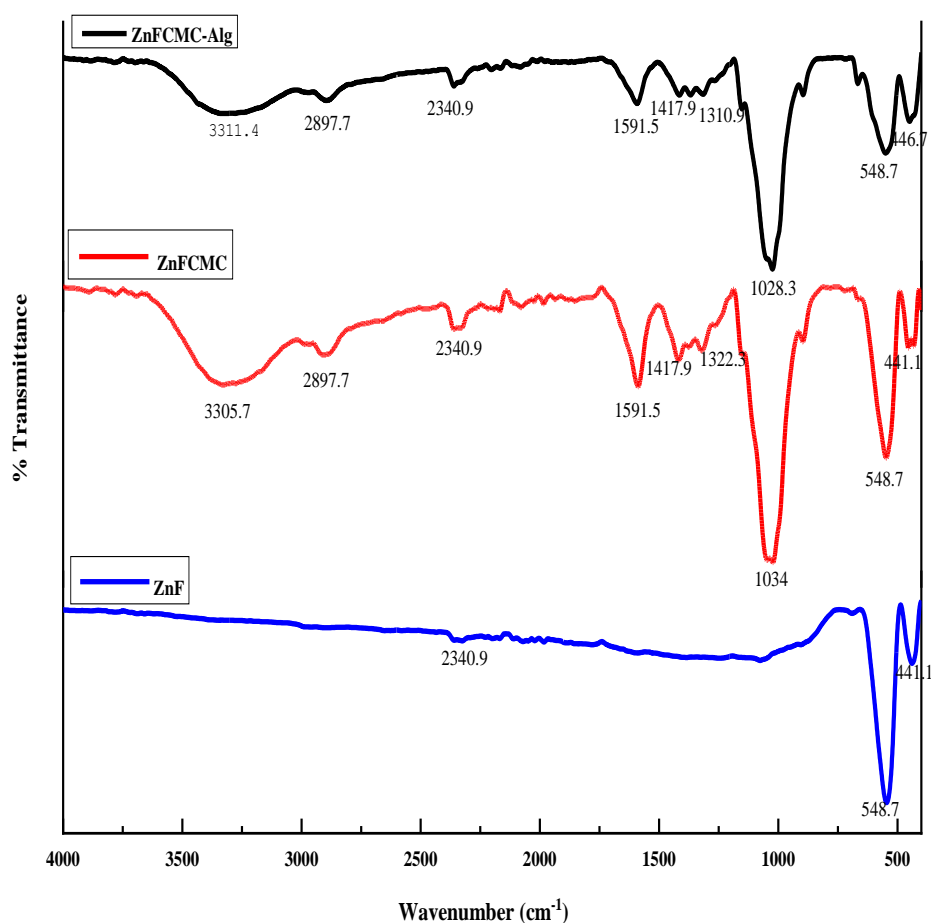


**Figure 4.5.1- FTIR spectra of ZnF, ZnFCMC and ZnFCMC-Alg composite**

#### 4.5.3 X-ray Diffraction (XRD)

XRD spectra of ZnF, ZnFCMC and ZnFCMC-Alg composite was shown in figure 4.5.2. Different diffraction peaks of ZnF appeared at  $2\theta \sim 30, 33.2, 35.3, 42.5, 54.0, 56.6$  and  $62.2^\circ$  having Bragg's reflection peaks as (220), (311), (222), (400), (422), (333) (440)<sup>154</sup>. The peaks showed that ZnF in the spinel-like structure has greater crystallinity and phase purity. However, similar diffraction peaks with slight difference seemed in XRD pattern of ZnFCMC and ZnFCMC-Alg composite. The reason could be that on modification of surface, magnetic composite's size is increased. That caused the shift in the XRD angle<sup>155</sup>. The ZnCMC and ZnFCMC-Alg retained crystallinity and spinel character afterwards surface modification as indicated by XRD image. By using the Scherrer formula, the mean crystallite size of ZnF, ZnFCMC and ZnFCMC-Alg was determined as 31.2 nm, 34.43 nm and 46.03 nm<sup>49, 78</sup>.

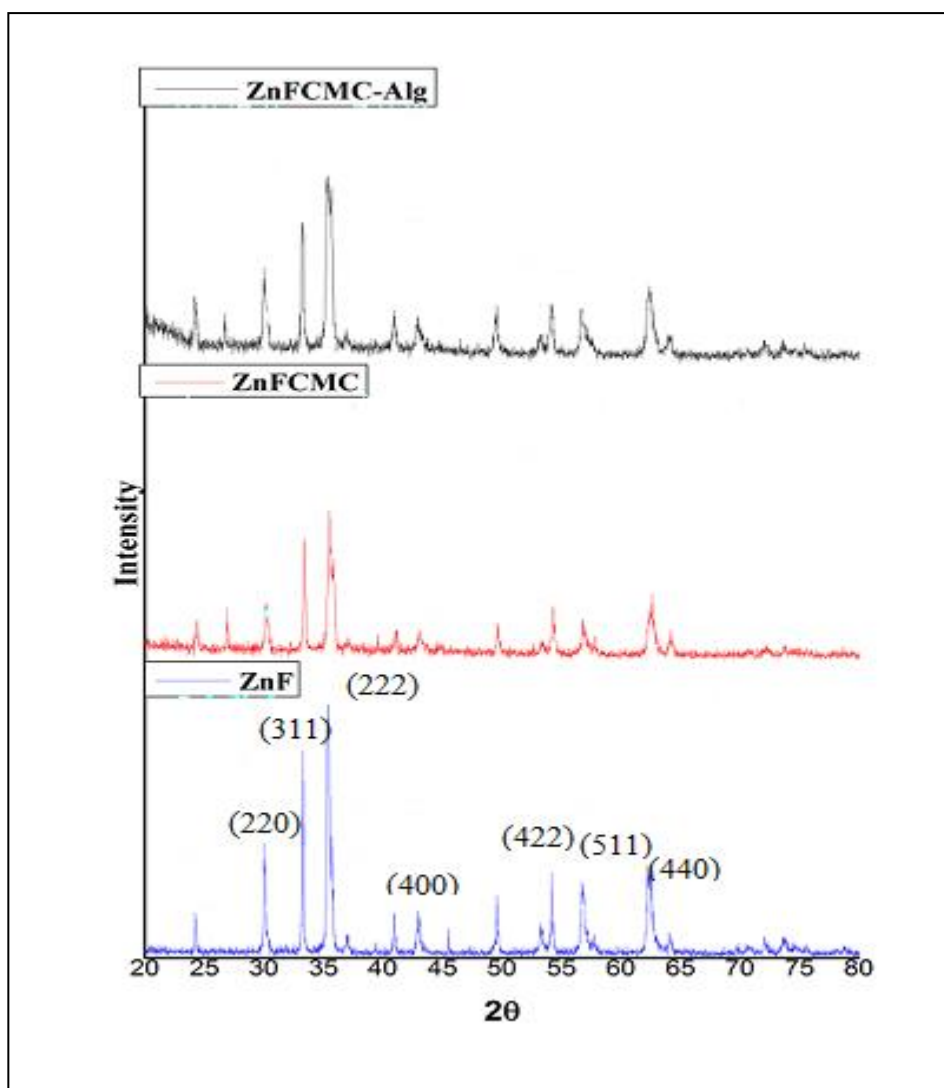
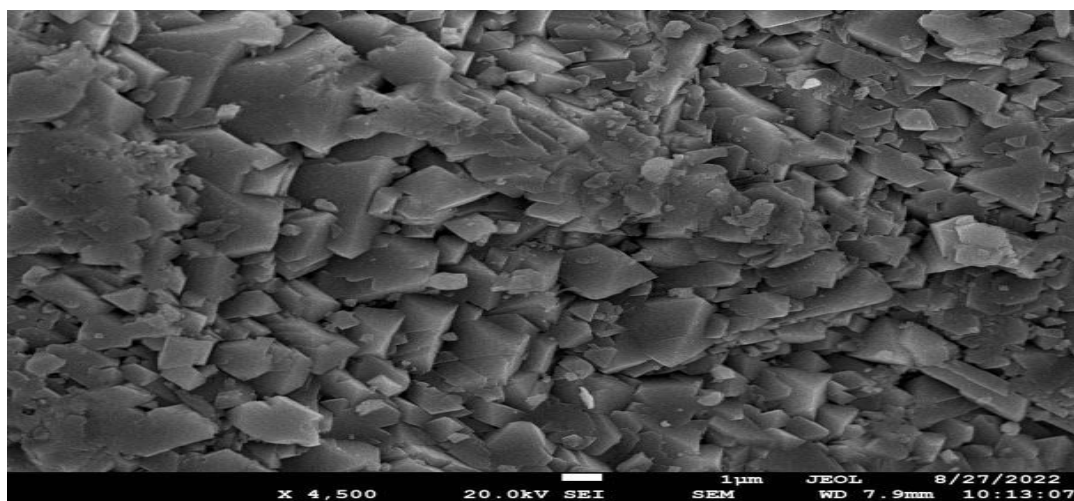


**Figure 4.5.2- XRD spectra of ZnF, ZnFCMC and ZnFCMC-Alg composite**

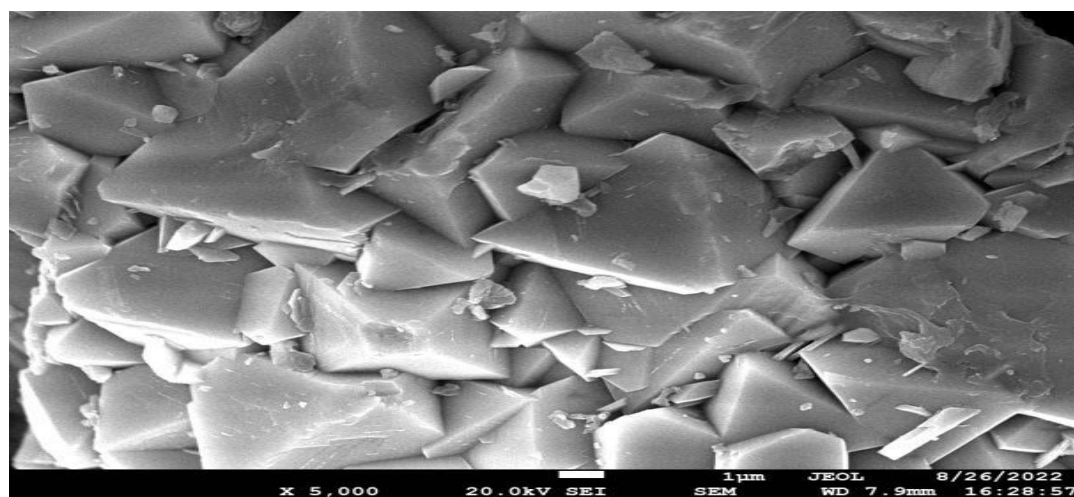
#### **4.5.4 Field Emission Scanning Electron Microscopy (FESEM)**

Figure 4.5.3 (a, b, c) displays the SEM images of ZnF, ZnFCMC and ZnFCMC-Alg. The crystalline structure of ZnF that is depicted by the XRD spectra was also confirmed by SEM image which shows its shape as the roughly spherical homogeneous particles that are uniformly distributed. The SEM image also shows the agglomeration of some of the particles <sup>156</sup>. The average size range of zinc ferrite was found to be 1.58  $\mu\text{m}$  and for ZnFCMC it was 2.80  $\mu\text{m}$  that indicated that the size of ZnFCMC was larger than uncoated ZnF. The surface was found to be uneven and more porous in ZnFCMC as shown in figure 4.5.3 (b). The layer of organic biopolymer content encasing the magnetic nanoparticles may have contributed to the decrease in agglomeration. In the ZnFCMC-Alg composite, the cross-section also revealed an interior with increased surface porosity. Raising the porosity of a composite material can help cationic dye particles freely diffuse

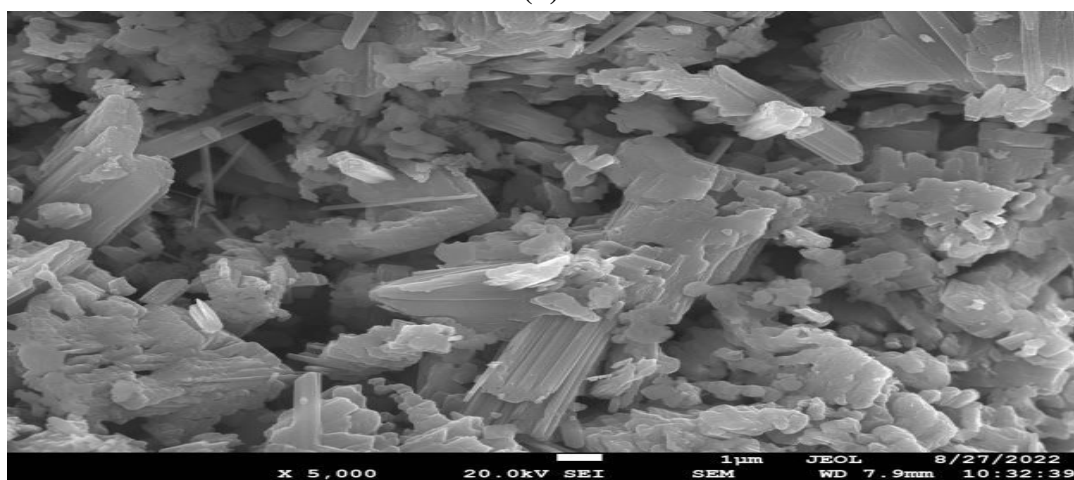
over its surface<sup>65, 126</sup>.



(a)



(b)



(c)

**Figure 4.5.3- FESEM pictures of (a) ZnF (b) ZnFCMC (c) ZnFCMC-Alg**

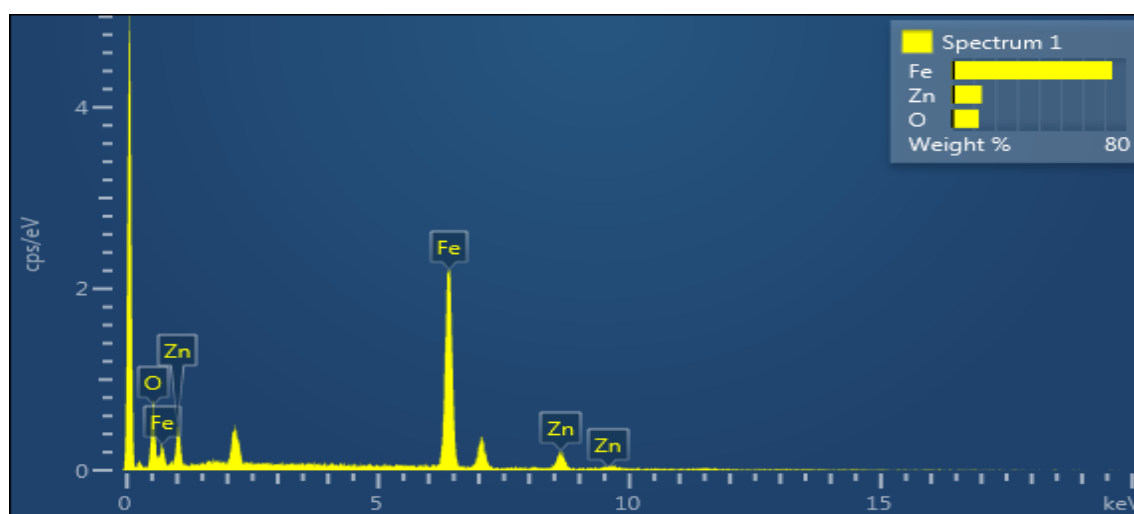
#### 4.5.5 Energy Dispersive Spectra (EDS)

Figure 4.5.4 (a, b and c) displayed the EDS spectra of ZnF, ZnFCMC, and ZnFCMC-Alg composites, each of which exhibits a unique peak for a constituent element. The atomic and weight percentages of each sample together with its elemental composition was shown in table 4.5.1.

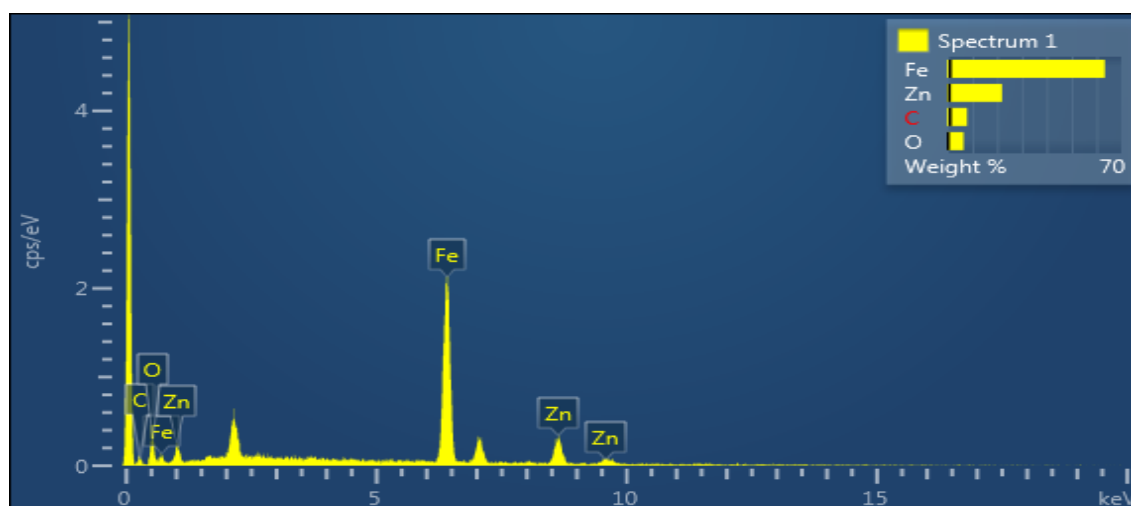
As per the findings, the ZnFCMC-Alg composite had a larger amount of carbon content compared to ZnFCMC. It verified that the surface of zinc ferrite has been successfully modified by carboxymethyl cellulose and sodium alginate <sup>49, 53</sup>.

**Table 4.5.1- Composition of elements in ZnF, ZnFCMC and ZnFCMC-Alg composite**

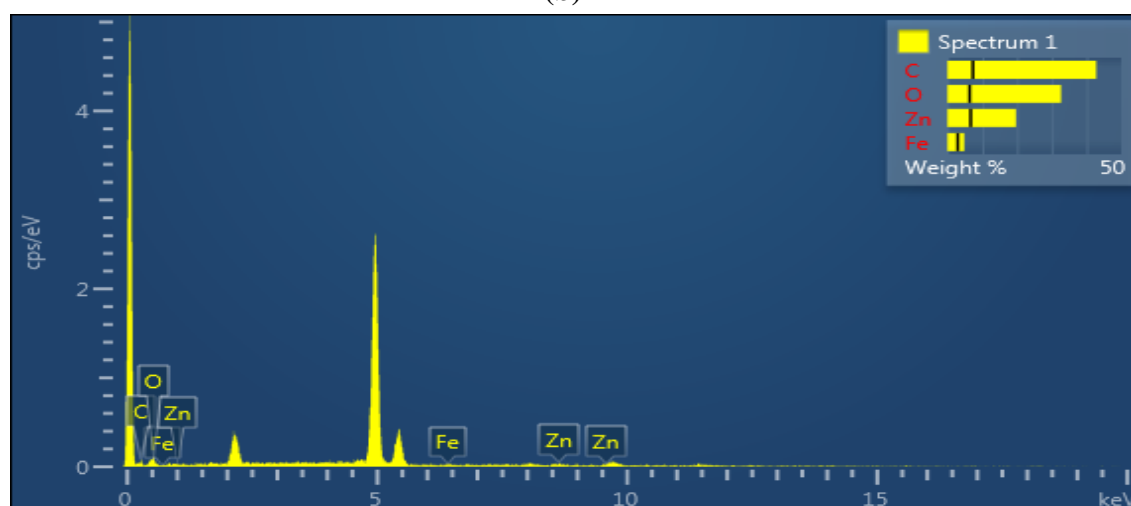
Element	ZnF		ZnFCMC		ZnFCMC-Alg composite	
	Weight %	Atomic %	Weight %	Atomic %	Weight %	Atomic %
C	-	-	7.96	26.03	42.77	59.42
O	12.47	33.74	6.57	16.14	32.70	34.10
Fe	73.61	57.05	63.44	44.61	4.85	1.45
Zn	13.92	9.22	22.03	13.23	19.68	5.02
Total	100.00	-	100.00	-	100.00	-



(a)



(b)



(c)

**Figure 4.5.4- Energy Dispersive spectra of (a) ZnF (b) ZnFCMC (c) ZnFCMC-Alg**

#### 4.5.6 Thermogravimetric Analysis (TGA)

Thermo gravimetric analysis is the technique to study the thermal stability of ZnF, ZnFCMC and ZnFCMC-Alg composite. In this technique, the sample was heated in air atmosphere with temperature ranged from range 30°C to 800°C having heating rate 10°C/minute. Figure 4.5.5 shows TGA curve of ZnF, ZnFCMC and ZnFCMC-Alg biopolymer.

At temperatures of roughly 100°C, both samples showed a 4-6% weight loss which may be caused by evaporation of moisture trapped in the samples. Around 250°C, additional weight loss of 2-5% was observed for ZnFCMC and ZnFCMC-Alg due to breakdown and loss of -OH groups in CMC and alginate while 15-30% weight loss at 350°C in

ZnFCMC and ZnFCMC-Alg composite. The degradation and breakdown of organic functional groups of polymeric chain in the composite may be the cause of this weight loss. No further weight loss was noticed up to temperature 400-800°C<sup>53, 126, 155</sup>. These results revealed that in 1 g of composite around 0.213 g of CMC and 0.338g of CMC-sodium alginate was attached.

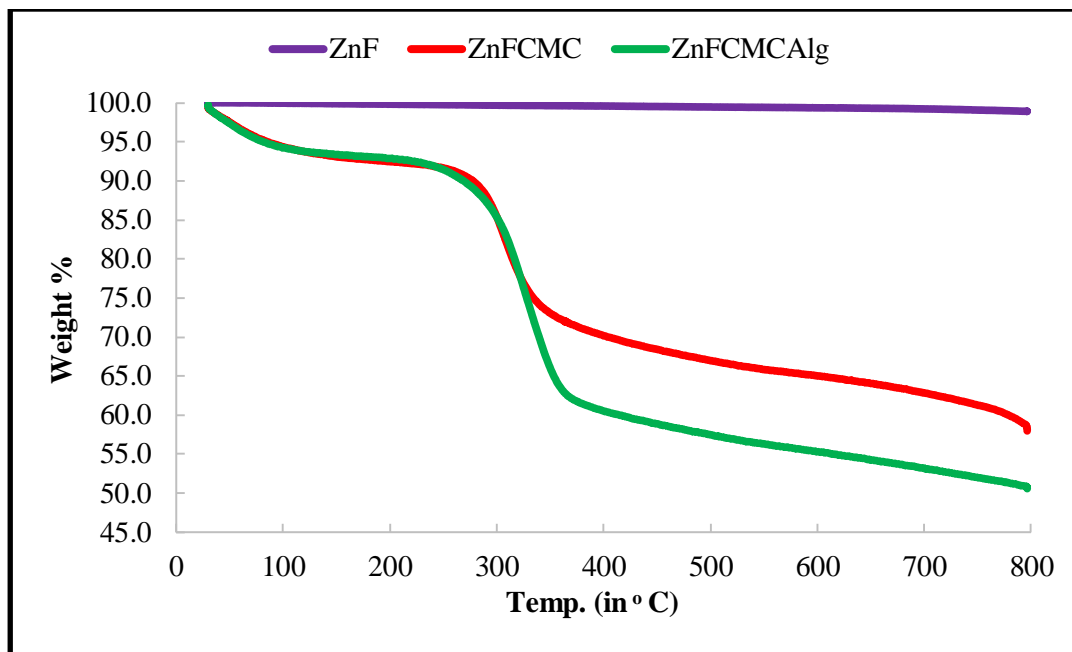


**Figure 4.5.5- TGA curves of ZnF, ZnFCMC and ZnFCMC-Alg composite**

#### 4.5.7 Vibration Scanning Magnetometry (VSM)

Magnetic properties of the synthesized samples were calculated by measuring the change in magnetization of sample with respect to changing magnetic field. Figure 4.5.6 shows the magnetization saturation of 12.28 emu/g, 11.16 emu/g and 8.62 emu/g respectively for ZnF, ZnFCMC and ZnFCMC-Alg composite. This magnetization was considered due to the presence of  $\text{Fe}_3\text{O}_4$  nanoparticles. As a result of polymerization, the slight increase in mass of ZnFCMC and ZnFCMC-Alg and decrease in percentage content of Fe from 57.05% to 44.61% and 1.45% in ZnF, ZnFCMC and ZnFCMC-Alg respectively could be the reason of reduced magnetization as shown in table 4.5.1. The composite can be magnetically separated as it still possessed magnetic properties<sup>53, 57</sup>.

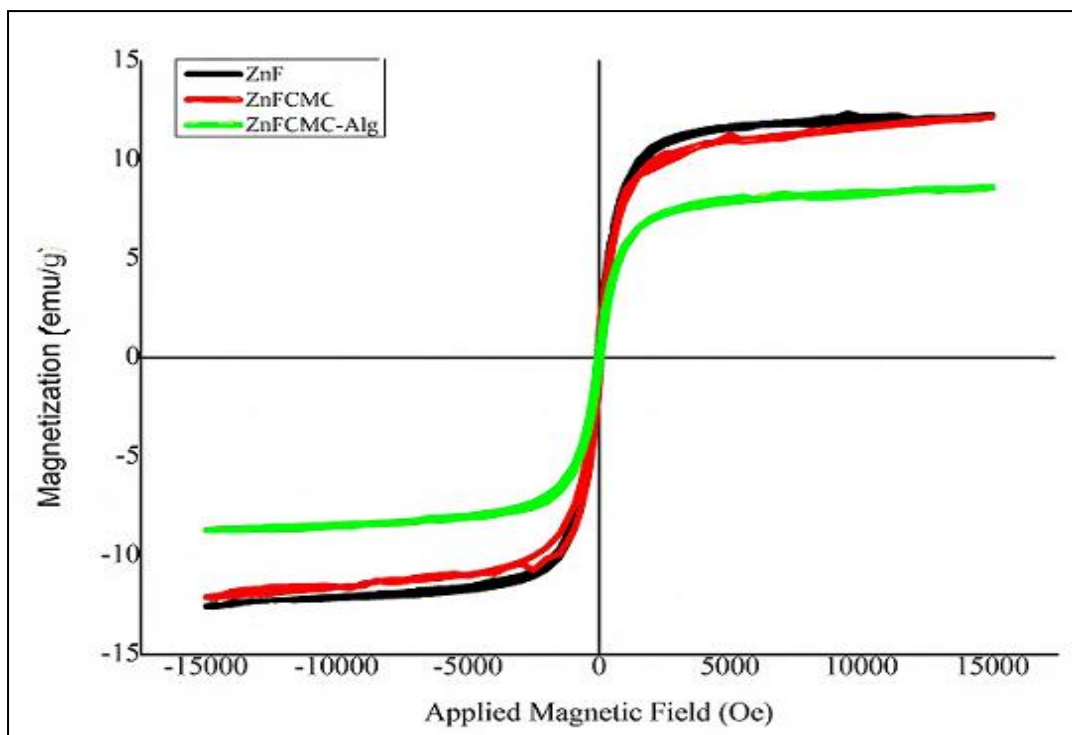


**Figure 4.5.6- Magnetization curve of ZnF, ZnFCMC and ZnFCMC-Alg composite**

#### 4.5.8 pH of point zero charge (pHpzc)

The pH of point zero charge (pHpzc) of prepared material represents the value of pH at which net surface charge of adsorbent is nil. Solid addition method was employed for calculating the pHpzc of magnetic composite <sup>49</sup>. Figure 4.5.7 shows the graph between  $\Delta\text{pH}_{(\text{Initial-final})}$  versus  $\text{pH}_{(\text{initial})}$  for ZnFCMC and ZnFCMC-Alg composite. The calculated values of pHpzc for ZnFCMC and ZnFCMC-Alg composite the computed values of pHpzc are 7.6 and 8.0 respectively. The pHpzc value is important factor in adsorption process as it would depict the charge on the adsorbent's surface. If the pH of the solution is less than pHpzc value, then the surface charge on the adsorbent would become positive and negatively charged species (anions) would be adsorbed. Conversely, if the pH of the solution is above the pHpzc value, then there would be net negative charge on the surface of adsorbent and it would attract positively charged species (cations). It revealed that the surface of the magnetic composite would have net positive and negative charge below and above this pH respectively <sup>49, 149, 158</sup>.



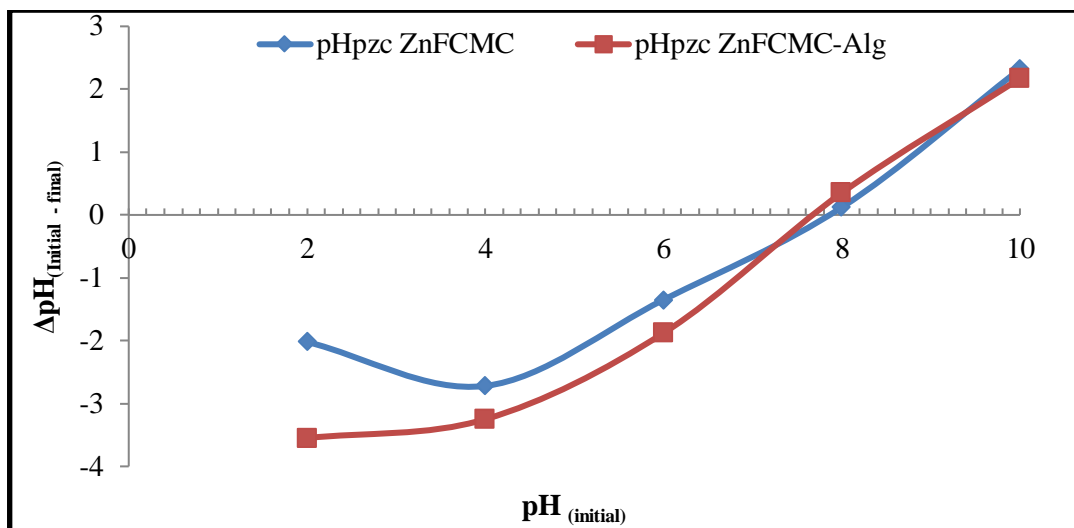


**Figure 4.4.7- pHpzc of ZnFCMC and ZnFCMC-Alg**

#### 4.5.9 Brunauer-Emmett-Teller (BET) Analysis

The BET analysis is the technique employed for the characterization of ZnF, ZnFCMC and ZnFCMC-Alg composite in terms of specific area, pore volume and pore diameter. Table 4.5.2 shows the results of BET analysis. As compared to pure ZnF, the surface area is decreased while pore diameter of the ZnFCMC and ZnFCMC-Alg composite were larger, which supports the successful surface modification of pure ZnF due to increase in the size of the particle. These findings confirm the effective attachment of the alginate component to the pure ZnF surface.

**Table 4.5.2- Results of BET analysis of ZnF, ZnFCMC and ZnFCMC-Alg composite**

Parameters	ZnF	ZnFCMC	ZnFCMC-Alg
Specific surface Area (in m <sup>2</sup> / g)	1.111	1.002	0.852
Total pore volume (cm <sup>3</sup> /g)	0.00343	0.00223	0.00393
Average Pore diameter (nm)	8.904	12.356	18.415

#### 4.5.10 Result of Batch Adsorption Studies of single and binary dye systems for ZnFCMC and ZnFCMC-Alg composite

##### 4.5.11 Effect of contact time

The process of adsorption is time dependent. To study this effect, a known quantity (0.1 g) of adsorbent (ZnFCMC and ZnFCMC-Alg) was added to dye solutions with known concentrations (50 mg/L for single dye system while 20 mg/L for binary dye systems

respectively) of 50 mL volumes in 250 mL Erlenmeyer flasks for fixed temperature at 150 rpm in a thermostatic shaker. The flasks were taken out of the shaker after the fixed time interval and lowered concentrations of dyes were measured with the help of the UV spectrophotometer (Shimadzu UV-1800).

Figure 4.5.8 illustrates the influence of contact time on concentration (Ct) and removal percentage for CV and MB in both single as well as binary dye systems. It was observed that the removal percentage increases rapidly before reaching equilibrium over time. This was caused by the adsorbent's surface having more available empty spaces. Consequently, empty spaces eventually filled up entirely and the adsorption rate slowed down till equilibrium was reached overtime <sup>49</sup>.

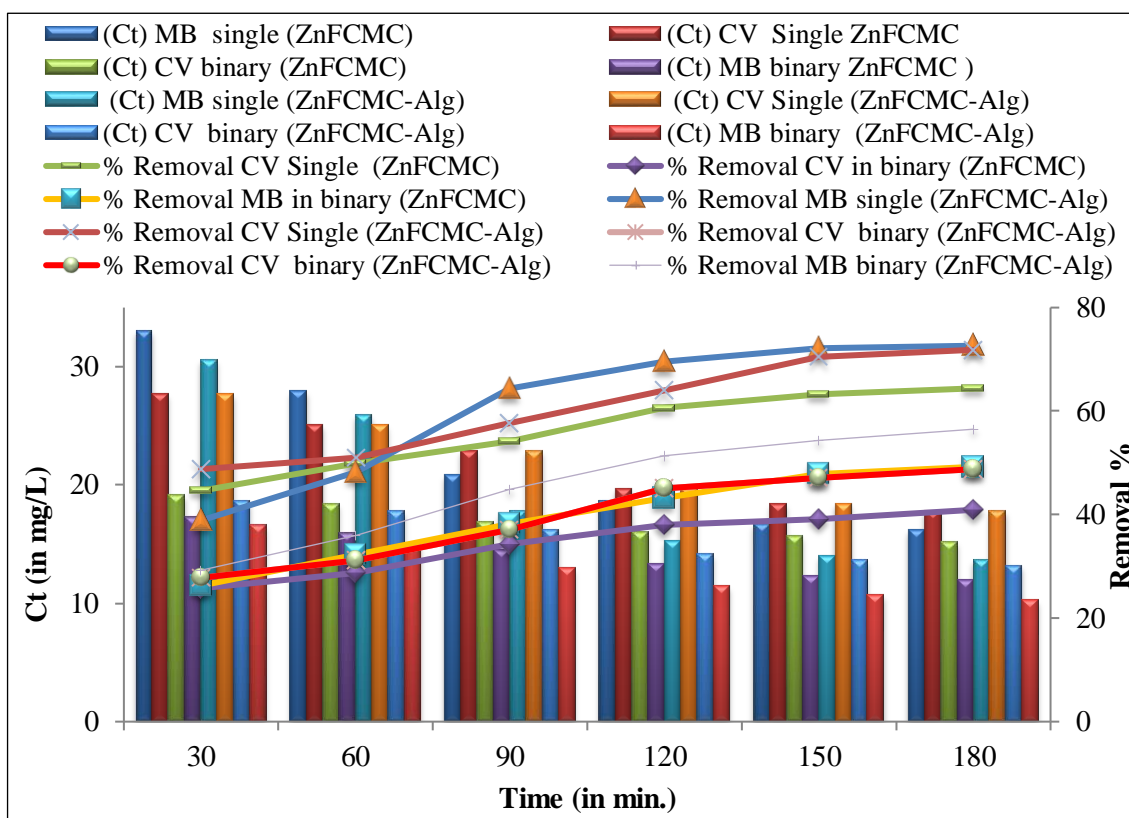


**Figure 4.5.8- Effect of contact time in single as well as binary dye system**

#### 4.5.12 Effect of adsorbent dose

The influence of adsorbent dosage amount on the percentage removal of dyes in both single as well as binary systems by using ZnFCMC and ZnFCMC-Alg is shown in Figure 4.5.9. A solution with known dye concentrations (50 mg/L for single dye system and 20 mg/L for binary dye system) and adsorbent doses (0.1 g to 0.5 g) was used to study this effect. It was found that adding more adsorbent enhanced the removal percentage from

63.49% to 76.39% of MB and 44.51% to 70.88% of CV by ZnFCMC while 77.57% to 90.29% for MB and 47.26% to 77.47% of CV by ZnFCMC-Alg in single dye system. When compared to a single dye system, the binary dye system is found to have a lower dye removal percentage. An increase in the removal percentage could be the result of more active sites become available as the adsorbent dosage increases in single and binary dye systems <sup>65</sup>. In the present work, 0.5 g of adsorbent was the optimal adsorbent dosage.

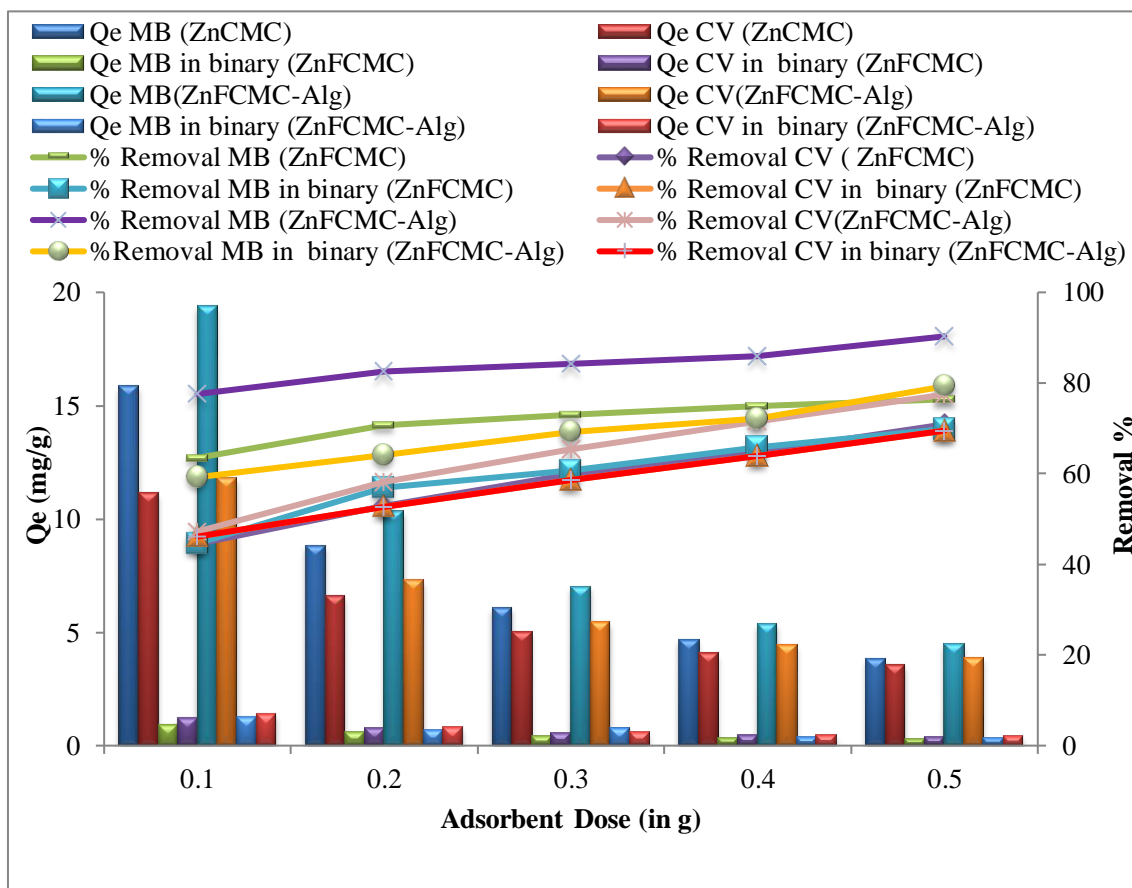


**Figure 4.5.9- Effect of adsorbent dosage in single as well as binary dye system**

#### 4.5.13 Effect of pH

The pH has direct effect on the material's adsorption behaviour since it changed the charge on the surface of the adsorbent. The investigation was carried out with a single dye system at different pH values between 2 and 10, with 50 mg/L initial dye concentration and 0.1 g adsorbent dose allowing for 3 hours time to attain equilibrium. The effect of pH on removal percentage of MB and CV dye solution for adsorbents is displayed in figure 4.5.10. At pH = 8, the maximum removal percentage was observed as 65.72% and 71.48% by using ZnFCMC for MB dye while 62.79% and 66.83% by using ZnFCMC-Alg for CV dye respectively and then further decreased.

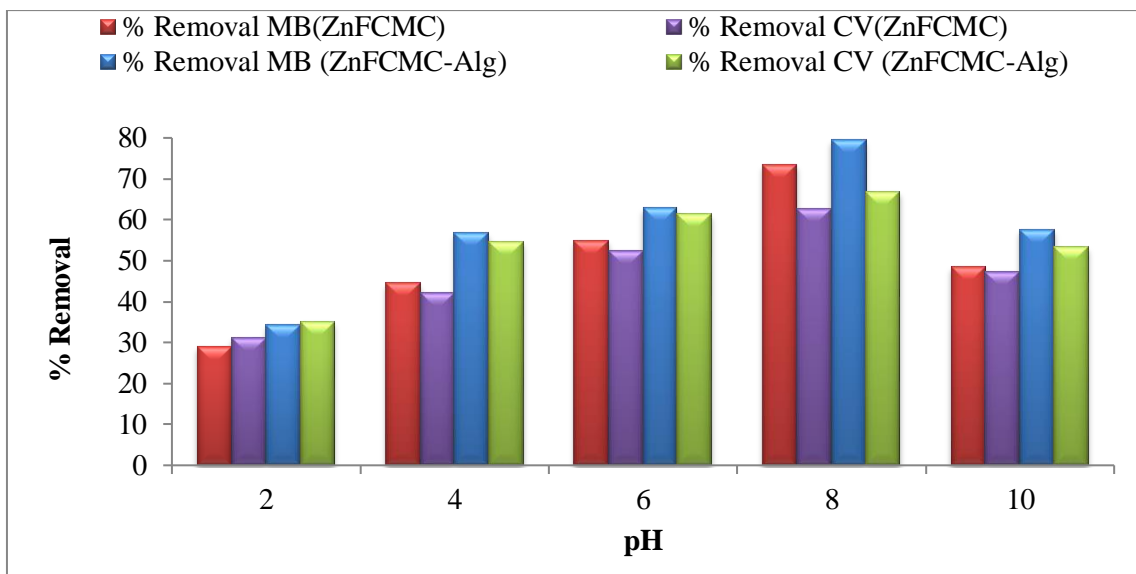


**Figure 4.5.10- Effect of pH on removal percentage of MB and CV dye**

The ZnFCMC-Alg composite behaved anionic below  $pH_{pzc} = 8.0$  and at low pH values, the electrostatic attractive forces were reduced. MB dye molecules and  $H^+$  ions competed to stick to the adsorbent surface because at lower pH values, there were more  $H^+$  ions in the aqueous solution. While comparing with  $H^+$  ions, these  $H^+$  ions are smaller and bind to the empty site more quickly, cationic dye molecules interact less electrostatically with the adsorbent surface. As pH increased, the adsorbent and dye molecules' electrostatic interaction intensified leading to increase in the degree of adsorption due to drop in surface charge density <sup>49, 143</sup>.

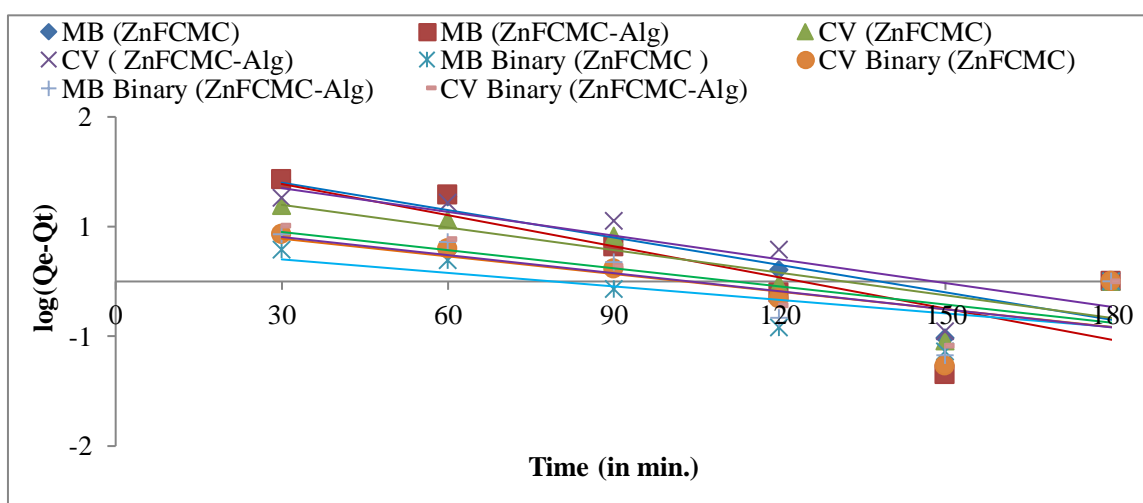
#### 4.5.14 Adsorption Kinetics

The adsorption behaviour in relation to time is determined by adsorption kinetics. Several models like the Lagergren pseudo-first order model, Lagergren pseudo-second order, Weber-Morris diffusion model and Elovich model of kinetics were employed for studying adsorption behavior <sup>78, 158</sup>.

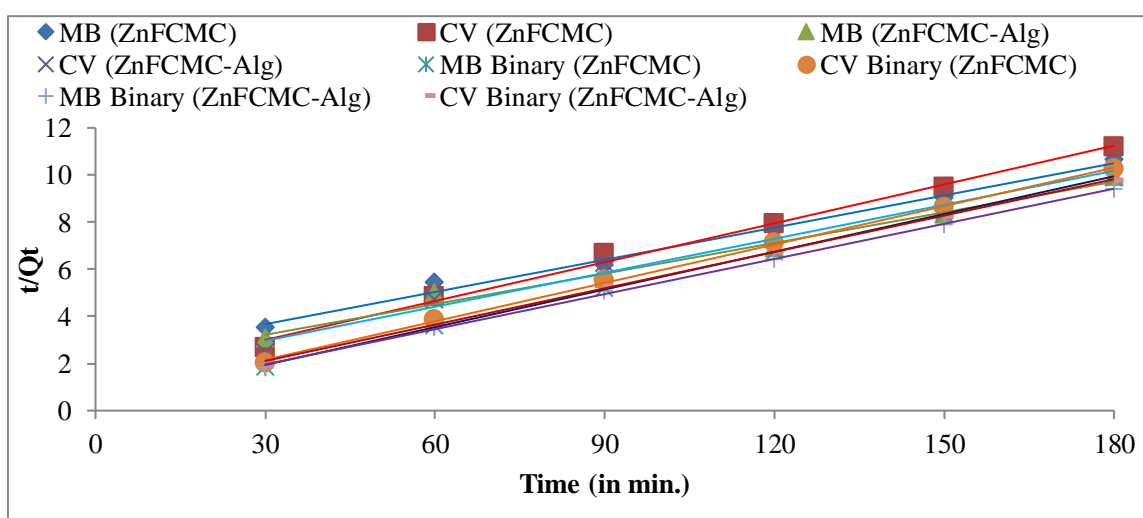
Table 4.5.3 and 4.5.4 shows the summary of the different adsorption constants computed for various models in both single as well as binary dye systems. The computed correlation coefficients ( $R^2$ ) values were compared to assess the fitness of several kinetic models. The adsorption behaviour will be chemisorption in nature if the data fits the kinetic model of pseudo second order; if not, it will be physical adsorption provided the data fulfill pseudo first order kinetics <sup>78</sup>. It was cleared from the results that among the numerous kinetic models, Lagergren pseudo-second order model best fit the adsorption

data as it had the highest  $R^2$  value. It showed that the adsorption process is carried out by the chemisorption mode between the molecules of dyes and adsorbent.

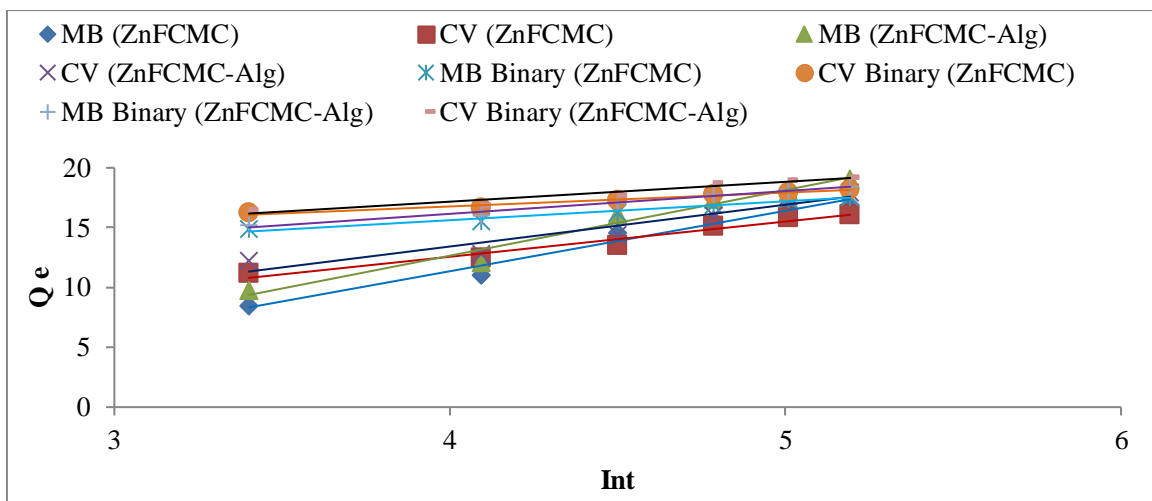
The Weber-Morris intra-particle diffusion model that determines the diffusion behaviour was used to analyze the adsorption behavior by plotting a graph between  $Q_t$  versus  $t^{0.5}$ . If that is the only rate determining step, then the origin must be crossed by a straight line. Figure 4.5.11 (d) showed that in the case of both adsorbents in both single as well as binary dye systems, the plot is non-linear and the line does not cross the origin. It showed that the factors other than intra particle diffusion may influence the adsorption rate<sup>49, 78</sup>.



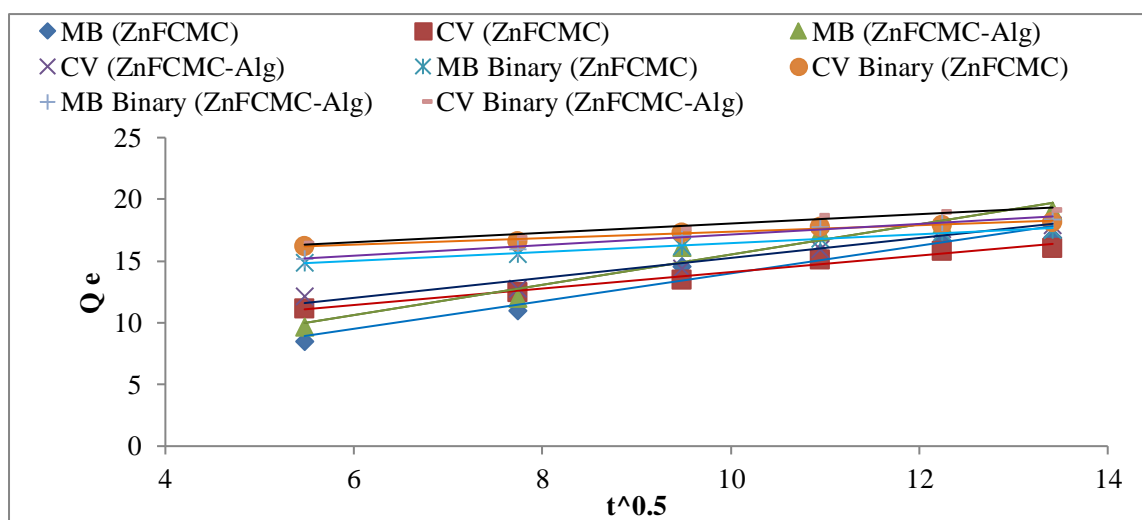
(a)



(b)



(c)



(d)

**Figure 4.5.11- Various kinetic models (a) Pseudo first order (b) Pseudo second order (c) Elovich (d) Weber-Morris diffusion model**

**Table 4.5.3- Calculated values of adsorption constants of different kinetic models for ZnFCMC and ZnFCMC-Alg at 298K in single dye system**

System→ Kinetic model ↓	Parameter	Single MB (ZnFCMC)	Single CV ZnFCMC)	Single MB (ZnFCMC- Alg)	Single CV (ZnFCMC- Alg)
<b>Lagergern Pseudo first order</b>	$Q_e$	14.151	11.682	14.894	8.037
	$k_1$	0.0191	0.0166	0.0219	0.0159

	$R^2$	0.777	0.741	0.670	0.702
<b>Lagergren Psuedo second order</b>	$Q_e$	21.978	18.182	23.095	20.79
	$h$	0.434	0.74	0.521	0.657
	$K_2$	0.009	0.0022	0.001	0.0015
	$R^2$	0.992	0.994	0.987	0.984
<b>Elovich model</b>	$\alpha$	29.08	3.85	29.79	4.08
	$\beta$	0.198	0.339	0.182	0.286
	$R^2$	0.975	0.966	0.969	0.903
<b>Weber -Morris Model</b>	$K_{id}$	1.122	0.667	1.226	0.809
	$I$	2.78	7.43	3.26	7.16
	$R^2$	0.950	0.981	0.956	0.957

**Table 4.5.4- Calculated values of adsorption constants of different kinetic models for ZnFCMC and ZnFCMC-Alg at 298K in binary dye system**

System→ Kinetic model ↓	Parameter	MB in binary (ZnFCMC)	CV in binary (ZnFCMC)	MB in binary (ZnFCMC- Alg)	CV in binary (ZnFCMC- Alg)
<b>Lagergren Pseudo first order</b>	$Q_e$	2.108	3.548	3.715	4.13
	$k_1$	0.0092	0.0115	0.0115	0.0115
	$R^2$	0.412	0.501	0.521	0.596
<b>Lagergren Psuedo second order</b>	$Q_e$	18.867	18.518	20.408	19.608
	$h$	2.958	1.89	2.118	1.776
	$K_2$	0.0083	0.0055	0.0051	0.0046

	$R^2$	0.999	0.998	0.998	0.999
<b>Elovich model</b>	$\alpha$	569.14	406.79	169.59	955.91
	$\beta$	0.632	0.863	0.526	0.603
	$R^2$	0.975	0.964	0.977	0.932
<b>Weber-Morris Model</b>	$K_{id}$	0.358	0.262	0.429	0.378
	I	12.86	14.75	12.85	14.25
	$R^2$	0.992	0.975	0.981	0.960

#### 4.5.15 Effect of Concentration

The impact of concentration of both dyes MB and CV was studied for the adsorbents ZnFCMC and ZnFCMC-Alg in both single as well as binary dye system. The initial dye concentration was taken between 50 and 250 mg/L (single dye system) and 20 and 100 mg/L (binary dye system) respectively. The adsorption capabilities of both adsorbents increased as the initial concentration of the dye solution increased as shown in figure 4.5.12 and 4.5.13 reaching a maximum at 250 mg/L in single dye system a maximum at 250 mg/L in single dye and 100 mg/L in binary dye system. It is because of the reason that as the dye concentration rises, more interactions took place between the adsorbent and adsorbate molecules. However, in both dye systems the removal percentage decreases as the solution's concentration increases. This may be the result of the adsorbent's surface having less accessible active sites as the dye concentration increases<sup>49, 149</sup>. At three distinct temperatures 25°C, 30°C and 35°C, the impact of concentration was examined. For both adsorbents, the adsorption capacity increased with rise in temperature. It was due to the reason that as the temperature increases, the interaction between the adsorbent and adsorbate occurs more quickly. It is because of the reason that the number of pores got increased with the rise in temperature. As a result of it, the surface area of the adsorbent also get increased that results in speeding up the adsorption process<sup>49, 78, 143</sup>.



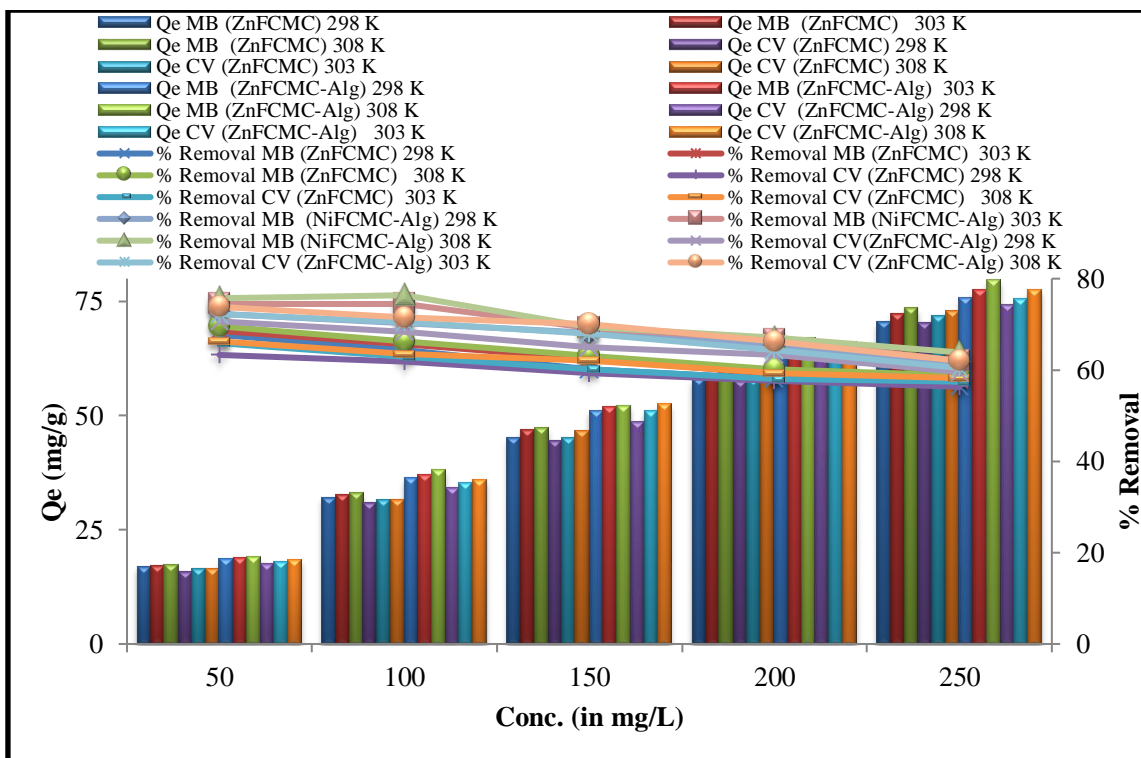


Figure 4.5.12- Effect of concentration on  $Q_e$  and percentage removal in single dye system

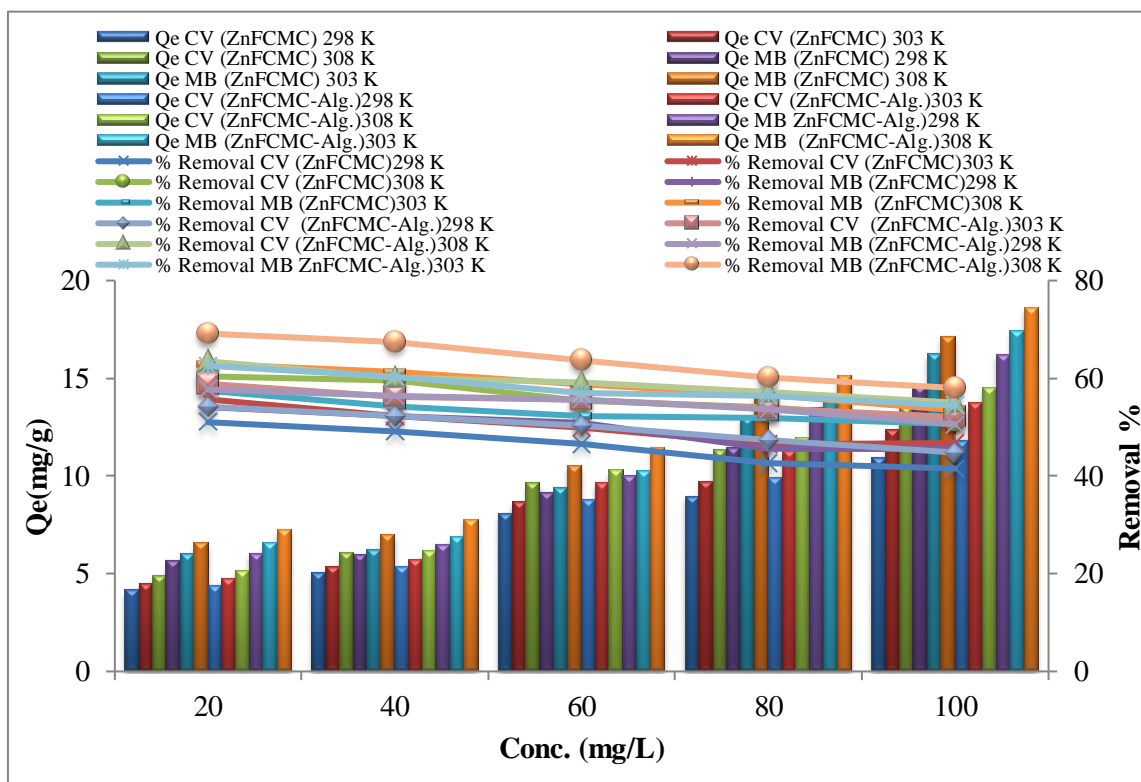


Figure 4.5.13- Effect of concentration on  $Q_e$  and percentage removal in binary dye system

#### 4.5.16 Adsorption Isotherms

The adsorption behavior was studied for various adsorption isotherms models viz. Langmuir, Freundlich, Temkin, and Dubinin-Radushkevich (D-R) in different dye systems. Figure 4.5.14 shows the calculated values of various constants by using the slope and intercept of graphs. In table 4.5.5 and 4.5.6, various adsorption isotherm models were compared on the basis of their correlation values ( $R^2$ ) and the results showed that the Langmuir model fits the adsorption data more precisely with highest  $R^2$  value among different isotherm models. It showed that the active sites are consistently arranged on the surface of magnetic bio-composite. It was found that the Langmuir adsorption capabilities in single dye system were 166.7 and 200.0 mg/g for MB while 250.0, 200.0 mg/g for CV and 45.45 and 55.56 mg/g for MB and 33.33 and 43.48 mg/g CV in binary dye system for ZnFCMC and ZnFCMC-Alg adsorbents respectively. The removal percentage in binary dye system was found lesser as compared to single dye system due to the antagonistic effects of the dyes in former case resulting in decreased removal efficiency. In a binary system, different dye molecules exhibit a variety of attractive forces that combine to form strong bonds. The decrease in dye adsorption behaviour in binary systems is a result of this strong bonding <sup>49, 116</sup>.

One of the crucial variables associated with the Langmuir adsorption isotherm is the separation factor ( $R_L$ ), which depicts the spontaneity of the adsorption process. According to the computed value of  $R_L$ , there are four types of adsorption behaviour: unfavourable ( $R_L > 1$ ), linear ( $R_L = 1$ ), favourable ( $0 < R_L < 1$ ) and irreversible ( $R_L = 0$ ). In the present study, the value of  $R_L$  lies in range 0-1 that shows that the Langmuir adsorption isotherm was advantageous in this study.

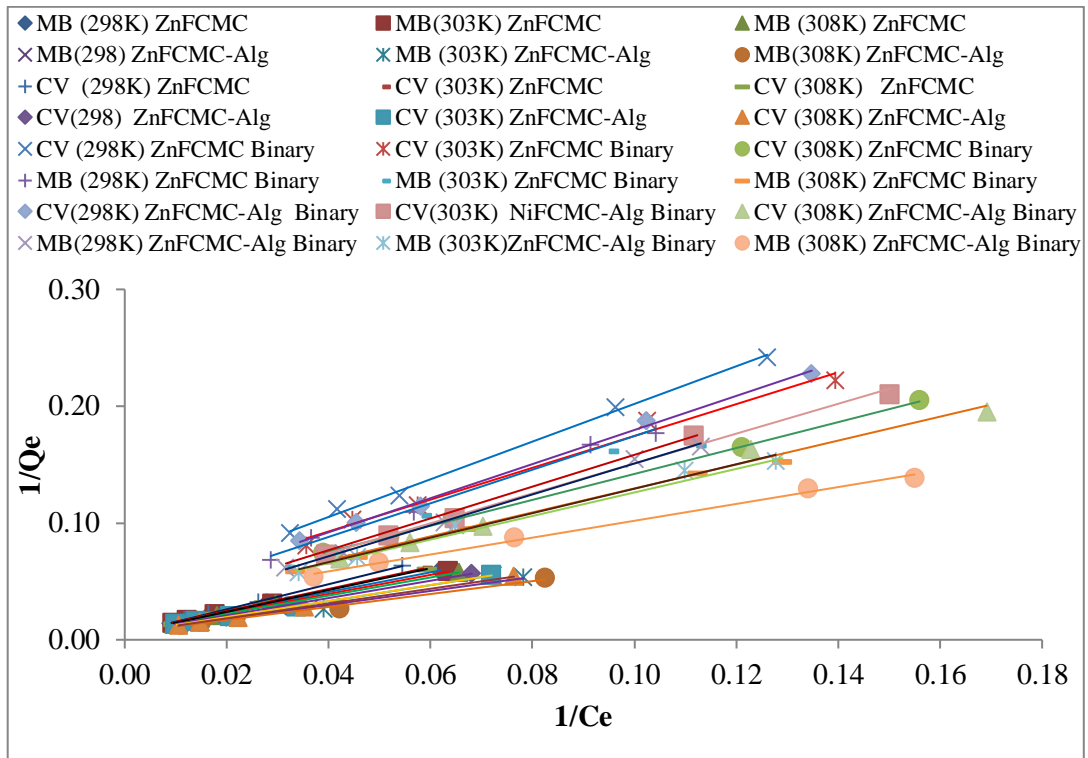
The adsorption energy ( $E$ ) that represents the type of adsorption in D-R model is an important parameter. Physical adsorption will occur if the predicted adsorption energy is less than 50 kJ/mol; if not, chemisorption will occur. The determined value of adsorption energy for the ZnFCMC and ZnFCMC-Alg adsorbents in single and binary systems as shown in table 4.5.5 and 4.5.6 was larger than 100 kJ/mol indicating that chemisorption occurred throughout the current study.

**Table 4.5.5- Computed values for various constants of different adsorption isotherm models at 25°C, 30°C and 35° C in single dye system ZnFCMC and ZnFCMC-Alg composite**

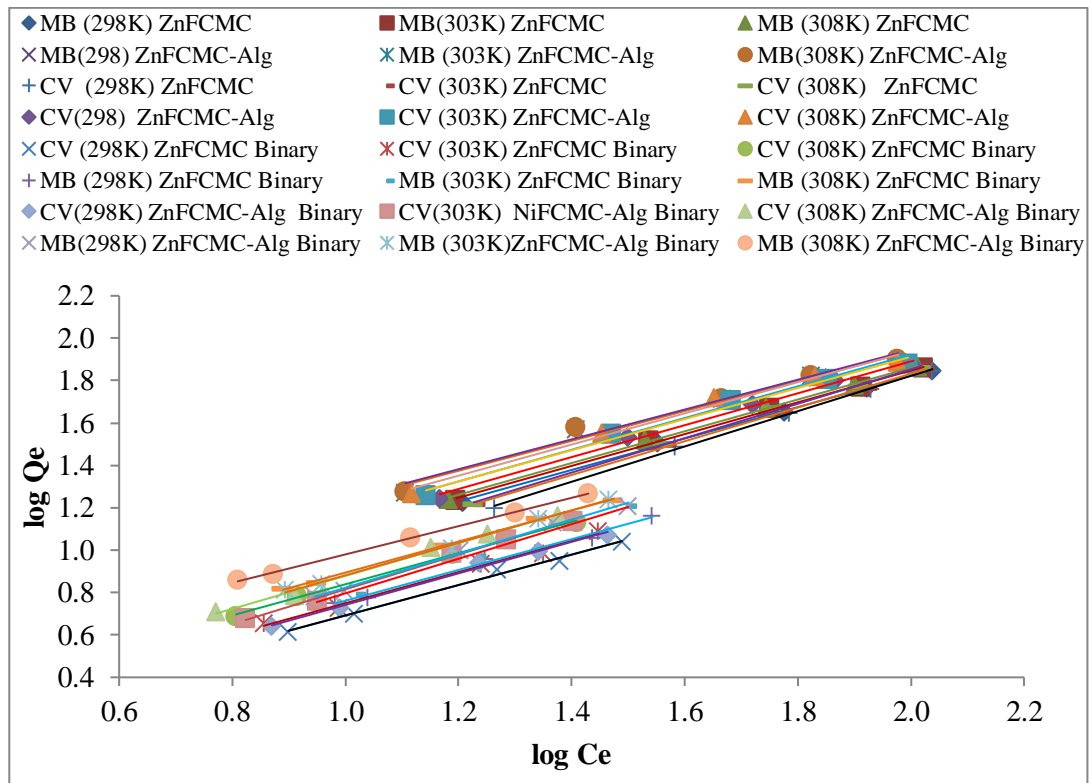
System→ Isotherm model ↓	Constant	Single MB (ZnFCMC)			Single CV (ZnFCMC)			Single MB (ZnFCMC-Alg)			Single CV (ZnFCMC-Alg)		
Temperature		25°C	30°C	35°C	25°C	30°C	35°C	25°C	30°C	35°C	25°C	30°C	35°C
<b>Langmuir</b>	<b>Q</b>	142.86	166.67	166.67	250.00	200.00	200.00	200.00	200.00	166.67	166.67	200.00	200.00
	<b>B</b>	0.0083	0.0073	0.0077	0.0037	0.0053	0.0054	0.0073	0.0083	0.0108	0.0081	0.0073	0.0079
	<b>R<sup>2</sup></b>	0.998	0.999	0.999	0.999	0.999	0.999	0.999	0.993	0.987	0.999	0.999	0.999
	<b>R<sub>L</sub></b>	0.706	0.731	0.722	0.844	0.791	0.789	0.733	0.707	0.649	0.712	0.733	0.717
<b>Freundlich</b>	<b>K<sub>f</sub></b>	2.187	2.223	2.301	1.432	1.734	1.694	2.667	3.381	3.443	2.426	2.767	2.944
	<b>1/n</b>	0.741	0.75	0.749	0.833	0.796	0.811	0.748	0.704	0.703	0.752	0.735	0.735
	<b>R<sup>2</sup></b>	0.998	0.997	0.998	0.998	0.998	0.998	0.987	0.978	0.978	0.994	0.988	0.986
<b>Temkin</b>	<b>b<sub>T</sub></b>	92.1	89.1	88.1	84.2	86.2	83.3	83.4	86.1	86.1	85.4	85.4	83.3
	<b>A</b>	0.102	0.104	0.107	0.082	0.091	0.091	0.121	0.142	0.152	0.112	0.123	0.129
	<b>R<sup>2</sup></b>	0.965	0.97	0.967	0.966	0.957	0.966	0.987	0.993	0.985	0.98	0.99	0.989
<b>D-R model</b>	<b>Q<sub>m</sub></b>	55.9	57.6	51.9	56.6	56.5	58.0	63.2	64.9	66.0	60.6	62.4	63.8
	<b>K</b>	6×10 <sup>-5</sup>	5×10 <sup>-5</sup>	4×10 <sup>-5</sup>	8×10 <sup>-5</sup>	7×10 <sup>-5</sup>	6×10 <sup>-5</sup>	4×10 <sup>-5</sup>	3×10 <sup>-5</sup>	3×10 <sup>-5</sup>	5×10 <sup>-5</sup>	4×10 <sup>-5</sup>	4×10 <sup>-5</sup>
	<b>R<sup>2</sup></b>	0.86	0.867	0.820	0.874	0.857	0.862	0.912	0.912	0.914	0.877	0.891	0.885
	<b>E</b>	91.29	100	111.8	79.1	84.5	91.3	111.8	129.1	129.1	100.0	111.8	111.8

**Table 4.5.6- Computed values for various constants of different adsorption isotherm models at 25°C, 30°C and 35° C in binary dye system for ZnFCMC and ZnFCMC-Alg composites**

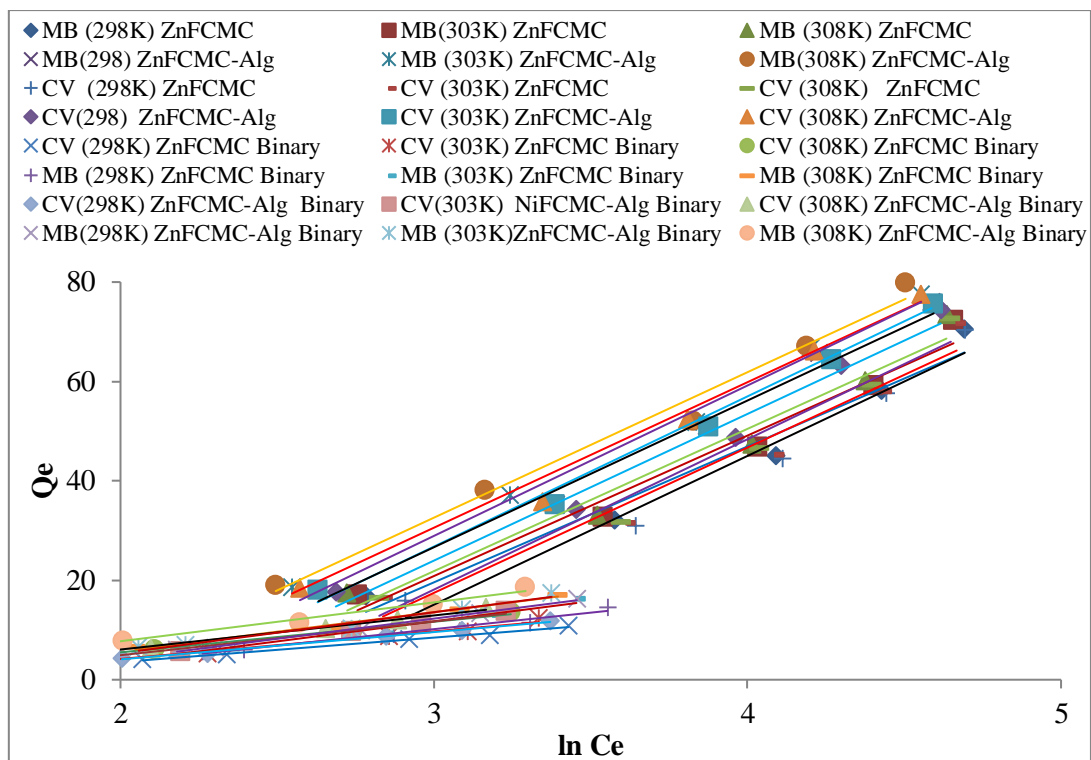
System→	Constant	CV in Binary (ZnFCMC)			MB in Binary (ZnFCMC)			CV in Binary (ZnFCMCAlg)			MB in Binary ( ZnFCMC-Alg)		
Isotherm model ↓													
Temperature		25°C	30°C	35°C	25°C	30°C	35°C	25°C	30°C	35°C	25°C	30°C	35°C
<b>Langmuir</b>	<b>Q</b>	25.00	26.32	33.33	45.45	40.00	32.26	30.30	43.48	37.04	55.56	41.67	34.48
	<b>B</b>	0.0248	0.0279	0.0208	0.0162	0.0248	0.0279	0.0226	0.0179	0.0263	0.0136	0.0229	0.0402
	<b>R<sup>2</sup></b>	0.996	0.987	0.992	0.978	0.995	0.999	0.997	0.992	0.988	0.997	0.987	0.994
	<b>R<sub>L</sub></b>	0.667	0.641	0.704	0.755	0.667	0.63	0.689	0.736	0.655	0.786	0.686	0.554
<b>Freundlich</b>	<b>K<sub>f</sub></b>	1.059	1.03	1.271	1.084	1.045	1.448	1.002	1.012	1.265	1.047	1.309	2.051
	<b>1/n</b>	0.717	0.736	0.726	0.726	0.815	0.732	0.743	0.82	0.776	0.802	0.764	0.667
	<b>R<sup>2</sup></b>	0.983	0.982	0.989	0.991	0.991	0.997	0.990	0.990	0.987	0.981	0.984	0.989
<b>Temkin</b>	<b>b<sub>T</sub></b>	511.5	454.1	409.2	379.7	311.5	318.9	458.4	370.8	367.5	310.8	305.8	322.3
	<b>A</b>	0.278	0.287	0.331	0.231	0.213	0.279	0.285	0.279	0.328	0.227	0.259	0.364
	<b>R<sup>2</sup></b>	0.987	0.966	0.992	0.976	0.966	0.989	0.994	0.984	0.984	0.994	0.971	0.982
<b>D-R model</b>	<b>Q<sub>m</sub></b>	10.7	11.2	12.9	13.6	15.0	16.2	11.3	12.9	13.5	15.9	16.1	16.9
	<b>K</b>	1×10 <sup>-5</sup>	9×10 <sup>-5</sup>	8×10 <sup>-6</sup>	2×10 <sup>-5</sup>	1×10 <sup>-5</sup>	1×10 <sup>-5</sup>	1×10 <sup>-5</sup>	9×10 <sup>-6</sup>	7×10 <sup>-6</sup>	1×10 <sup>-5</sup>	1×10 <sup>-5</sup>	7×10 <sup>-6</sup>
	<b>R<sup>2</sup></b>	0.937	0.894	0.945	0.930	0.886	0.929	0.939	0.914	0.902	0.949	0.898	0.914
	<b>E</b>	223.6	235.7	250	158.1	223.6	223.6	223.6	235.7	267.3	223.6	223.6	267.3



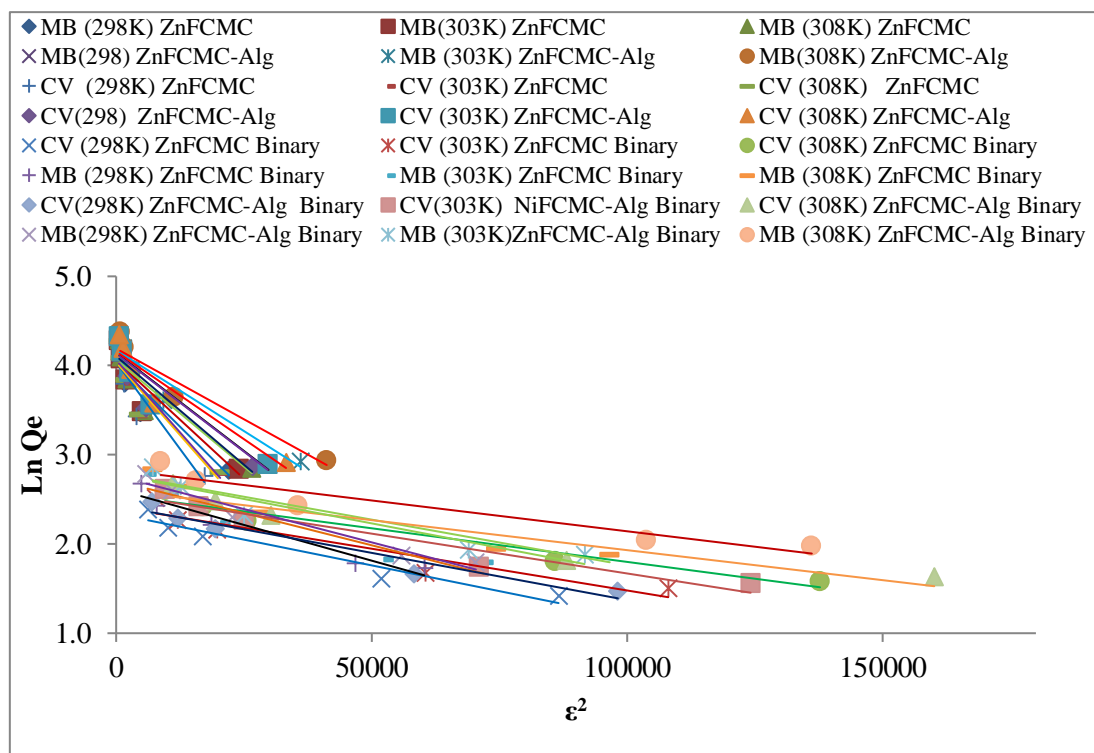
(a)



(b)



(c)



(d)

**Figure 4.5.14- Various adsoption isotherms plots (a) Langmuir (b)Freundlich (c) Temkin (d) D-R isotherm**

From the literature review, the adsorption studies with different adsorbents were reviewed. Table 4.5.7 represents the Langmuir adsorption capacities of different adsorbents for adsorption of both MB and CV dyes as reported in previous studies. On comparing, it was observed that NiFCMC, ZnFCMC, NiFCMC-Alg and ZnFCMC-Alg composites might be suitable eco-friendly adsorbent to remove MB and CV dyes from aqueous solution. Among these four composites, ZnFCMC and ZnFCMC-Alg composite have high adsorption capacity to remove MB and CV dyes in single as well as binary dye system from aqueous solution.

**Table 4.5.7- Comparative study of adsorption capabilities of different adsorption materials for MB and CV dyes**

Adsorption material	Adsorption Capabitiy for CV (mg/g)	Adsorption Capability for MB (mg/g)	Reference
Palm Kernal fiber	78.9	95.4	162
CMC/k-carrageenan/activated montmorillonite composite beads	-	12.25	134
Alginate coated perlite beads	-	104.1	108
Cyanthilium cinereum(L) H. Rob (CCLHR	-	76.33	163
Paspalum maritimum (PMT)	-	56.18	
CMC-Alg/GO hydrogel beads	-	78.5	120
Eucalyptus Camdulensis Biochar	56	123.3	164
Citrullus colocynthis seeds (CCS)	-	18.83	165
Citrullus colocynthis peels (CCP)	-	4.48	
CMC-Poly(acrylic acid-co- acrylamide) nanocomposite	-	34.3	60

PVA/CMC/Turmeric film	-	6.27	122
Sodium Alginate/ Lignin micro beads	-	254.3	113
Alginate/Clinoptilolite/ Fe <sub>3</sub> O <sub>4</sub>	16.52 (single), 15.79 (binary) 11.47 (binary)	-	61
3-Allyloxy-2-hydroxy-1- propanesulfonic acid sodium salt	-	79.42	139
CMC/ Acrylamide/ N- Vinylpyrrolidone(CMC-AM- NVP) copolymer	-	81.96	119
NiFCMC  NiFCMC-Alg composite	112.35 (single), 16.10 (binary) 97.08 (single), 21.23 (binary)	113.60 (single), 25.57 (binary) 99.01(single) 29.85 (binary)	Present study
ZnFCMC  ZnFCMC-Alg composite	250.0 (single), 33.33 (binary) 200.00 (single), 43.48 (binary)	166.67 (single), 45.45 (binary) 200.00 (single), 55.56 (binary)	Present study

#### 4.5.17 Adsorption Thermodynamics

Adsorption thermodynamics determines the amount of energy evolved from initial to final state in the adsorption process.  $H^\circ$  (Enthalpy of adsorption),  $G^\circ$  (Gibbs free energy) and  $S^\circ$  (entropy) are three thermodynamic characteristics employed to study the adsorption behaviour.

From the values of slope and intercept of linear plot of  $\ln K_d$  vs  $1/T$  the values of  $H^\circ$  and  $S^\circ$  are calculated as shown in figure 4.5.15 and 4.5.16. Various adsorption thermodynamic parameters were calculated and listed in table 4.5.9. The adsorbate and adsorbent exhibited a strong interaction as evidenced by the computed values of two parameters viz.  $\Delta H^\circ$  and  $\Delta S^\circ$  for both adsorbents which were found to be positive suggesting that the adsorption process was endothermic. In both dye systems, the calculated  $\Delta G^\circ$  value was



negative, which confirms the spontaneous nature of adsorption process<sup>49, 78, 162</sup>.

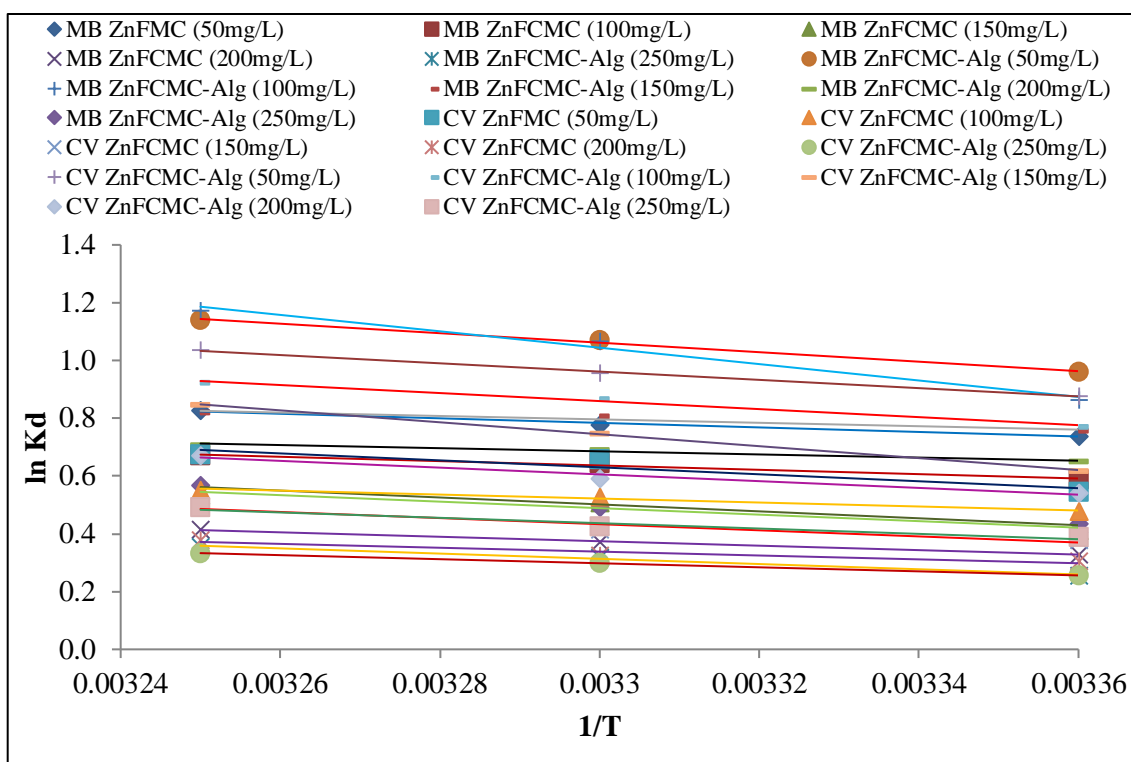


Figure 4.5.15- Graph between  $\ln K_d$  vs  $1/T$  for MB and CV in single dye system

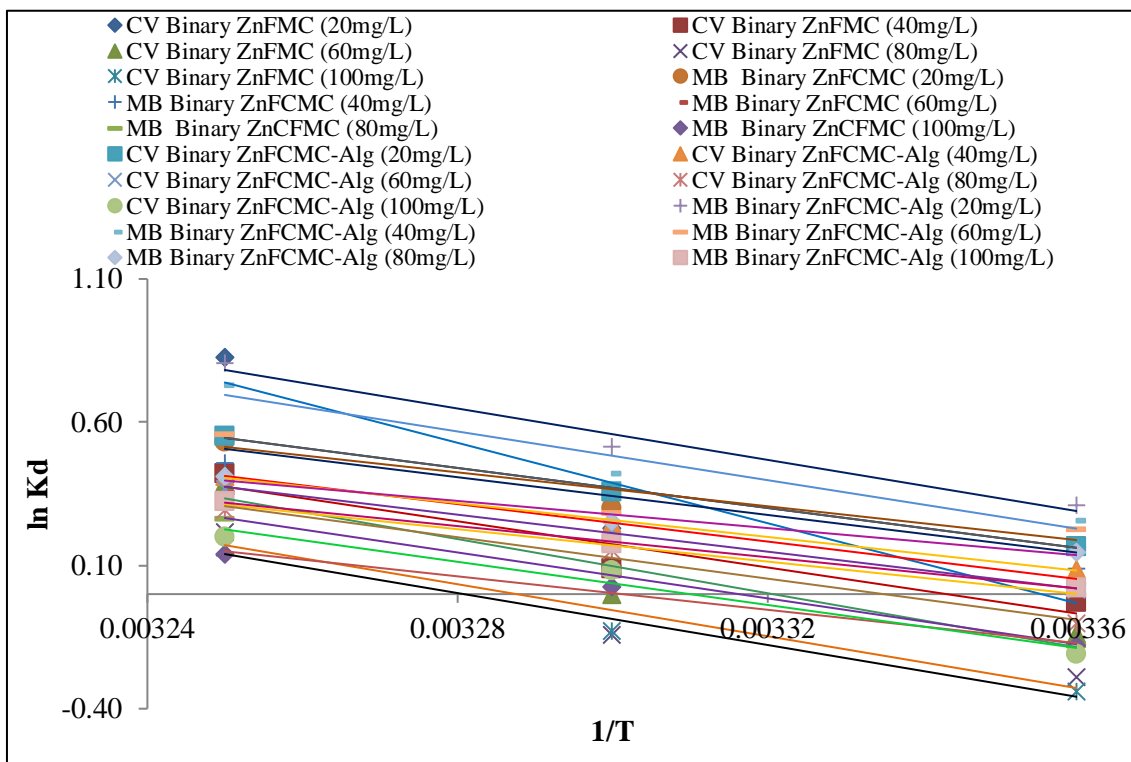


Figure 4.5.16- Graph between  $\ln K_d$  vs  $1/T$  for MB and CV in binary dye system

**Table 4.5.8- Calculated values of  $\Delta H^\circ$ ,  $\Delta S^\circ$  and  $\Delta G^\circ$  in both dye systems (single and binary)**

<b>System</b>	<b>Conc. (mg/L)</b>	<b><math>\Delta H^\circ</math> (KJ/mol)</b>	<b><math>\Delta S^\circ</math> (KJ/mol/ K)</b>	<b><math>\Delta G^\circ</math> (25°C) (kJ/mol)</b>	<b><math>\Delta G^\circ</math> (30°C) (kJ/mol)</b>	<b><math>\Delta G^\circ</math> (35°C) (kJ/mol)</b>
<b>Single CV ZnFCMC</b>	50	10.0	0.038	-1.350	-1.657	-1.729
	100	5.7	0.023	-1.185	-1.330	-1.415
	150	8.8	0.033	-0.936	-1.045	-1.269
	200	5.6	0.021	-0.753	-0.819	-0.971
	250	5.8	0.022	-0.631	-0.756	-0.850
<b>Single MB ZnFCMC</b>	50	6.5	0.028	-1.831	-1.962	-2.115
	100	6.2	0.026	-1.458	-1.622	-1.715
	150	9.3	0.035	-1.022	-1.277	-1.369
	200	6.4	0.024	-0.814	-0.936	-1.061
	250	7.5	0.027	-0.636	-0.800	-0.912
<b>Single CV ZnFCMC- Alg</b>	50	11.9	0.047	-2.175	-2.407	-2.653
	100	11.5	0.045	-1.914	-2.187	-2.367
	150	17.2	0.063	-1.535	-1.885	-2.167
	200	9.7	0.037	-1.343	-1.488	-1.720
	250	7.7	0.029	-0.959	-1.068	-1.254
<b>Single MB ZnFCMC- Alg</b>	50	13.7	0.054	-2.376	-2.695	-2.918
	100	23.6	0.086	-2.138	-2.690	-3.003
	150	4.9	0.023	-1.873	-2.031	-2.100
	200	4.5	0.021	-1.611	-1.744	-1.817
	250	10.0	0.037	-1.078	-1.234	-1.455
<b>CV in binary</b>	20	58.3	0.196	-0.099	-0.574	-1.079
	40	33.5	0.112	-0.085	-0.227	-0.995

<b>(ZnFCMC)</b>	60	39.3	0.130	-0.336	-0.007	-0.556
	80	37.7	0.124	-0.731	-0.355	-0.416
	100	37.7	0.124	-0.848	-0.322	-0.136
<b>MB in binary (ZnFCMC)</b>	20	27.4	0.093	-0.407	-0.300	-1.356
	40	27.2	0.092	-0.223	-0.167	-1.170
	60	23.5	0.079	-0.088	-0.094	-0.905
	80	33.3	0.110	-0.442	-0.072	-0.671
	100	24.3	0.080	-0.447	-0.025	-0.354
<b>CV in binary (ZnFCMC-Alg)</b>	20	29.0	0.099	-0.414	-0.901	-1.414
	40	24.5	0.083	-0.215	-0.623	-1.055
	60	26.8	0.090	-0.036	-0.563	-0.943
	80	30.0	0.100	-0.254	-0.388	-0.749
	100	31.3	0.104	-0.517	-0.210	-0.516
<b>MB in binary (ZnFCMC-Alg)</b>	20	37.2	0.128	-0.768	-1.292	-2.066
	40	35.3	0.120	-0.638	-1.055	-1.869
	60	24.6	0.084	-0.559	-0.713	-1.431
	80	19.7	0.067	-0.363	-0.638	-1.049
	100	22.6	0.076	-0.058	-0.442	-0.828

#### 4.5.18 Regeneration of Adsorbent

In recycling, regeneration efficiency significantly influenced the adsorbent performance and cost-effectiveness of the adsorbent. To regenerate the ZnFCMC and ZnFCMC-Alg composite in the present work, 0.1N HCl was used as the desorbing solvent. The regeneration capacity was examined over a maximum of five cycles. Table 4.5.9 and figure 4.5.17 displayed the regeneration capacity and percentage weight loss for each adsorbent. From the table, it was evident that after five cycles, the regeneration efficiency percentages for ZnFCMC and ZnFCMC-Alg in single dye system remained 78.8%,

81.3% for MB and 70.8%, 76.4% for CV. Additionally, the weight loss for five cycles of adsorption-desorption was also determined. In a single MB and CV study, the weight loss was 17.4%, 20.8%, and 21.6%, 26.6% for ZnFCMC and ZnFCMC-Alg adsorbent respectively. The findings showed that for both single as well as binary dye systems, ZnFCMC and ZnFCMC-Alg composite were efficient and inexpensive dye removal alternatives.

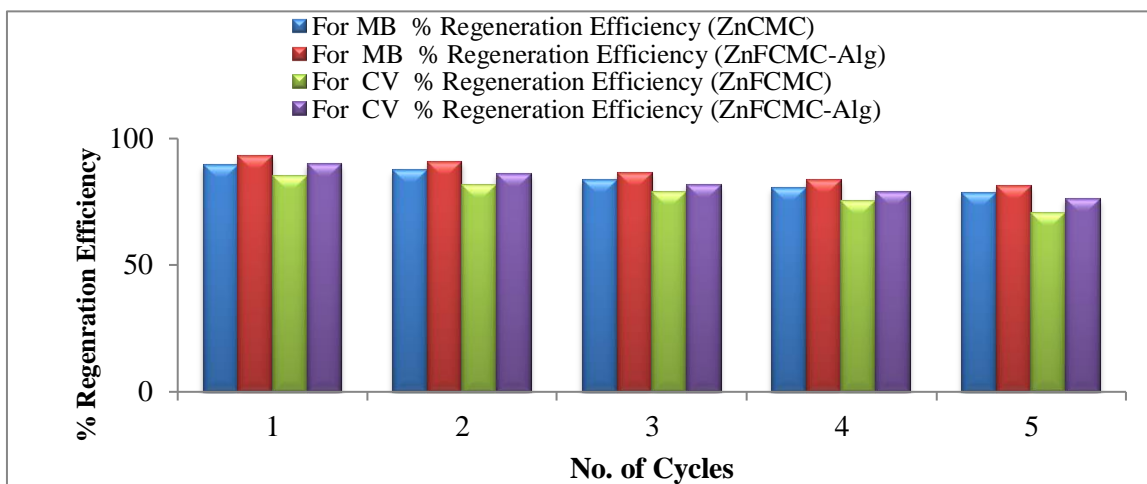


**Figure 4.5.17- Percentage regeneration efficiency of ZnFCMC and ZnFCMC-Alg adsorbent**

In order to properly dispose of the adsorbents loaded with MB and CV dyes, the characteristics of the materials and their possible effects on the environment need to be carefully considered. The regeneration and reuse of the adsorbents would be the primary method and in the present study, the regenerating and reusing the spent adsorbent upto five cycles of desorption-adsorption have been employed. The dyes like MB and CV can be desorbed from the adsorbent by employing suitable solvents or mild acidic solutions like 0.1 N HCl.

For safe disposal of metal ferrites, recycling is the preferred way as these ferrites contain valuable metals that can be extracted and reused. It is carried out by hydrometallurgical processes like acid leaching, reduction, purification and co-precipitation <sup>166, 167</sup>. Carboxymethyl cellulose (CMC) and alginates are generally considered safe for disposal due to their environmentally friendly, biodegradable and non-toxic nature. The proper disposal techniques like biodegradation by micro-organism, safe encapsulation and stabilized material to minimize leaching and environment contamination need to be considered as per standard waste management practices <sup>168, 169</sup>.

**Table 4.5.9- Percentage regeneration efficiency of ZnFCMC and ZnFCMC-Alg adsorbent**

<b>No.of Cycles</b>	<b>For MB % Regeneration Efficiency (ZnCMC)</b>	<b>For MB % Regeneration Efficiency (ZnFCMC-Alg)</b>	<b>For CV % Regeneration Efficiency (ZnFCMC)</b>	<b>For CV % Regeneration Efficiency (ZnFCMC-Alg)</b>	<b>Adsorbent weight loss % following five cycles (for MB )</b>		<b>Adsorbent weight loss % following five cycles (for CV )</b>	
					<b>ZnFCMC</b>	<b>ZnFCMC-Alg</b>	<b>ZnFCMC</b>	<b>ZnFCMC-Alg</b>
1	90.70	93.31	85.05	90.04	17.4	20.8	21.64	26.6
2	87.47	90.98	81.85	86.12				
3	83.65	86.41	79.00	81.85				
4	80.68	83.65	75.44	79.29				
5	78.82	81.32	70.82	76.46				

#### 4.5.19 Mechanism of Adsorption

Figure 4.5.18 shows a general mechanism that has been developed as a result of observations from the current investigation. The removal of cationic dyes and metal ions from an aqueous medium depends critically on modification of the surface of metal ferrites viz. nickel and zinc ferrites by carboxymethyl cellulose and sodium alginate. Due to the presence of various functional groups especially -OH and -COOH on the surface of linear chain structures of carboxymethyl cellulose and alginate which serve as binding sites for adsorption. Both the adsorbate and adsorbent molecules interact electrostatically as a result of these functional groups present on the adsorbents' surface. When functional groups like -OH and -COOH are present, the adsorbent's surface becomes negatively charged which encouraged positively charged dyes and metal ions to stick to it and increased removal efficiency. The process of adsorption was favoured by chemisorption mode.

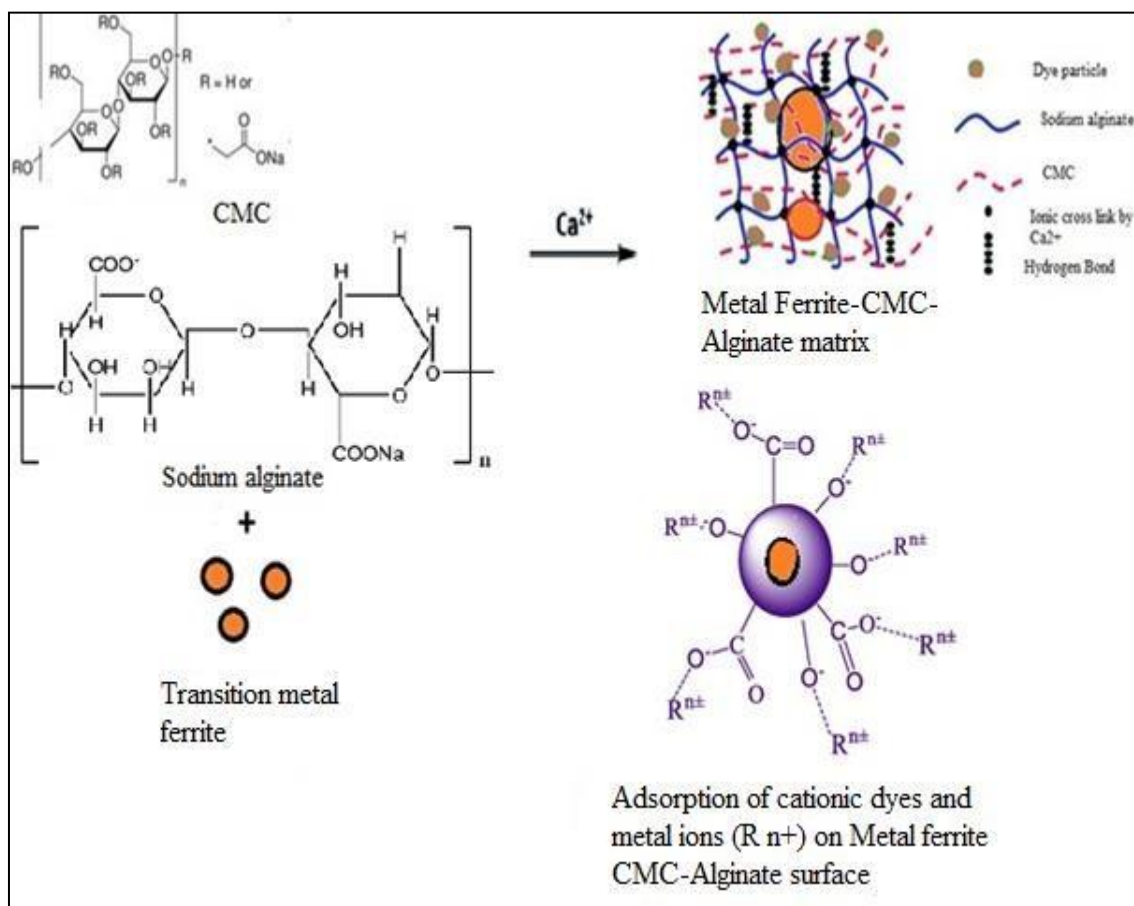
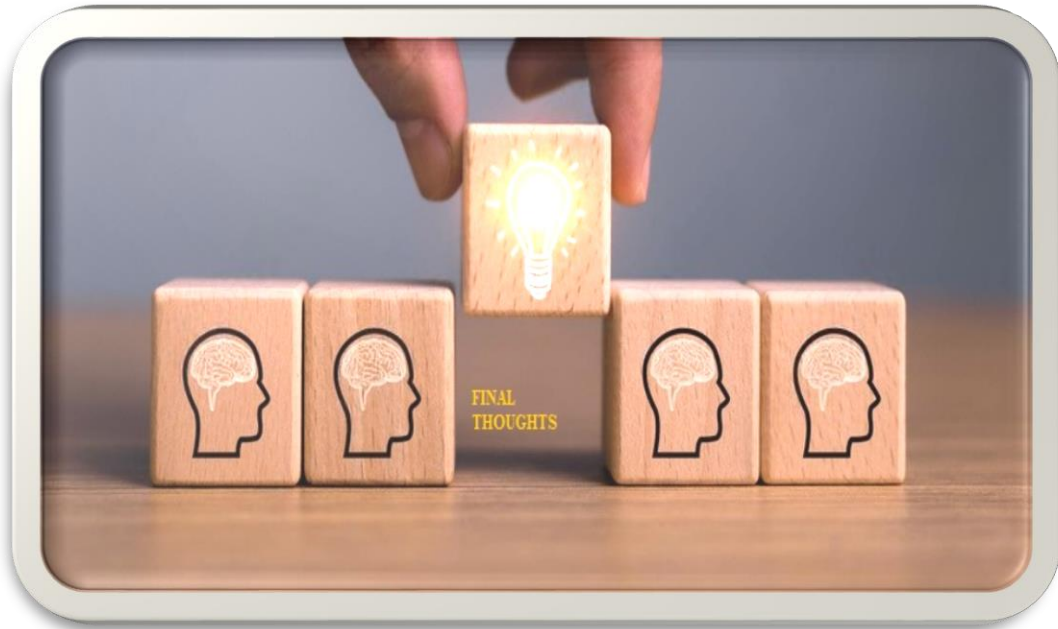


**Figure 4.5.18- Adsorption mechanism of cationic dyes and metal ion on Metal CMC-Alginate composite surface**



## **CHAPTER 5**

### **SUMMARY AND CONCLUSIONS**

## 5.0 Summary and Conclusions

In the current research work, the carboxymethyl cellulose was synthesized from the cellulose extracted from the corncob- an agricultural waste. The synthesis of different transition metal spinel ferrites such as NiF and ZnF was done and their surface modification was carried out with carboxymethyl cellulose and sodium alginate to form NiFCMC, ZnFMC, NiFCMC-Alg and ZnFCMC-Alg for their potential use as adsorbents for the removal of dyes and metal ions. These adsorbents were characterized and their surface morphology was studied by number of methods including FTIR (Fourier Transform Infrared Spectroscopy), XRD (X-Ray Diffraction), FESEM (Field emission scanning electron microscopy), EDS (Energy-dispersive spectra), BET (Brunauer-Emmett-Teller), TGA (Thermogravimetric analysis), VSM (Vibration sample magnetometry) and pH<sub>pzc</sub> (pH of point zero charge). The important findings of this research are listed below:

- The carboxymethyl cellulose (CMC) was synthesized from extracted cellulose by alkalization and etherification methods. Characterization of prepared CMC was carried out by FTIR, XRD and SEM techniques. Back titration method was used to determine the Degree of Substitution (DS). The synthesized CMC obtained has a large DS value of 2.27, purity of 91.65% and yield of 1.20 g/g, water and oil holding capacity of 3.81 g/g and 1.66 g/g respectively. The high degree of substitution is achieved in this work.
- FTIR spectra of various transition metal ferrites shows two strong peaks at 500-600 cm<sup>-1</sup> and 400-450 cm<sup>-1</sup> respectively which corresponds to the metal-oxygen bond at the tetrahedral and octahedral site that confirm the formation of spinel metal ferrites. A significant distinct peak at 3305-3317.7 cm<sup>-1</sup> was observed in the spectra for NiFCMC, NiFCMC-Alg, ZnFCMC and ZnFCMC-Alg. This peak is attributed to the stretching vibration of the hydroxyl (-OH) group while the aliphatic -CH stretching of the ether part generated by carboxymethylation of cellulose was shown at 2897.7-2913 cm<sup>-1</sup>. The presence of other significant peaks confirmed the presence of particular functional groups which revealed the successful surface modification of different metal ferrite with carboxymethylcellulose and sodium alginate.
- XRD studies showed that different metal ferrites (NiF, ZnF) in the spinel like structure have greater crystallinity and phase purity. However, similar diffraction peaks with slight variation in XRD pattern was observed in case of NiFCMC, ZnFCMC and NiFCMC-Alg and ZnFCMC-Alg composite. The reason could be that on modification of surface,



magnetic composite's size is increased. That causes the shift in the XRD angle. The average crystalline size of 21 nm for NiF, 31.2 nm for ZnF, 25.63 nm for NiFCMC, 34.43 nm for ZnFCMC, 38.42 nm for NiFCMC-Alg and 46.03 nm for ZnFCMC-Alg was calculated by the use of the Scherrer formula. However, it has been observed that different composites retain the phase purity with spinel character even on surface modification.

- FESEM analysis inferred that the typical size range of NiF, ZnF was 0.549  $\mu\text{m}$ , 1.58  $\mu\text{m}$  while that of NiFCMC and ZnFCMC was found to be 3.5  $\mu\text{m}$  and 2.80  $\mu\text{m}$  respectively. It was proposed that NiFCMC and ZnFCMC had a greater size and increased porosity compared to uncoated NiF and ZnF. Due to coating of biopolymer on the surface of NiF and ZnF, the agglomeration was reduced. Moreover, the cross-section of the NiFCMC-Alg and ZnFCMC-Alg composite revealed an interior with increased surface porosity. Elemental composition of different ferrites and their composites was shown by EDS analysis. The results revealed that there was no carbon content in pure NiF and ZnF but found in synthesized composites. Compared to NiFCMC and ZnFCMC composites, NiFCMC-Alg and ZnFCMC-Alg have a higher percentage of carbon content. It confirmed the attachment of carboxymethyl cellulose and sodium alginate on the surface of metal ferrites.
- The BET technique was employed to describe the various metal ferrites and their composites according to a particular area. The calculated surface area of NiF, ZnF, NiFCMC, ZnFCMC, NiFCMC-Alg and ZnFCMC-Alg composite was found to be 8.532, 1.111, 1.889, 1.002, 0.985 and 0.852  $\text{m}^2/\text{g}$  respectively. As compared to pure NiF and ZnF, the surface area was decreased while pore diameter of the NiFCMC, ZnFCMC, NiFCMC-Alg and ZnFCMC-Alg composite were larger, which supports the successful surface modification of pure metal ferrites due to increase in the size of the particle. These findings confirmed the effective attachment of CMC and polymer component to the pure NiF and ZnF.
- The thermogravimetric (TGA) analysis method was used to examine the thermal stability of the different metal ferrites and their composites. The results showed that up to temperature of 450°C NiFCMC, ZnFCMC, NiFCMC-Alg and ZnFCMC-Alg composites were thermally stable. Up to a temperature range of 600–800°C, no additional weight loss was observed. The average amount of different polymers attached on the surface of metal ferrites was calculated by TGA. These results showed that 0.193 g of CMC and 0.245 g

of CMC-sodium alginate were attached in 1 g of composite material in NiF while 0.213 g of CMC and 0.338 g of CMC-sodium alginate were attached in 1 g of composite material in ZnF respectively.

- VSM (Vibration Scanning Magnetometry) analysis determined the magnetic characteristics of composites by measuring the sample's magnetization with respect to an applied magnetic field. The measurement revealed a relatively low magnetization saturation value for NiF, NiFCMC, and NiFCMC-Alg of 0.59, 0.43 and 0.21 emu/g and 12.28, 11.16 and 8.62 emu/g for ZnF, ZnFCMC and ZnFCMC-Alg respectively. An incremental mass gain due to polymerization in NiFCMC, ZnFCMC, NiFCMC-Alg and ZnFCMC-Alg along with decrease in percent content of Fe in polymer composites as compared to metal ferrites could be the cause of a drop in the magnetisation value.
  - The pH<sub>pzc</sub> of the synthesized composite is the pH value at which the surface of the adsorbent has net zero charge. Solid addition method was employed for determining pH<sub>pzc</sub> of magnetic composite. The computed value of pH<sub>pzc</sub> for NiFCMC, ZnFCMC, NiFCMC-Alg and ZnFCMC-Alg was found as 6.8, 7.7, 7.6 and 8.0 respectively. It indicated that the magnetic composite's surface would have net positive and negative charge below and above this pH.
- **Adsorption study of Dyes/ Metal ions with Metal Ferrite-Biopolymer Composites**
- It was observed that NiFCMC, NiFCMC-Alg and ZnFCMC and ZnFCMC-Alg composites showed the maximum percentage removal to remove MB and CV dyes when compared with their metal ferrites in preliminary studies. The congo red (CR) anionic dye shows less removal percentage with NiFCMC, NiFCMC-Alg and ZnFCMC and ZnFCMC-Alg composites as compared to NiF and ZnF. As there are negatively charged functional groups -COO<sup>-</sup> and -OH present in the structure of CMC and alginate so surface become negatively charge. The positive charged dyes get attracted towards surface of the adsorbent carrying negatively charge functional groups and get attached and their removal percentage increased while in case of CR anionic dye, due to existence of similar charges on adsorbent's surface as well as on anionic dye, their removal percentage decreased. In case of neutral dye (Eosin Blue), the removal percentage decreased in NiFCMC and NiFCMC-Alg and no results were observed with ZnFCMC and ZnFCMC-Alg. So, it can be inferred that the synthesized adsorbents had high selectivity towards cationic dyes only. So, for studying the adsorption behaviour of cationic dyes MB and CV, the composites NiFCMC, NiFCMC-Alg, ZnFCMC and

ZnFCMC-Alg were used in aqueous medium.

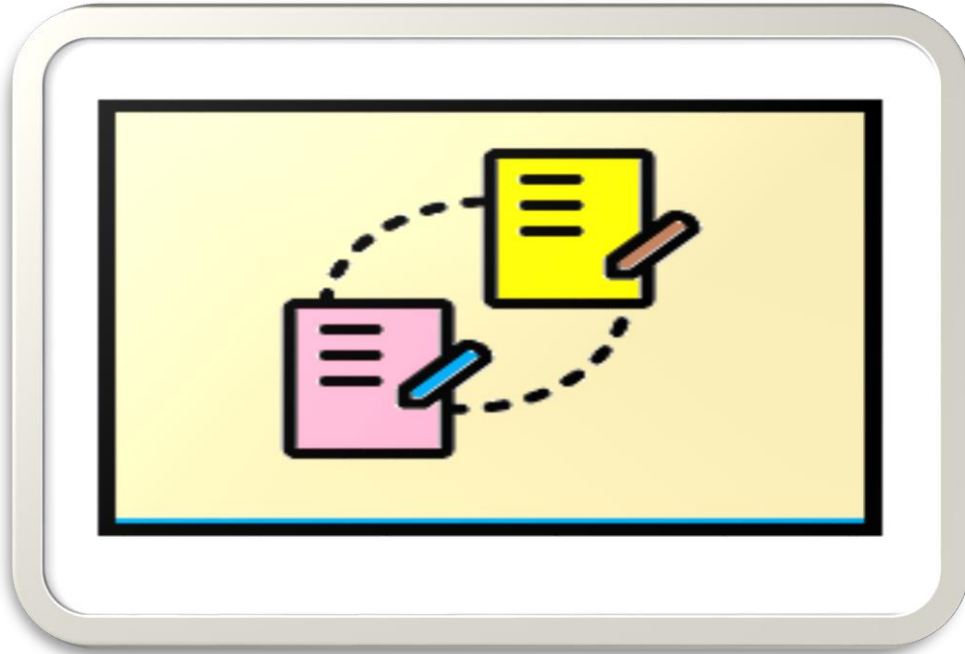
- The percentage removal of nickel ions was found to more than by using NiFCMC and NiFCMC-Alg as compared to pure NiF as well as ZnFCMC and ZnFCMC-Alg composite. So, for further detailed study of removal of nickel ions from aqueous medium, NiFCMC and NiFCMC-Alg composites were selected. The metal ferrites and their composites with CMC and alginate biopolymer did not give reproducible results with fluoride ions. The presence of specific functional groups such as -OH and -COO- on the surface of adsorbents that carry a negative charge and fluoride ions being anionic get repelled by these groups so show less removal percentage.
- The adsorption results of metal ferrites with their biopolymer composites in binary dye system were found to be lesser as compared to respective single dye system. The reason for this decrease in absorption potential may be formation of stronger bonds due to various types of interactions viz. electrostatic and  $\pi$ - $\pi$  interactions existed between different dye molecules. As a result, in the binary dye system, the percentage removal efficiency decreased.
- The data from the adsorption studies of dyes and metal ions in single and binary systems was analyzed among the several kinetic models of adsorption including the Lagergren pseudo-first and second order model, Elovich model and Weber-Morris diffusion model. It was found that the data was best fitted by Lagergren pseudo- second order model as it had the highest  $R^2$  value. It revealed that the dye and adsorbent undergo chemical adsorption. The Weber-Morris Intra particle diffusion model showed that in the case of all adsorbents for both systems, the graph is not linear and the line fails to run through its point of origin. It was shown that the rate of adsorption may be influenced by variables other than intra-particle diffusion.

The percentage removal of dyes and metal ions in single and binary system was found to be increased with increase in adsorbent dose due to increase in the availability of additional active sites for the adsorption to occur. The adsorption process is directly impacted by pH since it changes the charge on the adsorbent's surface. The results of the adsorption revealed that the pH at which the removal percentage was found maximum was 8.0. The adsorption capabilities of the adsorbents increased with increasing starting dye and metal ions concentration. With the increase in concentration, more interactions existed between the adsorbent and adsorbate molecules. On the other hand, in both dye systems the removal percentage decreased as the solution's concentration increased. This may be the result of the adsorbent's surface having less accessible active sites as the dye

concentration increased. At three different temperatures 25°C, 30°C and 35°C, it was observed that with rise in temperature, the adsorption capacity of the dye/ metal ions increased. It is due to the reason that the interaction between the adsorbent and adsorbate occurs more quickly as temperature rises.

The adsorption behaviour was studied for various models of adsorption isotherms like Langmuir, Freundlich, Temkin, and Dubinin-Radushkevich (D-R) in different metal ions and dye systems for different adsorbents. The findings showed that among the several isotherm models, the Langmuir model provided the most accurate representation of the adsorption data as indicated by the highest  $R^2$  value. It showed the uniform distribution of active sites on the homogenous surface of magnetic biocomposite. The formation of the monolayer and uniform adsorption on the adsorbent surface took place.

- The study of adsorption thermodynamic was done with different adsorbents for metal ions, single and binary dye systems. The thermodynamic parameters like  $\Delta H^\circ$ ,  $\Delta G^\circ$  and  $\Delta S^\circ$  were calculated and it was found that value of  $\Delta H^\circ$  was positive suggesting the endothermic nature of adsorption process. The calculated value for  $\Delta S^\circ$  was also positive showing that the randomness increased at the interface of adsorbate and adsorbent. Similarly, the value of  $\Delta G^\circ$  was found to be negative suggesting that the current adsorption process was spontaneous in nature.
- The regeneration capability of different adsorbents was calculated up to five cycles in metal ions and single dye system. It was revealed from the results that NiFCMC and NiFCMC-Alg retained the regeneration efficiency of 81.3% and 77.2% for metal ions, 78.6%, 81.3% for MB and 72.2%, 76.1% for CV in single dye system. Whereas for ZnFCMC and ZnFCMC-Alg, the regeneration efficiency remained 78.8%, 81.3% for MB and 70.8%, 76.4% for CV in single dye system. The findings showed that the synthesized NiFCMC, ZnFCMC, NiFCMC-Alg and ZnFCMC-Alg composites were inexpensive and efficient alternatives for removal of both metal ions and dyes for industrial purpose.
- It can be concluded from the present study that ZnFCMC and ZnFCMC-Alg composite has higher adsorption capability than NiFCMC and NiFCMC-Alg composite for both dye systems viz. single and double. For Ni (II) ions, NiFCMC and NiFCMC-Alg showed good results in aqueous medium. For the regeneration studies, ZnFCMC and ZnFCMC-Alg showed higher regeneration efficiency than NiFCMC and NiFCMC-Alg after five cycles. It can be inferred that magnetic composites of ZnF proved as valuable, eco-friendly and economical alternative for removal of dyes and metal ion from wastewater.



## REFERENCES

- (1) Katheresan, V.; Kansedo, J.; Lau, S. Y. Efficiency of Various Recent Wastewater Dye Removal Methods: A Review. *J. Environ. Chem. Eng.* **2018**, *6* (4), 4676–4697. <https://doi.org/10.1016/j.jece.2018.06.060>.
- (2) Mehra, S.; Singh, M.; Chadha, P. Adverse Impact of Textile Dyes on the Aquatic Environment as Well as on Human Beings. *Toxicol. Int.* **2021**, 165–176. <https://doi.org/10.18311/ti/2021/v28i2/26798>.
- (3) Chao, H. Book Review. *J. Inorg. Biochem.* **2014**, *138*, 144. <https://doi.org/10.1016/j.jinorgbio.2014.05.004>.
- (4) Kahlon, S. K.; Sharma, G.; Julka, J. M.; Kumar, A.; Sharma, S.; Stadler, F. J. Impact of Heavy Metals and Nanoparticles on Aquatic Biota. *Environ. Chem. Lett.* **2018**, *16* (3), 919–946. <https://doi.org/10.1007/s10311-018-0737-4>.
- (5) Reddy, K. R.; Gomes, V. G.; Hassan, M. Carbon Functionalized TiO<sub>2</sub> Nanofibers for High Efficiency Photocatalysis. *Mater. Res. Express* **2014**, *1* (1), 015012. <https://doi.org/10.1088/2053-1591/1/1/015012>.
- (6) Crini, G.; Lichtfouse, E. Advantages and Disadvantages of Techniques Used for Wastewater Treatment. *Environ. Chem. Lett.* **2019**, *17* (1), 145–155. <https://doi.org/10.1007/s10311-018-0785-9>.
- (7) Kumar, M.; Dosanjh, H. S.; Singh, H. Magnetic Zinc Ferrite-Chitosan Bio-Composite: Synthesis, Characterization and Adsorption Behavior Studies for Cationic Dyes in Single and Binary Systems. *J. Inorg. Organomet. Polym. Mater.* **2018**, *28* (3), 880–898. <https://doi.org/10.1007/s10904-017-0752-0>.
- (8) Alaqarbeh, M. Adsorption Phenomena: Definition, Mechanisms, and Adsorption Types: Short Review. **2021**, *Rhazes Green and Appl. Chem.* *13*, 43-51.
- (9) Ma, A.; Abushaikha, A.; Allen, S. J.; McKay, G. Ion Exchange Homogeneous Surface Diffusion Modelling by Binary Site Resin for the Removal of Nickel Ions from Wastewater in Fixed Beds. *Chem. Eng. J.* **2019**, *358*, 1–10. <https://doi.org/10.1016/j.cej.2018.09.135>.
- (10) Baker, R. W. *Membrane Technology and Applications*, 3. ed.; Wiley: Chichester, 2012.
- (11) Hube, S.; Eskafi, M.; Hrafnkelsdóttir, K. F.; Bjarnadóttir, B.; Bjarnadóttir, M. Á.; Axelsdóttir, S.; Wu, B. Direct Membrane Filtration for Wastewater Treatment and Resource Recovery: A Review. *Sci. Total Environ.* **2020**, *710*, 136375. <https://doi.org/10.1016/j.scitotenv.2019.136375>.
- (12) Cui, H.; Huang, X.; Yu, Z.; Chen, P.; Cao, X. Application Progress of Enhanced

- Coagulation in Water Treatment. *RSC Adv.* **2020**, *10* (34), 20231–20244. <https://doi.org/10.1039/D0RA02979C>.
- (13) Zhang, Y.; Duan, X. Chemical Precipitation of Heavy Metals from Wastewater by Using the Synthetical Magnesium Hydroxy Carbonate. *Water Sci. Technol.* **2020**, *81* (6), 1130–1136. <https://doi.org/10.2166/wst.2020.208>.
  - (14) Ahmed, S.; Aktar, S.; Zaman, S.; Jahan, R. A.; Bari, Md. L. Use of Natural Bio-Sorbent in Removing Dye, Heavy Metal and Antibiotic-Resistant Bacteria from Industrial Wastewater. *Appl. Water Sci.* **2020**, *10* (5), 107. <https://doi.org/10.1007/s13201-020-01200-8>.
  - (15) Madiraju, S. V. H.; Hung, Y.-T.; Paul, H. H.-C. Synthetic Wastewater Treatment Using Agro-Based Adsorbents. *Walailak J. Sci. Technol. WJST* **2021**, *18* (11). <https://doi.org/10.48048/wjst.2021.10337>.
  - (16) Yagub, M. T.; Sen, T. K.; Afroze, S.; Ang, H. M. Dye and Its Removal from Aqueous Solution by Adsorption: A Review. *Adv. Colloid Interface Sci.* **2014**, *209*, 172–184. <https://doi.org/10.1016/j.cis.2014.04.002>.
  - (17) Achour, Y.; Bahsis, L.; Ablouh, E.-H.; Yazid, H.; Laamari, M. R.; Haddad, M. E. Insight into Adsorption Mechanism of Congo Red Dye onto Bombax Buonopozense Bark Activated-Carbon Using Central Composite Design and DFT Studies. *Surf. Interfaces* **2021**, *23*, 100977. <https://doi.org/10.1016/j.surf.2021.100977>.
  - (18) El-Azazy, M.; El-Shafie, A. S.; Issa, A. A.; Al-Sulaiti, M.; Al-Yafie, J.; Shomar, B.; Al-Saad, K. Potato Peels as an Adsorbent for Heavy Metals from Aqueous Solutions: Eco-Structuring of a Green Adsorbent Operating Plackett–Burman Design. *J. Chem.* **2019**, 1–14. <https://doi.org/10.1155/2019/4926240>.
  - (19) Soleimani, M.; Kaghazchi, T. Low-Cost Adsorbents from Agricultural By-Products Impregnated with Phosphoric Acid. **2014**, 3.
  - (20) Reddy, D. H. K.; Yun, Y.-S. Spinel Ferrite Magnetic Adsorbents: Alternative Future Materials for Water Purification? *Coord. Chem. Rev.* **2016**, *315*, 90–111. <https://doi.org/10.1016/j.ccr.2016.01.012>.
  - (21) Jamshaid, A.; Iqbal, J.; Hamid, A.; Ghauri, M.; Muhammad, N.; Nasrullah, A.; Rafiq, S.; Shah, N. S. Fabrication and Evaluation of Cellulose-Alginate-Hydroxyapatite Beads for the Removal of Heavy Metal Ions from Aqueous Solutions. *Z. Für Phys. Chem.* **2019**, *233* (9), 1351–1375. <https://doi.org/10.1515/zpch-2018-1287>.
  - (22) Ayob, A.; Alias, S.; Dahlan, F. A.; Santiagoo, R.; Abdullah, A. Z.; Teng, T. T.

Kinetic Removal of Cr (VI) In Aqueous Solution By Carboxymethyl Cellulose - Stabilized Nano Zero-Valent Iron Particles. *Maced J Chem Chem Eng* **2015**, 34(2), 295-308.

- (23) Cai, Y.; Yuan, F.; Wang, X.; Sun, Z.; Chen, Y.; Liu, Z.; Wang, X.; Yang, S.; Wang, S. Synthesis of Core–Shell Structured Fe<sub>3</sub>O<sub>4</sub>@carboxymethyl Cellulose Magnetic Composite for Highly Efficient Removal of Eu (III). *Cellulose* **2017**, 24 (1), 175–190. <https://doi.org/10.1007/s10570-016-1094-8>.
- (24) Erkaya, I. A.; Arica, M. Y.; Akbulut, A.; Bayramoglu, G. Biosorption of Uranium (VI) by Free and Entrapped Chlamydomonas Reinhardtii: Kinetic, Equilibrium and Thermodynamic Studies. *J. Radioanal. Nucl. Chem.* **2014**, 299 (3), 1993–2003. <https://doi.org/10.1007/s10967-014-2964-x>.
- (25) Jia, F.; Liu, H.; Zhang, G. Preparation of Carboxymethyl Cellulose from Corncob. *Procedia Environ. Sci.* **2016**, 31, 98–102. <https://doi.org/10.1016/j.proenv.2016.02.013>.
- (26) Singh, R. K.; Singh, A. K. Optimization of Reaction Conditions for Preparing Carboxymethyl Cellulose from Corn Cob Agricultural Waste. *Waste Biomass Valorization* **2013**, 4 (1), 129–137. <https://doi.org/10.1007/s12649-012-9123-9>.
- (27) Saputra, A. H.; Qadhaiyna, L.; Pitaloka, A. B. Synthesis and Characterization of Carboxymethyl Cellulose (CMC) from Water Hyacinth Using Ethanol-Isobutyl Alcohol Mixture as the Solvents. *Int. J. Chem. Eng. Appl.* **2014**, 5 (1), 36–40. <https://doi.org/10.7763/IJCEA.2014.V5.347>.
- (28) Mondal, Md. I. H.; Yeasmin, Mst. S.; Rahman, Md. S. Preparation of Food Grade Carboxymethyl Cellulose from Corn Husk Agrowaste. *Int. J. Biol. Macromol.* **2015**, 79, 144–150. <https://doi.org/10.1016/j.ijbiomac.2015.04.061>.
- (29) Haleem, N.; Arshad, M.; Shahid, M.; Tahir, M. A. Synthesis of Carboxymethyl Cellulose from Waste of Cotton Ginning Industry. *Carbohydr. Polym.* **2014**, 113, 249–255. <https://doi.org/10.1016/j.carbpol.2014.07.023>.
- (30) Shui, T.; Feng, S.; Chen, G.; Li, A.; Yuan, Z.; Shui, H.; Kuboki, T.; Xu, C. Synthesis of Sodium Carboxymethyl Cellulose Using Bleached Crude Cellulose Fractionated from Cornstalk. *Biomass Bioenergy* **2017**, 105, 51–58. <https://doi.org/10.1016/j.biombioe.2017.06.016>.
- (31) Alizadeh Asl, S.; Mousavi, M.; Labbafi, M. Synthesis and Characterization of Carboxymethyl Cellulose from Sugarcane Bagasse. *J. Food Process. Technol.* **2017**, 08 (08). <https://doi.org/10.4172/2157-7110.1000687>.



- (32) Moussa, I.; Khiari, R.; Moussa, A.; Belgacem, M. N.; Mhenni, M. F. Preparation and Characterization of Carboxymethyl Cellulose with a High Degree of Substitution from Agricultural Wastes. *Fibers Polym.* **2019**, *20* (5), 933–943. <https://doi.org/10.1007/s12221-019-8665-x>.
- (33) Joshi, G.; Naithani, S.; Varshney, V. K.; Bisht, S. S.; Rana, V.; Gupta, P. K. Synthesis and Characterization of Carboxymethyl Cellulose from Office Waste Paper: A Greener Approach towards Waste Management. *Waste Manag.* **2015**, *38*, 33–40. <https://doi.org/10.1016/j.wasman.2014.11.015>.
- (34) Tasaso, P. Optimization of Reaction Conditions for Synthesis of Carboxymethyl Cellulose from Oil Palm Fronds. *Int. J. Chem. Eng. Appl.* **2015**, *6* (2), 101–104. <https://doi.org/10.7763/IJCEA.2015.V6.460>.
- (35) Youssif, A. A. A.; Hassan M., T. Synthesis and Characteristic of Carboxymethyl Cellulose from Baobab (*Adansonia Digitata* L.) Fruit Shell. *Int. J. Eng. Appl. Sci. IJEAS* **2018**, *5* (12). <https://doi.org/10.31873/IJEAS.5.12.02>.
- (36) Klunklin, W.; Jantanasakulwong, K.; Phimolsiripol, Y.; Leksawasdi, N.; Seesuriyachan, P.; Chaiyasom, T.; Insomphun, C.; Phongthai, S.; Jantrawut, P.; Sommano, S. R.; Punyodom, W.; Reungsang, A.; Ngo, T. M. P.; Rachtanapun, P. Synthesis, Characterization, and Application of Carboxymethyl Cellulose from Asparagus Stalk End. *Polymers* **2020**, *13* (1), 81. <https://doi.org/10.3390/polym13010081>.
- (37) Laribi, N.; Maatoug, S.; Low-cost Carboxymethyl holocellulose and carboxymethyl cellulose from wheat straw. *Cellul. Chem. Technol.* **2020**, *54* (3-4), 225–236. <https://doi.org/10.35812/Cellulose Chem Technol.2020.54.24>.
- (38) Rodsamran, P.; Sothornvit, R. Carboxymethyl Cellulose from Rice Stubble Waste. *J. Sci. Technol.* **2020**, *42* (2), 454-460.
- (39) Yimlamai, B.; Choorit, W.; Chisti, Y.; Prasertsan, P. Cellulose from Oil Palm Empty Fruit Bunch Fiber and Its Conversion to Carboxymethylcellulose. *J. Chem. Technol. Biotechnol.* **2021**, *96* (6), 1656–1666. <https://doi.org/10.1002/jctb.6689>.
- (40) Rahman, M. M.; Alam, M.; Rahman, M. M.; Susan, M. A. B. H.; Shaikh, Md. A. A.; Nayeem, J.; Jahan, M. S. A Novel Approach in Increasing Carboxymethylation Reaction of Cellulose. *Carbohydr. Polym. Technol. Appl.* **2022**, *4*, 100236. <https://doi.org/10.1016/j.carpta.2022.100236>.
- (41) Pujokaroni, A. S.; Ichiura, H. Preparation of Carboxymethyl Cellulose (CMC) Derived from Palm Fiber Waste: Effect of Ozone Pretreatment on CMC Properties.

October 4, 2022. <https://doi.org/10.21203/rs.3.rs-1496346/v2>.

- (42) Joyline, G.; Gachoki, K. P.; Ngunjiri, G. A.; Nyambura, N. C.; Shigwenya, M. E. High Swelling Carboxymethyl Cellulose Synthesized from Coconut Fibers. *J. Nat. Fibers* **2023**, *20* (2), 2283549. <https://doi.org/10.1080/15440478.2023.2283549>.
- (43) Fouad, H.; Jawaid, M.; Karim, Z.; Meraj, A.; Abu-Jdayil, B.; Nasef, M. M.; Sarmin, S. N. Preparation and Characterization of Carboxymethyl Microcrystalline Cellulose from Pineapple Leaf Fibre. *Sci. Rep.* **2024**, *14* (1), 23286. <https://doi.org/10.1038/s41598-024-73860-4>.
- (44) Gautam, P. K.; Singh, A.; Misra, K.; Sahoo, A. K.; Samanta, S. K. Synthesis and Applications of Biogenic Nanomaterials in Drinking and Wastewater Treatment. *J. Environ. Manage.* **2019**, *231*, 734–748. <https://doi.org/10.1016/j.jenvman.2018.10.104>.
- (45) Qu, X.; Alvarez, P. J. J.; Li, Q. Applications of Nanotechnology in Water and Wastewater Treatment. *Water Res.* **2013**, *47* (12), 3931–3946. <https://doi.org/10.1016/j.watres.2012.09.058>.
- (46) Kumari, P.; Alam, M.; Siddiqi, W. A. Usage of Nanoparticles as Adsorbents for Waste Water Treatment: An Emerging Trend. *Sustain. Mater. Technol.* **2019**, *22*, e00128. <https://doi.org/10.1016/j.susmat.2019.e00128>.
- (47) Sivashankar, R.; Sathya, A. B.; Vasantharaj, K.; Sivasubramanian, V. Magnetic Composite an Environmental Super Adsorbent for Dye Sequestration – A Review. *Environ. Nanotechnol. Monit. Manag.* **2014**, *1–2*, 36–49. <https://doi.org/10.1016/j.enmm.2014.06.001>.
- (48) Ž. Lazarević, Z.; Jovalekić, Č.; Milutinović, A.; Sekulić, D.; Ivanovski, V. N.; Rečnik, A.; Cekić, B.; Ž. Romčević, N. Nanodimensional Spinel  $\text{NiFe}_2\text{O}_4$  and  $\text{ZnFe}_2\text{O}_4$  Ferrites Prepared by Soft Mechanochemical Synthesis. *J. Appl. Phys.* **2013**, *113* (18), 187221. <https://doi.org/10.1063/1.4801962>.
- (49) Kumar, M.; Dosanjh, H. S.; Singh, H. Magnetic Zinc Ferrite–Alginate Biopolymer Composite: As an Alternative Adsorbent for the Removal of Dyes in Single and Ternary Dye System. *J. Inorg. Organomet. Polym. Mater.* **2018**, *28* (5), 1688–1705. <https://doi.org/10.1007/s10904-018-0839-2>.
- (50) Prithviraj Swamy, P. M.; Basavaraja, S.; Lagashetty, A.; Srinivas Rao, N. V.; Nijagunappa, R.; Venkataraman, A. Synthesis and Characterization of Zinc Ferrite Nanoparticles Obtained by Self-Propagating Low-Temperature Combustion Method. *Bull. Mater. Sci.* **2011**, *34* (7), 1325–1330. <https://doi.org/10.1007/s12034->

- (51) Mažeika, K.; Bėčytė, V.; Tykhonenko-Polishchuk, Y. O.; Kulyk, M. M.; Yelenich, O. V.; Tovstolytkin, A. I. Comparison between Magnetic Properties of  $\text{CoFe}_2\text{O}_4$  and  $\text{CoFe}_2\text{O}_4$ -Polypyrrole Nanoparticles. *Lith. J. Phys.* **2018**, 58 (3). <https://doi.org/10.3952/physics.v58i3.3815>.
- (52) Diodati, S.; Pandolfo, L.; Caneschi, A.; Gialanella, S.; Gross, S. Green and Low Temperature Synthesis of Nanocrystalline Transition Metal Ferrites by Simple Wet Chemistry Routes. *Nano Res.* **2014**, 7 (7), 1027–1042. <https://doi.org/10.1007/s12274-014-0466-3>.
- (53) Wu, S.; Guo, J.; Wang, Y.; Huang, C.; Hu, Y. Facile Preparation of Magnetic Sodium Alginate/Carboxymethyl Cellulose Composite Hydrogel for Removal of Heavy Metal Ions from Aqueous Solution. *J. Mater. Sci.* **2021**, 56 (23), 13096–13107. <https://doi.org/10.1007/s10853-021-06044-4>.
- (54) Kefeni, K. K.; Msagati, T. A. M.; Mamba, B. B. Ferrite Nanoparticles: Synthesis, Characterisation and Applications in Electronic Device. *Mater. Sci. Eng. B* **2017**, 215, 37–55. <https://doi.org/10.1016/j.mseb.2016.11.002>.
- (55) Badaik, B.; Chowdhury, Study On Structural And Magnetic Properties Of  $\text{Mn}_{(1-x)}\text{Zn}_x\text{Fe}_2\text{O}_4$  Prepared By Solid-State Reaction Method Method, A Bachelor of Technology in Ceramic Engineering , Department of Ceramic Engineering , National Institute of Technology, Rourkela, 2015.
- (56) Perez, T.; Pasquini, D.; De Faria Lima, A.; Rosa, E. V.; Sousa, M. H.; Cerqueira, D. A.; De Moraes, L. C. Efficient Removal of Lead Ions from Water by Magnetic Nanosorbents Based on Manganese Ferrite Nanoparticles Capped with Thin Layers of Modified Biopolymers. *J. Environ. Chem. Eng.* **2019**, 7 (1), 102892. <https://doi.org/10.1016/j.jece.2019.102892>.
- (57) Arica, M. Y.; Bayramoglu, G. Polyaniline Coated Magnetic Carboxymethylcellulose Beads for Selective Removal of Uranium Ions from Aqueous Solution. *J. Radioanal. Nucl. Chem.* **2016**, 310 (2), 711–724. <https://doi.org/10.1007/s10967-016-4828-z>.
- (58) Dahlan, N. A.; Veeramachineni, A. K.; Langford, S. J.; Pushpamalar, J. Developing of a Magnetite Film of Carboxymethyl Cellulose Grafted Carboxymethyl Polyvinyl Alcohol (CMC- g -CMPVA) for Copper Removal. *Carbohydr. Polym.* **2017**, 173, 619–630. <https://doi.org/10.1016/j.carbpol.2017.06.008>.
- (59) Sagadevan, S.; Chowdhury, Z. Z.; Rafique, R. F. Preparation and Characterization

- of Nickel Ferrite Nanoparticles via Co-Precipitation Method. *Mater. Res.* **2018**, *21* (2). <https://doi.org/10.1590/1980-5373-mr-2016-0533>.
- (60) Zhou, Y.; Li, T.; Shen, J.; Meng, Y.; Tong, S.; Guan, Q.; Xia, X. Core-Shell Structured Magnetic Carboxymethyl Cellulose-Based Hydrogel Nanosorbents for Effective Adsorption of Methylene Blue from Aqueous Solution. *Polymers* **2021**, *13* (18), 3054. <https://doi.org/10.3390/polym13183054>.
- (61) Noori, M.; Tahmasebpour, M.; Nami, S. H. Adsorption Removal of Crystal Violet in Single and Binary Systems onto Low-Cost Iron Oxide Nanoparticles Coated Clinoptilolite Powders/Granules. June 14, 2022. <https://doi.org/10.21203/rs.3.rs-1727993/v1>.
- (62) Sajjia, M.; Oubaha, M.; Hasanuzzaman, M.; Olabi, A. G. Developments of Cobalt Ferrite Nanoparticles Prepared by the Sol–Gel Process. *Ceram. Int.* **2014**, *40* (1), 1147–1154. <https://doi.org/10.1016/j.ceramint.2013.06.116>.
- (63) Iqbal, F.; Mutalib, M. I. A.; Shaharun, M. S.; Khan, M.; Abdullah, B. Synthesis of  $\text{ZnFe}_2\text{O}_4$  Using Sol-Gel Method: Effect of Different Calcination Parameters. *Procedia Eng.* **2016**, *148*, 787–794. <https://doi.org/10.1016/j.proeng.2016.06.563>.
- (64) Kumar, M.; Chauhan, S.; Pandey, H. Effect of Gd (III) Substitution on Structural, Morphological, and Magnetic Properties of  $\text{BiFeO}_3$  Nanoparticles. *J. Sol-Gel Sci. Technol.* **2024**, *109* (1), 272–282. <https://doi.org/10.1007/s10971-023-06269-6>.
- (65) Yu, C.; Li, H.; Ma, H.; Zhang, L.; Li, Y.; Lin, Q. Characteristics and Mechanism of Cu(II) Adsorption on Prepared Calcium Alginate/Carboxymethyl cellulose@ $\text{MnFe}_2\text{O}_4$ . *Polym. Bull.* **2022**, *79* (2), 1201–1216. <https://doi.org/10.1007/s00289-021-03555-7>.
- (66) Zhang, Y.; Kang, Z.; Chen, D. Process of Synthesizing High Saturation Magnetization  $\text{Ni}_{0.5}\text{Zn}_{0.5}\text{Fe}_2\text{O}_4$  by Microwave Assisted Ball Milling. *Mater. Lett.* **2014**, *133*, 259–261. <https://doi.org/10.1016/j.matlet.2014.07.031>.
- (67) Naik, T. R. R.; Joshi, N.; Shivashankar, S. A.; Bindu, P. J. Low-Temperature Microwave-Assisted Synthesis and Antifungal Activity of  $\text{CoFe}_2\text{O}_4$  Nanoparticles. *J. Mat. NanoSci.* **2019**, *6*(2), 67-72.
- (68) Kumar, S.; Sharma, A.; Singh, M.; Sharma, S. P. Simple Synthesis and Magnetic Properties of Nickel-Zinc Ferrites Nanoparticles by Using Aloe Vera Extract Solution. *Arch. Appl. Sci. Res.*, **2013**, *5* (6):145-151.
- (69) Kumar, M.; Dosanjh, H. S.; Singh, H. Biopolymer Modified Transition Metal Spinel Ferrites for Removal of Fluoride Ions from Water. *Environ. Nanotechnol.*

*Monit. Manag.* **2019**, *12*, 100237. <https://doi.org/10.1016/j.enmm.2019.100237>.

- (70) Kumar, S.; Singh, J.; Kaur, H.; Singh, H.; Singh Dosanjh, H. Microstructural and Magnetic Properties of Zn Substituted Nickel Ferrite Synthesised by Facile Solution Combustion Method. *Micro Nano Lett.* **2019**, *14* (7), 727–731. <https://doi.org/10.1049/mnl.2018.5217>.
- (71) An, G. H.; Hwang, T.-Y.; Kim, J.; Kim, J.; Kang, N.; Kim, S.; Choi, Y.-M.; Choa, Y.H. Barium Hexaferrite Nanoparticles with High Magnetic Properties by Salt-Assisted Ultrasonic Spray Pyrolysis. *J. Alloys Compd.* **2014**, *583*, 145–150. <https://doi.org/10.1016/j.jallcom.2013.08.105>.
- (72) Joy, J.; Krishnamoorthy, A.; Tanna, A.; Kamathe, V.; Nagar, R.; Srinivasan, S. Recent Developments on the Synthesis of Nanocomposite Materials via Ball Milling Approach for Energy Storage Applications. *Appl. Sci.* **2022**, *12* (18), 9312. <https://doi.org/10.3390/app12189312>.
- (73) Ghaemi, M.; Absalan, G.; Sheikhan, L. Adsorption Characteristics of Titan Yellow and Congo Red on CoFe<sub>2</sub>O<sub>4</sub> Magnetic Nanoparticles. *J. Iran. Chem. Soc.* **2014**, *11* (6), 1759–1766. <https://doi.org/10.1007/s13738-014-0448-0>.
- (74) Yang, X.; Wang, Z.; Jing, M.; Liu, R.; Song, F.; Shen, X. Magnetic Nanocomposite Ba-Ferrite/ $\alpha$ -Iron Hollow Microfiber: A Multifunctional 1D Space Platform for Dyes Removal and Microwave Absorption. *Ceram. Int.* **2014**, *40* (10), 15585–15594. <https://doi.org/10.1016/j.ceramint.2014.07.035>.
- (75) Srivastava, V.; Sharma, Y. C.; Sillanpää, M. Application of Nano-Magnesso Ferrite (n-MgFe<sub>2</sub>O<sub>4</sub>) for the Removal of Co (II) Ions from Synthetic Wastewater: Kinetic, Equilibrium and Thermodynamic Studies. *Appl. Surf. Sci.* **2015**, *338*, 42–54. <https://doi.org/10.1016/j.apsusc.2015.02.072>.
- (76) Xue, Z.; Wang, T.; Chen, B.; Malkoske, T.; Yu, S.; Tang, Y. Degradation of Tetracycline with BiFeO<sub>3</sub> Prepared by a Simple Hydrothermal Method. *Materials* **2015**, *8* (9), 6360–6378. <https://doi.org/10.3390/ma8095310>.
- (77) Kalpakli, Yasemen. Removal of Cu (II) from Aqueous Solutions Using Magnetite: A Kinetic, Equilibrium Study. *Adv. Environ. Res.* **2015**, *4* (2), 119–133. <https://doi.org/10.12989/AER.2015.4.2.119>.
- (78) Singh, M.; Dosanjh, H. S.; Singh, H. Surface Modified Spinel Cobalt Ferrite Nanoparticles for Cationic Dye Removal: Kinetics and Thermodynamics Studies. *J. Water Process Eng.* **2016**, *11*, 152–161. <https://doi.org/10.1016/j.jwpe.2016.05.006>.
- (79) Ouyang, H.; Liu, S.; Liu, D.; Wang, Y.; Xu, S.; Pan, S. Fabrication of Magnetic

Cobalt-Nickel Ferrite Nanoparticles for the Adsorption of Methyl Blue in Aqueous Solutions. *Mater. Res. Express* **2021**, 8 (10), 105013. <https://doi.org/10.1088/2053-1591/ac3106>.

- (80) Shi, S.; Dong, Q.; Wang, Y.; Zhang, X.; Zhu, S.; Chow, Y. T.; Wang, X.; Zhu, L.; Zhang, G.; Xu, D. Self-Supporting Super Hydrophilic  $\text{MgFe}_2\text{O}_4$  Flexible Fibers for Pb(II) Adsorption. *Sep. Purif. Technol.* **2021**, 266, 118584. <https://doi.org/10.1016/j.seppur.2021.118584>.
- (81) Sonu; Sharma, S.; Dutta, V.; Raizada, P.; Hosseini-Bandegharai, A.; Thakur, V.; Nguyen, V.H.; VanLe, Q.; Singh, P. An Overview of Heterojunctioned  $\text{ZnFe}_2\text{O}_4$  Photocatalyst for Enhanced Oxidative Water Purification. *J. Environ. Chem. Eng.* **2021**, 9 (5), 105812. <https://doi.org/10.1016/j.jece.2021.105812>.
- (82) Kharisov, B. I.; Dias, H. V. R.; Kharissova, O. V. Mini-Review: Ferrite Nanoparticles in the Catalysis. *Arab. J. Chem.* **2019**, 12 (7), 1234–1246. <https://doi.org/10.1016/j.arabjc.2014.10.049>.
- (83) Gómez-Pastora, J.; Bringas, E.; Ortiz, I. Recent Progress and Future Challenges on the Use of High Performance Magnetic Nano-Adsorbents in Environmental Applications. *Chem. Eng. J.* **2014**, 256, 187–204. <https://doi.org/10.1016/j.cej.2014.06.119>.
- (84) Ahalya, K.; Suriyanarayanan, N.; Ranjithkumar, V. Effect of Cobalt Substitution on Structural and Magnetic Properties and Chromium Adsorption of Manganese Ferrite Nano Particles. *J. Magn. Magn. Mater.* **2014**, 372, 208–213. <https://doi.org/10.1016/j.jmmm.2014.07.030>.
- (85) Abbas, N.; Rubab, N.; Sadiq, N.; Manzoor, S.; Khan, M. I.; Fernandez Garcia, J.; Barbosa Aragao, I.; Tariq, M.; Akhtar, Z.; Yasmin, G. Aluminum-Doped Cobalt Ferrite as an Efficient Photocatalyst for the Abatement of Methylene Blue. *Water* **2020**, 12 (8), 2285. <https://doi.org/10.3390/w12082285>.
- (86) Neyaz, N.; Siddiqui, W. A.; Nair, K. K. Application of Surface Functionalized Iron Oxide Nanomaterials as a Nanosorbents in Extraction of Toxic Heavy Metals from Ground Water: A Review. *Int. Journal Environ. Sci.* **2014**, 4(4).
- (87) Das, S.; Bououdina, M.; Manoharan, C. The Influence of Cationic Surfactant CTAB on Optical, Dielectric and Magnetic Properties of Cobalt Ferrite Nanoparticles. *Ceram. Int.* **2020**, 46 (8), 11705–11716. <https://doi.org/10.1016/j.ceramint.2020.01.202>.
- (88) Pandey, N.; Shukla, S. K.; Singh, N. B. Water Purification by Polymer

- Nanocomposites: An Overview. *Nanocomposites* **2017**, 3 (2), 47–66. <https://doi.org/10.1080/20550324.2017.1329983>.
- (89) Yang, S.; Guo, Z.; Sheng, G.; Wang, X. Investigation of the Sequestration Mechanisms of Cd (II) and 1-Naphthol on Discharged Multi-Walled Carbon Nanotubes in Aqueous Environment. *Sci. Total Environ.* **2012**, 420, 214–221. <https://doi.org/10.1016/j.scitotenv.2012.01.018>.
- (90) Burakov, A. E.; Galunin, E. V.; Burakova, I. V.; Kucheroval, A. E.; Agarwal, S.; Tkachev, A. G.; Gupta, V. K. Adsorption of Heavy Metals on Conventional and Nanostructured Materials for Wastewater Treatment Purposes: A Review. *Ecotoxicol. Environ. Saf.* **2018**, 148, 702–712. <https://doi.org/10.1016/j.ecoenv.2017.11.034>.
- (91) Naghizadeh, A.; Karimi, A.; Derakhshani, E.; Esform, A. Single-walled Carbon Nanotubes (SWCNTs) as an Efficient Adsorbent for Removal of Reactive Dyes from Water Solution: Equilibrium, Kinetic, and Thermodynamic. *Environ. Qual. Manag.* **2022**, 31 (4), 133–140. <https://doi.org/10.1002/tqem.21753>.
- (92) Chen, H.; Li, J.; Shao, D.; Ren, X.; Wang, X. Poly(Acrylic Acid) Grafted Multiwall Carbon Nanotubes by Plasma Techniques for Co (II) Removal from Aqueous Solution. *Chem. Eng. J.* **2012**, 210, 475–481. <https://doi.org/10.1016/j.cej.2012.08.082>.
- (93) Wang, S.; Ng, C. W.; Wang, W.; Li, Q.; Hao, Z. Synergistic and Competitive Adsorption of Organic Dyes on Multiwalled Carbon Nanotubes. *Chem. Eng. J.* **2012**, 197, 34–40. <https://doi.org/10.1016/j.cej.2012.05.008>.
- (94) Abraham, T. N.; Kumar, R.; Misra, R. K.; Jain, S. K. Poly(Vinyl Alcohol)-based MWCNT Hydrogel for Lead Ion Removal from Contaminated Water. *J. Appl. Polym. Sci.* **2012**, 125 (S1). <https://doi.org/10.1002/app.35666>.
- (95) Pillay, K.; Cukrowska, E. M.; Coville, N. J. Improved Uptake of Mercury by Sulphur-Containing Carbon Nanotubes. *Microchem. J.* **2013**, 108, 124–130. <https://doi.org/10.1016/j.microc.2012.10.014>.
- (96) Salam, M. A. Coating Carbon Nanotubes with Crystalline Manganese Dioxide Nanoparticles and Their Application for Lead Ions Removal from Model and Real Water. *Colloids Surf. Physicochem. Eng. Asp.* **2013**, 419, 69–79. <https://doi.org/10.1016/j.colsurfa.2012.11.064>.
- (97) Maleki, A.; Hamesadeghi, U.; Daraei, H.; Hayati, B.; Najafi, F.; McKay, G.; Rezaee, R. Amine Functionalized Multi-Walled Carbon Nanotubes: Single and

- Binary Systems for High Capacity Dye Removal. *Chem. Eng. J.* **2017**, *313*, 826–835. <https://doi.org/10.1016/j.cej.2016.10.058>.
- (98) Côa, F.; Strauss, M.; Clemente, Z.; Rodrigues Neto, L. L.; Lopes, J. R.; Alencar, R. S.; Souza Filho, A. G.; Alves, O. L.; Castro, V. L. S. S.; Barbieri, E.; Martinez, D. S. T. Coating Carbon Nanotubes with Humic Acid Using an Eco-Friendly Mechanochemical Method: Application for Cu(II) Ions Removal from Water and Aquatic Ecotoxicity. *Sci. Total Environ.* **2017**, *607–608*, 1479–1486. <https://doi.org/10.1016/j.scitotenv.2017.07.045>.
- (99) Ruan, Z.; Tian, Y.; Ruan, J.; Cui, G.; Iqbal, K.; Iqbal, A.; Ye, H.; Yang, Z.; Yan, S. Synthesis of Hydroxyapatite/Multi-Walled Carbon Nanotubes for the Removal of Fluoride Ions from Solution. *Appl. Surf. Sci.* **2017**, *412*, 578–590. <https://doi.org/10.1016/j.apsusc.2017.03.215>.
- (100) Mallakpour, S.; Rashidimoghadam, S. Starch/MWCNT-Vitamin C Nanocomposites: Electrical, Thermal Properties and Their Utilization for Removal of Methyl Orange. *Carbohydr. Polym.* **2017**, *169*, 23–32. <https://doi.org/10.1016/j.carbpol.2017.03.081>.
- (101) Rahmati, N.; Rahimnejad, M.; Pourali, M.; Muallah, S. K. Effective removal of nickel ions from aqueous solution using multi-wall carbon nanotube functionalized by glycerol-based deep eutectic solvent. *Colloid Interface Sci. Commun.* **2021**, *40*, 100347. <https://doi.org/10.1016/j.colcom.2020.100347>.
- (102) Zhao, W.; Hao, C.; Guo, Y.; Shao, W.; Tian, Y.; Zhao, P. Optimization of Adsorption Conditions Using Response Surface Methodology for Tetracycline Removal by MnFe<sub>2</sub>O<sub>4</sub>/Multi-Wall Carbon Nanotubes. *Water* **2023**, *15* (13), 2392. <https://doi.org/10.3390/w15132392>.
- (103) Yao, Y.; Miao, S.; Liu, S.; Ma, L. P.; Sun, H.; Wang, S. Synthesis, Characterization, and Adsorption Properties of Magnetic Fe<sub>3</sub>O<sub>4</sub>@graphene Nanocomposite. *Chem. Eng. J.* **2012**, *184*, 326–332. <https://doi.org/10.1016/j.cej.2011.12.017>.
- (104) Mahmoodi, N. M. Magnetic Ferrite Nanoparticle–Alginate Composite: Synthesis, Characterization and Binary System Dye Removal. *J. Taiwan Inst. Chem. Eng.* **2013**, *44* (2), 322–330. <https://doi.org/10.1016/j.jtice.2012.11.014>.
- (105) Deng, J.-H.; Zhang, X.-R.; Zeng, G.-M.; Gong, J.-L.; Niu, Q.-Y.; Liang, J. Simultaneous Removal of Cd (II) and Ionic Dyes from Aqueous Solution Using Magnetic Graphene Oxide Nanocomposite as an Adsorbent. *Chem. Eng. J.* **2013**,



226, 189–200. <https://doi.org/10.1016/j.cej.2013.04.045>.

- (106) Wu, K.; Jing, C.; Zhang, J.; Liu, T.; Yang, S.; Wang, W. Magnetic Fe<sub>3</sub>O<sub>4</sub>@CuO Nanocomposite Assembled on Graphene Oxide Sheets for the Enhanced Removal of Arsenic (III/V) from Water. *Appl. Surf. Sci.* **2019**, *466*, 746–756. <https://doi.org/10.1016/j.apsusc.2018.10.091>.
- (107) Attar, K.; Demey, H.; Bouazza, D.; Sastre, A. M. Sorption and Desorption Studies of Pb (II) and Ni (II) from Aqueous Solutions by a New Composite Based on Alginate and Magadiite Materials. *Polymers* **2019**, *11* (2), 340. <https://doi.org/10.3390/polym11020340>.
- (108) Parlayici, Ş. Alginate-Coated Perlite Beads for the Efficient Removal of Methylene Blue, Malachite Green, and Methyl Violet from Aqueous Solutions: Kinetic, Thermodynamic, and Equilibrium Studies. *J. Anal. Sci. Technol.* **2019**, *10* (1), 4. <https://doi.org/10.1186/s40543-019-0165-5>.
- (109) Ablouh, E.; Hanani, Z.; Eladlani, N.; Rhazi, M.; Taourirte, M. Chitosan Microspheres/Sodium Alginate Hybrid Beads: An Efficient Green Adsorbent for Heavy Metals Removal from Aqueous Solutions. *Sustain. Environ. Res.* **2019**, *29* (1), 5. <https://doi.org/10.1186/s42834-019-0004-9>.
- (110) Yadav, S.; Asthana, A.; Chakraborty, R.; Jain, B.; Singh, A. K.; Carabineiro, S. A. C.; Susan, Md. A. B. H. Cationic Dye Removal Using Novel Magnetic/Activated Charcoal/β-Cyclodextrin/Alginate Polymer Nanocomposite. *Nanomaterials* **2020**, *10* (1), 170. <https://doi.org/10.3390/nano10010170>.
- (111) Othman, I.; Abu Haija, M.; Kannan, P.; Banat, F. Adsorptive Removal of Methylene Blue from Water Using High-Performance Alginate-Based Beads. *Water. Air. Soil Pollut.* **2020**, *231* (8), 396. <https://doi.org/10.1007/s11270-020-04751-3>.
- (112) Hamza, M. F.; Hamad, N. A.; Hamad, D. M.; Khalafalla, M. S.; Abdel-Rahman, A. A.-H.; Zeid, I. F.; Wei, Y.; Hessien, M. M.; Fouda, A.; Salem, W. M. Synthesis of Eco-Friendly Biopolymer, Alginate-Chitosan Composite to Adsorb the Heavy Metals, Cd (II) and Pb (II) from Contaminated Effluents. *Materials* **2021**, *14* (9), 2189. <https://doi.org/10.3390/ma14092189>.
- (113) Chen, T.; Liu, H.; Gao, J.; Hu, G.; Zhao, Y.; Tang, X.; Han, X. Efficient Removal of Methylene Blue by Bio-Based Sodium Alginate/Lignin Composite Hydrogel Beads. *Polymers* **2022**, *14* (14), 2917. <https://doi.org/10.3390/polym14142917>.
- (114) Patel, P. K.; Pandey, L. M.; Uppaluri, R. V. S. Highly Effective Removal of Multi-

- Heavy Metals from Simulated Industrial Effluent through an Adsorption Process Employing Carboxymethyl-Chitosan Composites. *Environ. Res.* **2024**, *240*, 117502. <https://doi.org/10.1016/j.envres.2023.117502>.
- (115) Sando, M. S.; Farhan, A. M. Quaternary Biocomposite of Chitosan-Polyvinyl Alcohol/Food Grade Algae/ Montmorillonite Clay for Cationic Methyl Violet 2B Dye Removal: Optimization and Desirability Functions. **2024**, <https://doi.org/10.21203/rs.3.rs-4502784/v1>.
- (116) Sharma, D.; Jasrotia, R.; Singh, R.; Singh, J.; Mittal, S.; Singh, H. Novel Magnetic Metal Ferrite-Mango Starch Composite for the Removal of Dyes in Single and Ternary Dye Mixtures from Aqueous Solutions: Kinetic and Thermodynamic Studies. *Indian Chem. Eng.* **2024**, 1–23. <https://doi.org/10.1080/00194506.2024.2408021>.
- (117) Qiu, L.; Shao, Z.; Wang, D.; Wang, F.; Wang, W.; Wang, J. Novel Polymer Li-Ion Binder Carboxymethyl Cellulose Derivative Enhanced Electrochemical Performance for Li-Ion Batteries. *Carbohydr. Polym.* **2014**, *112*, 532–538. <https://doi.org/10.1016/j.carbpol.2014.06.034>.
- (118) Wang, J.; Liu, M.; Duan, C.; Sun, J.; Xu, Y. Preparation and Characterization of Cellulose-Based Adsorbent and Its Application in Heavy Metal Ions Removal. *Carbohydr. Polym.* **2019**, *206*, 837–843. <https://doi.org/10.1016/j.carbpol.2018.11.059>.
- (119) Belaid, A.; Hocine, T.; Bouras, B.; Tennouga, L.; Benabadji, K. I.; Benhabib, K. Modified Biopolymer as Adsorbent for Methylene Blue Dye Removal. **2024**, *Phys. Chem. Res.*, *12* (1), 189–204. doi: 10.22036/pcr.2023.393442.2325. *12* (1).
- (120) Allouss, D.; Essamlali, Y.; Amadine, O.; Chakir, A.; Zahouily, M. Response Surface Methodology for Optimization of Methylene Blue Adsorption onto Carboxymethyl Cellulose-Based Hydrogel Beads: Adsorption Kinetics, Isotherm, Thermodynamics and Reusability Studies. *RSC Adv.* **2019**, *9* (65), 37858–37869. <https://doi.org/10.1039/C9RA06450H>.
- (121) Omer, A. M.; Elgarhy, G. S.; El-Subruiti, G. M.; Khalifa, R. E.; Eltaweil, A. S. Fabrication of Novel Iminodiacetic Acid-Functionalized Carboxymethyl Cellulose Microbeads for Efficient Removal of Cationic Crystal Violet Dye from Aqueous Solutions. *Int. J. Biol. Macromol.* **2020**, *148*, 1072–1083. <https://doi.org/10.1016/j.ijbiomac.2020.01.182>.
- (122) Radoor, S.; Karayil, J.; Jayakumar, A.; Parameswaranpillai, J.; Lee, J.; Siengchin,

- S. Ecofriendly and Low-Cost Bio Adsorbent for Efficient Removal of Methylene Blue from Aqueous Solution. *Sci. Rep.* **2022**, *12* (1), 20580. <https://doi.org/10.1038/s41598-022-22936-0>.
- (123) Dewangan, T.; Tiwari, A.; Bajpai, A. K. Removal of Chromium(VI) Ions by Adsorption onto Binary Biopolymeric Beads of Sodium Alginate and Carboxymethyl Cellulose. *J. Dispers. Sci. Technol.* **2011**, *32* (8), 1075–1082. <https://doi.org/10.1080/01932691003659403>.
- (124) Vani, J. S.; Rao, K. M.; Reddy, N. S. G. Synthesis and Characterization of Sodium Carboxy Methyl Cellulose/Poly (Acrylamide) Magnetic Nano Composite Semi Ipn's for Removal of Heavy Metal Ions. *World J. Nano Sci. Technol.*, **2013**, *2* (1): 33-41.
- (125) Mosafari, M.; Nemati, S.; Khataee, A.; Nasser, S.; Hashemi, A. A. Removal of Arsenic (III, V) from Aqueous Solution by Nanoscale Zero-Valent Iron Stabilized with Starch and Carboxymethyl Cellulose. *J. Environ. Health Sci. Eng.* **2014**, *12* (1), 74. <https://doi.org/10.1186/2052-336X-12-74>.
- (126) Ahmad, M.; Manzoor, K.; Ahmad, S.; Ikram, S. Preparation, Kinetics, Thermodynamics, and Mechanism Evaluation of Thiosemicarbazide Modified Green Carboxymethyl Cellulose as an Efficient Cu (II) Adsorbent. *J. Chem. Eng. Data* **2018**, *63* (6), 1905–1916. <https://doi.org/10.1021/acs.jced.7b01008>.
- (127) Lin, Y.; Cao, Y.; Song, Q.; Gao, J.; Jia, P.; Alsulami, H.; Amin Kutbi, M. Synthesis of Poly(Acrylic Acid)-Grafted Carboxymethyl Cellulose for Efficient Removal of Copper Ions. *J. Renew. Mater.* **2019**, *7* (12), 1403–1414. <https://doi.org/10.32604/jrm.2019.08380>.
- (128) Manzoor, K.; Ahmad, M.; Ahmad, S.; Ikram, S. Synthesis, Characterization, Kinetics, and Thermodynamics of EDTA-Modified Chitosan-Carboxymethyl Cellulose as Cu (II) Ion Adsorbent. *ACS Omega* **2019**, *4* (17), 17425–17437. <https://doi.org/10.1021/acsomega.9b02214>.
- (129) Angaru, G. K. R.; Choi, Y.-L.; Lingamdinne, L. P.; Koduru, J. R.; Yang, J.-K.; Chang, Y.-Y.; Karri, R. R. Portable SA/CMC Entrapped Bimetallic Magnetic Fly Ash Zeolite Spheres for Heavy Metals Contaminated Industrial Effluents Treatment via Batch and Column Studies. *Sci. Rep.* **2022**, *12* (1), 3430. <https://doi.org/10.1038/s41598-022-07274-5>.
- (130) Moradi, Z.; Alihosseini, A.; Ghadami, A. Adsorption Removal of Arsenic from Aqueous Solution by Carboxymethyl cellulose (CMC) Modified with

- Montmorillonite. *Results Mater.* **2023**, *17*, 100378.  
<https://doi.org/10.1016/j.rinma.2023.100378>.
- (131) Michelle, L.-Y. L.; Ahmad, I.; Phang, S.-W. Preparation and Optimization of Polyaniline/ Titanium Dioxide/ Carboxymethyl Cellulose Powder for Effective Nickel Adsorption. *Sains Malays.* **2024**, *53* (7), 1661–1676.  
<https://doi.org/10.17576/jsm-2024-5307-14>.
- (132) Zhang, G.; Yi, L.; Deng, H.; Sun, P. Dyes Adsorption Using a Synthetic Carboxymethyl Cellulose-Acrylic Acid Adsorbent. *J. Environ. Sci.* **2014**, *26* (5), 1203–1211. [https://doi.org/10.1016/S1001-0742\(13\)60513-6](https://doi.org/10.1016/S1001-0742(13)60513-6).
- (133) Lin, Q.; Gao, M.; Chang, J.; Ma, H. Adsorption Properties of Crosslinking Carboxymethyl Cellulose Grafting Dimethyldiallylammonium Chloride for Cationic and Anionic Dyes. *Carbohydr. Polym.* **2016**, *151*, 283–294.  
<https://doi.org/10.1016/j.carbpol.2016.05.064>.
- (134) Liu, C.; Omer, A. M.; Ouyang, X. Adsorptive Removal of Cationic Methylene Blue Dye Using Carboxymethyl Cellulose/k-Carrageenan/Activated Montmorillonite Composite Beads: Isotherm and Kinetic Studies. *Int. J. Biol. Macromol.* **2018**, *106*, 823–833. <https://doi.org/10.1016/j.ijbiomac.2017.08.084>.
- (135) Chen, R.; Yang, S.; Liu, B.; Liao, Y. Eco-Friendly Semi-Interpenetrating Polymer Network Hydrogels of Sodium Carboxymethyl Cellulose/Gelatin for Methylene Blue Removal. *Materials* **2023**, *16* (9), 3385. <https://doi.org/10.3390/ma16093385>.
- (136) Hussain, S.; Salman, M.; Farooq, U.; Zahid, F.; Yasmeen, S.; Al-Ahmary, K. M.; Ahmed, M. Fabrication of Carboxymethyl Cellulose/Graphene Oxide/ZnO Composite Hydrogel for Efficient Removal of Fuchsin Dye from Aqueous Media. *Int. J. Biol. Macromol.* **2024**, *277*, 134104.  
<https://doi.org/10.1016/j.ijbiomac.2024.134104>.
- (137) Sirach, R.; Dave, P. N. Artificial Neural Network Modelling and Experimental Investigations of Malachite Green Adsorption on Novel Carboxymethyl Cellulose/ $\beta$ -Cyclodextrin/Nickel Cobaltite Composite. *Heliyon* **2024**, *10* (13), e33820. <https://doi.org/10.1016/j.heliyon.2024.e33820>.
- (138) Kaur, N.; Kaur, M. Comparative Studies on Impact of Synthesis Methods on Structural and Magnetic Properties of Magnesium Ferrite Nanoparticles. *Process. Appl. Ceram.* **2014**, *8* (3), 137–143. <https://doi.org/10.2298/PAC1403137K>.
- (139) Elkony, A. M.; Ibrahim, A. G.; Abu El-Farh, M. H.; Abdelhai, F. Synthesis of Acrylamide-Co-3-Allyloxy-2-Hydroxy-1-Propanesulfonic Acid Sodium Salt

- Hydrogel for Efficient Adsorption of Methylene Blue Dye. *Int. J. Environ. Anal. Chem.* **2023**, *103* (8), 1751–1770. <https://doi.org/10.1080/03067319.2021.1882447>.
- (140) Watkins, D.; Nuruddin, Md.; Hosur, M.; Tcherbi-Narteh, A.; Jeelani, S. Extraction and Characterization of Lignin from Different Biomass Resources. *J. Mater. Res. Technol.* **2015**, *4* (1), 26–32. <https://doi.org/10.1016/j.jmrt.2014.10.009>.
- (141) Singh, H.; Rattan, V. K. Adsorption of Nickel from Aqueous Solutions Using Low Cost Biowaste Adsorbents. *Water Qual. Res. J.* **2011**, *46* (3), 239–249. <https://doi.org/10.2166/wqrjc.2011.024>.
- (142) Rajabi, H. R.; Razmpour, S. Synthesis, Characterization and Application of Ion Imprinted Polymeric Nanobeads for Highly Selective Preconcentration and Spectrophotometric Determination of Ni(II) ion in Water Samples. *Spectrochim. Acta. A. Mol. Biomol. Spectrosc.* **2016**, *153*, 45–52. <https://doi.org/10.1016/j.saa.2015.08.010>.
- (143) Li, X.; Wang, Y.; Li, Y.; Zhou, L.; Jia, X. Biosorption Behaviors of Biosorbents Based on Microorganisms Immobilized by Ca-Alginate for Removing Lead (II) from Aqueous Solution. *Biotechnol. Bioprocess Eng.* **2011**, *16* (4), 808–820. <https://doi.org/10.1007/s12257-010-0434-z>.
- (144) Mahmoodi, N. M. Surface Modification of Magnetic Nanoparticle and Dye Removal from Ternary Systems. *J. Ind. Eng. Chem.* **2015**, *27*, 251–259. <https://doi.org/10.1016/j.jiec.2014.12.042>.
- (145) Ibrahim, A. G.; Abdel Hai, F.; Abd El-Wahab, H.; Aboelanin, H. Methylene Blue Removal Using a Novel Hydrogel Containing 3-Allyloxy-2-hydroxy-1-propanesulfonic Acid Sodium Salt. *Adv. Polym. Technol.* **2018**, *37* (8), 3561–3573. <https://doi.org/10.1002/adv.22140>.
- (146) Lima, É. C.; Adebayo, M. A.; Machado, F. M. Kinetic and Equilibrium Models of Adsorption. In *Carbon Nanomaterials as Adsorbents for Environmental and Biological Applications*; Bergmann, C. P., Machado, F. M., Eds.; Carbon Nanostructures; Springer International Publishing: Cham, 2015; pp 33–69. [https://doi.org/10.1007/978-3-319-18875-1\\_3](https://doi.org/10.1007/978-3-319-18875-1_3).
- (147) Saucier, C.; Karthickeyan, P.; Ranjithkumar, V.; Lima, E. C.; Dos Reis, G. S.; De Brum, I. A. S. Efficient Removal of Amoxicillin and Paracetamol from Aqueous Solutions Using Magnetic Activated Carbon. *Environ. Sci. Pollut. Res.* **2017**, *24* (6), 5918–5932. <https://doi.org/10.1007/s11356-016-8304-7>.
- (148) Mondal, N. K. Natural Banana (*Musa Acuminata*) Peel: An Unconventional

- Adsorbent for Removal of Fluoride from Aqueous Solution through Batch Study. *Water Conserv. Sci. Eng.* **2017**, 1 (4), 223–232. <https://doi.org/10.1007/s41101-016-0015-x>.
- (149) Jasrotia, R.; Singh, R.; Sharma, D.; Singh, J.; Mittal, S.; Singh, H. A Sustainable Approach for Enhancing Cationic Dyes Adsorption in Single and Multiple Systems Using Novel Nano Ferrites Modified with Walnut Shell. *Chemistry Select* **2024**, 9 (18), e202304810. <https://doi.org/10.1002/slct.202304810>.
- (150) Pertiwi, A.; Yulianti, E.; Khoiroh, L. M.; Yusniyanti, F. Variation of Alginate: Carboxymethyl Cellulose on Making Beads CMC from Cellulose of Corn Stalk;; Malang, East Java, Indonesia, 2021. <https://doi.org/10.2991/assehr.k.210421.126>.
- (151) Riyajan, S.-A.; Nuim, J. Interaction of Green Polymer Blend of Modified Sodium Alginate and Carboxymethyl Cellulose Encapsulation of Turmeric Extract. *Int. J. Polym. Sci.* **2013**, 1–10. <https://doi.org/10.1155/2013/364253>.
- (152) Mahmood, A.; Bano, S.; Kim, S.-G.; Lee, K.-H. Water–Methanol Separation Characteristics of Annealed SA/PVA Complex Membranes. *J. Membr. Sci.* **2012**, 415–416, 360–367. <https://doi.org/10.1016/j.memsci.2012.05.020>.
- (153) Zhang, Q.; Wang, D.; Bei, Y.; Ren, S.; Fang, G. Flocculation Performance of Trimethyl Quaternary Ammonium Salt of Lignin-Sodium Alginate Polyampholyte. *BioResources* **2013**, 8 (3), 3544–3555. <https://doi.org/10.15376/biores.8.3.3544-3555>.
- (154) Yattinahalli, S. S.; Kapatkar, S. B.; Mathad, S. N. Structural and Mechanical Properties of a Nano Ferrite. *Adv. Sci. Focus* **2014**, 2 (1), 42–46. <https://doi.org/10.1166/asfo.2014.1079>.
- (155) Dongol, M.; El-Denglawey, A.; Abd El Sadek, M. S.; Yahia, I. S. Thermal Annealing Effect on the Structural and the Optical Properties of Nano CdTe Films. *Optik* **2015**, 126 (14), 1352–1357. <https://doi.org/10.1016/j.ijleo.2015.04.048>.
- (156) Kanagarajan, S. V.; Thiagarajan, D. Carboxymethyl Cellulose-Functionalised Magnetic Nanocarriers for pH Responsive Delivery of Curcumin in Cancer Therapy. *Mater. Res. Express* **2018**, 6 (1), 016105. <https://doi.org/10.1088/2053-1591/aadc94>.
- (157) Dai, H.; Zhang, H.; Ma, L.; Zhou, H.; Yu, Y.; Guo, T.; Zhang, Y.; Huang, H. Green pH/Magnetic Sensitive Hydrogels Based on Pineapple Peel Cellulose and Polyvinyl Alcohol: Synthesis, Characterization and Naringin Prolonged Release. *Carbohydr. Polym.* **2019**, 209, 51–61. <https://doi.org/10.1016/j.carbpol.2019.01.014>.

- (158) Konicki, W.; Sibera, D.; Mijowska, E.; Lendzion-Bieluń, Z.; Narkiewicz, U. Equilibrium and Kinetic Studies on Acid Dye Acid Red 88 Adsorption by Magnetic ZnFe<sub>2</sub>O<sub>4</sub> Spinel Ferrite Nanoparticles. *J. Colloid Interface Sci.* **2013**, *398*, 152–160. <https://doi.org/10.1016/j.jcis.2013.02.021>.
- (159) Kandisa, R. V.; Saibaba Kv, N. Dye Removal by Adsorption: A Review. *J. Bioremediation Biodegrad.* **2016**, *07* (06). <https://doi.org/10.4172/2155-6199.1000371>.
- (160) Torres-Caban, R.; Vega-Olivencia, C. A.; Mina-Camilde, N. Adsorption of Ni<sup>2+</sup> and Cd (II) from Water by Calcium Alginate/Spent Coffee Grounds Composite Beads. *Appl. Sci.* **2019**, *9* (21), 4531. <https://doi.org/10.3390/app9214531>.
- (161) Zdujić, A.; Trivunac, K.; Pejić, B.; Vukčević, M.; Kostić, M.; Milivojević, M. A Comparative Study of Ni (II) Removal from Aqueous Solutions on Ca-Alginate Beads and Alginate-Impregnated Hemp Fibers. *Fibers Polym.* **2021**, *22* (1), 9–18. <https://doi.org/10.1007/s12221-021-9814-6>.
- (162) El-Sayed, G. O. Removal of Methylene Blue and Crystal Violet from Aqueous Solutions by Palm Kernel Fiber. *Desalination* **2011**, *272* (1–3), 225–232. <https://doi.org/10.1016/j.desal.2011.01.025>.
- (163) Silva, F.; Nascimento, L.; Brito, M.; Da Silva, K.; Paschoal, W.; Fujiyama, R. Biosorption of Methylene Blue Dye Using Natural Biosorbents Made from Weeds. *Materials* **2019**, *12* (15), 2486. <https://doi.org/10.3390/ma12152486>.
- (164) Amin, M. T.; Alazba, A. A.; Shafiq, M. Successful Application of Eucalyptus Camdulensis Biochar in the Batch Adsorption of Crystal Violet and Methylene Blue Dyes from Aqueous Solution. *Sustainability* **2021**, *13* (7), 3600. <https://doi.org/10.3390/su13073600>.
- (165) Alghamdi, W. M.; El Mannoubi, I. Investigation of Seeds and Peels of Citrullus Colocynthis as Efficient Natural Adsorbent for Methylene Blue Dye. *Processes* **2021**, *9* (8), 1279. <https://doi.org/10.3390/pr9081279>.
- (166) Li, Y.-C.; Zhuo, S.-N.; Peng, B.; Min, X.-B.; Liu, H.; Ke, Y. Comprehensive Recycling of Zinc and Iron from Smelting Waste Containing Zinc Ferrite by Oriented Transformation with SO<sub>2</sub>. *J. Clean. Prod.* **2020**, *263*, 121468. <https://doi.org/10.1016/j.jclepro.2020.121468>.
- (167) Mei, L.; Iizuka, A.; Shibata, E. Recent Progress on Utilization of Metal-Rich Wastes in Ferrite Processing: A Review. *Waste Biomass Valorization* **2018**, *9* (9), 1669–1679. <https://doi.org/10.1007/s12649-017-9909-x>.

- (168) Ouedraogo, A. S.; Kumar, A.; Frazier, R.; Sallam, K. A. Comparative Life Cycle Assessment of Landfilling with Sustainable Waste Management Methods for Municipal Solid Wastes. *Environments* **2024**, *11* (11), 248. <https://doi.org/10.3390/environments11110248>.
- (169) Hashem, A.; Farag, S.; Badawy, S. M. Carboxymethyl Cellulose: Past Innovations, Present Applications, and Future Horizons. *Re. Chem.* **2024**, <https://doi.org/10.1016/j.rechem.2025.102534>.



## List of Publications

### Papers Published

1. **R. Singh**, J. Singh, Sonika and H. Singh, "Green Synthesis of carboxymethyl cellulose from agricultural waste- its characterization" *Journal of Physics: Conference Series*, 2022,012144, doi:10.1088/1742-6596/2267/1/012144.
2. **R Singh**, R. Jasrotia, D. Sharma, J. Singh, S. Mittal and H. Singh, "Recyclable magnetic nickel ferrite-carboxymethyl cellulose-sodium alginate bio-composite for efficient removal of nickel ion from water" *Journal of Dispersion Science and Technology*, pp 1-12, 2024, doi.org/10.1080/01932691.2024.2320302.
3. R. Jasrotia, **R. Singh**, D. Sharma, J. Singh, S. Mittal, H. Singh "A Sustainable Approach for Enhancing Cationic Dyes Adsorption in Single and Multiple Systems using Novel Nano Ferrites Modified with Walnut Shell" *Chemistry Select*, vol 9, no. 18, p. E202304810, 2024, doi.org/10.1002/slct.202304810.
4. D. Sharma, R. Jasrotia, **R. Singh**, J. Singh, S. Mittal and H. Singh, "Novel magnetic metal ferrite-mango starch composite for the removal of dyes in single and ternary dye mixtures from aqueous solutions: kinetic and thermodynamic studies" *Indian Chemical Engineer*, 2024, doi.org/10.1080/00194506.2024.2408021.
5. **R Singh**, R. Jasrotia, D. Sharma, J. Singh, S. Mittal and H. Singh, "Selective Removal of Cationic Dyes in Single and Multiple Dye Systems by Recyclable Spinel Ferrite-Biopolymer Based Composites" *Chemical Engineering Communications*, (Communicated).

### Conferences Attended

1. The poster presentation of paper of title "Green Synthesis of carboxymethyl cellulose from agricultural waste- its characterization" was presented in the the International Conference on Recent Advances in Fundamental and Applied Sciences (RAFAS 2021) held on June 25-26, 2021 organized by School of Chemical Engineering and Physical Sciences, Lovely Professional University, Punjab.
2. The poster presentation of paper of title "Synthesis, Characterization and Adsorption Behaviour Studies of Magnetic Nickel Ferrite-CMC-Sodium Alginate Bio-Composite for Efficient Removal of Nickel metal Ion in Aqueous Medium" was presented in 14<sup>th</sup> National Conference on Chemistry for Sustainable Future (CSF-2024) held on March 06-07, 2024 at Department of Chemistry, Punjabi University, Patiala.

## Green synthesis of carboxymethyl cellulose from agricultural waste its characterization

R Singh, J Singh, Sonika and H Singh

School of Chemical Engineering and Physical Sciences, Lovely Professional University,

Phagwara, Punjab, India

**Email:** *rajinder.choudhary@gmail.com*

**Abstract:** In the present study, corncob (an agricultural waste) has been explored as a source of cellulose. Cellulose was extracted from corncob through removal of hemicellulose and lignin. The carboxymethyl cellulose (CMC) was then synthesized from extracted cellulose by alkalization and etherification with 30% NaOH and 120% monochloro acetic acid (MCA) in ethanol medium respectively. Characterization of prepared CMC was carried out by various techniques like Fourier Transform Infra-Red (FTIR) spectroscopy, X-Ray Diffraction (XRD) and Scanning Electron Microscopy (SEM). Back titration method was used to determine the Degree of Substitution (DS). The synthesized CMC obtained has a large DS value of 2.27. The purity of CMC was high at 91.65% and showed a yield of 1.20g/g, intrinsic viscosity of 1.02, water holding capacity 3.81g/g and oil holding capacity 1.66g/g. Higher degree of substitution is achieved in this work. The synthesized product is effective suitable additive for food and various pharmaceuticals industries.

**Keywords:** Corncob, Cellulose, Carboxymethyl cellulose (CMC), Alkalization, Etherification, Degree of Substitution (DS)

### 1. Introduction

Cellulose is the major and important natural polymer on earth which can be found in all kinds of plants. It is the component of cell wall and plant biomass (30%), wood (over 50%) that can be explored as underdone material for synthesis of various cellulose derivatives [1]. Due to biodegradable nature, low cost and abundant availability of cellulose sources, their use has been increased in material science and innovation. The cellulose fibres are being used in textile, paper, packaging, pharmaceutical industries and many more [2]. To meet the increasing demand of cellulose and to reduce dependency on wood sources, non-wood materials are explored as alternative sources of cellulose.

Cellulose is a long, linear polymer made up of glucose units joined by  $\beta$ -1, 4 glycosidic bonds formed by condensation process. In plants, it is found along with other substances like lignin and hemicelluloses having composition of 40-55% cellulose, 25-40% hemicelluloses and 15-35% lignin. Carboxymethyl cellulose (CMC), a common derivative of cellulose which is a water soluble, anionic polysaccharide contains carboxyl ( $-\text{COO}$ ) and hydroxyl ( $-\text{OH}$ ) groups for interactions with positively.

111

Views

2

CrossRef citations to date

0

Altmetric

Research Article

## Recyclable magnetic nickel ferrite–carboxymethyl cellulose–sodium alginate bio-composite for efficient removal of nickel ion from water

Rajinder Singh Rimzim Jasrotia Dimple Sharma Jandeep Singh Sunil Mittal & Harmander Singh

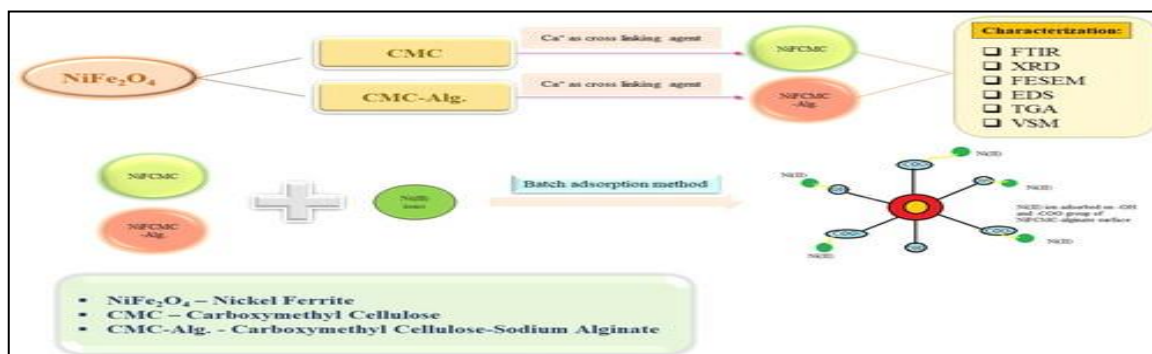
Received 17 Oct 2023, Accepted 13 Feb 2024, Published online: 27 Feb 2024

<https://doi.org/10.1080/01932691.2024.2320302>

### Abstract

In waste water treatment, magnetic bio-composites are frequently investigated as an adsorbent recently due to their great capacity for adsorption and affordability. In this current work, an attempt has been made to develop spinel nickel ferrite–carboxymethyl cellulose (NiFCMC) composite and modified its surface by alginate polymer to form NiFCMC–Alg composite. Several techniques were utilized to characterize these adsorbents including Fourier transform infrared spectroscopy, x-ray diffraction, field emission scanning electron microscopy, energy-dispersive spectra, thermogravimetric analysis, vibration sample magnetometry and pH of point zero charge. These adsorbents were explored to check their potentiality to remove Ni (II) ions in aqueous medium on various parameters such as contact time, initial metal ion concentration, pH, adsorbent dose and temperature. The optimum time for establishment of equilibrium was 180 minutes at pH 8 with adsorbent dose of 0.1 g. Results of kinetic studies revealed that the best fit for the metal ion adsorption data was the Lagergren pseudo-second-order mode indicating the chemisorption nature. Likewise, the Langmuir isotherm model also showed good agreement with adsorption equilibrium data with maximum adsorption capacities  $47.84 \pm 2.39$  and  $60.24 \pm 3.01$  mg/g for NiFCMC and NiFCMC–Alg respectively. The calculated adsorption thermodynamic parameters confirmed the spontaneous nature of adsorption process. The regeneration efficiency of both adsorbents was studied for five cycles and showed significant results. This study has shown that NiFCMC and NiFCMC–Alg can be a good substitute for removing Ni (II) ions in aqueous medium.

### GRAPHICAL ABSTRACT



# A Sustainable Approach for Enhancing Cationic Dyes Adsorption in Single and Multiple Systems using Novel Nano Ferrites Modified with Walnut Shell

Rimzim Jasrotia,<sup>[a]</sup> Rajinder Singh,<sup>[a]</sup> Dimple Sharma,<sup>[a]</sup> Jandeep Singh,<sup>[a]</sup> Sunil Mittal,<sup>[b]</sup> and Harminder Singh\*<sup>[a]</sup>


[a] R. Jasrotia, R. Singh, D. Sharma, J. Singh, H. Singh

School of Chemical Engineering and Physical Sciences, Lovely Professional University, Phagwara, Punjab, 144411, India

E-mail: harminder\_env@yahoo.com

[b] S. Mittal

Department of Environmental Science and Technology, Central University of Punjab, Bathinda, Punjab, India

 Supporting information for this article is available on the WWW under <https://doi.org/10.1002/slct.202304810>

Walnut shell has been used in various experimental studies for different dyes removal, but it is exciting to study the adsorption behaviour of bio-waste (walnut shell) in combination with spinel zinc ferrite which resulted in the formation of a novel material having magnetic properties and help in easy separation after the wastewater treatment. Novel magnetic walnut shell zinc ferrite (WSZF) composite has been synthesized and used to remove Malachite Green and Methylene Blue from aqueous solution in single and binary dye systems. Different techniques have been used to characterize the composite such as Fourier Transform Infrared Spectroscopy, X-Ray Diffraction, Field Emission Scanning Electron Microscopy, Energy Dispersive Spectroscopy, Thermogravimetric Analysis and pHzpc. Adsorption of dyes were studied to see the effect of time, pH,

adsorbent dose, dye concentration and temperature. The Lagergren pseudo second order model fitted well among various kinetic models employed. Langmuir adsorption isotherm best fitted with maximum adsorption capacities of 86.20 and 169.5 mg/g in single dye and 23.92 and 18 mg/g respectively in binary dye system for Malachite Green and Methylene Blue. Process was spontaneous and  $\Delta H^\circ$  were found positive, confirmed endothermic process of adsorption. The composite's regeneration capacity was studied for five cycles and at the end of five cycle the efficiency of the material was found to be around 80 % for both single as well as binary dye systems. It is concluded that the chosen WSZF will be the optimum solution for cationic dyes removal.

## 1. Introduction

Rapid increase in population growth, various industrial activities, climatic variations etc. leads to the deterioration of available fresh water resources in the whole world.<sup>[1]</sup> Industries such as paint, plastic, leather, food processing, textile, pharmaceutical industries etc. are using dyes as colorants in their production process.<sup>[2]</sup> Dyes are used by industries in large quantities and discharged directly into water bodies without their treatment.<sup>[3]</sup> The discharge of harmful pollutants into water bodies can cause mutagenicity, embryo toxicity and carcinogenicity.<sup>[4]</sup> The dyes are of basically synthetic origin which possess complex molecular structure, thus shows more stability and difficulty in biodegradation.<sup>[1]</sup> The dyes can be categorized as cationic, anionic and non-ionic dyes.<sup>[5]</sup> Approximately ten thousand types and about  $7 \times 10^5$  tons of different dyes are produced by these industries annually.<sup>[6]</sup> Even at very low concentration, dyes are easily visible to naked eye. Dyes contain harmful components which are toxic in nature that can damage aquatic life, human life and may also result in the disruption of ecological balance. Therefore, presence of dyes in the water body beyond maximum permissible limits affects the quality of water and also results in the inhibition of sunlight penetration which ultimately affects the photosynthetic activity.



Check for updates

# Novel magnetic metal ferrite-mango starch composite for the removal of dyes in single and ternary dye mixtures from aqueous solutions: kinetic and thermodynamic studies

Dimple Sharma<sup>a</sup>, Rimzim Jasrotia<sup>a</sup>, Rajinder Singh<sup>a</sup>, Jandeep Singh<sup>a</sup>, Sunil Mittal<sup>b</sup> and Harminder Singh<sup>a</sup>

<sup>a</sup>School of Chemical Engineering and Physical Sciences, Lovely Professional University, Phagwara, India;

<sup>b</sup>Department of Environmental Science and Technology, Central University of Punjab, Bathinda, India

## ABSTRACT

Magnetic metal ferrites attached to biowastes are proven to be promising adsorbents for the removal of dyes from water. Magnetic composites with biopolymers are gaining interest in the field of treatment of wastewater because of their selective nature, recyclability, low cost and environmental compatibility. In this work, Zinc ferrite composite with starch, extracted from mango seed kernel (ZFNMS) was synthesised. Characterisation techniques, such as FTIR, XRD, FESEM, BET, TGA and pH<sub>zpc</sub>, were used for the structural analysis of ZFNMS. ZFNMS was used to remove Methylene blue, Crystal violet and Brilliant green dyes in single and multiple (ternary) dye systems. The kinetics of adsorption by ZFNMS revealed that pseudo-second-order of kinetics was most appropriate for this study. Maximum adsorption capacities using ZFNMS for CV, BG and MB dyes were 142.9, 101.2 and 105.8 mg/g, respectively. The values of adsorption energies using ZFNMS were 200.5, 494.3 and 183.6 KJ/mol for CV, BG and MB dyes, respectively. Thermodynamic data revealed the spontaneous nature of the adsorption of dyes by ZFNMS and it was found that chemical adsorption was taking place in the present study. Regeneration of the adsorbent was done for successive five cycles and showed significant results. Thus ZFNMS is an ideal adsorbent for cationic dyes removal from water.

## ARTICLE HISTORY

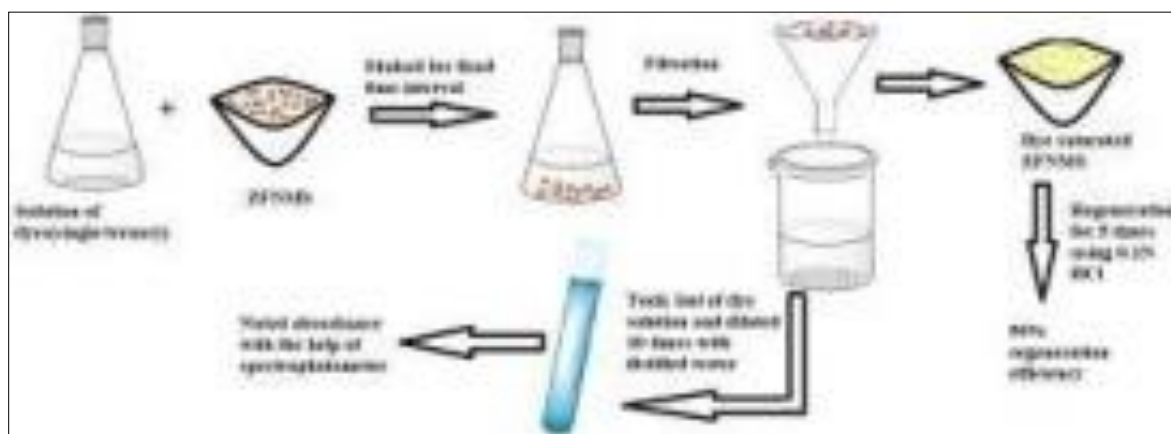
Received 25 June 2024

Accepted 18 September

2024

## KEYWORDS

Ternary dyes; spinel ferrites; adsorption; kinetics; Langmuir



## 1. Introduction

With the increase in the population, industrialisation also increased proportionately, thereby increasing the use of chemicals, which cause pollution and associated effects [1]. The scarcity of clean water is the main problem which our society is facing today. Dyes have been used in various industries, such as textile industries, printing presses, drugs, etc. These used dyes have been discarded into water bodies before any treatment [2]. Their direct disposal into water bodies causes various mutagenic and carcinogenic diseases. So, there is a challenge before us to develop a sustainable method for the treatment of dye-containing water before its discharge into water bodies.

# Removal of Cationic Dyes in Single and Multiple Dye Systems by Recyclable Spinel Ferrite-Biopolymer Based Composites

Rajinder Singh<sup>1</sup>, Rimzim<sup>1</sup>, Dimple Sharma<sup>1</sup>, Jandeep Singh<sup>1</sup>, Sunil Mittal<sup>2</sup> and Harminder Singh<sup>1\*</sup>

<sup>1</sup>School of Chemical Engineering and Physical Sciences, Lovely Professional University, Phagwara, Punjab–144411, India

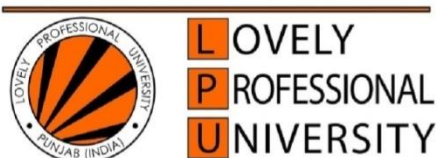
<sup>2</sup>Department of Environmental Science and Technology, Central University of Punjab, Bathinda, Punjab, India

Corresponding Author: harminder\_env@yahoo.com

## Abstract

Currently, due to remarkable adsorption capacity and cost, magnetic bio-composites have been extensively used as an efficient adsorbent in wastewater treatment. The present work aims to produce spinel NiFCMC (nickel ferrite carboxymethyl cellulose) and NiFCMC-Alg (nickel ferrite carboxymethyl cellulose-Alginate) composites. These adsorbents were characterized by number of characterization techniques including FTIR (Fourier Transform Infrared Spectroscopy), FE-SEM (Field Emission Scanning Electron Microscopy), EDS (Energy Dispersive Spectra), TGA (Thermogravimetric Analysis), XRD (X-Ray Diffraction), VSM (Vibration Sample Magnetometry) and  $\text{pH}_{\text{pzc}}$  (pH of point zero charge). Several parameters like contact time, pH, adsorbent dose, initial dye concentration and temperature were studied. To attain equilibrium, 0.1 g adsorbent dose at pH 8, time duration 180 minutes and initial concentration 50 mg/L and 20 mg/L for single and binary dye system respectively were considered optimal. Kinetic analysis showed that the pseudo second order model which signifies chemisorption, fits best with the adsorption data. Conversely, the Langmuir model for adsorption equilibrium proved to be the best fit with the data. With regard to Crystal Violet (CV) and Methylene Blue (MB), the greatest adsorption capabilities for NiFCMC and NiFCMC-Alg were 113.6 mg/g and 99.01 mg/g for single dye system and 16.10 mg/g, 25.57 mg/g, 21.23 mg/g and 29.85 mg/g respectively for binary dye system. For up to six cycles of the regeneration, effectiveness of both adsorbents were studied and showed significant results. The results of this study showed that NiFCMC and NiFCMC-Alg may serve as effective alternatives for removing dyes in single and binary systems.

**Key words:** Ferrite, carboxymethyl cellulose, alginate, adsorption, isotherm, regeneration



*Transforming Education Transforming India*

Certificate No. 225326



## **Certificate of Participation**

This is to certify that Mr. Rajinder Singh  
of Lovely Professional University  
has given poster presentation on Green Synthesis Of Carboxymethyl Cellulose From Agricultural Waste Its  
Characterization

*in the International Conference on "Recent Advances in Fundamental and Applied Sciences" (RAFAS 2021) held on June 25-26, 2021, organized by School of Chemical Engineering and Physical Sciences, Lovely Faculty of Technology and Sciences, Lovely Professional University, Punjab.*

Date of Issue : 15-07-2021

Place of Issue: Phagwara (India)

Prepared by  
(Administrative Officer-Records)

Organizing Secretary  
(RAFAS 2021)

Convener  
(RAFAS 2021)



14<sup>th</sup> National Conference on Chemistry for the Sustainable Future

(CSF-2024)

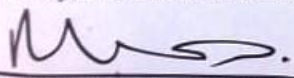
March 06-07, 2024

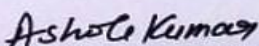
Department of Chemistry, Punjabi University, Patiala

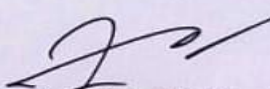


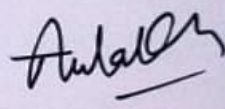
CERTIFICATE

This is to certify that Prof. /Dr. /Mr. /Ms. Rajinder Singh of School of Chemical engg and Physical Sci, LPU has participated / presented a poster / given an oral presentation/delivered an invited lecture / chaired a technical session entitled Synthesis, characterization Aqueous medium in the 14<sup>th</sup> National Conference on Chemistry for the Sustainable Future (CSF-2024), organized by the Department of Chemistry, Punjabi University, Patiala on March 06-07, 2024.

  
Prof. (Dr.) Mohamad Yusuf  
Convener

  
Prof. (Dr.) Ashok K. Malik  
Coordinator

  
Prof. (Dr.) Baljit Singh  
Co-Coordinator

  
Dr. J.S. Aulakh  
Organizing Secretary